



LUND UNIVERSITY

Molecular, micro- and ultrastructural investigations of labile tissues in deep time

Gren, Johan

2017

Document Version:

Publisher's PDF, also known as Version of record

[Link to publication](#)

Citation for published version (APA):

Gren, J. (2017). *Molecular, micro- and ultrastructural investigations of labile tissues in deep time*. [Doctoral Thesis (compilation), Lithosphere and Biosphere Science]. Lund University, Faculty of Science, Department of Geology, Lithosphere and Biosphere Science.

Total number of authors:

1

General rights

Unless other specific re-use rights are stated the following general rights apply:

Copyright and moral rights for the publications made accessible in the public portal are retained by the authors and/or other copyright owners and it is a condition of accessing publications that users recognise and abide by the legal requirements associated with these rights.

- Users may download and print one copy of any publication from the public portal for the purpose of private study or research.
- You may not further distribute the material or use it for any profit-making activity or commercial gain
- You may freely distribute the URL identifying the publication in the public portal

Read more about Creative commons licenses: <https://creativecommons.org/licenses/>

Take down policy

If you believe that this document breaches copyright please contact us providing details, and we will remove access to the work immediately and investigate your claim.

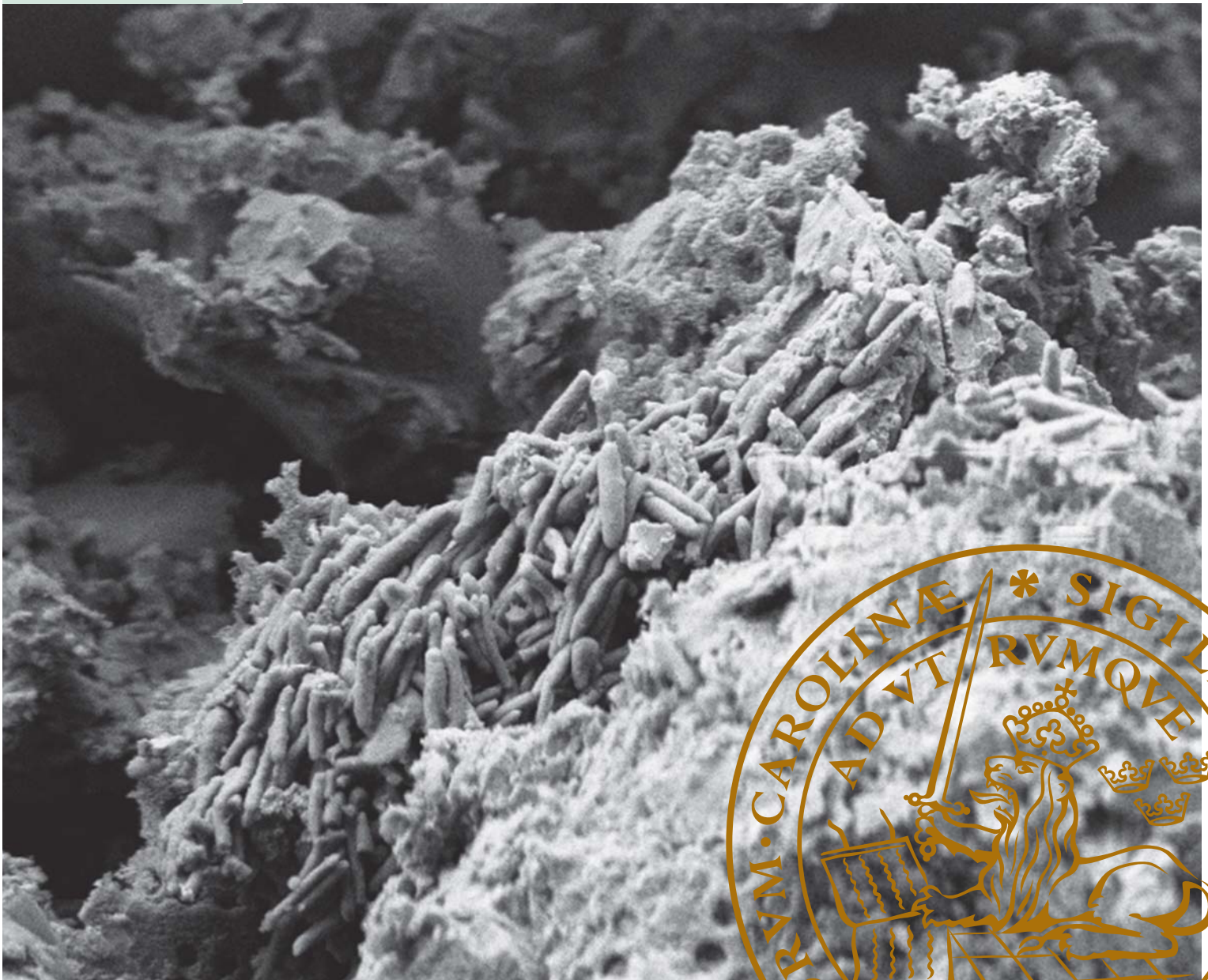
LUND UNIVERSITY

PO Box 117
221 00 Lund
+46 46-222 00 00

Molecular, micro- and ultrastructural investigations of labile tissues in deep time

JOHAN A. GREN

LITHOSPHERE AND BIOSPHERE SCIENCE | DEPARTMENT OF GEOLOGY | LUND UNIVERSITY 2018



Molecular, micro- and ultrastructural investigations of labile tissues in deep time

This dissertation encompasses six scientific papers presenting investigations of microstructures and molecular analyses of various fossil tissues. Using an array of analytical tools, combining established methods with state-of-the art techniques, a series of case studies are presented. These cases take on fossils belonging to a variety of taxa of different geological ages and localities. I provide compelling evidence for the presence of the pigment melanin in the fossil record, often occurring in close association with microstructures that resemble melanosomes. The microstructures do, however, overlap in size and shape with bacteria, making chemical analyses necessary to discern their origin and, subsequently, basing interpretations of biology, ecology or colour reconstructions on their presence.

The author, Johan Gren, is a geologist trained in the profession at Lund University. His interest for palaeontology has been present since childhood. In high school, Johan volunteered in the collections of the Royal Tyrell Museum of Paleontology in Drumheller, Canada, and since then the path has been clear. His interest in the life of long extinct organisms is still as vivid as it can be, and the ever growing collection of miniature dinosaurs serves to remind everyone of his true passion.



Molecular, micro- and ultrastructural investigations of labile tissues in deep time

Johan A. Gren



LUND
UNIVERSITY

Lithosphere and Biosphere Science
Department of Geology

DOCTORAL DISSERTATION

by due permission of the Faculty of Science, Lund University, Sweden.
To be defended in Pangea, Department of Geology, Sölvegatan 12, Lund
on the 19th of January 2018 at 13:15.

Faculty opponent

Dr. Maria E. McNamara
University College Cork

© Johan Gren

Front cover: FEG-SEM image of elongate microstructures in the fossil feather FUM-1980

Back cover: The author. In a bow tie. Photo credit: Stefan Johansson

Lithosphere and Biosphere Science
Department of Geology
Faculty of Science

ISBN 978-91-87847-34-9 (print)

ISBN 978-91-87847-35-6 (pdf)

ISSN 1651-6648

Printed in Sweden by Media-Tryck, Lund University, Lund 2018

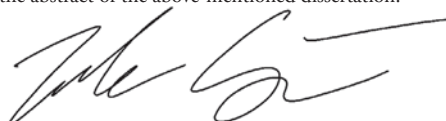


KLIMATKOMPENSERAT
PAPPER



Organization LUND UNIVERSITY Department of Geology Sölvegatan 12 SE-223 62 Lund Sweden Author: Johan A. Gren	Document name DOCTORAL DISSERTATION
Date of issue: 19 January 2018	
Sponsoring organization: –	
Title and subtitle: Molecular, micro- and ultrastructural investigations of labile tissues in deep time	
<p>Abstract</p> <p>This thesis comprises investigations of microstructures and molecular remains, preserved in a variety of fossil specimens. The results are presented in six papers, collectively aiming to thoroughly examine fossil traces of such remains by employing a combination of both established and relatively new analytical methods. The main questions asked are: What can we learn about the biology, ecology and behaviour of ancient organisms by studying these fossilised remnants, and what methods are best suited to accomplish this?</p> <p>The work presented herein has been conducted through a series of case studies performed on fossils representing an array of taxa, collected from different geological ages and settings. Methods applied include light and electron microscopy, computed tomography, and molecular analyses, such as time-of-flight secondary ion mass spectrometry, IR microspectroscopy and X-ray absorption spectroscopy.</p> <p>Microscopic analysis and histology of teeth from Mesozoic marine reptiles allowed calculations of dentine formation and tooth replacement rates. My findings include evidence that while teeth of larger mosasaur taxa took longer time to develop, their dentine formation rates were more rapid, relative to that of smaller species.</p> <p>In other fossils, microscopic investigations of eye, skin and feather remnants revealed aggregations of micro-metre-sized, sub-rounded to elongate structures. Because similar microbodies have previously been described alternatively as relict melanosomes (i.e. pigment-containing, eukaryotic cellular organelles) and lithified bacteria, my co-authors and I performed chemical and molecular analyses in order to explore the affinity of these structures. To ascertain the chemical identity of our fossil samples, corresponding analyses were carried out also on molecularly similar compounds, including modern eumelanin, as controls. My studies show chemical evidence of animal eumelanin in close association with the microbodies, advocating the melanosome interpretation for the analysed specimens.</p> <p>Beyond the results reported in the included papers, this thesis provides a short review of melanin formation in vertebrate eyes and integument, as well as in fungi and bacteria which also produce this type of pigment. An overview of the various methods applied is presented and followed by a discussion about possible outcomes and pitfalls when studying fossil microstructures and molecular palaeontology. Whereas remnant melanosomes could potentially provide new insight into a multitude of biological and ecological aspects of ancient life, there is still no straight-forward approach to determine the affinity of ‘melanosome-like’ microstructures found in fossils. Therefore, a thorough investigation of such remains, including chemical analyses, should be applied in each study – at least until a consensus has been reached regarding the minimum amount of criteria to be used for a confident recognition.</p>	
Key words: eumelanin, fossils, histology, integument, IR microspectroscopy, melanin, melanosomes, molecular palaeontology, ToF-SIMS, XAS	
Classification system and/or index terms (if any): –	
Supplementary bibliographical information: –	Language: English
ISSN and key title: 1651-6648 LITHOLUND THESES	
ISBN: 978-91-87847-34-9	
Recipient's notes: –	Number of pages 105
Price: –	
Security classification: –	

I, the undersigned, being the copyright owner of the abstract of the above-mentioned dissertation, hereby grant to all reference sources permission to publish and disseminate the abstract of the above-mentioned dissertation.

Signature: 

Date: 4 December 2017

Preface

To begin this thesis, I would like to take a moment for reflection.

I believe that science is completely driven by curiosity, and that new discoveries always start with a question. And there is one question to rule them all:

“Why?”

One word, simple as that, can sprout ideas, inspire explorations and investigations and lead to great scientific discoveries.

But it can also be immensely frightening.

Why?

Because there always comes a point when there is no answer to the question. Whatever the context, if the question “*Why?*” is repeatedly posed, the answers will become successively vaguer, until the one inevitable answer left is “*I don’t know*”.

I guess that the question itself is not what horrifies us. It is the fear of not having an answer. And that is the foundation of science: To find answers to new questions.

Therefore, in a way, you can say that science is built on fear. I would argue that it is healthy kind of fear, though, a fear that always keeps us moving. We are chasing the “*Why?*”, while running as fast as we can from ignorance. If we hesitate, or even slow down, “*I don’t know*” will eventually catch up.

So I will keep running. Keep chasing the question in pursuit of a better answer, whatever my questions may be. Never stop being curious. Always learn. I will do it because I am afraid of not having an answer.

Why it scares me?

I don’t know.

Contents

1. SCOPE OF THE THESIS	9
2. INTRODUCTION	9
3. METHODS	10
4. MELANIN	10
Melanin chemistry	10
Melanosomes	10
Melanin in different tissues	12
5. SUMMARY OF PAPERS	14
Paper I: Dental histology of mosasaurs and a marine crocodylian from the Campanian (Upper Cretaceous) of southern Sweden: incremental growth lines and dentine formation rates.	14
Paper II: Skin pigmentation provides evidence of convergent melanism in extinct marine reptiles.	14
Paper III: Interpreting melanin-based coloration through deep time: a critical review.	15
Paper IV: Molecular composition and ultrastructure of Jurassic paravian feathers.	15
Paper V: Molecular and microstructural inventory of an isolated fossil bird feather from the Eocene Fur Formation of Denmark	16
Paper VI: Skeletal and soft tissue anatomy of an Early Permian temnospondyl amphibian from the Saar-Nahe Basin of south-western Germany	16
6. DISCUSSION	16
Fossil colours	17
Adaptation and behaviour	18
7. CONCLUSIONS	19
8. ACKNOWLEDGEMENTS	20
9. REFERENCES	21
SVENSK SAMMANFATTNING	24
PAPER I-VI	25

List of publications

- Paper I: **Gren, J.A.** and Lindgren, J. 2014: Dental histology of mosasaurs and a marine crocodylian from the Campanian (Upper Cretaceous) of southern Sweden: incremental growth lines and dentine formation rates. *Geological Magazine* 151, 134–143. (doi:10.1017/S0016756813000526)
- Paper II: Lindgren, J., Sjövall, P., Carney, R.M., Uvdal, P., **Gren, J.A.**, Dyke, G., Schultz, B.P., Shawkey, M.D., Barnes, K.R. and Polcyn, M.J. 2014: Skin pigmentation provides evidence of convergent melanism in extinct marine reptiles. *Nature* 506, 484–488. (doi:10.1038/nature12899)
- Paper III: Lindgren, J., Moyer, A., Schweitzer, M.H., Sjövall, P., Uvdal, P., Nilsson, D.E., Heimdal, J., Engdahl, A., **Gren, J.A.**, Schultz, B.P. and Kear, B.P. 2015a: Interpreting melanin-based coloration through deep time: a critical review. *Proceedings of the Royal Society B* 282, 20150614. (doi:10.1098/rspb.2015.0614)
- Paper IV: Lindgren, J., Sjövall, P., Carney, R.M., Cincotta, A., Uvdal, P., Hutcheson, S.W., Gustafsson, O., Lefevre, U., Escuillie, F., Heimdal, J., Engdahl, A., **Gren, J.A.**, Kear, B.P., Wakamatsu, K., Yans, J. and Godefroit, P. 2015b: Molecular composition and ultrastructure of Jurassic paravian feathers. *Scientific Reports* 5, 13520. (doi:10.1038/srep13520)
- Paper V: **Gren, J.A.**, Sjövall, P., Eriksson, M.E., Sylvestersen, R.L., Marone, F., Sigfridsson Clauss, K.G.V., Taylor, G.J., Carlson, S., Uvdal, P., Lindgren, J. 2017: Molecular and microstructural inventory of an isolated fossil bird feather from the Eocene Fur Formation of Denmark. *Palaeontology* 60, 73–90. (doi:10.1111/pala.12271)
- Paper VI: **Gren, J.A.**, Hall, S.A., Sachs, S. and Kokfelt, U. 2017: Skeletal and soft tissue anatomy of an Early Permian temnospondyl amphibian from the Saar-Nahe Basin of south-western Germany. *Manuscript in prep.*

1. Scope of the thesis

The general scope of this thesis is to investigate micro- and ultrastructural features of exceptionally preserved fossils collected from a variety of spatially and temporally separated localities. Additionally, analyses of chemical and molecular remains are employed to ascertain the affinity of preserved soft tissues. This is conducted through a series of case studies, each applying a variety of both new and established methods as a means to bring clarity to a few key questions

- What can we learn about the biology, ecology or behaviour of extinct animals by studying their preserved microstructures?
- Which methods are best suited to achieve this and to avoid ambiguous or erroneous conclusions?

2. Introduction

In order to understand the history of life and the evolution of organisms, it is imperative to study the fossil record. Certain locations around the world provide especially detailed windows into the past thanks to a superior preservation of the fossils. These localities, known as *Fossil Konservat Lagerstätten*, sometimes produce fossils that retain details of labile tissues (e.g. skin, feathers or eyes) that otherwise decay soon after the carcasses are buried (e.g. Briggs & McMahon 2015). The presence of such features presents us with an opportunity to study aspects of extinct animals that are unattainable by looking at fossil bones alone.

Historically, palaeontology has largely entailed the description and classification of extinct organisms based on their skeletal remains. While this is still an important element of palaeontological research, advancements in biology and ecology together with the development of new analytical techniques have expanded the field to become a broad interdisciplinary subject (e.g. Edwards *et al.* 2014). As an example, although serial sectioning of bone and teeth was applied already a century ago through stepwise grinding, with each increment depicted by a drawing of the observed surface (e.g. Sollas 1903), this is now more-or-less routinely carried out by means of computed tomography and digital reconstructions. Not only does this technological development save time and effort, but in many cases it also prevents the destruction of precious fossil material. Furthermore, a multitude of recent studies on exceptionally preserved specimens have applied state-

of-the-art methodologies to investigate the presence of remnant microstructures and biomolecules, thereby hoping to gain deeper knowledge about the life histories of extinct animals.

For instance, reconstructions of pigmentation patterns and colours (possibly providing information on ecological adaptation and behaviour) were until recently thought impossible (Edwards *et al.* 2014). However, a study by Vinther *et al.* (2008) brought this into new light. In that study, the authors proposed a reinterpretation of micro-metre-sized, elongate to sub-rounded structures found in eye and plumage remains of fossil birds. Observed by means of electron microscopy, these microstructures were identified as fossil melanosomes (eukaryotic, pigment bearing cellular organelles). Similar structures were described in the 1980s by Michael Wuttke and co-workers, who observed such microbodies in fossilised skin, hair and feathers of various animals from the Eocene Messel pit of south-western Germany and referred to them as lithified bacteria (Wuttke 1983; Willems & Wuttke 1987). These different interpretations have spurred a lively debate on the affinity of ‘melanosome-like’ microbodies, hitherto without any general consensus; while some authors still favour a microbial origin of the structures (e.g. Franzen *et al.* 2015), others have embraced the melanosome interpretation (e.g. Clarke *et al.* 2010; Li *et al.* 2010, 2012; Colleary *et al.* 2015; Vinther 2015, 2016). In between these groups, there are authors advocating a thorough investigation – including chemical analyses – for each individual study (e.g. Moyer *et al.* 2014; Schweitzer *et al.* 2015; Paper III). While this approach inherently requires more time and resources, the latter authors argue that it is necessary in order to avoid unsubstantiated or erroneous conclusions being introduced in the literature.

To be able to discuss deep time preservation potential of biomolecules, such as melanic pigments, it is necessary to consider the structural constituents of the compounds, their mode of deposition and organization within different tissues, and how we can distinguish them in chemical analyses. Furthermore, because the nomenclature has changed over time, a brief review of the terminology is necessary.

3. Methods

In the papers presented herein, a number of different techniques for analysing the structure and chemistry of various fossil tissues have been employed. Some of these, including conventional light microscopy (CLM) and scanning and transmission electron microscopy (SEM and TEM, respectively), are well established and widely used in palaeontology as well as other fields, and therefore do not call for a methodological overview. Other methods (e.g. computed tomography) are relatively new but have quickly been integrated in studies of fossil remains, and a few (e.g. ToF-SIMS) have just recently gained recognition in palaeontological studies and their full potential may still not be entirely appreciated. Brief overviews for some of these techniques and their applications in palaeontology are presented below (Boxes 1–3).

The methods of choice vary between each paper presented in this thesis (i.e. Papers I–VI), primarily because the aim of each case study is rather different. Some of the applied techniques have proven particularly effective and have thus been utilised repeatedly (e.g. ToF-SIMS; Box 1), whereas others – while providing important results – have proven relatively inefficient with respect to the desired scientific output (e.g. CT imaging of fossil surfaces). Additionally, some methods are not applicable for certain samples due to physical constraints; for instance, high-resolution surface analysis of a fossil feather (FUM-1980) using synchrotron-based CT was complicated due to the large size of the specimen (Paper V), and would not have been feasible for an even larger fossil.

Table 1: Methods applied in the different papers.

Methods applied	
Paper I	CLM
Paper II	CLM, SEM-EDX, ToF-SIMS
Paper III	SEM-EDX, TEM, ToF-SIMS, IR microspectroscopy
Paper IV	SEM-EDX, TEM, ToF-SIMS, IR microspectroscopy
Paper V	CLM, SEM-EDX, ToF-SIMS, XAS, CT
Paper VI	CLM, SEM-EDX, TEM, CT

4. Melanin

Coining of the term ‘melanin’ is usually credited to the Swedish chemist Jöns Jacob Berzelius (1840) in his *Lehrbuch der Chemie*. The term derives from the Greek word *melanos*, simply meaning ‘dark’ and it was originally used to describe the dark pigmentation in eye membranes. The

term has since then been widely used to include essentially any type of dark, organic pigmentation, without direct structural, biogenic or functional inferences (d’Ischia *et al.* 2013). In light of this potential cause of ambiguity, a more restrictive terminology was proposed by d’Ischia *et al.* (2013) who advocated a subdivision of ‘melanin’ into four categories: *eumelanin*, *pheomelanin*, *neuromelanin* and *pyomelanin*. According to this nomenclature, eumelanin comprises a heterogeneous group of dark brown to black eukaryote pigments formed through the oxidation and polymerisation of tyrosine (see below). Similarly, pheomelanin is a tyrosine-related eukaryote pigment. It is a sulfur-containing melanin subgroup, responsible for reddish and buff colouration. Neuromelanin is a dark pigment produced in neurons and primarily found within the substantia nigra of the brain. Finally, pyomelanins include the dark pigments produced by microorganisms.

Melanin chemistry

Despite a broad scientific interest for these compounds, not least in terms of cancer research, the precise chemistry of different types of melanin is still incompletely known (Prota 2012). Eu- and pheomelanin are both derived from the amino acid tyrosine, catalysed by the enzyme tyrosinase (Prota 2012). From a dopaquinone precursor, the two melanin types thereafter follow slightly different pathways. Eumelanin is formed through interaction with dihydroxyindole (DHI) and dihydroxyindole carboxylic acid (DHICA), whereas pheomelanin synthesis notably includes interaction with the amino acid cysteine, thereby incorporating a sulfur group that is not present in eumelanin. However, the chemical structure of the larger, polymerized melanin molecules is still largely unknown. This is in part related to the process of isolation and extraction of melanin, which influences the chemical structure of the pigment (Liu *et al.* 2003).

Melanosomes

In eukaryotes, melanin is synthesised within specific cellular organelles called melanosomes. The term was first proposed by Seiji *et al.* (1961) who studied the cells responsible for melanin production, ‘melanocytes’. These authors described the melanosome as a ‘cell organelle with internal structure and tyrosinase activity’ (Seiji *et al.* 1961, fig. 13), measuring c. 0.1–0.4 μm in diameter, further developing into larger ‘granules’ (up to 20 μm in diameter) within the melanocyte. This terminology has later been revised, however, and to avoid ambiguity the fully melanised units are herein referred to as melano-

Box 1: ToF-SIMS

Time-of-flight secondary ion mass spectrometry (ToF-SIMS) has over the past decade emerged as one of the key methods in molecular palaeontology. Although ToF-SIMS has been used for well over 20 years, primarily applied to analyse inorganic and polymer surfaces (Vickerman 2001), it has only recently gained recognition as a means to identify biomolecules, such as eumelanin, in fossil samples (see Thiel & Sjövall 2011).

In principle, the instrument consists of two parts: an ion gun that bombards the sample surface with high-energy (primary) ions, and a time-of-flight mass spectrometer for mass-resolved detection of the (secondary) ions that are emitted from the sample surface (Fig 1). The obtained mass spectra provide molecular information about the sample surface, and imaging of specific molecular species is accomplished by scanning the primary ion beam over the selected analysis area. For molecular identification, comparisons can be made between the spectral features of the analysed sample and those of reference samples; for example, when looking for traces of melanic compounds in fossil tissues (see e.g. Papers III–IV).

Although the irradiation of the sample by the ion gun is indeed a destructive process (effectively removing material from the sample surface), ToF-SIMS is still regarded as a practically non-destructive method thanks to the minute sample area affected (usually

on the sub-mm scale) and the minimal sample depth that is affected (typically the outermost 1–10 nm of the sample surface; see Thiel & Sjövall 2011). The marginal interference with the sample integrity and high sensitivity of this method makes it effective for studying rare fossil material. These parameters, together with the possibility to study molecular composition *in situ* on the sample, make ToF-SIMS a more effective technique for identifying fossil biomarkers than comparable methods such as coupled gas- or liquid chromatography/mass spectrometry (GC/MS and LC/MS, respectively), which require larger sample sizes and sample homogenisation, preventing spatial distribution analyses of compounds and consuming the sample in the process.

Benefits

- Provides high resolution molecular data
- Offers spatial distribution data over the sample surface
- Virtually non-destructive

Drawbacks

- Requires a ‘fresh’, uncontaminated surface
- Only provides data for the sample surface
- Interpretation of the complex data output may be time consuming and requires a specialist

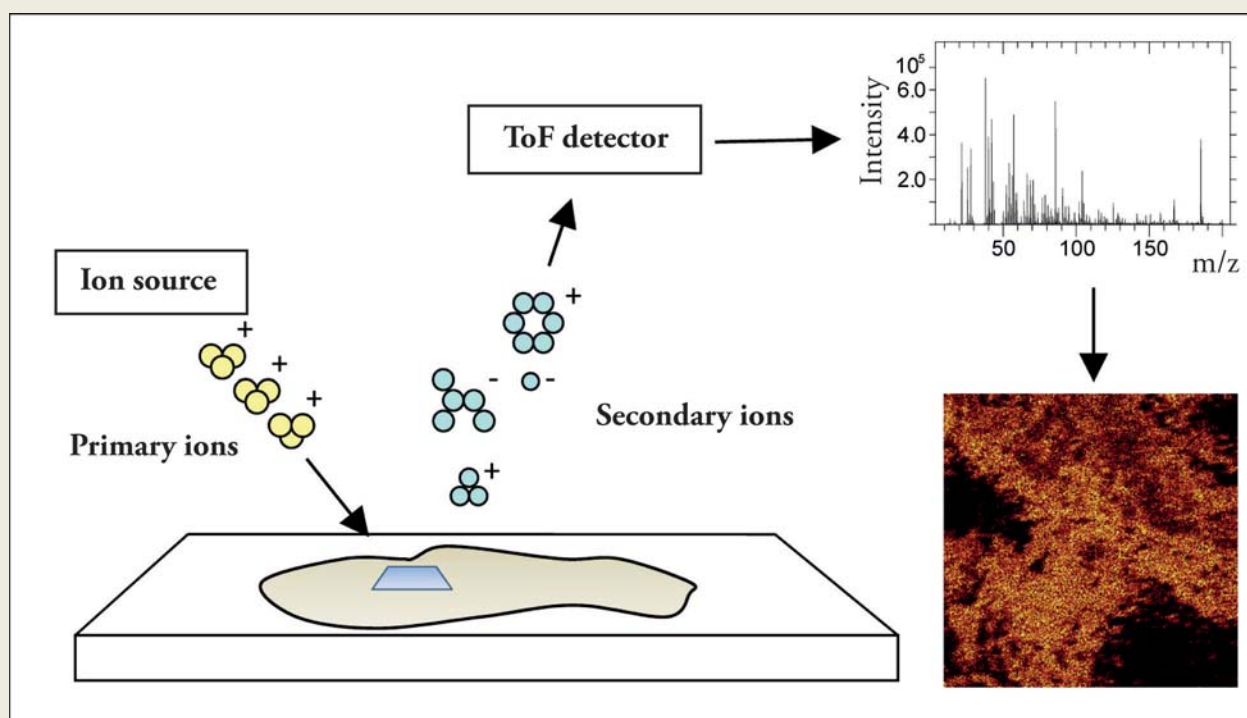


Fig. 1: Schematic illustration of the ToF-SIMS analysis (reprinted with permission from Thiel & Sjövall 2011, fig. 1).

somes, whereas ‘melanin granules’ represent the smaller aggregates of polymerised melanin within the melanosome (*sensu* Simon & Peles 2010). Such melanin granules normally measure 10–30 nm in diameter, although pheomelanin granules of up to 80 nm have been reported (see Liu *et al.* 2005a). Furthermore, melanosome development is subdivided into four stages; stage I and II melanosomes are considered melanosome precursors or premelanosomes, as melanin synthesis commences at stage III. Thereafter the melanosomes are gradually filled with melanin until they reach the fully melanised, ‘mature’, stage IV. At this stage, the melanin granules can often be discerned on the melanosome surface, giving it a rough appearance (see Liu *et al.* 2003, figs 2–3; Lindgren *et al.* 2017, fig 2). Mature melanosomes are transported to the periphery of the cell, from where they can be transferred to other target cells (such as keratinocytes in the epidermis, or forming the epithelium between the choroid and the photoreceptor layer in the vertebrate eye; Marks & Seabra 2001; Wasmeier *et al.* 2008).

Melanin in different tissues

Because melanin is deposited in different ways between tissue types, this has implications for the paleontological interpretation of its occurrence in association with fossils.

In vertebrate **eyes**, melanin is present in melanosomes situated in various tissues, including the iris, retina, choroid and retinal pigment epithelium (RPE). Most studies on melanin and melanosomes in the vertebrate eye have been performed on RPE tissue, where melanosomes are especially abundant and extraction protocols are established (e.g. Liu *et al.* 2005b). In contrast to most other tissues, where melanosome synthesis is a continuous process throughout the life of the organism, RPE melanosomes are primarily generated in the embryonic stage and are retained throughout life (although there is a debate whether or not some melanin synthesis occurs in adult RPE; see Schraermeyer & Heimann 1999; Lopes *et al.* 2007; Wasmeier *et al.* 2008). RPE melanosomes are heterogeneous in size and shape, ranging from sub-spherical (c. $0.8 \times 0.6 \mu\text{m}$) to rod-shaped (c. $2.3 \times 0.7 \mu\text{m}$) morphologies (measurements from bovine RPE melanosomes; see Liu *et al.* 2005b; cf. Paper III, fig 1c). Eumelanin is the dominating melanin moiety in the RPE with pheomelanin occurring in significantly lower quantities. This led Liu *et al.* (2005b) to conclude that the hypothesis of melanosome shape being dependent on melanin type is not valid for RPE melanosomes. Rather, these authors suggested that melanosome shape is influenced by the origin of the pigmented cells, where neural ectoderm-derived cells mainly contain rod-shaped melanosomes whereas sub-spherical morphologies are primarily present in neural crest-derived cells. The full function of melanin within the RPE is

Box 2: XAS

X-ray absorption spectroscopy (XAS) is often utilised as a means for assessing the nuclear geometry and electron structure of a target element (Koningsberger & Prins 1988). The technique uses X-rays to excite electrons in the sample, causing the electron to either move to an unoccupied higher energy state in the atom shell or leave the atom as a photoelectron. By recording at what energy levels these events take place, a spectrum carrying detailed information about the atomic relationships (including metal content, oxidation state and coordination of metal species) within the sample is produced.

Because melanic pigments often incorporate heavy metals (including Cu, Fe and Mn) into their macromolecular structure (e.g. Liu *et al.* 2004), XAS can be used to target these metals and determine whether there are organically bound metal species in the sample or if the metal content is derived from the sedimentary matrix (Barden *et al.* 2014). Despite not being a standalone method for characterising biomol-

ecules, XAS can corroborate results from other analyses (e.g., ToF-SIMS, electron microscopy) and provide a separate line of evidence for biologically derived compounds in a fossil sample (cf. Paper V).

Benefits

- Qualitatively assesses metal content of the sample
- Separate line of evidence for organically bound materials
- Non-destructive *in situ* analyses

Drawbacks

- Large spot size (often mm scale)
- Results are difficult to quantify
- *in situ* analyses may penetrate ‘through’ the sample into underlying sediment

Box 3: IR microspectroscopy

For material analyses at the molecular scale, IR microspectroscopy is a versatile method, applied in a variety of contexts. The technique uses the naturally occurring molecular vibration frequencies to identify relationships between atoms in a molecule. By sending infrared light through the sample, a spectrum can be recorded for when the frequency of this light matches the frequency of the molecular vibrations. Such spectra can then be compared to reference samples of similar compounds and their structural differences can be determined (Atkins & de Paula 2009).

The resulting spectra contain a significant amount of information that may be used as ‘fingerprints’ for organic and biological material (Atkins & de Paula 2009). Moreover, spatial distributions of the material can be analysed, giving insight into microstructural organisation and physical–chemical properties of the sample. The ability to identify and quantify single molecular species makes this method highly effective for distinguishing between, for example, melanin

and structurally similar compounds (as demonstrated by e.g. Lindgren *et al.* 2012; Papers III–IV). IR microspectroscopy has therefore been repeatedly used in studies of fossil melanin (e.g. Barden *et al.* 2011; Wogelius *et al.* 2011; Lindgren *et al.* 2017).

Benefits

- Provides detailed information about molecular structure
- Requires only minute sample sizes
- Point analyses and spatial distribution mapping possible

Drawbacks

- Comparative method; requires reference samples
- Coinciding peaks from different sources may obscure results

not completely understood. Whereas it is clear that melanin plays an important part in the initial development of the eye, its role in the adult animal is uncertain (Lopes *et al.* 2007), though it has been proposed to influence photoprotection and act as an antioxidant (Schraermeyer & Heimann 1999).

Hair (or fur) is an integumentary structure unique to mammals. It is almost always pigmented and plays an important role in UV-protection, camouflage and sexual selection (Chapman 1986). In contrast to RPE melanosomes, the corresponding structures in (human) hair have indeed been shown to differ in shape depending on their type; whereas isolated eumelanosomes (collected from dark hair) generally appear rod-shaped, pheomelanosomes (from red hair) are smaller and retain a sub-spherical to ovoid morphology (Liu *et al.* 2005a). Moreover, red-hair melanosomes display a greater morphological variation and are smaller in size than black-hair melanosomes (Liu *et al.* 2005a). Hair melanin synthesis takes place in follicle melanocytes, from where mature hair melanosomes are stepwise transported to keratinocytes. This transport follows a slower pace than in the epidermis (see below), coupled to the hair growth cycle, subsequently leading to a noticeable abundance of mature (stage IV) melanosomes within hair melanocytes that is not seen in corresponding epidermal cells (Slominski *et al.* 2005). While arguing that the eumelanin-to-pheomelanin production

ratio can be controlled in the hair melanocyte, Slominski *et al.* (2005) also suggest that eumelanin production is never completely halted, thus always adding a eumelanin component to pheomelanosomes. After being transferred from the follicle to the hair shaft, melanosomes are firmly bound within a keratinous matrix (Liu *et al.* 2003) and organised in rows of medullary cells along the shaft centre (Behrendt *et al.* 2012).

Melanin synthesis and melanosome transport in vertebrate **skin** occurs similarly to in hair. In mammals, skin melanocytes are primarily situated close to the epidermal basement layer and exhibit dendritic extensions that provide close proximity to numerous keratin cells. After migration along the melanocyte dendrites, mature melanosomes are readily transported to epidermal keratinocytes (Wasmeier *et al.* 2008). In some vertebrates, particularly reptilian and amphibian taxa, other pigment cells (collectively referred to as chromatophores) are also present in the integument; while melanocytes can be found in the epidermis, the dermis of these animals hosts layers of different pigment cells, including reflective iridophores and yellow to bright red producing xanthophores (Bagnara 1986, Landmann 1986). These cells incorporate other pigments than melanin, such as carotenoids, which are not synthesised by the animal but rather ingested through their diet (Bagnara 1986).

Feather colours are often rich and varied, influenced by a number of different pigments. Some of these pigments (e.g. carotenoids) are well characterised, whereas others (e.g. porphyrins and pterins) have received considerably less attention (see Hill & McGraw 2006). Nevertheless, melanins are the most common source for feather pigmentation, responsible not only for black, grey, brown and reddish hues but also acting as the foundation of many structural colours (e.g., Durrer 1986; Prum 2006). Similarly to in other integumental structures (e.g. skin; see above), feather melanin is synthesised in melanocytes, where melanosomes are formed and transferred to feather barbule cells through dendritic extensions of the melanocytes (Durrer 1986). Within feather barbs and barbules, melanosomes are then enveloped in a keratinous matrix, sometimes with intricate structural organisation (Prum 2006). Furthermore, relationships between the morphology of feather melanosomes and the colour they produce have been proposed, suggesting that pheomelanosomes are generally round to oblate whereas eumelanosomes take on a more elongate shape (Clarke 2010; Li *et al.* 2010, 2012).

In addition to the above listed integumentary structures of vertebrates, it should be noted that melanin production also occurs in some **bacteria** and **fungi**. These groups do not, however, utilise the same pigment production pathways as vertebrates do. Melanogenesis in prokaryotes is still poorly understood as variants the pigment can be synthesised in a number of different ways; some genera (e.g. *Vibrio* sp.) can simultaneously produce multiple types of melanin, including pyomelanin and eumelanin (Plonka & Grabacka 2006). Generally, however, bacterial melanin does not incorporate nitrogen into its molecular structure, often making it molecularly distinct from its eukaryotic counterparts (although exceptions exist, see Plonka & Grabacka 2006). Furthermore, contrary to in eukaryotic cells, bacterial melanin is usually synthesised extracellularly, thereby observable as amorphous deposits (Tarangini & Mishra 2013), globular aggregates (Agodi *et al.* 1996) or sometimes electron-dense spots (Geng *et al.* 2010) when purified.

In melanin producing fungi, the pigment is usually confined to the cell wall (Romero-Martinez *et al.* 2000). There, it may be present as part of the wall proper or occur in the fibrillary matrix, slightly extending out from the wall (Butler & Day 1998). Moreover, melanin may be dislodged from the cell wall and can then be observed as ‘free’ granules within the cell. Whereas this pigment is still considered ‘wall bound’ based on its origin, extracellular melanin may also be present in fungi (see Bell & Wheeler 1986; Butler & Day 1998). However, due to the high durability of melanised cell walls, these can easily be isolated from other cellular material, resulting in a hollow ‘melanin ghost’ that retains the shape and size of the original cell (Wang *et al.* 1996). Melanogenesis in fungi

is known to follow several different pathways, although it is considered the formation of melanin primarily occurs from tyrosine and DOPA precursors (Bell & Wheeler 1986).

5. Summary of papers

Paper I: Dental histology of mosasaurs and a marine crocodylian from the Campanian (Upper Cretaceous) of southern Sweden: incremental growth lines and dentine formation rates.

In this paper we examine the formation rate of dentine in the teeth of three mosasaur taxa (*Dollosaurus* sp., cf. *Platecarpus*, and *Tylosaurus ivoensis*) and one marine crocodylian (*Aigialosuchus* sp.), all collected from the Upper Cretaceous of the Kristianstad Basin, southern Sweden, by studying incremental growth lines. Two types of incremental lines are identified; *lines of von Ebner* are opaque, concentric striations laid down following a daily rhythm caused by the periodic accumulation and mineralization of dentine, and *Andresen lines*, observable as broader dark bands following a depositional rate of 11–13 days/line. The measured consecutive lines of von Ebner are situated 6–34 µm apart (depending on taxon). By extrapolation, we can estimate the development times for the dentine layer at the level of sectioning for each taxon. Accordingly, we calculate that the teeth had grown for 426 days in *Dollosaurus*, 342 days in cf. *Platecarpus*, 487 days in *T. ivoensis* and 259 days in *Aigialosuchus* before they were lost. Although the largest tooth crown included in the study (*T. ivoensis*) has the highest rate of dentine formation, it still has the slowest formation rate, resulting in higher risk of long-term incapacity if the tooth was lost prematurely. However, we suggest that this could be compensated for by other adaptations of the dentition, such as more robust crowns and broader tooth bases.

Paper II: Skin pigmentation provides evidence of convergent melanism in extinct marine reptiles.

This contribution presents direct chemical evidence for integumental pigmentation in three separate lineages of extinct marine reptiles: ichthyosaurs, mosasaurs and

sea turtles. This is achieved by employing time-of-flight secondary ion mass spectrometry (ToF-SIMS) on skin samples from three specimens in order to determine the molecular composition of the fossil tissue remains. All samples are shown to possess remnants of the pigment eumelanin, which is the main constituent responsible for dark colouration in almost all extant vertebrates. By means of electron microscopy we observe that the pigment traces occur in close association with fossil melanosomes (micrometre-sized, melanin-bearing cellular organelles). Our results imply that these three distantly related reptiles were all, at least partly, dark in colour. While many extant marine animals express countershading (i.e. dark dorsal and light ventral colouration), some ichthyosaurs appear to have been uniformly dark coloured – a pattern also known from modern deep-diving animals.

Paper III: Interpreting melanin-based coloration through deep time: a critical review.

Here, we review the recent progress in the emerging field of molecular palaeontology, with focus on melanic pigments. This includes advances in methodology, the interpretation of fossil tissues based on different means of analysis, and inferences that can be made from these fossil structures. We discuss the differences in melanin synthesis between vertebrates and microorganisms, reports of melanin and melanosomes in the fossil record, and the durability of melanic pigments in deep time. In order to assess the strengths and limitations of various methods, we also present a case study where we investigate a dark pigmentation located within the orbit of teleost fish from the early Eocene of Denmark. Our analyses include both morphological examinations using SEM and TEM, and chemical analysis by means of ToF-SIMS and IR-microspectroscopy analysis. As a control, the chemistry of

natural and synthetic melanins is analysed and modern melanosomes and bacterial biofilms are morphologically compared to microbodies detected in the fossil 'eye'. Ultimately, we identify a number of potential pitfalls that require consideration in the identification of fossil melanosomes and, consequently, interpretations of colouration, biology and behaviour, and recommend thorough analyses of fossil tissue to avoid erroneous conclusions.

Paper IV: Molecular composition and ultrastructure of Jurassic paravian feathers.

This study comprises descriptions of micro- and ultrastructural details in a specimen of *Anchiornis huxleyi* from the western Liaoning Province of north-east China. This exceptional fossil is preserved with extensive traces of plumage adjacent to the skull, body and limbs, as well as around the tail. We examine small samples of plumage under SEM and TEM and observe accumulations of melanosome-like microbodies and fibrous tissues. To determine the affinity of these microstructures, we subject a feather sample to ToF-SIMS and IR-microspectroscopy analyses. This way, we obtain chemical and molecular data for the fossil residue, which we can compare to controls consisting of natural and synthetic melanins (including bacterial eu- and pyomelanin), keratin, microbial mats, and a number of chemical compounds that are structurally similar to melanin. We can conclude that the molecular signature of the fossilised plumage most closely resembles animal eumelanin, and that these traces occur in strong association with the melanosome-like microbodies. Moreover, we find that these microbodies are preserved within a matrix containing filamentous structures, presumably representing degraded keratin, and preserved as a eumelanin-calcium phosphate mixture.

Table 2. Johan Gren's contributions to papers.

	Paper I	Paper II	Paper III	Paper IV	Paper V	Paper VI
Concept and study design	X				X	X
Lab work	X			X	X	X
Data interpretation/analysis	X	X	X	X	X	X
Photography/Illustrations	X	X		X	X	X
Writing of manuscript	X				X	X
Comments on manuscript	X	X	X	X	X	X

Paper V: Molecular and microstructural inventory of an isolated fossil bird feather from the Eocene Fur Formation of Denmark

In this contribution, we analyse an isolated bird feather from the Eocene of Denmark by investigating its molecular composition in addition to providing a detailed study of its preserved micro- and ultrastructure. The exceptional fossil is preserved as a thin film, retaining barbs and barbules. Using electron microscopy, melanosome-like microbodies of two distinct morphologies are identified; the proximal portion of the feather displays ovoid microbodies averaging $1.7 \times 0.5 \mu\text{m}$ in size, whereas the distal part holds smaller, highly elongate microbodies measuring $0.9 \times 0.2 \mu\text{m}$. By employing synchrotron-based μCT , we also create a three-dimensional rendering of the feather surface, and show that the microbodies reside within 5–10 μm large depressions, strongly resembling the medullary pith of modern feathers (where melanosomes are normally abundant). Furthermore, we use ToF-SIMS and X-ray absorption spectroscopy (XAS) to investigate the chemical composition of the feather residue, and demonstrate that the microbodies are associated with molecular compounds consistent with animal eumelanin. The size and shape of microbodies and the morphology of the proximal feather barbules show strong similarities with corresponding structures in modern parrots (Psittaciformes) – a group of birds that have previously been documented in the Fur Formation.

Paper VI: Skeletal and soft tissue anatomy of an Early Permian temnospondyl amphibian from the Saar-Nahe Basin of south-western Germany

This contribution includes a description of a nearly 300 million-year-old, exceptionally preserved larval amphibian fossil from the Saar-Nahe Basin, south-west Germany. The fossil displays a semi-articulated skeleton and several types of soft tissues, including a black pigmentation in the ‘eye’, a dark ‘skin’ halo demarcating the body outline, and remains of external gills. X-ray computed tomography was employed to construct a three-dimensional model of the skeleton, aiding in the visualization of obscured bones and benefiting the description of the specimen. Electron microscopy of the carbonaceous remains in the left eye of the specimen revealed sub-spherical microbodies, corresponding in overall morphology to modern melanosomes.

6. Discussion

Due to technological advancements and new methodologies, we are constantly gaining new insights into the biology and ecology of extinct organisms. Whether we apply state-of-the-art techniques, find new ways of employing conventional methods, or use a combination these, we can now learn about aspects of ancient life that until recently were thought to be impossible to gain. Studying different types of microstructures and molecular traces preserved in the fossil archive is a rather new concept, and we are still learning about the full potential of this information for our understanding of ancient life.

From the viewpoint of this thesis, a good place to start discussing preserved fossil microstructures is our contribution on mosasaur tooth histology (Paper I). While not strictly falling under ‘labile tissues’ as the thesis title suggests, this paper serves as an introduction to describing and interpreting preserved structures that are not perceivable by the naked eye. In Paper I, we show that dentine deposition in the teeth of large mosasaur species, such as *Tylosaurus ivoensis*, occurred at a higher rate than in relatively smaller species, such as cf. *Platecarpus*. However, because of the large tooth size in e.g. *T. ivoensis*, the full formation of the tooth crown was still slower than in smaller mosasaur taxa. This suggests an evolutionary adaptation of the animals, where an increased pace of tooth formation can prevent long-time feeding incapacity due to loss of teeth also in larger species with enormous tooth crowns (Paper I).

Whereas the research focus of this paper is on the dentine formation rate and tooth replacement rates, there may be other information available by studying the dental microstructures of extinct animals. For instance, the observed incremental lines provide a very high (daily) resolution of dentine deposition during the time of tooth formation. As our findings show that mosasaur teeth had grown for about 11–15 months (depending on species) before they were lost they could thus, in theory, be used to show variations over a year in the life of extinct animals, given that differences in the dentinal layer were to be observed. Cyclic variations in fossil corals are, for instance, frequently studied to infer palaeoclimate using LA-ICPMS (e.g. Allison *et al.* 2007) and although the chemistry of fossil teeth may be altered during diagenesis (e.g. Kohn *et al.* 1999), such methodology could potentially be applied to discern differences in composition during tooth development. However, as we point out in our study (Paper I), to expand the knowledge about these microstructures (and their possible biological implications), investigations encompassing a larger sample set would be required. Some authors have shown the feasibility of studying histology in fossil tissues by means of other methods, such as com-

puted tomography (e.g. Sanchez *et al.* 2012). The contrast differences in the dentine would, however, not be large enough to use this method for mapping of the incremental lines. Therefore, a traditional (destructive) sectioning is still the preferred method for visualising these hard tissue microstructures.

In Papers II–VI, a shared focus point has been the identification and interpretation of fossil soft tissue structures, and in particular the traces of melanosome-like microbodies and their occurrence in relation to molecular traces of the pigment eumelanin. It has repeatedly been argued in this thesis (and the papers it includes) that we need to be cautious when discussing the origin of microstructures in fossil tissues. For example, while melanosome-like microbodies are frequently observed in various fossil specimens, they undeniably share morphological features with both microbes and modern melanosomes (e.g. Moyer *et al.* 2014). As a result, we need several independent lines of evidence to confidently assign the microbodies as one or the other. That being said, there are, as highlighted in this thesis, several ways to acquire independent lines of evidence for determining the affinity of fossil microstructures. Apart from visualisation of the microstructures by conventional or electron microscopy, the chemical/molecular content of fossil samples can be investigated using e.g. ToF-SIMS (Paper II–V), IR-microspectroscopy (Paper III–IV) or XAS (Paper V). Moreover, organisation and distribution patterns of surface structures can be studied using computed tomography (Paper V), although this may be difficult and time-consuming, especially if the fossil remains are similar to the surrounding sediment with regard to density, or if they are present only in very limited quantities. Therefore, in some cases, atomic force microscopy (AFM) may be a viable method for the investigation of surface topography in fossil tissues. In palaeontology, AFM is not widely used and has mainly been applied to hard tissues, such as tooth enamel (Xia *et al.* 2015) and coccoliths (Henriksen *et al.* 2004); its application to fossil soft structures has merely been touched upon (e.g. collagen fibres in demineralised bone, Schweitzer *et al.* 2007; plant cytoplasm, Wang *et al.* 2008). The possible applications of this technique in palaeontology are thus not fully explored and should be investigated further in the future. Similarly, a relatively new method for studies of fossil tissue is *in situ* immunohistochemistry, which has provided important new insights into the preservation of endogenous biomolecules in various fossil taxa (e.g. dinosaurs, Moyer *et al.* 2016; turtles, Lindgren *et al.* 2017), and should continue to see application in molecular palaeontology in the future.

So, if fossilised microbodies are observed and can be interpreted as remnant melanosomes (beyond reasonable doubt), then *what can they tell us?*

Fossil colours

The full function of melanin is not completely understood and it varies between the tissues where it is deposited (see section 4 above). However, there is broad consensus that the pigment plays a role in photoprotection, protection against free radicals and (when present in integumental tissues, such as skin and feathers) in inter- and intraspecific signalling. Because the latter role of the pigment perhaps is the most conspicuous one, much recent research on fossil pigments has been devoted to colour interpretations, especially in early birds and feathered dinosaurs (e.g. Clarke *et al.* 2010; Li *et al.* 2010, 2012; Smithwick *et al.* 2017), but also in non-avian dinosaurs (e.g. Brown *et al.* 2017) and several marine reptiles (e.g. Paper II). There are, however, some issues that need to be addressed before making such interpretations, including: (i) that melanic pigmentation is not solely responsible for colouration; (ii) the correlation between melanosome morphology and perceived colour may not be fully understood; and (iii), importantly, microbody morphology may be altered during diagenesis (McNamara *et al.* 2013).

(i) In addition to colours produced by melanic pigments (i.e. dark brown to black by eumelanin, reddish to brown by pheomelanin), a phenomenon known as ‘structural colours’ (e.g. Prum 2006) make matters more complicated. Structural colouration is an extensive topic – its details falling well beyond the scope of this thesis – but nonetheless an issue that should be considered if interpretations regarding original colouration of animals are to be made. Particularly known from bird feathers (but also in many insects and other organisms), structural colours arise due to optical interference patterns created on the nanoscale. In part produced by melanosome organisation within the feather barbules, this type of structural interference is responsible for the iridescence seen in, for example, peacock feathers; while peacock feathers retain eumelanosomes producing a dark brown pigment, the organisation of microbodies within the feather barbules gives rise to their characteristic hues of blue, green and yellow (e.g. Zi *et al.* 2003). Some authors have made interpretations of iridescence in fossil feathers based on the organisation of microbody imprints (e.g. Vinther *et al.* 2010; Li *et al.* 2012). Furthermore, it has been argued that iridescence may be discerned by melanosome shape (Li *et al.* 2012). If this is accurate, it could contribute to the interpretation of the fossil feather FUM-1980 (Paper V), which retains melanosomes overlapping in morphology with modern iridescent melanosomes (*sensu* Li *et al.* 2012). It should be noted, though, that because of their inherent dependence on structure, reconstructions of iridescent colours in fossils should be undertaken with particular caution, and possible taphonomic and diagenetic processes affecting sample integrity should be accounted for (see below).

(ii) In the past decade, some authors (e.g. Clarke *et al.* 2010; Li *et al.* 2010, 2012; Smithwick *et al.* 2017) have used the shape of ‘fossil melanosomes’ to reconstruct the colouration of extinct animals based on a large dataset of melanosome measurements from modern bird feathers, released by Li *et al.* (2012, supplementary database S1). The dataset contains measurements of melanosomes from hundreds of bird species, grouping them into five colour classes (black, brown, grey, iridescent and penguin; the latter including melanosomes with morphologies distinct for members of the penguin family Spheniscidae; see Li *et al.* 2012). While these data have been successfully used to statistically predict the colour produced by melanosomes of certain morphologies (Li *et al.* 2010, 2012), the quality of the dataset may be debated. Each bird species included in the dataset is represented by one entry, using the average measurements of between 5–30 melanosomes from the same (contour) feather (Matthew Shawkey 2015, pers. comm.). As it has been observed that melanosome shape is highly variable even within a single feather (e.g. Paper V), the dataset should be expanded to include melanosome measurements from different parts of several feathers collected from multiple individuals. Despite being a large and undoubtedly time consuming undertaking, such an expansion would substantially reinforce the quality of the data.

(iii) When discussing the interpretation of preserved fossil microstructures, we must bear in mind the aspect of deep time and thereby consider those long-term processes acting on the material. In some cases, maturation experiments have been performed, simulating the lapse of time by exposing melanosomes to elevated pressures and temperatures (e.g. McNamara *et al.* 2013; Colleary *et al.* 2015). While these studies have demonstrated the remarkable resilience of melanosomes and their associated melanin, it is not feasible to reconstruct the full geological history of a specimen that has been influenced by geological processes over millions (or, in some cases, even hundreds of millions) of years. This becomes particularly evident when we consider different (superficial) appearances of structures that over the past decade have been interpreted as evidence for melanosomes in the fossil archive; that is, structures including everything from sub-rounded to elongate impressions in an amorphous, often mineralized, matrix (e.g. Zhang *et al.* 2010, figs 1–4) to three-dimensional bodies of different shapes and sizes – ranging from c. 0.15 μm (Glass *et al.* 2012) up to over 1.7 μm (Zhang *et al.* 2010; Paper V) – have all been described as ‘fossil melanosomes’ or imprints thereof. While melanosome morphology is known to be highly variable also in extant animals, this noticeable morphological variation alone advocates caution when discussing affinity of the microstructures. Furthermore, maturation experiments have confirmed geometric alteration of melanosomes under elevated temperature and pressure

conditions, with increasingly greater alteration at higher temperatures (McNamara *et al.* 2013).

Nonetheless, if microbodies observed in fossil samples are confidently shown to be remnant melanosomes and the above issues are taken into account, partial colour reconstructions in extinct animals may be feasible. Furthermore, such interpretations could potentially also provide insights into other biological and physiological traits.

Adaptation and behaviour

In addition to interpretations of potential colouration of fossil creatures, traces of their pigments (and associated structures) can contribute to our knowledge about how the animals were adapted to their environment, and possibly also about their behaviour. In Paper II, we discuss the presence of melanosomes, intimately associated with molecular traces of eumelanin, in three separate lineages of extinct marine reptiles (an Eocene turtle, a Cretaceous mosasaur and a Jurassic ichthyosaur, Fig 2). We reason that the inferred dark pigmentation may have been an evolutionary adaptation influencing thermoregulation and growth rates, as has been observed in modern animals (e.g. Clusella Trullas *et al.* 2007, 2009). Moreover, pigmentation often contributes to camouflage, and many modern marine creatures (including marine turtles, e.g. *Chelonia mydas*) have developed ‘countershading’ (i.e. a dark dorsum and a light ventrum) for concealment in their open pelagic habitat (Bustard 1970). A similar case has been suggested for other fossil marine turtles (Lindgren *et al.* 2017), and countershading has also been reported in exceptionally preserved fossil fish (Gottfried 1989). Because ichthyosaur fossils repeatedly have been found with impressions of uniformly dark soft body outlines, and we show that such ‘skin’ impressions contain eumelanin traces, we suggest that this indicates a uniformly dark pigmentation in life. This inconspicuous pattern fits well with the theory of a deep-diving behaviour among these creatures (see Motani 2005), as the limited amount of light at greater depths would favour dark animals in terms of camouflage (Paper II). Our findings can thus aid in interpretations of the behaviour and life environments of these extinct creatures. It should be noted, however, that the methods used for identification of pigment remains are highly localised to a spot on each sample, and that interpretations on colour patterning based on these must be performed with caution (Edwards *et al.* 2014). Additionally, whereas the presence of preserved melanin is strongly indicative of animal pigmentation, a lack thereof does not necessarily suggest unpigmented tissue, as these remains may have been lost due to taphonomic and/or diagenetic processes.



Fig. 2: Artists interpretation of the marine reptiles studied in Paper II. From top to bottom: a marine turtle, an ichthyosaur and a mosasaur. Illustration by Stefan Sølberg.

A few other inferences on behaviour and physiology have also been published in the recent literature: Li *et al.* (2010) suggested that their findings of differently-shaped melanosome-like microbodies in the plumage of the feathered dinosaur *Anchiornis* advocate pigmentation patterns used in inter- or intraspecific signalling, potentially acting as a factor for sexual selection (but see also Paper IV for a more conservative interpretation). Another feathered dinosaur (*Sinosauropteryx*) was recently studied by Smithwick *et al.* (2017). Based on the presence and distribution of remnant microbodies, interpreted as pheomelanosomes (cf. Zhang *et al.* 2010), a countershading pigmentation patterning was proposed (Smithwick *et al.* 2017). Moreover, the authors reconstructed pigment patterns including a

striped tail and a ‘bandit mask’ around the eyes, contributing to interpretations of habitat preference, predator–prey relationships and physiological adaptations (Smithwick *et al.* 2017).

7. Conclusions

In this thesis, I have investigated a number of molecular, micro- and ultrastructural remnants in fossil soft tissues from several animal groups of different age. This has been done as a series of case studies, employing novel as well as established methods. Whereas it is indeed possible to make interpretations on the biology of extinct animals based on microstructural and molecular remains, it is imperative to understand that our window into the past is inherently a narrow one. Thus, broad or generalised interpretations can be dangerous when based on minute samples.

Over the course of this PhD project, the ‘melanosomes versus microbes’-dilemma has been repeatedly debated from a variety of viewpoints. Whereas the discussion has not reached any general consensus, the results presented herein (Papers II–V) show that there are methods available for assigning ‘melanosome-like’ microbodies to remnant melanosomes with some confidence and that more independent lines of evidence render a more trustworthy diagnosis. Using such methods, including analyses of tissue chemistry (e.g. ToF-SIMS), will limit the risk of introducing erroneous conclusions into the literature.

There is still much work to be done in the study of fossil microstructures, such as ‘melanosome-like’ microbodies, as there is currently no straightforward way of determining their origin. For now, a multi-proxy approach using several independent lines of evidence is recommended before making assumptions on microbody affinity and implications based on these structures.

8. Acknowledgements

This PhD project was funded by the Department of Geology, Lund University. Additional funding was provided through grants by the Faculty of Science, Lund University (<http://www.science.lu.se/>) and by the Royal Physiographic Society of Lund (<http://www.fysiografen.se/en/>).

First and foremost, I thank my supervisors, Johan and Mats. Without your guidance none of this would have been possible. The two of you have been fundamental parts of my academic path for well over a decade and I thank you for not losing faith. Johan – thank you for important lessons not only in palaeontology, but also in critical thinking, sincere representation of data, and scientific ethics. And, of course, the valuable lesson of always double-checking the departure time on the train tickets. Mats – thank you for always being available for comments and suggestions on my work. And thank you for the music. Finally, thank you both for always leaving your doors open. I could probably have used them more.

I thank my co-authors and collaborators who have been a tremendous resource for input and feedback: Kenneth Barnes, Stefan Carlson, Ryan Carney, Aude Cincotta, Gareth Dyke, Anders Engdahl, François Escuillié, Pascal Godefroit, Ola Gustafsson, Stephen Hall, Jimmy Heimdal, Steven Hutcheson, Ben Kear, Ulla Kokfelt, Ulysse Lefèvre, Federica Marone, Alison Moyer, Dan Nilsson, Mike Polcyn, Sven Sachs, Bo Schultz, Mary Schweitzer, Matt Shawkey, Kajsa Sigfridsson Clauss, Peter Sjövall, Rene Sylvestersen, Gavin Taylor, Per Uvdal, Kazumasa Wakamatsu and Johan Yans.

I thank the department staff who have been my teachers, colleagues, peers and friends for so many years now. Honourable mentions go out to Mikael and Anders S who constantly listen to the students and make sure all voices count. To Ulf, who can lighten up any Friday evening over a beer. And, of course, Per Ahlberg. You may not be aware of it, Per, but you are the reason I ended up in Lund in the first place: When I was applying to universities, I wrote to the student coordinators of the geology departments in Lund and Uppsala, asking about their palaeontology programmes. You sent me a personal letter and appended the course catalogue, highlighting all relevant courses. About a week later, an e-mail arrived from Uppsala, telling me to check their website. Thank you, Per, for caring. You will always be the real Per Ahlberg to me.

Thank you, all current and past PhD students who have made my time at the department both enlightening and fun. An extra shout out to the other PhDs out of class 2005: Dr Sanna, Dr Mimmi, Dr Maria and my mentor and friend, Dr Andy. May your papers always receive fair peer review. To the ones livening up the office: Dr Karolina, Dr Anders, Dr Ashley and Maria. You are often the biggest reason to go to work. And sometimes the reason leave. I love you. Elisabeth and Vicky. You're close. Just do it. I know you can.

Thanks to all people around me during my time here, including Helsingkrona Nation, FN-kören, Tornakören and Ostrochorus. To Helsingkronaspexet, Jesperspexet, Lundaspexarna, Krischanstaspäaxet, Spegatspexet, Lundakarnevalen and Bataljonen, for the time on and around the stage. It truly helped me to survive.

To Grøn.

To Teo, Lovisa and Mattis, because everyone needs a support group. Rock and roll. See you in Olam.

Mor och Far: Ord är överflödiga.

Tack.

9. References

- Agodi, A., Stefani, S., Corsaro, C., Campanile, F., Gribaldo, S. and Sichel, G. 1996: Study of a melanic pigment of *Proteus mirabilis*. *Research in Microbiology* 147, 167–174.
- Allison, N., Finch, A.A., Webster, J.M. and Clague, D.A. 2007: Palaeoenvironmental records from fossil corals: The effects of submarine diagenesis on temperature and climate estimates. *Geochimica et Cosmochimica Acta* 71, 4693–4703.
- Atkins, P. and de Paula, J. 2009: *Elements of physical chemistry*. Oxford university press, New York, 600 pp.
- Bagnara, J. 1986: The skin of amphibia: Pigments cells. In Bereiter-Hahn, J., Matoltsy, A. G., Richards, K. S. (eds.), *Biology of the Integument, 2: Vertebrates*, 136–149. Springer Verlag, Berlin.
- Barden, H.E., Wogelius, R.A., Li, D., Manning, P.L., Edwards, N.P. and van Dongen, B.E. 2011: Morphological and geochemical evidence of eumelanin preservation in the feathers of the Early Cretaceous bird, *Gansus yumenensis*. *PLoS ONE* 6, e25494.
- Barden, H.E., Bergmann, U., Edwards, N.P., Egerton, V.M., Manning, P.L., Perry, S., van Veelen, A., Wogelius, R.A. and van Dongen, B.E. 2014: Bacteria or melanosomes? A geochemical analysis of micro-bodies on a tadpole from the Oligocene Enspel Formation of Germany. *Palaeobiodiversity and Palaeoenvironments* 95, 33–45.
- Behrendt, K., Klatte, J., Pofahl, R., Bloch, W., Smyth, N., Tschardtke, M., Krieg, T., Paus, R., Niessen, C., Niemann, C., Brakebusch, C. and Haase, I. 2012: A function for Rac1 in the terminal differentiation and pigmentation of hair. *Journal of Cell Science* 125, 896–905.
- Bell, A.A. and Wheeler, M.H. 1986: Biosynthesis and functions of fungal melanins. *Annual Review of Phytopathology* 24, 411–451.
- Berzelius, J.J. 1840: *Lehrbuch der Chemie*. Arnoldische Buchhandlung, Leipzig, 801 pp.
- Briggs, D.E.G. and McMahon, S. 2015: The role of experiments in investigating the taphonomy of exceptional preservation. *Palaeontology* 59, 1–11.
- Brown, C.M., Henderson, D.M., Vinther, J., Fletcher, I., Sistiaga, A., Herrera, J. and Summons, R.E. 2017: An exceptionally preserved three-dimensional armored dinosaur reveals insights into coloration and Cretaceous predator-prey dynamics. *Current Biology* 27, 2514–2521.e3.
- Bustard, R.H. 1970: The adaptive significance of coloration in hatchling Green Sea Turtles. *Herpetologica* 26, 224–227.
- Butler, M.J. and Day, A.W. 1998: Fungal melanins: a review. *Canadian Journal of Microbiology* 44, 1115–1136.
- Chapman, R.E. 1986: The skin of mammals: Hair, wool, quill, nail, claw, hoof, and horn. In Bereiter-Hahn, J., Matoltsy, A. G., Richards, K. S. (eds.), *Biology of the Integument, 2: Vertebrates*, 293–317. Springer Verlag, Berlin.
- Clarke, J.A., Ksepka, D.T., Salas-Gismondi, R., Altamirano, A.J., Shawkey, M.D., D’Alba, L., Vinther, J., DeVries, T.J. and Baby, P. 2010: Fossil evidence for evolution of the shape and color of penguin feathers. *Science* 330, 954–957.
- Clusella-Trullas, S., van Wyk, J.H. and Spotila, J.R. 2009: Thermal benefits of melanism in cordylid lizards: A theoretical and field test. *Ecology* 90, 2297–2312.
- Clusella Trullas, S., van Wyk, J.H. and Spotila, J.R. 2007: Thermal melanism in ectotherms. *Journal of Thermal Biology* 32, 235–245.
- Colleary, C., Dolocan, A., Gardner, J., Singh, S., Wuttke, M., Rabenstein, R., Habersetzer, J., Schaal, S., Fesha, M., Clemens, M., Jacobs, B.F., Currano, E.D., Jacobs, L.L., Sylvestersen, R.L., Gabbott, S.E. and Vinther, J. 2015: Chemical, experimental, and morphological evidence for diagenetically altered melanin in exceptionally preserved fossils. *Proceedings of the National Academy of Sciences* 112, 12592–12597.
- d’Ischia, M., Wakamatsu, K., Napolitano, A., Briganti, S., Garcia-Borron, J.C., Kovacs, D., Meredith, P., Pezzella, A., Picardo, M., Sarna, T., Simon, J.D. and Ito, S. 2013: Melanins and melanogenesis: methods, standards, protocols. *Pigment Cell & Melanoma Research* 26, 616–633.
- Durrer, H. 1986: The skin of birds: Colouration. In Bereiter-Hahn, J., Matoltsy, A. G., Richards, K. S. (eds.), *Biology of the Integument, 2: Vertebrates*, 239–247. Springer Verlag, Berlin.
- Edwards, N.P., Manning, P.L. and Wogelius, R.A. 2014: Pigments through time. *Pigment Cell & Melanoma Research* 27, 684–685.
- Franzen, J.L., Aurich, C. and Habersetzer, J. 2015: Description of a well preserved fetus of the European Eocene equoid *Eurohippus messelensis*. *PLoS One* 10, e0137985.
- Geng, J., Yuan, P., Shao, C., Yu, S.B., Zhou, B., Zhou, P. and Chen, X.D. 2010: Bacterial melanin interacts with double-stranded DNA with high affinity and may inhibit cell metabolism *in vivo*. *Archives of Microbiology* 192, 321–329.

- Glass, K., Ito, S., Wilby, P.R., Sota, T., Nakamura, A., Bowers, C.R., Vinther, J., Dutta, S., Summons, R., Briggs, D.E., Wakamatsu, K. and Simon, J.D. 2012: Direct chemical evidence for eumelanin pigment from the Jurassic period. *Proceedings of the National Academy of Sciences* 109, 10218–10223.
- Gottfried, M.D. 1989: Earliest fossil evidence for protective pigmentation in an actinopterygian fish. *Historical Biology* 3, 79–83.
- Henriksen, K., Young, J.R., Bown, P.R. and Stipp, S.L.S. 2004: Coccolith biomineralisation studied with atomic force microscopy. *Palaeontology* 47, 725–743.
- Hill, G.E. and McGraw, K.J. 2006: *Bird Coloration, Volume 1: Mechanisms and Measurements*. Harvard University Press, Cambridge, MA, 640 pp.
- Kohn, M.J., Schoeninger, M.J. and Barker, W.W. 1999: Altered states: Effects of diagenesis on fossil tooth chemistry. *Geochimica et Cosmochimica Acta* 63, 2737–2747.
- Koningsberger, D.C. and Prins, R. 1988: *X-ray absorption: principles, applications, techniques of EXAFS, SEXAFS, and XANES*. John Wiley & Sons, Inc., New York, 688 pp.
- Landmann, L. 1986: The skin of reptiles: Epidermis and dermis. In Bereiter-Hahn, J., Matoltsy, A. G., Richards, K. S. (eds.), *Biology of the Integument, 2: Vertebrates*, 150–193. Springer Verlag, Berlin.
- Li, Q., Gao, K.Q., Meng, Q., Clarke, J.A., Shawkey, M.D., D’Alba, L., Pei, R., Ellison, M., Norell, M.A. and Vinther, J. 2012: Reconstruction of *Microraptor* and the evolution of iridescent plumage. *Science* 335, 1215–1219.
- Li, Q., Gao, K.Q., Vinther, J., Shawkey, M.D., Clarke, J.A., D’Alba, L., Meng, Q., Briggs, D.E. and Prum, R.O. 2010: Plumage color patterns of an extinct dinosaur. *Science* 327, 1369–1372.
- Lindgren, J., Kuriyama, T., Madsen, H., Sjövall, P., Zheng, W., Uvdal, P., Engdahl, A., Moyer, A.E., Gren, J.A., Kamezaki, N., Ueno, S. and Schweitzer, M.H. 2017: Biochemistry and adaptive colouration of an exceptionally preserved juvenile fossil sea turtle. *Scientific Reports* 7, e13324.
- Lindgren, J., Uvdal, P., Sjövall, P., Nilsson, D.E., Engdahl, A., Schultz, B.P. and Thiel, V. 2012: Molecular preservation of the pigment melanin in fossil melanosomes. *Nature Communications* 3, 824.
- Liu, Y., Hong, L., Kempf, V.R., Wakamatsu, K., Ito, S. and Simon, J.D. 2004: Ion-exchange and adsorption of Fe(III) by *Sepia* melanin. *Pigment Cell Research* 17, 262–269.
- Liu, Y., Kempf, V.R., Nofsinger, J.B., Weinert, E.E., Rudnicki, M., Wakamatsu, K., Ito, S. and Simon, J.D. 2003: Comparison of the structural and physical properties of human hair eumelanin following enzymatic or acid/base extraction. *Pigment Cell Research* 16, 355–365.
- Liu, Y., Hong, L., Wakamatsu, K., Ito, S., Adhyaru, B., Cheng, C.Y., Bowers, C.R. and Simon, J.D. 2005a: Comparison of structural and chemical properties of black and red human hair melanosomes. *Photochemistry & Photobiology* 81, 135–144.
- Liu, Y., Hong, L., Wakamatsu, K., Ito, S., Adhyaru, B.B., Cheng, C.-Y., Bowers, C.R. and Simon, J.D. 2005b: Comparisons of the structural and chemical properties of melanosomes isolated from retinal pigment epithelium, iris, and choroid of newborn and mature bovine eyes. *Photochemistry and Photobiology* 81, 510–516.
- Lopes, V.S., Wasmeier, C., Seabra, M.C. and Futter, C.E. 2007: Melanosome maturation defect in Rab38-deficient retinal pigment epithelium results in instability of immature melanosomes during transient melanogenesis. *Molecular Biology of the Cell* 18, 3914–3927.
- Marks, M.S. and Seabra, M.C. 2001: The melanosome: membrane dynamics in black and white. *Nature Reviews Molecular Cell Biology* 2, 738–748.
- McNamara, M.E., Briggs, D.E., Orr, P.J., Field, D.J. and Wang, Z. 2013: Experimental maturation of feathers: implications for reconstructions of fossil feather colour. *Biology Letters* 9, 20130184.
- Motani, R. 2005: Evolution of fish-shaped reptiles (Reptilia: Ichthyopterygia) in their physical environments and constraints. *Annual Review of Earth and Planetary Sciences* 33, 395–420.
- Moyer, A.E., Zheng, W. and Schweitzer, M.H. 2016: Microscopic and immunohistochemical analyses of the claw of the nesting dinosaur, *Citipati osmolskae*. *Proceedings of The Royal Society B* 283, 20161997.
- Moyer, A.E., Zheng, W., Johnson, E.A., Lamanna, M.C., Li, D., Lacovara, K.J. and Schweitzer, M.H. 2014: Melanosomes or microbes: Testing an alternative hypothesis for the origin of microbodies in fossil feathers. *Scientific Reports* 4, 4233.
- Plonka, P.M. and Grabacka, M. 2006: Melanin synthesis in microorganisms – biotechnological and medical aspects. *Acta biochimica Polonica* 53, 429–443.
- Prota, G. 2012: *Melanins and melanogenesis*. Academic press, San Diego, 290 pp.
- Prum, R.O. 2006: Anatomy, physics and evolution of structural colours. In Hill, G. E., McGraw, K. J. (eds.), *Bird Coloration, Vol. 1. Mechanisms and Measurements*, 295–353. Harvard University Press, Cambridge, MA.

- Romero-Martinez, R., Wheeler, M., Guerrero-Plata, A., Rico, G. and Torres-Guerrero, H. 2000: Biosynthesis and functions of melanin in *Sporothrix schenckii*. *Infection and Immunity* 68, 3696–3703.
- Sanchez, S., Ahlberg, P.E., Trinajstic, K.M., Mirone, A. and Tafforeau, P. 2012: Three-dimensional synchrotron virtual paleohistology: A new insight into the world of fossil bone microstructures. *Microscopy and Microanalysis* 18, 1095–1105.
- Schraermeyer, U. and Heimann, K. 1999: Current understanding on the role of retinal pigment epithelium and its pigmentation. *Pigment Cell Research* 12, 219–236.
- Schweitzer, M.H., Lindgren, J. and Moyer, A.E. 2015: Melanosomes and ancient coloration re-examined: A response to Vinther 2015 (DOI 10.1002/bies.201500018). *BioEssays* 37, 1174–1183.
- Schweitzer, M.H., Suo, Z., Avci, R., Asara, J.M., Allen, M.A., Arce, F.T. and Horner, J.R. 2007: Analyses of soft tissue from *Tyrannosaurus rex* suggest the presence of protein. *Science* 316, 277–280.
- Seiji, M., Fitzpatrick, T.B. and Birbeck, M.S.C. 1961: The melanosome: a distinctive subcellular particle of mammalian melanocytes and the site of melanogenesis. *Journal of Investigative Dermatology* 36, 243–252.
- Simon, J.D. and Peles, D.N. 2010: The red and the black. *Accounts of Chemical Research* 43, 1452–1460.
- Slominski, A., Wortsman, J., Plonka, P.M., Schallreuter, K.U., Paus, R. and Tobin, D.J. 2005: Hair follicle pigmentation. *Journal of Investigative Dermatology* 124, 13–21.
- Smithwick, F.M., Nicholls, R., Cuthill, I.C. and Vinther, J. 2017: Countershading and stripes in the theropod dinosaur *Sinosauropteryx* reveal heterogeneous habitats in the Early Cretaceous Jehol Biota. *Current Biology* 27, 3337–3343.e2.
- Sollas, W.J. 1903: A method for investigation of fossils by serial sections. *Philosophical Transactions of the Royal Society B: Biological Sciences* 196, 259–265.
- Tarangini, K. and Mishra, S. 2013: Production, characterization and analysis of melanin from isolated marine *Pseudomonas* sp. using vegetable waste. *Research Journal of Engineering Sciences* 2, 40–46.
- Thiel, V. and Sjövall, P. 2011: Using time-of-flight secondary ion mass spectrometry to study biomarkers. *Annual Review of Earth and Planetary Sciences* 39, 125–156.
- Vickerman, J.C. 2001: ToF-SIMS – an overview. In Vickerman, J. C., Briggs, D. (eds.), *ToF-SIMS: Surface Analysis by Mass Spectrometry*, 1–36. IM Publications, Chichester.
- Vinther, J. 2015: A guide to the field of palaeo colour: Melanin and other pigments can fossilise: Reconstructing colour patterns from ancient organisms can give new insights to ecology and behaviour. *Bioessays* 37, 643–656.
- Vinther, J. 2016: Fossil melanosomes or bacteria? A wealth of findings favours melanosomes. *BioEssays* 38, 220–225.
- Vinther, J., Briggs, D.E., Prum, R.O. and Saranathan, V. 2008: The colour of fossil feathers. *Biology Letters* 4, 522–525.
- Vinther, J., Briggs, D.E., Clarke, J., Mayr, G. and Prum, R.O. 2010: Structural coloration in a fossil feather. *Biology Letters* 6, 128–131.
- Wang, X., Yu, J. and Fang, X. 2008: An AFM Observation on Fossil Cytoplasm. *Acta Geologica Sinica - English Edition* 82, 1141–1145.
- Wang, Y., Aisen, P. and Casadevall, A. 1996: Melanin, melanin ‘ghosts,’ and melanin composition in *Cryptococcus neoformans*. *Infection and Immunity* 64, 2420–2424.
- Wasmeier, C., Hume, A.N., Bolasco, G. and Seabra, M.C. 2008: Melanosomes at a glance. *Journal of Cell Science* 121, 3995–3999.
- Willems, H. and Wuttke, M. 1987: Lithogenese lakustriner Dolomite und mikrobiell induzierte Weichteilerhaltung bei Tetrapoden des Unter-Rotliegenden (Perm, Saar-Nahe Becken, SW-Deutschland). *Neues Jahrbuch für Geologie und Paläontologie, Abhandlungen* 174, 213–238.
- Wogelius, R.A., Manning, P.L., Barden, H.E., Edwards, N.P., Webb, S.M., Sellers, W.I., Taylor, K.G., Larson, P.L., Dodson, P., You, H., Da-qing, L. and Bergmann, U. 2011: Trace metals as biomarkers for eumelanin pigment in the fossil record. *Science* 333, 1622–1626.
- Wuttke, M. 1983: Weichteil-Erhaltung durch lithifizierte Mikroorganismen bei mittel-eosänen Vertebraten aus den Ölschiefern der Grube Messel bei Darmstadt. *Senckenbergiana lethaea* 64, 509–527.
- Xia, J., Zheng, J., Huang, D., Tian, Z.R., Chen, L., Zhou, Z., Ungar, P.S. and Qian, L. 2015: New model to explain tooth wear with implications for microwear formation and diet reconstruction. *Proceedings of the National Academy of Sciences* 112, 10669–10672.
- Zhang, F., Kearns, S.L., Orr, P.J., Benton, M.J., Zhou, Z., Johnson, D., Xu, X. and Wang, X. 2010: Fossilized melanosomes and the colour of Cretaceous dinosaurs and birds. *Nature* 463, 1075–1078.
- Zi, J., Yu, X., Li, Y., Hu, X., Xu, C., Wang, X., Liu, X. and Fu, R. 2003: Coloration strategies in peacock feathers. *Proceedings of the National Academy of Sciences* 100, 12576–12578.

Svensk sammanfattning

Denna avhandling behandlar en mängd mikrostrukturella och molekylära lämningar som påträffats i ett antal fossil. Resultaten presenteras i sex vetenskapliga artiklar med det gemensamma syftet att grundligt studera dessa lämningar med hjälp av såväl nya som vedertagna analysmetoder. Avhandlingens huvudsakliga frågeställningar är dels vad denna typ av fossila spår kan säga om de studerade djurens biologi, ekologi och beteende, samt vilka analysmetoder som är bäst lämpade för att kunna utröna detta.

Avhandlingen baseras på en serie fallstudier där jag undersökt fossil från ett flertal olika djurgrupper från olika geologiska tidsåldrar. Fossilerna är insamlade från ett antal geologiska lokaler runtom i världen. Bland de metoder som använts kan nämnas ljus- och elektronmikroskopi, datortomografi och molekylära analyser. De senare innefattar bland annat s.k. ToF-SIMS (en mycket känslig spektrometrimetod för att studera ytstrukturer), infraröd mikrospektroskopi och röntgenabsorptionsspektroskopi.

Bland resultaten finner vi att man genom mikroskopi och histologisk analys av tänder från bland annat mosasaurier (jättelika, numera utdöda marina reptiler) kan beräkna dentinets (tandvävnadens) bildningshastighet. Eftersom dentinbildningen ligger till grund för tändernas tillväxthastighet kan man dra slutsatser om djurens tandersättningscykler (i likhet med nu levande reptiler bytte dessa djur regelbundet sina tänder). Jag påvisar också att tänderna hos större mosasaurierarter tog längre tid att nå full storlek än tänderna hos mindre arter. Dock skedde dentinbildningen med högre hastighet i de större tänderna, vilket innebar att djuren snabbare kunde ersätta förlorade tänder.

Genom studier av ögon, hud och fjädrar från en mängd fossil observerade jag ansamlingar av mikrometerstora,

runda till avlånga kroppar i den bevarade vävnaden. Liknande mikrostrukturer har tidigare, vid olika tillfällen, beskrivits som så kallade melanosomer (dvs. pigmentbärande cellorganeller) och som fossiliserade bakterier. För att kunna säkerställa mikrokropparnas härkomst utförde jag och mina medförfattare molekylära och ultrastrukturella analyser av de fossila bildningarna och jämförde sedan resultaten med motsvarande analyser av modernt melanin och andra liknande kemiska föreningar. Resultaten visar mycket riktigt att molekylära rester av eumelanin återfinns i nära anslutning till de observerade mikrostrukturerna, vilket tydligt talar för att de är melanosomer.

Utöver de studier som redovisas i de bifogade vetenskapliga artiklarna så inkluderar avhandlingen även en kort redogörelse för hur melanin uppträder i ögon, hud och fjädrar hos olika ryggradsdjur, samt dess förekomst i vissa svampar och bakterier. En översikt över de olika metoder som tillämpats i projekten presenteras, och följs av en diskussion om de möjliga slutsatser som kan dras och de svårigheter som bör beaktas inom denna typ av paleontologi.

Bevarade melanosomer kan potentiellt bidra med information rörande ett flertal biologiska och ekologiska företeelser som inte tidigare kunnat beaktas hos förhistoriskt liv. Det råder dock ännu ingen konsensus kring hur vi enklast kan säkerställa dessa "melanosomliknande" mikrostrukturers ursprung. Jag anser därför att en grundlig undersökning av sådana fossila rester, inklusive kemiska analyser, bör tillämpas för varje enskild studie – åtminstone tills vi uppnått enighet kring vilka kriterier som måste uppfyllas för att mikrofossilerna ska kunna identifieras med säkerhet.



PAPER I

Overleaf: Thin sectioned mosasaur tooth (cf. *Platycarpus*)

Dental histology of mosasaurs and a marine crocodylian from the Campanian (Upper Cretaceous) of southern Sweden: incremental growth lines and dentine formation rates

JOHAN A. GREN* & JOHAN LINDGREN

Department of Geology, Lund University, Sölvegatan 12, SE-223 62 Lund, Sweden

(Received 5 October 2012; accepted 30 May 2013)

Abstract – Mosasaurs are an extinct group of secondarily adapted aquatic lizards that became the dominant marine tetrapods in the Late Cretaceous oceans. They continuously shed and replaced their teeth in order to maintain a functional dentition at all times; however, the process of tooth development in mosasaurs is still incompletely known. Based on incremental line width measurements and growth line counts, we assess dentine formation rates in three mosasaur taxa (*Dollosaurus*, cf. *Platecarpus* and *Tylosaurus*) and one genus of marine crocodylian (*Aigialosuchus*), all from the lower Campanian (Upper Cretaceous) of southernmost Sweden. Two sets of periodic dentinal markings characterized by concentric, alternating opaque and transparent laminae are recognized: one set comprising thin bands situated 6–34 μm apart (depending on taxon), which is superimposed onto a second set of coarser bands where spaces vary between 102 and 275 μm . Assuming that the finer striations represent daily increments (i.e. lines of von Ebner), it is estimated that the deposition of dentine at the sectioned level of the tooth-crowns took 342 (cf. *Platecarpus*), 426 (*Dollosaurus*), 487 (*Tylosaurus*) and 259 (*Aigialosuchus*) days, respectively. The coarser bands contain between 11 and 13 thin striations each, and are thus considered to be homologous to similar periodic dentinal markings in extant vertebrates, i.e. Andresen lines. Prolonged tooth development times in large-toothed taxa, such as *Tylosaurus*, presumably increased the risk of long-term incapacity to capture prey after dental trauma, an evolutionary trade-off which may have been compensated for by allometric modifications of the teeth.

Keywords: Andresen, dentine, histology, increments, Mosasauridae, teeth, von Ebner.

1. Introduction

In most living reptiles, teeth are continuously shed and replaced to ensure a regular bite and a lifelong capability to engulf prey (Richman & Handrigan, 2011). However, the process of tooth development in many fossil reptilian groups has only recently become a topic of study (Erickson, 1996a; Zaher & Rieppel, 1999; Rieppel & Kearney, 2005; Caldwell, 2007; Chinsamy, Tunçöglü & Thomas, 2010, 2012). Hence, in order to gain a deeper understanding of the odontogenesis in Mosasauridae, a speciose family of secondarily aquatic lizards that became the dominant marine tetrapods in the Late Cretaceous about 98–66 million years ago, we examined periodic dentinal markings in a small number of isolated marginal tooth-crowns collected from the marine Cretaceous of southern Sweden.

Examination of incremental growth lines is an effective method of assessing dentine formation rates and tooth development times in both extant and extinct vertebrates (e.g. Erickson, 1996a and references therein). Incremental markings form through periodic alterations in collagen fibre trajectories and/or variations in the mineralization process (Kawasaki, Tanaka & Ishikawa, 1980; Bhaskar, 1991; Erickson, 1996b;

Nanci, 2008), thereby providing a continuous and often permanent record of the odontogenesis (Erickson, 1996a). Such increments also contribute to our understanding of those mechanisms that underlie morphological change (Dean, 2000), and are thus of importance in the scientific fields of developmental and evolutionary biology.

Despite being illustrated already in the mid-1800s by Richard Owen (1841, 1845; see Erickson, 1996a), the importance of dentinal laminations was not recognized until the works of Andresen (1898) and von Ebner (1902, 1906). These latter authors described concentric striations in the teeth of humans and other primates that are now being referred to as incremental lines of von Ebner and Andresen, respectively (e.g. Dean & Scandrett, 1996). Long-period Andresen lines are spaced between 4 and 14 days apart owing to endogenous biorhythms (Kawasaki, Tanaka & Ishikawa, 1980; Dean & Scandrett, 1996; Dean, 2000), and usually contain short-period lines of von Ebner, where the distance between each lamination represents the daily secretion of dentine (Bhaskar, 1991; Dean, 1995, 1998; Dean & Scandrett, 1996; Hillson, 2005).

Using periodic chemical (i.e. fluorochrome) labelling, Erickson (1996b) was able to determine the rate and duration of dentine secretion in the modern crocodylians *Alligator mississippiensis* and *Caiman crocodylus*. Moreover, by counting and measuring

*E-mail: johan.gren@geol.lu.se

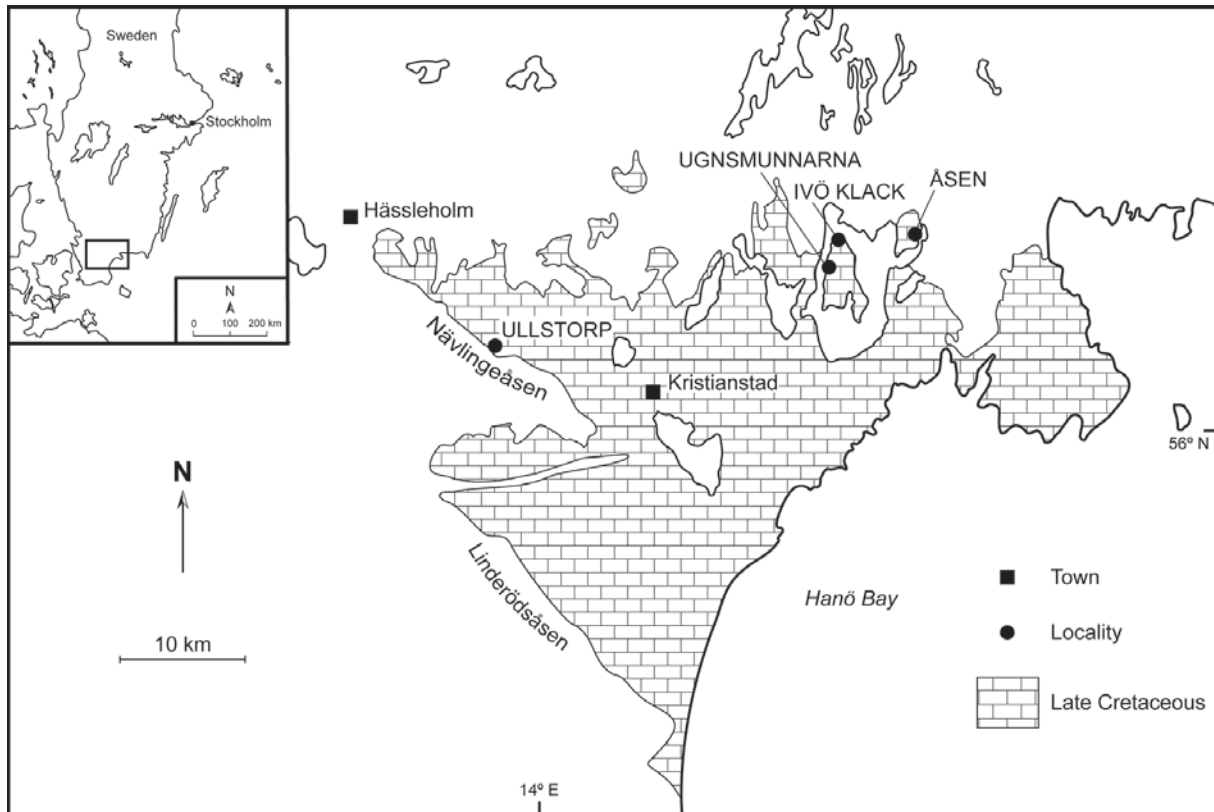


Figure 1. Geological map of southernmost Sweden showing the location of the Kristianstad Basin in the northeastern corner of the province of Skåne and the localities from which the analyzed teeth were collected (modified from Lindgren & Siverson, 2002, fig. 1).

the increments laid down between the fluorochrome injections, he (Erickson, 1996b) demonstrated that these laminations form on a daily basis (as they do in most amniotes; e.g. Erickson, 1996a, b; Kamiya *et al.* 2006; Nanci, 2008; Kierdorf *et al.* 2009). Subsequently, Erickson (1996a) broadened his investigation to also include Mesozoic crocodylians and nonavian dinosaurs. Comparable markings were found in the fossilized teeth of both groups, to suggest homology given their close phylogenetic relationship (Erickson, 1996a). More recently, Chinsamy, Tunçöglü & Thomas (2010, 2012) demonstrated the presence of periodic dentinal increments in a tooth-crown of the derived mosasaur *Mosasauros hoffmanni*, and building on Erickson's (1996a, b) model, they estimated that it took 511 days to deposit the dentine at the level of sectioning.

In the present contribution, concentric laminations observed in histological sections of three isolated mosasaur teeth (assigned to *Dollosaurus* sp., cf. *Platecarpus* and *Tylosaurus ivoensis*, respectively) from the Kristianstad Basin, southernmost Sweden, are compared to morphologically similar markings in a tooth-crown of the marine crocodylian *Aigialosuchus* sp. collected from the same area. We begin with a description of various microstructural features that have previously been used to determine crocodylian and mosasaur dentine secretion rates (see Erickson 1996a, b; Chinsamy, Tunçöglü & Thomas, 2010, 2012). We then estimate the time it took to develop the dentine at the level of

sectioning. Finally, we conclude with a brief discussion on tooth development times and replacement rates in mosasaurs.

2. Geological setting

The Cretaceous deposits of the Kristianstad Basin *sensu* Erlström & Gabrielson (1992) are bordered to the southwest by the Linderödsåsen and Nävlingeåsen horst ridges, whereas the northern demarcation is more diffuse with several outliers of marine strata of Campanian–Maastrichtian age (Fig. 1). The Cretaceous sediments comprise primarily shallow marine calcarenites, calcisiltites and calcareous sandstones, although terrigenous material in conglomerates and boulder beds indicates that nearby land served as important source areas (Christensen, 1975). For more comprehensive descriptions of the geology, development and depositional environments of the Kristianstad Basin, see Christensen (1975), Bergström & Sundquist (1978), Lidmar-Bergström (1982) and Erlström & Gabrielson (1986, 1992).

With the exception of a single *Aigialosuchus* sp. tooth (LO 11621 *t*) from the lowermost Campanian (*Goniotoothis granulataquadrata* belemnite Zone, Ullstorp site; see Erlström & Gabrielson, 1986 and Siverson, 1993 for locality information), all fossils examined herein were collected from strata representing a narrow stratigraphic interval (i.e. the informal

Table 1. Measurements and section locations of sampled tooth-crowns

Taxon	Crown height (mm)	Crown width (mm)	Crown length (mm)	Section locations (mm from base, mid-crown; apical section)
<i>Aigialosuchus</i> sp. (LO 11621 <i>t</i>)	9	8	6	5; 8
<i>Dollosaurus</i> sp. (LO 11622 <i>t</i>)	23	16	14	8; 19
cf. <i>Platecarpus</i> sp. (LO 11623 <i>t</i>)	33	17	13	10; 23
<i>Tylosaurus ivoensis</i> (LO 11624 <i>t</i>)	45	31	25	21; 35

Belemnellocomax mammillatus zone) corresponding to the highest belemnite zone in the lower part of the European two-fold division of the Campanian Stage (see Christensen, 1975). Three localities exposing sediments of latest early Campanian age (Åsen, Ivö Klack and Ugnsmunarna; Fig. 1) produced the teeth described below. For locality information, see Lindgren & Siverson (2002), Lindgren *et al.* (2007) and Eriksson *et al.* (2011, fig. 2).

3. Methodology

The material selected for histological analysis comprises four isolated, presumably shed marginal tooth-crowns (LO 11621 *t* – LO 11624 *t*) representing three genera of mosasaurs (*Dollosaurus*, cf. *Platecarpus* and *Tylosaurus*) and one genus of crocodylian (*Aigialosuchus*). Comparisons with more complete dentitions in mosasaur and crocodylian skeletons from North America and west-central Europe (see Lindgren & Siverson, 2002, 2004, 2005; Lindgren, 2005*a, b*) suggest that all teeth originate from the mid-section of the dental ramus in sub-adult to adult individuals.

Prior to sampling, all tooth-crowns were measured (Table 1), photographed (the crowns were covered with ammonium chloride prior to being photographed) and moulded. Thereafter, the teeth were vacuum-embedded in a clear polyester resin, and millimetre-thick transverse sections were produced using a slow-speed diamond saw (the precise location of each section is listed in Table 1). Additionally, a partial longitudinal section was produced from LO 11621 *t* (*Aigialosuchus* sp.) because previous studies (e.g. Erickson, 1996*b*) have indicated that longitudinal sections may provide additional histological details. The thin-sections were mounted on petrographic slides using polyester resin, ground to optical translucency (i.e. to about 50–100 µm thickness), polished on a felt pad with aluminium oxide powder, and imaged (at × 5–40 magnification) using a Nikon DS-Fi1 camera attached to a binocular microscope. Histological features were documented with particular focus on incremental growth line distribution, spacing and counts. Notes were made also on other potential endogenous markings, as well as on enamel thickness, state of the osteocyte lacunocanalicular system, and possible taphonomic/diagenetic artefacts. In accordance with the published methodology of, for ex-

ample, Dean (1998), Erickson (1996*a, b*) and Nanci (2008), the different types of incremental laminations were identified based on their widths and morphology. In each section examined, the most complete sequences of short- and (if present) long-period lines were measured using an image analysis software (NIS-Elements BR 3.10) from digital micrographs, and the average distance between the individual lines was calculated. These numbers were then extrapolated to include the entire thickness of the dentine (measured using the multipoint circle tool in NIS-Elements BR 3.10) in order to obtain values of the total dentine accumulation at the level of sectioning.

Depository acronym. LO – Department of Geology, Lund University, Lund, Sweden.

4. Histological analyses

The dental morphology of the mosasaur and crocodylian taxa dealt with in this work has been described in detail by, for example, Persson (1959, 1963), Lindgren (2005*a, b*) and Lindgren & Siverson (2002, 2004, 2005); here we provide additional microstructural data obtained from recent histological analyses. Basic measurements, such as tooth-crown height, width and length (as preserved), are presented in Table 1.

4.a. LO 11622 *t* (*Dollosaurus* sp.)

Two transverse histological sections were made from LO 11622 *t* (Fig. 2); one near the apex and one at approximately mid-crown height. The apical section preserves closely spaced dentinal tubules that radiate from the margin of the pulp cavity and outward. Numerous odontocyte lacunae are also visible, and these are oriented with their long axis parallel to the tubules. A small number of laminations run parallel to the pulp circumference. The lines are faint, irregularly spaced and too few to allow a confident quantitative analysis. Numerous taphonomically induced micro-cracks are also present, and these have served as loci for bacterial or fungal activity (cf. Underwood, Mitchell & Veltkamp, 1999), resulting in the partial loss of endogenous microstructures.

The transverse section taken at mid-crown height is similar to the apical one in that it contains multiple radially oriented dentinal tubules and elongated

4

J. A. GREN & J. LINDGREN

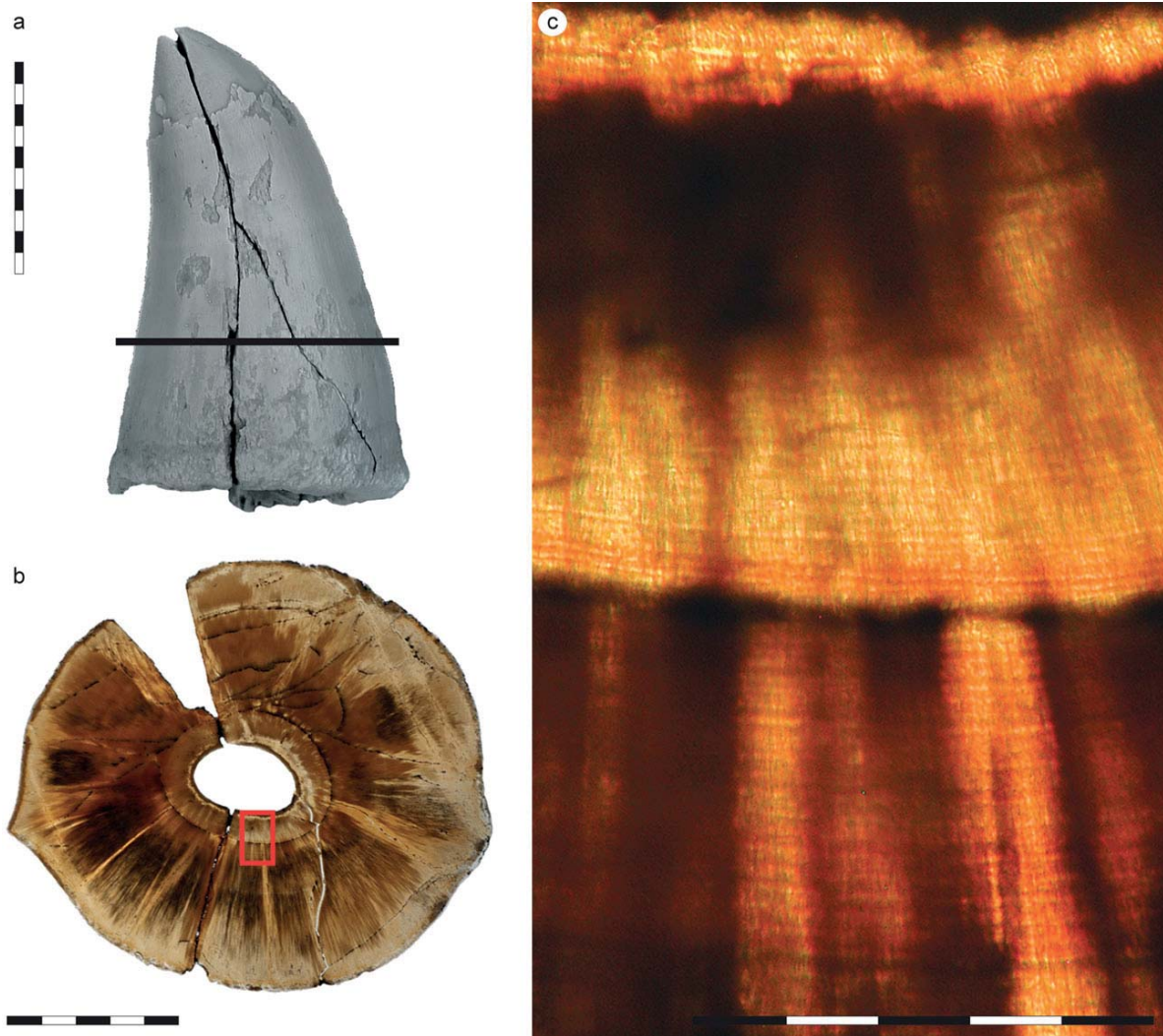


Figure 2. (Colour online) *Dollosaurus* sp., LO 11622 *t*, isolated marginal tooth-crown. (a) Specimen photographed in labial view prior to histological analysis. Level of sectioning is marked with a horizontal bar. (b) Transverse mid-crown section of LO 11622 *t* (labial side faces downwards). (c) Demarcated area in (b) showing periodic incremental markings here interpreted as lines of von Ebner. Scale bars represent 10 mm (a), 5 mm (b) and 500 μm (c).

odontocyte lacunae (Fig. 2b). However, those areas affected by microorganisms are considerably smaller, and consequently the dentine is rich in preserved increments (some of which are accentuated by secondarily deposited minerals). These laminations run perpendicularly to the tubules and are most pronounced in the peri-pulpal part of the dentine, where 105 consecutive lines with a size range of 8–23 μm and an average width of 12.2 μm were documented (Fig. 2c). By extrapolation (mean thickness of dentine = 5194 μm), the sectioned part of the tooth-crown holds a total of 426 periodic dentinal markings.

4.b. LO 11623 *t* (cf. *Platecarpus*)

Two transverse histological sections were made from LO 11623 *t* (Fig. 3): one close to the apex and one at approximately mid-crown height. In the apical section, the enamel displays one distinct and one faint lam-

ination. No increments were observed in the dentine; however, closely spaced dentinal tubules could be seen radiating from the vicinity of the pulp cavity and outward. The dentine is also rich in dark odontocyte lacunae with stubby canaliculi. As in LO 11622 *t*, the lacunae are elongate and oriented with their long axis parallel to the tubules. Diverging channels, joined in discrete networks and probably made by bone-boring bacteria and/or fungal hyphae, surround a number of taphonomically induced micro-cracks.

The enamel of the mid-crown section holds three weak and incomplete increments consisting of alternating dark and light bands. The section is rich in both endogenous microstructures and diagenetic artefacts, such as micro-fractures filled with brownish matter. Towards the circumference the dentine is largely deteriorated by microorganisms (Fig. 3b, c). Microborings are also present in the region of the pulp cavity, although some original structures, including darkly

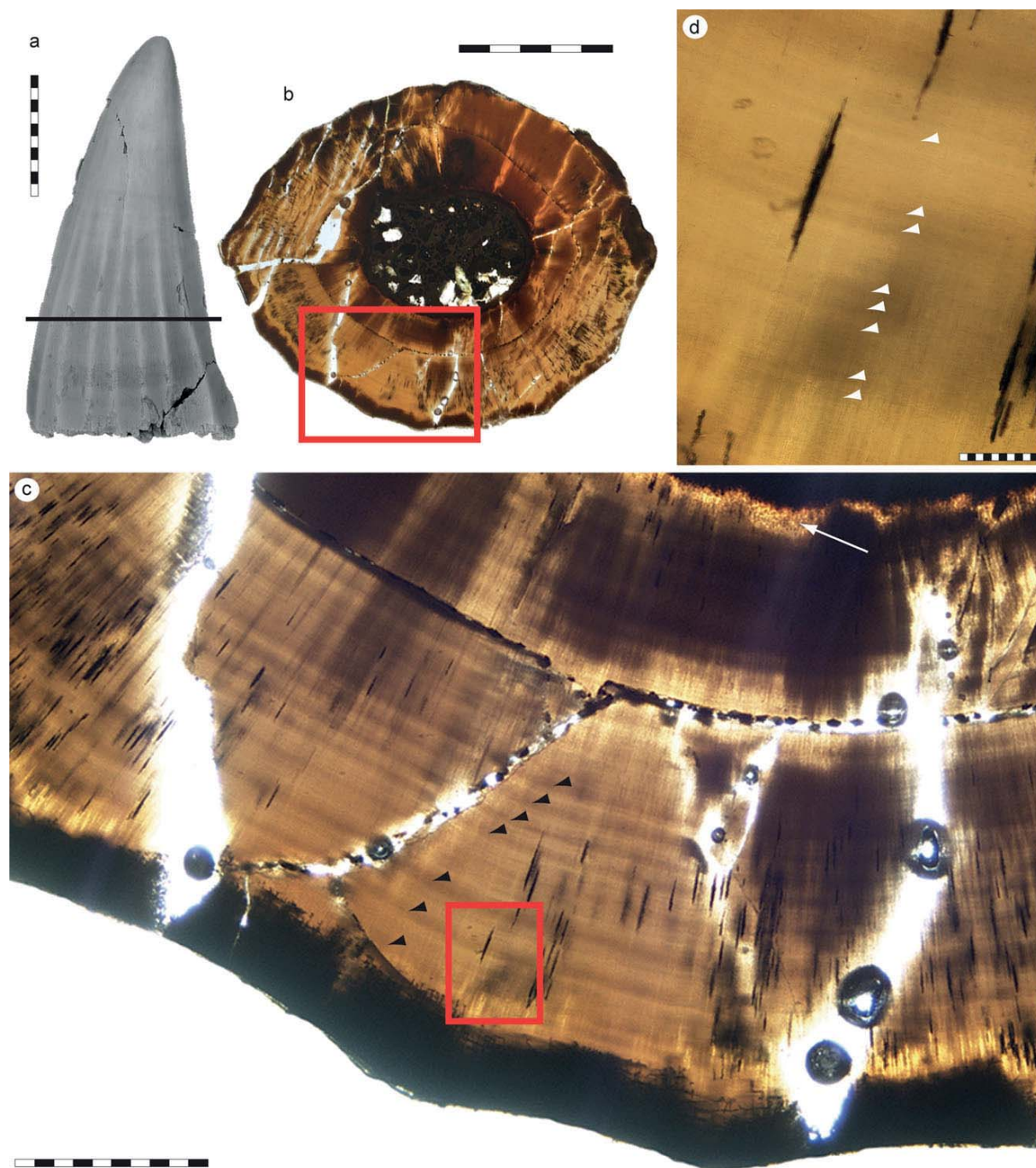


Figure 3. (Colour online) *cf. Platecarpus*, LO 11623 *t*, isolated marginal tooth-crown. (a) LO 11623 *t* in labial view prior to histological analysis. Level of sectioning is marked with a horizontal bar. (b) Transverse mid-crown section of LO 11623 *t* (labial side faces downwards). (c) Demarcated area in (b) showing long-period incremental markings (here interpreted as Andresen lines – black arrowheads), radially oriented dentinal tubules, possible calcospherites (arrow), and elongate osteocyte lacunae. (d) Demarcated area in (c) showing a second set of finer concentric laminations here interpreted as lines of von Ebner (better preserved striae are marked with white arrowheads). Scale bars represent 10 mm (a), 5 mm (b), 1 mm (c) and 100 μm (d).

stained mineral globules (possibly calcospherites) remain (Fig. 3c, white arrow). Radially oriented dentinal tubules and odontocyte lacunae are dispersed throughout the dentine (Fig. 3b, c, d). The blackish lacunae are elliptical, and remains of the canalicular system occur as thread-like extensions from the surfaces of the secondarily filled cavities (Fig. 3d). Two sets of incre-

mental growth lines were measured: one set of ten consecutive long-period lines, characterized by alternating opaque and transparent bands, with a size range of 102–201 μm and an average width of 141 μm (Fig. 3c), and one set of 128 short-period lines with a size range of 6–19 μm and an average width of 11.3 μm (Fig. 3d). By extrapolation, at the level of sectioning the tooth

6

J. A. GREN & J. LINDGREN

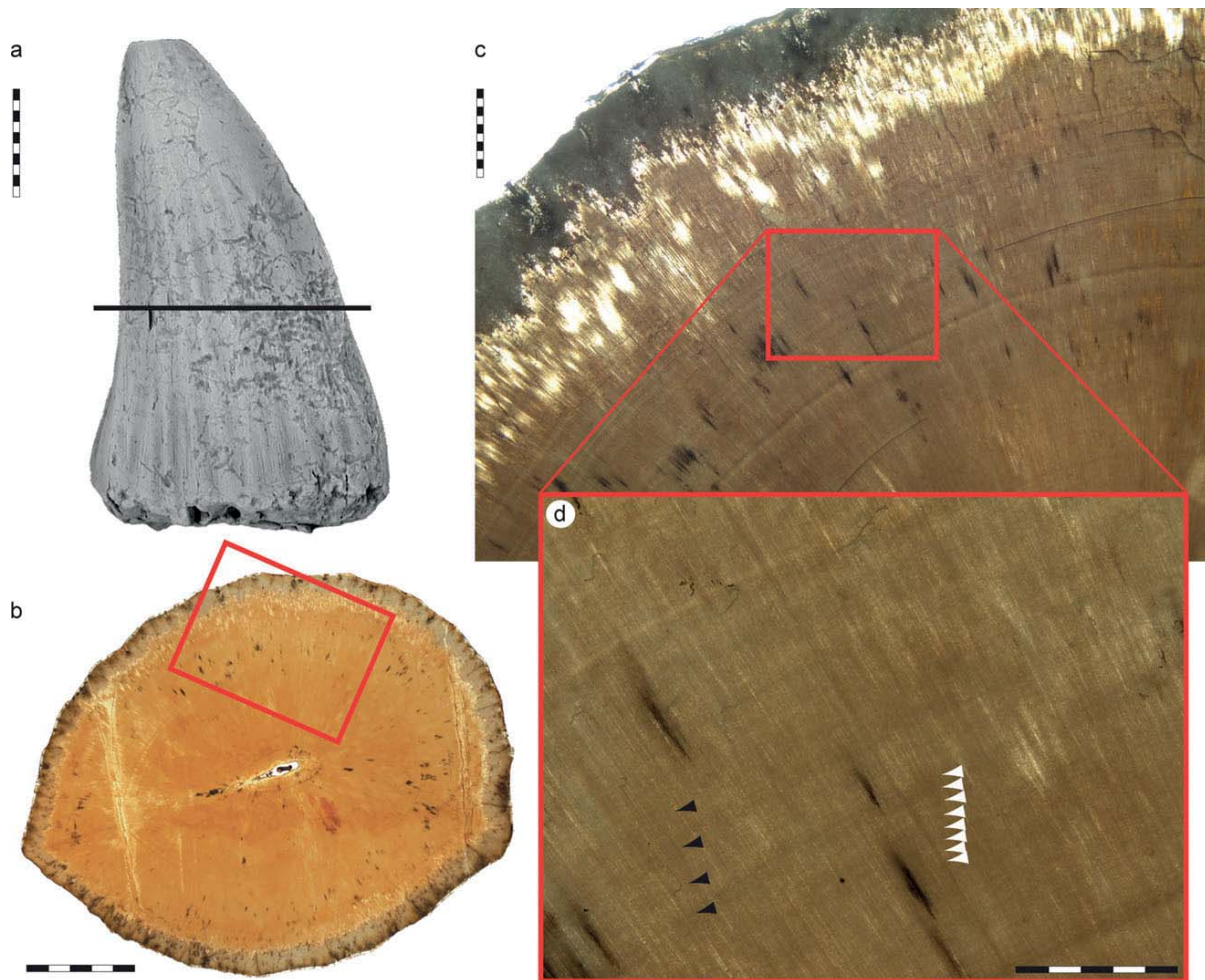


Figure 4. (Colour online) *Tylosaurus ivoensis*, LO 11624 *t*, isolated marginal tooth-crown. (a) Specimen photographed in labial view prior to histological analysis. Level of sectioning is marked with a horizontal bar. (b) Transverse mid-crown section of LO 11624 *t* (labial side faces downwards). (c) Demarcated area in (b) showing long-period incremental markings (here interpreted as Andresen lines), radially oriented dentinal tubules and elongate osteocyte lacunae. (d) Demarcated area in (c) showing presumed Andresen lines (black arrowheads) and a second set of finer concentric laminations here interpreted as lines of von Ebner (better preserved striae are marked with white arrowheads). Scale bars represent 10 mm (a), 5 mm (b), 1 mm (c) and 500 μm (d).

holds a total of 342 short-period lines with one long-period line for every twelfth or thirteenth short-period line (mean thickness of dentine = 3860 μm).

4.c. LO 11624 *t* (*Tylosaurus ivoensis*)

Two transverse histological sections were made from LO 11624 *t* (Fig. 4): one close to the apex and one at approximately mid-crown height. In the apical section, the enamel contains four incomplete increments. Evidence of bacterial or fungal activity is apparent towards the periphery of the dentine, thus limiting the amount of observable primary features in this part of the section. Odontocyte lacunae and dentinal tubules appear scattered throughout the dentine, the latter of these microstructures being intersected by a continuous set of 77 incremental laminations ranging in size from 10 to 26 μm and with an average width of 15.7 μm . Given that the thickness of the dentine is 6441 μm , there are

410 daily increments at the level of sectioning. Additionally, a few coarser markings occur among the short-period lines, roughly 100–200 μm apart.

In the mid-crown section, only one incremental line can be traced over some distance in the enamel. Although the perimeter of the dentine is remodelled by bone-boring bacteria and/or fungal hyphae, its inner parts are well preserved with abundant dentinal tubules and elongate odontocyte lacunae. One set comprising 16 consecutive long-period lines, with a size range of 122–275 μm and an average width of 219 μm , is present in the peri-pulpal dentine (Fig. 4d, black arrowheads). Additionally, there is one set of 82 short-period lines with a size range of 9–34 μm and an average width of 19.4 μm (Fig. 4d, white arrowheads). Thus, at the level of sectioning the tooth-crown holds a total of 487 short-period lines (mean thickness of dentine = 9440 μm) with one long-period line for every eleventh or twelfth short-period line.

Mosasaur tooth histology

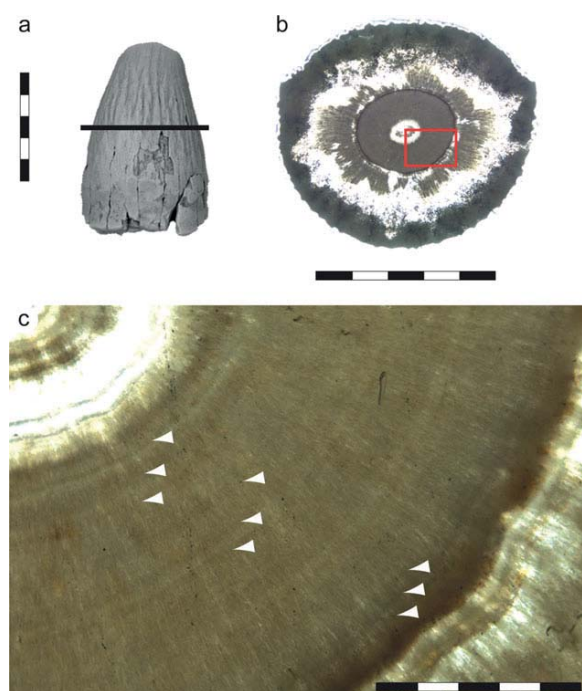


Figure 5. (Colour online) *Aigialosuchus* sp., LO 11621 *t*, isolated tooth-crown. (a) LO 11621 *t* as it appeared (in labial view) prior to histological analysis. Level of sectioning is marked with a horizontal bar. (b) Transverse mid-crown section of LO 11621 *t* (labial side faces downwards). (c) Demarcated area in (b) showing periodic incremental markings (arrowheads) here interpreted as lines of von Ebner. Scale bars represent 5 mm (a, b) and 500 μm (c).

4.d. LO 11621 *t* (*Aigialosuchus* sp.)

Three histological sections were made from LO 11621 *t* (Fig. 5): one transverse section close to the apex, one transverse section at approximately mid-crown height, and one longitudinal section near the base of the crown. In the apical section, the enamel holds three incomplete increments preserved as alternating opaque and transparent laminae. Most primary features of the dentine are obscured by an interconnected lattice of thread-like channels that was probably made by bone-boring bacteria and/or fungal hyphae, although densely spaced, radially oriented dentinal tubules and a few faint, concentric laminations are visible in some areas.

The section taken at mid-crown height is also partially affected by microorganisms, particularly in the peripheral parts of the dentine (Fig. 5b). Close to the pulp cavity, fine dentinal tubules extend radially from the crown centre and outward (Fig. 5c). These tubules are intersected perpendicularly by a number of concentric and gently undulating incremental growth lines (consisting of alternating dark and light bands) of somewhat varying widths (6–19 μm) and thickness (Fig. 5c, arrowheads). A strong band at about 1200 μm from the centre of the pulp cavity is surrounded by a micro-crack, about 1 μm wide. This crack indicates a weakening zone in the dentine, which may have been exploited by bacteria and/or fungi (Fig. 5c).

Proximal to the pulp cavity, increments are regular and well preserved, whereas distally, the laminations are more irregular and diffuse. Fifty-one consecutive short-period growth lines were measured, rendering an average width of 12.7 μm . By extrapolation (mean thickness of dentine = 3287 μm), the tooth-crown contains a total of 259 dentinal increments over the sectioned surface. The longitudinal section did not yield any additional information.

5. Discussion

Lines of von Ebner form through a circadian rhythm involving alternating accumulation and mineralization of dentine (Nanci, 2008), and the daily increments seen in extant crocodylian teeth are presumably deposited in a similar manner (Erickson, 1996b). The short-period markings observed in *Aigialosuchus* sp. have a morphology and size range consistent with the periodic increments documented by Erickson (1996b), and homologous increments are also found in *Dollosaurus* sp., cf. *Platecarpus* and *Tylosaurus ivoensis*, thus corroborating the presence of von Ebner's lines in Mesozoic crocodylian and mosasaur dentine (cf. Erickson, 1996a; Chinsamy, Tunoglu & Thomas, 2010, 2012).

Daily dentine formation rates (and incremental line widths) in modern amniotes are between 1 and 30 μm regardless of the size of the tooth (and animal), something that led Erickson (1996a) to conclude that there are important structural or physiological constraints that limit the amount of dentine that can form on a daily basis. The consequences of these restraints are interesting, particularly when considering animals that attain gigantic proportions. During the evolution of obligatory marine mosasaurs, body size increased and so did tooth size (Russell, 1967; Lingham-Soliar, 1995). However, the time required to develop the teeth seemingly increased as well, as indicated by the growth line counts in *T. ivoensis* (410 and 487 days at the apex and mid-crown section, respectively) and *Mosasaurus hoffmanni* (511 days; see Chinsamy, Tunoglu & Thomas, 2010, 2012) – two enormous species with massive marginal tooth-crowns – compared to cf. *Platecarpus* (342 days at mid-crown height) (the moderately robust crown of *Dollosaurus* sp. takes an intermediate position with 426 daily increments at mid-crown height). Although both *T. ivoensis* and *M. hoffmanni* undoubtedly were capable of eating almost anything that they encountered, including sea turtles and other mosasaurs (e.g. Massare, 1987 and references therein), the risk of long-term incapacity to overwhelm prey following breakage or other severe dental injuries may have been high (assuming that tooth replacement rates declined in conjunction with prolonged tooth development times, as they do in extant animals; cf. Kline & Cullum, 1984; Erickson, 1996a). Nonetheless, in similarity with the giant tyrannosaurid dinosaurs (see Erickson, 1996a), this evolutionary trade-off presumably was compensated for by allometric modifications of the teeth, including, for example, the

development of more robust crowns and broader tooth bases (Massare, 1987; Lingham-Soliar, 1995; Lindgren & Siverson, 2002). Not only did these adaptations enable the capture of larger prey items, but they also increased the resistance of the teeth to mechanical damage, thereby extending their functional longevity (Lingham-Soliar, 1995).

In addition to lines of von Ebner, coarser and more widely spaced incremental markings were observed in LO 11623 *t* (cf. *Platecarpus*) and LO 11624 *t* (*T. ivoensis*) (Figs. 3, 4). These long-period lines contain between 11 and 13 short-period lines each, to suggest formation periodicities similar to those of Andresen lines in extant animals (Dean & Scandrett, 1996). However, unlike typical Andresen lines, which are spaced on average between 15 and 30 μm apart (Dean & Scandrett, 1996), the long-period lines documented in this study have a mean width of 141 μm (cf. *Platecarpus*) and 219 μm (*T. ivoensis*), respectively. Assuming depository rhythms similar to those of Andresen lines, this would imply that the amount of dentine secreted at any given time was between 4 and 15 times higher in mosasaurs relative to modern mammals (cf. Dean & Scandrett, 1996). Given that mosasaurs, as opposed to most mammalian taxa, continuously shed and replaced their teeth, significantly higher tooth formation rates are expected (and in line with calculated tooth formation times in other reptilian groups, including *Aigialosuchus*, other crocodylians, and nonavian dinosaurs; Erickson, 1996*a, b*; Sereno *et al.* 2007; D'Emic *et al.* 2009). Nonetheless, in a study devoted to Bauer's (1898) collection of ichthyosaur tooth sections, Scheyer & Moser (2011) pointed out that similarly spaced incremental lines are variably assigned to as von Ebner and Andresen lines by different authors (see also Dean, 1998, 2000). Moreover, they (Scheyer & Moser, 2011) documented two sets of incremental markings in ichthyosaur dentine: a first set comprising very fine laminations situated about 2–3 μm apart, and a second set of coarser markings where spaces varied around 15–20 μm . Scheyer & Moser (2011) interpreted the thin, short-period lines as those of von Ebner based on their comparable thickness to the daily increments in human dentine, whereas the coarser, long-period lines were referred to as Andresen lines. If this interpretation is correct, then the short-period lines recorded in mosasaur and nonavian dinosaur dentine would represent Andresen lines, which in turn would result in even shorter tooth development times than those estimated by us and others (cf. Erickson, 1996*a*; Sereno *et al.* 2007; D'Emic *et al.* 2009; Chinsamy, Tunoglu & Thomas, 2010, 2012). However, increments with a periodicity of less than a day (infradian markings) have been identified in some animals (see Dean & Scandrett, 1996), and it should also be pointed out that Maxwell, Caldwell & Lamoureux (2012) failed to find any regular incremental banding pattern in their sample of sectioned ichthyosaur teeth. Even though we were unable to confirm the presence of laminations spaced less than about 6 μm apart, we cannot rule out the possib-

ility of three different sets of incremental markings in mosasaur dentine because of potential preservational artefacts, such as diagenetic colouration or secondary mineralization, which might obliterate the original ultrastructure of the dentine.

In order to fully understand the process of tooth development and replacement in mosasaurs, more comprehensive studies based on larger sample sizes are required. However, because the incremental growth lines observed in mosasaur marginal teeth are homologous to those in the dentine of extant animals, it is likely that the dentinal deposition rhythms we record herein represent primitive features that can be found in all tooth-bearing vertebrates.

Acknowledgements. We gratefully acknowledge logistical support for the project provided by the Department of Geology, Lund University. We thank Jan Rees, Peter Cederström and Filip Lindgren for collecting some of the specimens examined in this study and for putting their private collections at our disposal. This research was supported by grants from the Swedish Research Council, the Crafoord Foundation and the Royal Swedish Academy of Sciences.

References

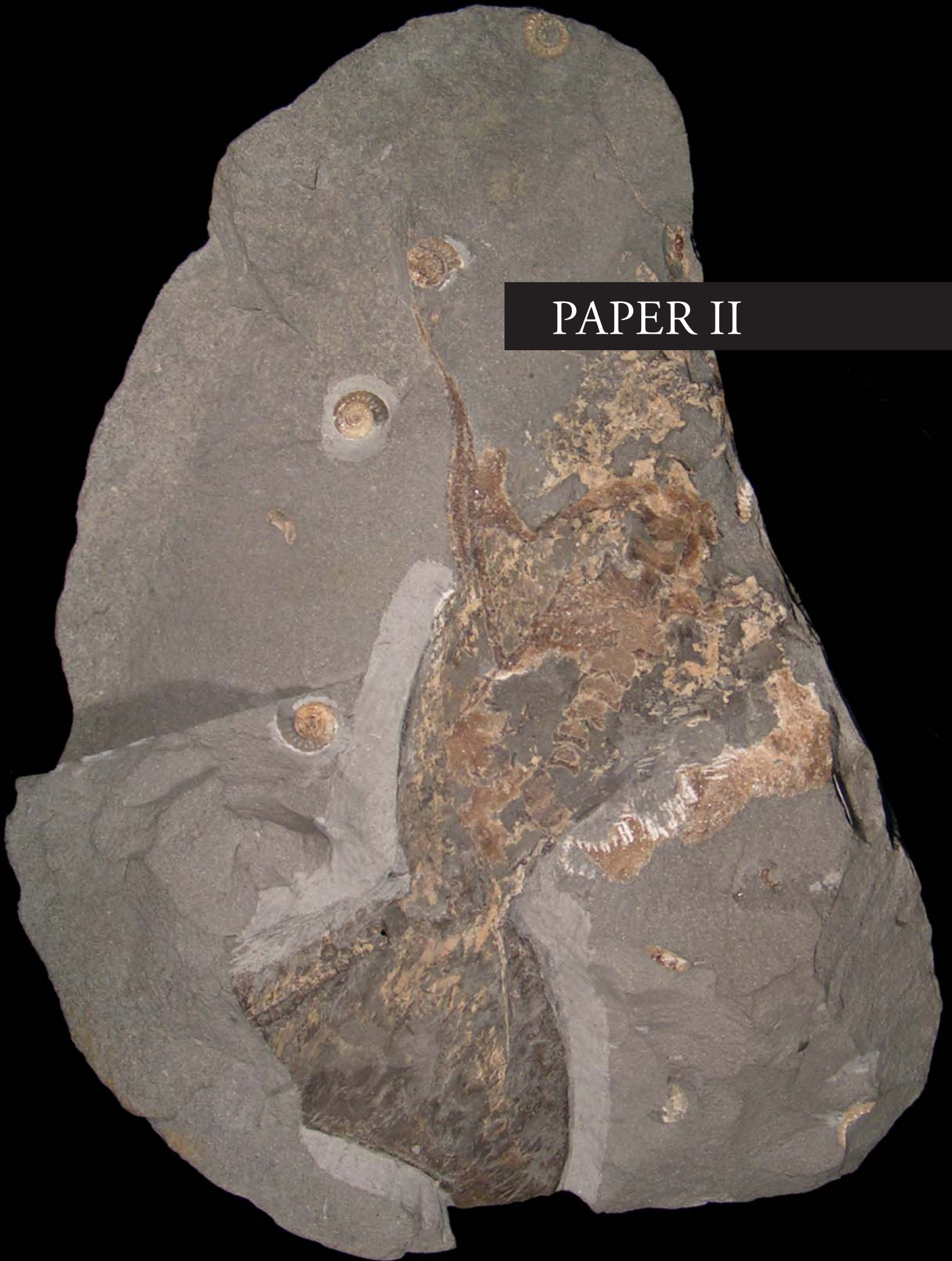
- ANDRESEN, V. 1898. Die Querstreifung des Dentins. *Deutsche Monatsschrift für Zahnheilkunde* **38**, 386–9.
- BAUER, F. 1898. Die Ichthyosaurier des oberen weissen Jura. *Palaeontographica* **44**, 283–328.
- BERGSTRÖM, J. & SUNDQUIST, B. 1978. Kritberggrunden. In *Beskrivning till Berggrundskartan och Flygmagnetiska Kartan Kristianstad SO* (eds K. A. Kornfält, J. Bergström, L. Carsrud, H. Henkel & B. Sundquist), pp. 55–99. Sveriges Geologiska Undersökning Af 121.
- BHASKAR, S. N. 1991. *Orban's Oral Histology and Embryology*, 11th ed. St Louis: Elsevier.
- CALDWELL, M. W. 2007. Ontogeny, anatomy and attachment of the dentition in mosasaurs (Mosasauridae: Squamata). *Zoological Journal of the Linnean Society* **149**, 687–700.
- CHINSAMY, A., TUNOĞLU, C. & THOMAS, D. B. 2010. Dental microstructure and geochemistry of *Mosasaurus hoffmanni* (Squamata) from the Late Cretaceous of Turkey. *Third Mosasaur Meeting, Muséum National d' Histoire Naturelle, Paris, 18–22 May 2010, Schedule, Abstracts, Field Trip*, p. 5.
- CHINSAMY, A., TUNOĞLU, C. & THOMAS, D. B. 2012. Dental microstructure and geochemistry of *Mosasaurus hoffmanni* (Squamata) from the Late Cretaceous of Turkey. *Bulletin de la Société Géologique de France* **183**, 85–92.
- CHRISTENSEN, W. K. 1975. Upper Cretaceous belemnites from the Kristianstad area in Scania. *Fossils and Strata* **7**, 1–69.
- DEAN, M. C. 1995. The nature and periodicity of incremental lines in primate dentine and their relationship to periradicular bands in OH 16 (*Homo habilis*). In *Aspects of Dental Biology; Paleontology, Anthropology and Evolution* (ed. J. Moggi-Cecchi), pp. 239–65. Florence: International Institute for the Study of Man.
- DEAN, M. C. 1998. Comparative observations on the spacing of short-period (von Ebner's) lines in dentine. *Archives of Oral Biology* **43**, 1009–21.

Mosasaur tooth histology

- DEAN, M. C. 2000. Incremental markings in enamel and dentine: what they can tell us about the way teeth grow. In *Development, Function and Evolution of Teeth* (eds M. F. Teaford, M. M. Smith & M. W. J. Ferguson), pp. 119–30. Cambridge: Cambridge University Press.
- DEAN, M. C. & SCANDRETT, A. E. 1996. The relation between long-period incremental markings in dentine and daily cross-striations in enamel in human teeth. *Archives of Oral Biology* **41**, 233–41.
- D'EMIC, M. D., WHITLOCK, J. A., SMITH, K. M., WILSON, J. A. & FISHER, D. C. 2009. The evolution of tooth replacement rates in sauropod dinosaurs. *Journal of Vertebrate Paleontology* **29**, 84A.
- EBNER, V. VON 1902. Histologie der Zähne mit Einschluss der Histogenese. In *Handbuch der Zahnheilkunde* (ed. J. Scheff), pp. 243–99. Wien: A. Holder.
- EBNER, V. VON 1906. Über die Entwicklung der leimgebenden Fibrillen, insbesondere im Zahnbein. *Sitzungsberichte der Mathematisch-Naturwissenschaftlichen Klasse der kaiserlichen Akademie der Wissenschaften in Wien* **115**, 281–347.
- ERICKSON, G. M. 1996a. Incremental lines of von Ebner in dinosaurs and the assessment of tooth replacement rates using growth line counts. *Proceedings of the National Academy of Sciences, USA* **93**, 14623–7.
- ERICKSON, G. M. 1996b. Daily deposition of dentine in juvenile *Alligator* and assessment of tooth replacement rates using incremental line counts. *Journal of Morphology* **228**, 189–94.
- ERIKSSON, M. E., LINDGREN, J., CHIN, K. & MÅNSBY, U. 2011. Coprolite morphotypes from the Upper Cretaceous of Sweden: novel views on an ancient ecosystem and implications for coprolite taphonomy. *Lethaia* **44**, 455–68.
- ERLSTRÖM, M. & GABRIELSON, J. 1986. The Upper Cretaceous clastic deposits of Ullstorp, Kristianstad Basin, Scania. *Geologiska Föreningens i Stockholm Förhandlingar* **107**, 241–54.
- ERLSTRÖM, M. & GABRIELSON, J. 1992. Petrology, fossil composition and depositional history of the Ignaberga limestone, Kristianstad Basin, Scania. *Sveriges Geologiska Undersökning* **Ca 80**, 1–30.
- HILLSON, S. 2005. *Teeth*, 2nd ed. Cambridge Manuals in Archaeology. Cambridge: Cambridge University Press.
- KAMIYA, H., YOSHIDA, T., KUSUHASHI, N. & MATSUOKA, H. 2006. Enamel texture of the tritylodontid mammal-like reptile, occurred from the lower Cretaceous in central Japan. *Materials Science and Engineering C* **26**, 707–9.
- KAWASAKI, K., TANAKA, S. & ISHIKAWA, T. 1980. On the daily incremental lines in human dentine. *Archives of Oral Biology* **24**, 939–43.
- KIERDORF, H., KIERDORF, U., WITZEL, C., INTOH, M. & DOBNEY, K. 2009. Developmental defects and post-mortem changes in archaeological pig teeth from Fais Island, Micronesia. *Journal of Archaeological Science* **36**, 1637–46.
- KLINE, L. W. & CULLUM, D. 1984. A long term study of the tooth replacement phenomenon in the young green iguana, *Iguana iguana*. *Journal of Herpetology* **18**, 176–85.
- LIDMAR-BERGSTRÖM, K. 1982. Pre-Quaternary geomorphological evolution in southern Fennoscandia. *Sveriges Geologiska Undersökning C* **785**, 1–202.
- LINDGREN, J. 2005a. The first record of *Hainosaurus* (Reptilia: Mosasauridae) from Sweden. *Journal of Paleontology* **79**, 1157–65.
- LINDGREN, J. 2005b. Dental and vertebral morphology of the enigmatic mosasaur *Dollosaurus* (Reptilia, Mosasauridae) from the lower Campanian (Upper Cretaceous) of southern Sweden. *Bulletin of the Geological Society of Denmark* **52**, 17–25.
- LINDGREN, J., CURRIE, P. J., SIVERSON, M., REES, J., CEDERSTRÖM, P. & LINDGREN, F. 2007. The first neoceratopsian dinosaur remains from Europe. *Palaeontology* **50**, 929–37.
- LINDGREN, J. & SIVERSON, M. 2002. *Tylosaurus ivoensis*: a giant mosasaur from the early Campanian of Sweden. *Transactions of the Royal Society of Edinburgh, Earth Sciences* **93**, 73–93.
- LINDGREN, J. & SIVERSON, M. 2004. The first record of the mosasaur *Clidastes* from Europe and its palaeogeographical implications. *Acta Palaeontologica Polonica* **49**, 219–34.
- LINDGREN, J. & SIVERSON, M. 2005. *Halisaurus sternbergi*, a small mosasaur with an intercontinental distribution. *Journal of Paleontology* **79**, 763–73.
- LINGHAM-SOLIAR, T. 1995. Anatomy and functional morphology of the largest marine reptile known, *Mosasauros hoffmanni* (Mosasauridae, Reptilia) from the Upper Cretaceous, Upper Maastrichtian of The Netherlands. *Philosophical Transactions of the Royal Society B: Biological Sciences* **347**, 155–80.
- MASSARE, J. A. 1987. Tooth morphology and prey preference of Mesozoic marine reptiles. *Journal of Vertebrate Paleontology* **7**, 121–37.
- MAXWELL, E. E., CALDWELL, M. W. & LAMOUREUX, D. O. 2012. Tooth histology, attachment, and replacement in the Ichthyopterygia reviewed in an evolutionary context. *Paläontologische Zeitschrift* **86**, 1–14.
- NANCI, A. 2008. *Ten Cate's Oral Histology: Development, Structure, and Function*, 7th ed. St Louis: Elsevier.
- OWEN, R. 1841. *Odontography; or, a Treatise on the Comparative Anatomy of the Teeth; their Physiological Relations, Mode of Development, and Microscopic Structure, in the Vertebrate Animals. Volume 1. Text*. London: Hippolyte Bailliére.
- OWEN, R. 1845. *Odontography; or, a Treatise on the Comparative Anatomy of the Teeth; their Physiological Relations, Mode of Development, and Microscopic Structure, in the Vertebrate Animals. Volume 2. Plates*. London: Hippolyte Bailliére.
- PERSSON, P. O. 1959. Reptiles from the Senonian (U. Cret.) of Scania (S. Sweden). *Arkiv för Mineralogi och Geologi* **2**, 431–78.
- PERSSON, P. O. 1963. Studies on Mesozoic marine reptile faunas with particular regard to the Plesiosauria. *Publications from the Institutes of Mineralogy, Paleontology and Quaternary Geology, University of Lund, Sweden* **118**, 1–15.
- RICHMAN, J. M. & HANDRIGAN, G. R. 2011. Reptilian tooth development. *Genesis* **49**, 247–60.
- RIEPEL, O. & KEARNEY, M. 2005. Tooth replacement in the Late Cretaceous mosasaur *Clidastes*. *Journal of Herpetology* **39**, 688–92.
- RUSSELL, D. A. 1967. Systematics and morphology of American mosasaurs (Reptilia, Sauria). *Peabody Museum of Natural History, Yale University, Bulletin* **23**, 1–241.
- SCHEYER, T. M. & MOSER, M. 2011. Survival of the thinnest: rediscovery of Bauer's (1898) ichthyosaur tooth sections from Upper Jurassic lithographic limestone quarries, south Germany. *Swiss Journal of Geosciences* **104**, 147–57.

- SERENO, P. C., WILSON, J. A., WITMER, L. M., WHITLOCK, J. A., MAGA, A., IDE, O. & ROWE, T. A. 2007. Structural extremes in a Cretaceous sauropod. *PLoS ONE* **2** (11), e1230, doi:10.1371/journal.pone.0001230.
- SIVERSON, M. 1993. Late Cretaceous and Danian neoselachians from southern Sweden. *Lund Publications in Geology* **110**, 1–28.
- UNDERWOOD, C. J., MITCHELL, S. F. & VELTKAMP, C. J. 1999. Microborings in mid-Cretaceous fish teeth. *Proceedings of the Yorkshire Geological Society* **52**, 269–74.
- ZAHER, H. & RIEPPEL, O. 1999. Tooth implantation and replacement in squamates, with special reference to mosasaur lizards and snakes. *American Museum Novitates* **3271**, 1–19.

PAPER II



Overleaf: The Jurassic ichthyosaur specimen YORYM 1993.338

LETTER

doi:10.1038/nature12899

Skin pigmentation provides evidence of convergent melanism in extinct marine reptiles

Johan Lindgren¹, Peter Sjövall², Ryan M. Carney³, Per Uvdal^{4,5}, Johan A. Gren¹, Gareth Dyke^{6,7}, Bo Pagh Schultz⁸, Matthew D. Shawkey⁹, Kenneth R. Barnes¹⁰ & Michael J. Polcyn¹¹

Throughout the animal kingdom, adaptive colouration serves critical functions ranging from inconspicuous camouflage to ostentatious sexual display, and can provide important information about the environment and biology of a particular organism^{1,2}. The most ubiquitous and abundant pigment, melanin, also has a diverse range of non-visual roles, including thermoregulation in ectotherms^{3,4}. However, little is known about the functional evolution of this important biochrome through deep time, owing to our limited ability to unambiguously identify traces of it in the fossil record². Here we present direct chemical evidence of pigmentation in fossilized skin, from three distantly related marine reptiles: a leatherback turtle⁵, a mosasaur⁶ and an ichthyosaur⁷. We demonstrate that dark traces of soft tissue in these fossils are dominated by molecularly preserved eumelanin, in intimate association with fossilized melanosomes. In addition, we suggest that contrary to the countershading of many pelagic animals^{8,9}, at least some ichthyosaurs were uniformly dark-coloured in life. Our analyses expand current knowledge of pigmentation in fossil integument beyond that of feathers^{2,10}, allowing for the reconstruction of colour over much greater ranges of extinct taxa and anatomy. In turn, our results provide evidence of convergent melanism in three disparate lineages of secondarily aquatic tetrapods. Based on extant marine analogues, we propose that the benefits of thermoregulation and/or crypsis are likely to have contributed to this melanisation, with the former having implications for the ability of each group to exploit cold environments.

On rare occasions, the fossil record reveals examples of exceptional preservation, in which decay-prone tissues, such as skin, are preserved as ‘an organic film’¹¹ with a high degree of morphological fidelity. These specimens provide information crucial to our understanding of ancient anatomy and evolutionary patterns. For example, the discovery of a dark-coloured ‘halo’ surrounding the skeleton of extraordinarily preserved ichthyosaurs (an extinct group of ocean-going reptiles⁷) in the 1890s drastically changed the prevailing image of these animals, revealing their remarkably derived, piscine body plan. Likewise, the preservation of carbonised scales in mosasaurs (another lineage of Mesozoic-era marine reptiles⁶) has greatly improved our understanding of how these ancient lizards evolved from land dwellers to pelagic cruisers¹².

Although such fossils have advanced our knowledge of the body plans of these animals, the origin and composition of the dark matter that forms preserved surface structures have yet to be resolved. Previous studies have shown that carbonised fossil ‘skin’ is rich in micrometre-sized spherical to rod-shaped bodies¹³. Morphologically, these structures resemble melanosomes (lysosome-related pigment organelles) but also microbes, and thus there has been debate over whether they represent fossilized remains of endogenous organelles^{10,14} or bacteria^{7,13}.

Therefore, to elucidate the molecular composition of putative fossilized skin, we analysed samples from three phylogenetically diverse marine reptiles—a 55-Myr-old leatherback turtle (FUM-N-1450; MUSERUM),

an 86-Myr-old mosasaur (SMU 76532; Shuler Museum of Paleontology) and a 196–190-Myr-old ichthyosaur (YORYM 1993.338; Yorkshire Museum) (Figs 1–4; see Supplementary Information)—using time-of-flight secondary ion mass spectrometry (ToF-SIMS) and scanning electron microscopy (SEM). ToF-SIMS provides detailed information on the composition and spatial distribution of surface molecules and chemical structures^{15,16}. In the three specimens, soft tissue anatomy associated with the skeletal elements is preserved as macroscopically amorphous, matt black material; however, SEM reveals masses of ovoid bodies, with long and short axes of approximately $0.8 \times 0.5 \mu\text{m}$ (turtle; Fig. 2b, c), $0.5 \times 0.3 \mu\text{m}$ (mosasaur; Fig. 3b, c) and $0.8 \times 0.5 \mu\text{m}$ (ichthyosaur; Fig. 4b, c) (Supplementary Information). These dimensions are consistent with those of melanosomes from extant lizards¹⁷ and bird feathers¹⁰. Energy-dispersive X-ray (EDX) microanalysis shows that carbon in these specimens is associated with the ‘skin’ but not the adjacent sedimentary matrix, suggesting that the former represents organic residues (Extended Data Fig. 1).

ToF-SIMS analysis produced negative-ion mass spectra from specific sample regions that closely match the spectrum obtained from natural eumelanin (Figs 2d, 3d and 4d and Extended Data Figs 2 and 3), indicating the presence of considerable amounts of this black to brown biochrome on the sampled surfaces. All relevant features of the standard

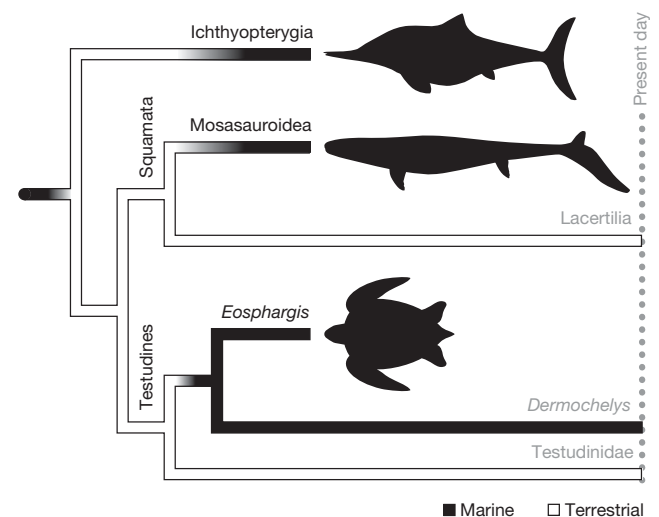


Figure 1 | Phylogenetic relationships of the three fossil marine reptiles examined in this study. Note that each lineage independently became secondarily aquatic (black branches, marine; white branches, terrestrial). Phylogeny is based on ref. 26; branch lengths and body sizes are not to respective scale.

¹Department of Geology, Lund University, SE-223 62 Lund, Sweden. ²SP Technical Research Institute of Sweden, Chemistry, Materials and Surfaces, SE-501 15 Borås, Sweden. ³Department of Ecology and Evolutionary Biology, Brown University, Providence, Rhode Island 02906, USA. ⁴MAX-IV laboratory, Lund University, SE-221 00 Lund, Sweden. ⁵Chemical Physics, Department of Chemistry, Lund University, SE-221 00 Lund, Sweden. ⁶Ocean and Earth Sciences, University of Southampton, Southampton SO14 3ZH, UK. ⁷Institute for Life Sciences, University of Southampton, Southampton SO14 3ZH, UK. ⁸MUSERUM, Natural History Division, Havnevej 14, 7800 Skive, Denmark. ⁹Integrated Bioscience Program, University of Akron, Akron, Ohio 44325, USA. ¹⁰Mosasaur Ranch Museum, Lajitas, Texas 79852, USA. ¹¹Roy M. Huffington Department of Earth Sciences, Southern Methodist University, Dallas, Texas 75275, USA.

RESEARCH LETTER

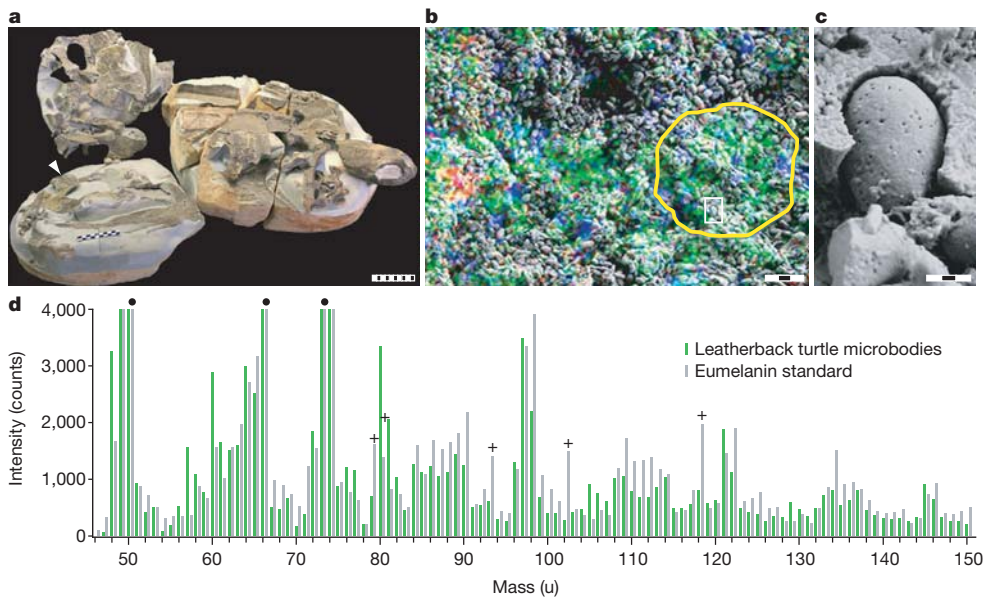


Figure 2 | SEM and ToF-SIMS data of fossil leatherback turtle FUM-N-1450. **a**, Photograph of specimen. Sampled skin structures are marked with an arrowhead. Scale bar, 10 cm. **b**, A semi-transparent ion image showing the spatial distribution of peaks characteristic of eumelanin (green; see Methods), silicon oxide (blue) and sulphate (red) superimposed onto a SEM image of the ‘skin’. Scale bar, 3 μ m. **c**, Enlargement of the demarcated area in **b** (white box) showing a melanosome-like microbody. Scale bar, 300 nm. **d**, Negative-ion

ToF-SIMS spectra from the area demarcated by a yellow line in **b** (‘Leatherback turtle microbodies’) and natural eumelanin. Filled circles (above grey bars) indicate peaks used to produce the eumelanin ion image in **b**, and plus symbols (above grey bars) indicate peaks from inorganic ions that are not part of the eumelanin structure (see Methods for further discussion). u, unified atomic mass unit.

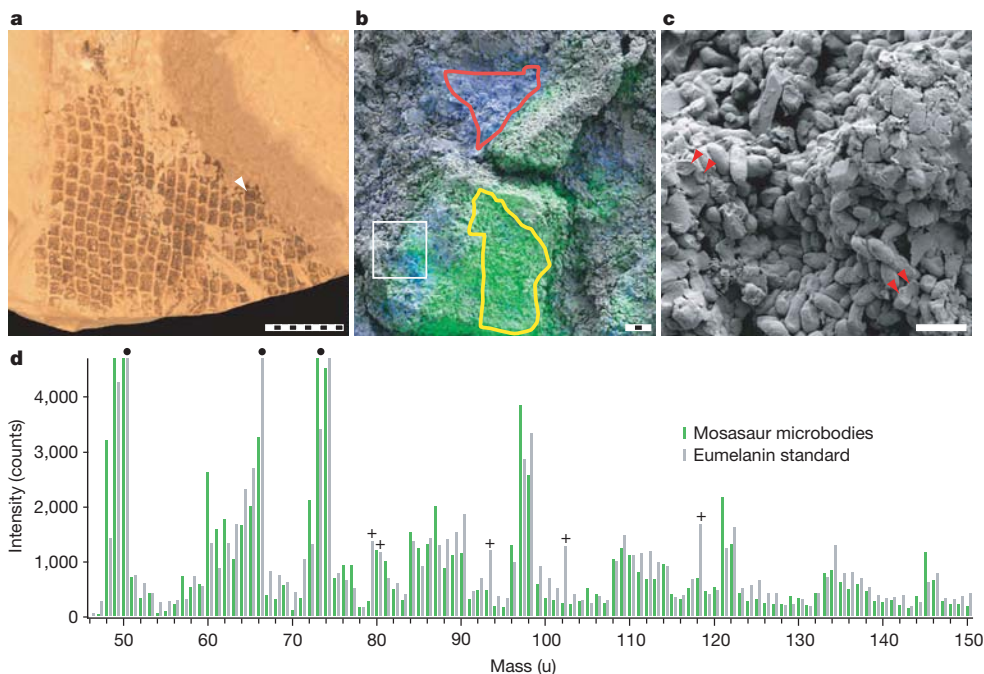


Figure 3 | SEM and ToF-SIMS data of mosasaur SMU 76532. **a**, Photograph of section with ‘scales’. Arrowhead indicates analysed area. Scale bar, 10 mm. **b**, A semi-transparent ion image showing the spatial distribution of peaks characteristic of eumelanin (green; see Methods) and silicon oxide (blue) superimposed onto a SEM image of the ‘scales’. The yellow line demarcates the area from which the spectrum presented in **d** (‘Mosasaur microbodies’) was collected, whereas the red line demarcates the area from which the upper spectrum in Extended Data Fig. 3 was collected. Scale bar, 3 μ m. **c**, Enlargement

of the demarcated area in **b** (white box) showing melanosome-like microbodies (arrowheads indicate solid interior; see Supplementary Information). Scale bar, 1 μ m. **d**, Negative-ion ToF-SIMS spectra from the area demarcated by a yellow line in **b** and natural eumelanin. Filled circles (above grey bars) indicate peaks used to produce the eumelanin ion image in **b**, and plus symbols (above grey bars) indicate peaks from inorganic ions that are not part of the eumelanin structure (see Methods for further discussion).

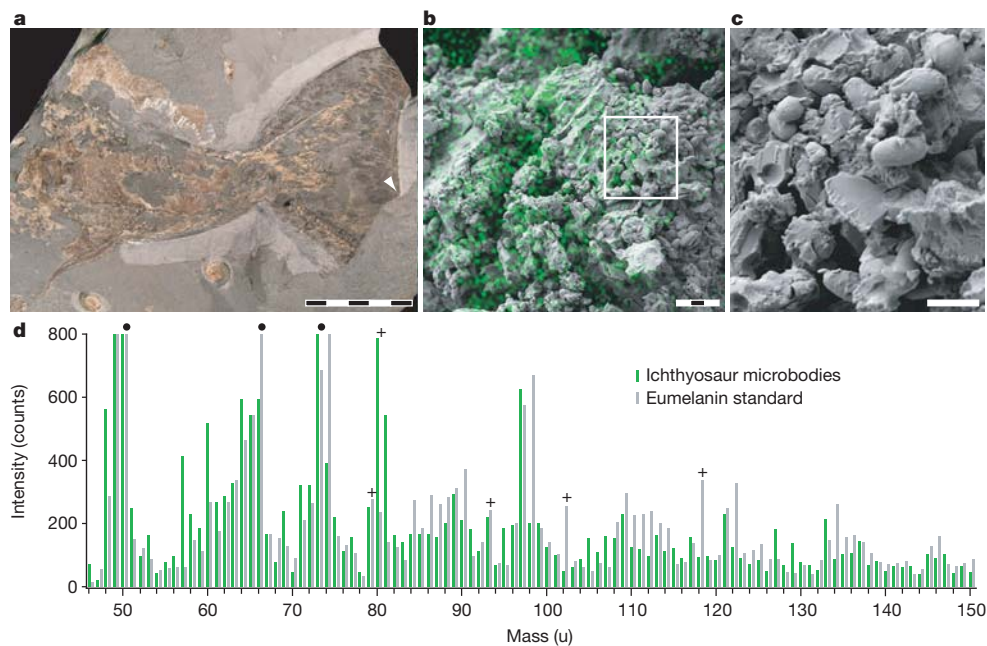


Figure 4 | SEM and ToF-SIMS data of ichthysaur YORYM 1993.338.

a, Photograph of specimen (caudal region and tail fin). The analysed area is indicated by an arrowhead. Scale bar, 5 cm. **b**, A semi-transparent ion image showing the spatial distribution of peaks characteristic of eumelanin (green; see Methods) superimposed onto a SEM image of the 'skin'. Scale bar, 3 μm . **c**, Enlargement of the demarcated area in **b** (white box) showing

melanosome-like microbodies. Scale bar, 1 μm . **d**, Negative-ion ToF-SIMS spectra of the 'skin' and natural eumelanin. Filled circles (above grey bars) indicate peaks used to produce the ion image in **b**, and plus symbols (above grey bars) indicate peaks from inorganic ions that are not part of the eumelanin structure (see Methods for further discussion).

spectrum are reproduced in the fossil spectra, including relative intensity distributions and precise peak positions (measured at 'high' mass resolution; see Extended Data Table 1) of all major peaks occurring at 49, 50, 66, 73, 74, 97, 98, 121, 122, 145, and 146 u (unified atomic mass unit), as well as several less intense peaks in the entire mass range up to 175 u. Moreover, all main eumelanin peaks show the same spatial distribution, demonstrating that they originate from the same molecular species (Extended Data Fig. 4). Importantly, superimposition of these data onto SEM micrographs shows that the eumelanin peaks from all three fossil specimens consistently appear in intimate association with melanosome-like microbodies (Figs 2b, 3b and 4b). Additional peaks representing other molecular structures, including silica (60, 76 and 77 u) and sulphate (80 u), display distinctly different spatial distributions not associated with melanin or the microbodies (Figs 2b and 3b and Extended Data Fig. 4).

The other main class of melanin pigment is phaeomelanin, which imparts red to yellow colours¹⁸. For a long time phaeomelanin was thought to be absent outside of mammals and birds, but it has recently been identified in Testudines¹⁸; phaeomelanosomes have also been found to fossilize¹⁰. However, the spectra from our three specimens do not indicate large amounts of phaeomelanin (Extended Data Fig. 5), and the ovoid microbodies are inconsistent with the spherical morphology of phaeomelanosomes¹⁰. Although minor contributions from compounds, such as phaeomelanin, cannot be excluded given the presence of sulphur (Extended Data Figs 4 and 6), the latter is likely to be diagenetic in origin (Supplementary Information). Ultimately, our molecular and imaging analyses provide compelling evidence that the organic content of the structures forming the 'skin' in all three specimens is dominated by eumelanin, and that the structures themselves represent fossilized melanosomes (see also Supplementary Information).

The fossil spectra are also inconsistent with those taken from three microbial mat samples¹⁶, as well as from nine molecular standards consisting of two compounds that are structurally similar to melanin, three porphyrin pigments, and four compounds that comprise the three other types of colour-producing cells (chromatophores) found in reptilian

integument: erythrophores, iridophores and xanthophores (Extended Data Figs 5 and 6; Supplementary Information)¹⁷. However, given that the relative preservation potential of non-melanic pigments and structural colour-producing chromatophores is believed to be relatively low², their absence may not necessarily indicate lack of original presence. Nevertheless, a relationship exists between melanin density and skin darkness^{3,17,19}, and the soft tissues in the fossil specimens are composed entirely of tightly packed melanosomes. Therefore, we conclude that the bodies of the three marine reptiles represented by these fossils originally had, at least partially, eumelanin colouration similar to the extant leatherback turtle, *Dermochelys coriacea* (Extended Data Fig. 7)⁵.

Given that animal pigmentation is subject to natural selection¹, the integumental melanisation we report was likely to have been advantageous to these organisms in life. One well-known modern example is thermal melanism, which provides faster heating and higher equilibrium temperatures through increased absorption of solar radiation due to lower albedo^{3,4}. This adaptation has been found to increase the fitness of various organisms in cold climates, including reptiles^{3,4}. Among extant reptiles, the leatherback turtle has the largest geographical and temperature ranges, including near-freezing waters in the Arctic Circle^{5,20}. The leatherback's ability to maintain a high core body temperature is generally attributed to an integrated suite of physiological and behavioural adaptations, including extremely large body size (gigantothermy)^{5,20}. It has also been suggested that the dark dorsal colouring of leatherbacks, coupled with their routinely observed, apparent basking behaviour, maximizes absorption of solar radiation²¹, and studies of leatherbacks foraging at high latitudes have revealed that these turtles surface for extended periods of time during daylight hours (peaking at around midday)^{5,21}. Furthermore, experimental results demonstrate that the black dorsal colouration of hatchlings of the related green sea turtle, *Chelonia mydas*, has an important role in elevating body temperature; this in turn is believed to increase growth rates during this vulnerable life history stage²². Thus, such thermal melanism presumably also has a role in leatherback turtles, particularly given that they inhabit colder environments (at

RESEARCH LETTER

least as sub-adults and adults⁵) and exhibit the fastest growth rates of any living turtle²³. Adult leatherbacks also retain this black colouration—unlike adult green sea turtles²² and despite lower growth rates compared to their juvenile stage²³—which may be due in part to thermal selective pressure throughout ontogeny. In addition, results from physical and theoretical modelling predict more advantageous thermal melanism in larger organisms³.

It is therefore feasible that selective pressures for fast growth, large size and/or homeothermy also selected for melanisation in extant (and fossil) leatherbacks. It is interesting to note that Eocene-epoch leatherback turtles also ranged into cold, high-latitude climates²⁴, and thus presumably possessed thermoregulatory adaptations comparable to those found in extant *Dermodochelys*. Similar selective pressures are likely to have acted on mosasaurs and ichthyosaurs as well, both of which were fast-growing, large and homeothermic^{25,26}. This homeothermy, which is likely to have been augmented by the thermal advantages of melanised skin during the sea-surfacing behaviours of these obligate air-breathers, allowed exploitation of ecological niches near the Arctic and Antarctic^{24,25,27}.

Pigmentation is often a multi-functional trait^{1,2}, and thus may have performed other non-mutually-exclusive roles, such as camouflage. For example, in addition to thermoregulation, the black colouration of green sea turtle hatchlings provides countershading (a dark dorsum and light ventrum), a simple but effective form of concealment against predators above, and below, the water surface²². Many other living aquatic organisms are countershaded^{9,22}, including *Dermodochelys*⁵, and this is occasionally also observed in exceptionally preserved fossils⁸. However, assuming that the black body outlines of ichthyosaur fossils with a full 'skin' envelope (Extended Data Fig. 8) represent endogenous pigments and/or organelles as reported here in YORYM 1993.338, we infer that these animals were uniformly dark-coloured in life. Some extant marine animals, including the deep diving sperm whale, *Physeter macrocephalus*, have a uniform dark colouration, and it has been suggested that this colour scheme acts as background matching in low light environments⁹. Although this is not a statistically supported association among cetaceans⁹, such a function in ichthyosaurs would nonetheless be consistent with their inferred deep diving habits⁷. The particular distribution of dark and light pigments in mosasaurs is unknown; however, the keeled scales present in some forms would have reduced shininess and provided a non-reflective appearance¹². Similarly, we reason that both cryptic and thermal melanism in marine reptiles would tend to select against other types of chromatophores and structural colouration, which by their nature serve to reflect light. This is consistent with the matt black appearance of extant leatherback skin, which is also smooth in adults due to a lack of scales⁵, a feature believed to be shared by at least some derived ichthyosaurs^{7,11}. More speculative functions for the melanisation observed in these three fossil taxa include photoprotection from the continuous exposure to ultraviolet radiation while at the sea surface²⁸, and mechanical strengthening of the integumentary tissue²⁹; gene(s) responsible for the melanisation may also have had pleiotropic effects on other physiological or behavioural traits, such as increased aggressiveness³⁰.

Ultimately, our molecular approach provides an unprecedented level of confidence for the detection and characterization of pigment in fossilized integument. Furthermore, the ability to reconstruct colour in skin has great potential for a phylogenetically diverse range of fossil animals. Our results suggest that dark colouration in extinct marine reptiles may be common, as it is in extant marine amniotes^{5,9}; such convergence reflects the important evolutionary role that melanin played after each of these ancient reptile lineages returned to the sea.

METHODS SUMMARY

Preparation of samples. Small tissue samples were removed from each specimen using a sterile scalpel and rinsed multiple times in 96% ethanol and 'ultrapure' (Milli-Q) water, dried under a hood, and wrapped in aluminium foil until examination. Prior to ToF-SIMS analysis, the surface of each sample was partially removed

using a sterile scalpel, and the collected material was deposited on double-sided cellophane tape. Aluminium foil was used to cover all work areas, and surgical gloves were used in all handling of the 'skin' samples. Treatment of modern reference samples was identical to that of the fossil structures for all analyses.

Scanning electron microscopy. Initial screening was performed using a Hitachi S-3400N SEM on uncoated samples under low vacuum, and the elemental composition was determined via elemental mapping using EDX analysis (1,900 s scanning time at 15 keV, 62.0 μ A and a working distance of 10 mm). After ToF-SIMS analysis, the samples were sputter-coated with gold and re-examined using a Zeiss Supra 40VP scanning electron microscope (2 keV, working distance 3–5 mm, Everhart-Thornley secondary electron detector).

Time-of-flight secondary ion mass spectrometry. ToF-SIMS analyses in the static SIMS mode were performed in a ToF-SIMS IV instrument (IONTOF GmbH) using 25 keV Bi₃⁺ primary ions and low energy electron flooding for charge compensation. High mass resolution data ($m/\Delta m \sim 5,000$) were acquired at a spatial resolution of $\sim 3\text{--}4 \mu\text{m}$, whereas high image resolution data (spatial resolution $\sim 0.2\text{--}0.5 \mu\text{m}$) were obtained at a mass resolution of $m/\Delta m \sim 300$; in both cases at 256×256 pixels. Because the positive-ion spectra were found to show strong interference with the signal from the sedimentary matrix, only negative-ion data are presented here.

Online Content Any additional Methods, Extended Data display items and Source Data are available in the online version of the paper; references unique to these sections appear only in the online paper.

Received 9 October; accepted 22 November 2013.

Published online 8 January 2014.

- Hubbard, J. K., Uy, J. A. C., Hauber, M. E., Hoekstra, H. E. & Safran, R. J. Vertebrate pigmentation: from underlying genes to adaptive function. *Trends Genet.* **26**, 231–239 (2010).
- McNamara, M. E. The taphonomy of colour in fossil insects and feathers. *Palaeontology* **56**, 557–575 (2013).
- Clusella Trullas, S., van Wyk, J. H. & Spotila, J. R. Thermal melanism in ectotherms. *J. Therm. Biol.* **32**, 235–245 (2007).
- Clusella Trullas, S., van Wyk, J. H. & Spotila, J. R. Thermal benefits of melanism in cordylid lizards: a theoretical and field test. *Ecology* **90**, 2297–2312 (2009).
- Eckert, K. L., Wallace, B. P., Frazier, J. G., Eckert, S. A. & Pritchard, P. C. H. *Synopsis of the Biological Data on the Leatherback Sea Turtle (Dermodochelys coriacea)* (US Department of Interior, Fish and Wildlife Service, 2012).
- Lindgren, J., Kaddumi, H. F. & Polcyn, M. J. Soft tissue preservation in a fossil marine lizard with a bilobed tail fin. *Nature Commun.* **4**, 2423 (2013).
- Motani, R. Evolution of fish-shaped reptiles (Reptilia: Ichthyopterygia) in their physical environments and constraints. *Annu. Rev. Earth Planet. Sci.* **33**, 395–420 (2005).
- Gottfried, M. D. Earliest fossil evidence for protective pigmentation in an actinopterygian fish. *Hist. Biol.* **3**, 79–83 (1989).
- Caro, T., Beeman, K., Stankowich, T. & Whitehead, H. The functional significance of colouration in cetaceans. *Evol. Ecol.* **25**, 1231–1245 (2011).
- Li, Q. *et al.* Plumage color patterns of an extinct dinosaur. *Science* **327**, 1369–1372 (2010).
- Martill, D. M. An ichthyosaur with preserved soft tissue from the Sinemurian of southern England. *Palaeontology* **38**, 897–903 (1995).
- Lindgren, J., Alwmark, C., Caldwell, M. W. & Fiorillo, A. R. Skin of the Cretaceous mosasaur *Plotosaurus*: implications for aquatic adaptations in giant marine reptiles. *Biol. Lett.* **5**, 528–531 (2009).
- Martill, D. M. Prokaryote mats replacing soft tissues in Mesozoic marine reptiles. *Mod. Geol.* **11**, 265–269 (1987).
- Whitear, M. On the colour of an ichthyosaur. *Ann. Mag. Nat. Hist.* **9**, 742–744 (1956).
- Thiel, V. & Sjövall, P. Using time-of-flight secondary ion mass spectrometry to study biomarkers. *Annu. Rev. Earth Planet. Sci.* **39**, 125–156 (2011).
- Lindgren, J. *et al.* Molecular preservation of the pigment melanin in fossil melanosomes. *Nature Commun.* **3**, 824 (2012).
- Kuriyama, T., Miyaji, K., Sugimoto, M. & Hasegawa, M. Ultrastructure of the dermal chromatophores in a lizard (Scincidae: *Plestiodon latiscutatus*) with conspicuous body and tail coloration. *Zool. Sci.* **23**, 793–799 (2006).
- Roulin, A., Mafli, A. & Wakamatsu, K. Reptiles produce pheomelanin: evidence in the eastern Hermann's tortoise (*Eurotestudo boettgeri*). *J. Herpetol.* **47**, 258–261 (2013).
- Rosenblum, E. B., Hoekstra, H. E. & Nachman, M. W. Adaptive reptile color variation and the evolution of the *Mc1r* gene. *Evolution* **58**, 1794–1808 (2004).
- Bostrom, B. L., Jones, T. T., Hastings, M. & Jones, D. R. Behaviour and physiology: the thermal strategy of leatherback turtles. *PLoS ONE* **5**, e13925 (2010).
- James, M. C., Myers, R. A. & Ottensmeyer, C. A. Behaviour of leatherback sea turtles, *Dermodochelys coriacea*, during the migratory cycle. *Proc. R. Soc. Lond. B* **272**, 1547–1555 (2005).
- Bustard, H. R. The adaptive significance of coloration in hatchling green sea turtles. *Herpetologica* **26**, 224–227 (1970).

23. Zug, G. R. & Parham, J. F. Age and growth in leatherback turtles, *Dermochelys coriacea* (Testudines: Dermochelyidae): a skeletochronological analysis. *Chelonian Conserv. Biol.* **2**, 244–249 (1996).
24. Albright, L. B., Woodburne, M. O., Case, J. A. & Chaney, D. S. A leatherback sea turtle from the Eocene of Antarctica: implications for antiquity of gigantothermy in Dermochelyidae. *J. Vertebr. Paleontol.* **23**, 945–949 (2003).
25. Bernard, A. *et al.* Regulation of body temperature by some Mesozoic marine reptiles. *Science* **328**, 1379–1382 (2010).
26. Houssaye, A. Bone histology of aquatic reptiles: what does it tell us about secondary adaptation to an aquatic life? *Biol. J. Linn. Soc.* **108**, 3–21 (2013).
27. Rich, T. H., Vickers-Rich, P. & Gangloff, R. A. Polar dinosaurs. *Science* **295**, 979–980 (2002).
28. Martinez-Levasseur, L. M. *et al.* Whales use distinct strategies to counteract solar ultraviolet radiation. *Sci. Rep.* **3**, 2386 (2013).
29. McGraw, K. J. in *Bird Coloration* Vol. 1 (eds Hill, G. E. & McGraw, K. J.) 243–294 (Harvard Univ. Press, 2006).
30. Ducrest, A.-L., Keller, L. & Roulin, A. Pleiotropy in the melanocortin system, coloration and behavioural syndromes. *Trends Ecol. Evol.* **23**, 502–510 (2008).

Supplementary Information is available in the online version of the paper.

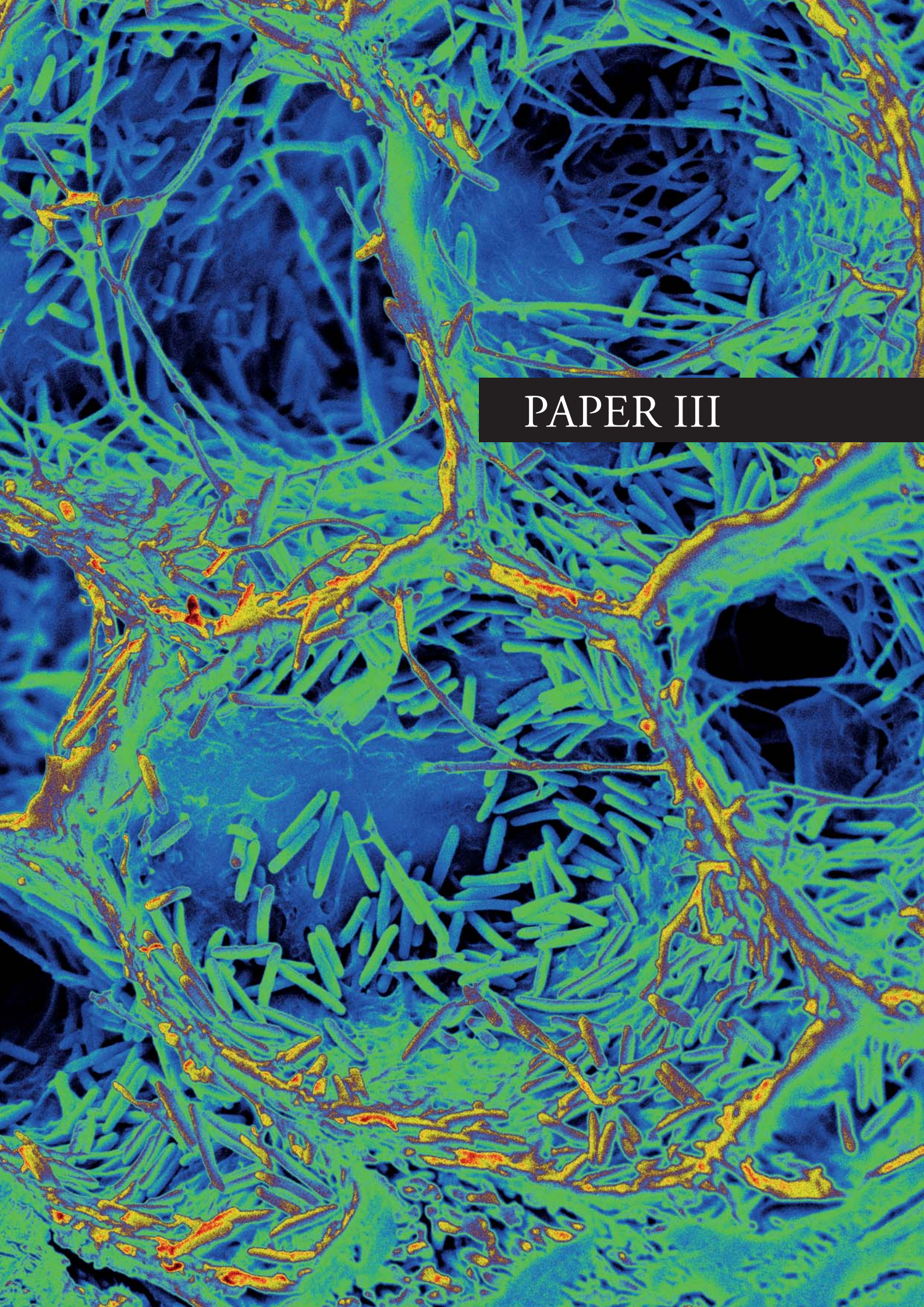
Acknowledgements We thank I. Gladstone, S. King and the Yorkshire Museum for permission to sample YORYM 1993.338, as well as J. Wyneken, P. Weston and L. Alibardi for providing and sectioning the extant leatherback turtle skin samples, respectively. B. P. Kear took the photograph of PMU R435 (Extended Data Fig. 8). This research was supported by grants from the Swedish Research Council, the Crafoord Foundation, the Royal Swedish Academy of Sciences (J.L.), VINNOVA Swedish Governmental Agency for Innovation Systems (P.S.), the National Geographic Society/Waitt Foundation (R.M.C.), the National Science Foundation, Human Frontiers Science Program, and Air Force Office of Scientific Research (M.D.S.).

Author Contributions J.L. designed the project. J.L., P.S., R.M.C. and G.D. wrote the manuscript. J.L., P.S., R.M.C., J.A.G. and P.U. prepared the images. G.D., B.P.S., M.D.S., K.R.B. and M.J.P. provided materials, observations and scientific interpretations. All authors discussed the results and provided input on the manuscript.

Author Information Reprints and permissions information is available at www.nature.com/reprints. The authors declare no competing financial interests. Readers are welcome to comment on the online version of the paper. Correspondence and requests for materials should be addressed to J.L. (johan.lindgren@geol.lu.se).

“Those who get it, get it.”

- Stefan Holm



PAPER III

Overleaf: False colour SEM image of elongate melanosomes in a modern bird feather barb (*Corvus* sp.)



Cite this article: Lindgren J *et al.* 2015 Interpreting melanin-based coloration through deep time: a critical review. *Proc. R. Soc. B* **282**: 20150614.
<http://dx.doi.org/10.1098/rspb.2015.0614>

Received: 17 March 2015
 Accepted: 23 July 2015

Subject Areas:

palaeontology, molecular biology, evolution

Keywords:

bacteria, eumelanin, melanosome, pheomelanin, pyomelanin, vertebrate

Author for correspondence:

Johan Lindgren
 e-mail: johan.lindgren@geol.lu.se

Electronic supplementary material is available at <http://dx.doi.org/10.1098/rspb.2015.0614> or via <http://rspb.royalsocietypublishing.org>.

Interpreting melanin-based coloration through deep time: a critical review

Johan Lindgren¹, Alison Moyer³, Mary H. Schweitzer^{1,3,4}, Peter Sjövall⁵, Per Uvdal^{6,7}, Dan E. Nilsson², Jimmy Heimdal⁶, Anders Engdahl⁶, Johan A. Gren¹, Bo Pagh Schultz⁸ and Benjamin P. Kear^{9,10}

¹Department of Geology, and ²Department of Biology, Lund University, 223 62 Lund, Sweden

³Department of Biological Sciences, North Carolina State University, Raleigh, NC 27695, USA

⁴North Carolina Museum of Natural Sciences, Raleigh, NC 27601, USA

⁵SP Technical Research Institute of Sweden, Chemistry, Materials and Surfaces, 501 15 Borås, Sweden

⁶MAX-IV laboratory, and ⁷Chemical Physics, Department of Chemistry, Lund University, 221 00 Lund, Sweden

⁸MUSERUM, Natural History Division, 7800 Skive, Denmark

⁹Museum of Evolution, and ¹⁰Palaeobiology Programme, Department of Earth Sciences, Uppsala University, 752 36 Uppsala, Sweden

Colour, derived primarily from melanin and/or carotenoid pigments, is integral to many aspects of behaviour in living vertebrates, including social signalling, sexual display and crypsis. Thus, identifying biochromes in extinct animals can shed light on the acquisition and evolution of these biological traits. Both eumelanin and melanin-containing cellular organelles (melanosomes) are preserved in fossils, but recognizing traces of ancient melanin-based coloration is fraught with interpretative ambiguity, especially when observations are based on morphological evidence alone. Assigning microbodies (or, more often reported, their 'mouldic impressions') as melanosome traces without adequately excluding a bacterial origin is also problematic because microbes are pervasive and intimately involved in organismal degradation. Additionally, some forms synthesize melanin. In this review, we survey both vertebrate and microbial melanization, and explore the conflicts influencing assessment of microbodies preserved in association with ancient animal soft tissues. We discuss the types of data used to interpret fossil melanosomes and evaluate whether these are sufficient for definitive diagnosis. Finally, we outline an integrated morphological and geochemical approach for detecting endogenous pigment remains and associated microstructures in multimillion-year-old fossils.

1. Introduction

The astonishing diversity of colour patterns seen in extant animals testifies to the important and multifunctional roles of melanin and other biological pigments (biochromes) in nature. Moreover, organic molecules (including eumelanin) can persist and be recognized over vast spans of geological time, and thereby evince crucial information about the history of life [1]. Preserved biochromes not only yield interpretations on the appearance of ancient organisms, but can also potentially elucidate their ecology and behaviour. They are therefore an insightful data source for resolving facets of palaeobiology and evolution.

For decades, scanning electron microscopy (SEM) and, more rarely, transmission electron microscopy (TEM) have been used to detect round to oblate microstructures (about 1–2 μm long) in exceptionally preserved vertebrate fossils (e.g. [2–5]). Until 2008, these minute bodies were interpreted as the remains of microorganisms that contribute to the decomposition of organic material (e.g. [4], but also see Voigt [6] and references therein). However, that year, Vinther *et al.* [7] re-described them as residual melanosomes: eukaryotic, melanin-containing cellular organelles, responsible in part for the coloration of integumentary structures, including skin, hair and feathers. They further suggested that the shape and arrangement of fossil melanosomes could be used to deduce plumage colours in ancient birds and non-avian dinosaurs [7], which led to inferences

about ecology and behaviour that have since been adopted by numerous studies (e.g. [8–10]).

Although information about the colour of extinct animals might provide important clues pertaining to lifestyles and habits, the reconstruction of specific tones and hues based on morphological evidence alone is not a straightforward process [11]. This is particularly pertinent when only SEM image data are considered, as these are demonstrably inadequate for discriminating between remnant melanosomes and pervasive bacteria [12]. Differentiation of melanosomes from microorganisms is necessary because they overlap in size, shape and distribution [12–14]. Moreover, microbes are always associated with decaying carcasses, and are known to fossilize as both organic (e.g. [15,16]) and inorganic traces (e.g. [17]). Another confounding issue is that microorganisms synthesize melanins [18,19], an ability that is most prevalent in bacteria inhabiting soil and marine environments [19]. Compounds arising from the degradation of melanic pigments have also been detected in microbial fossils, including fungal hyphae [20].

Defining colour from the shape of fossil microbodies (see [8,9]) has other limitations. Extant eumelanosomes (ellipsoidal organelles associated with dusky pigmentation [21], but also see below) can contain only eumelanin, but pheomelanosomes (spherical organelles associated with reddish pigmentation [21]) may not exist without a eumelanin complement [22]. Finally, the eumelanin-dominated eye pigments of vertebrates exhibit a random distribution of melanosome shapes that do not correlate with the type of melanin present [23,24].

Here, we address conceptual and methodological issues related to the interpretation of microbodies detected in fossilized animal tissues. As a framework, we briefly review melanosome formation in vertebrates (for brevity, we do not address invertebrate melanogenesis), focusing on physical and chemical properties of one of its main constituents: melanin. This moiety is thought to impart stability to the intracellular organelle, thereby enabling its preservation through deep time. Microbial melanization is also summarized for a practical character-based discrimination between fossil melanosomes and microorganismal cells. Our critical assessment of the methods commonly employed to identify fossil microstructures is intended to facilitate confident documentation and reduce the risk of insufficiently supported claims propagating in the literature.

2. Vertebrate melanogenesis

Structurally, melanins are heterogeneous biopolymers comprising a series of conjugated indole (resonant double-ring) moieties [25,26]. Several major melanin types exist in nature, but the most common are (dark brown-black) eumelanin and (red-yellow) pheomelanin [27]. Eumelanin is derived from enzyme-controlled oxidation of the amino acid tyrosine [28] to form a biochrome that is inherently resistant to degradation [25]; thus, its molecular structure is incompletely known [22,26]. Likewise, despite recognition that pheomelanin is produced from sulfur-containing benzothiazine units [28], its chemical structure is also not fully characterized [21].

In vertebrates, melanins are distributed through epidermal tissues and their derivatives, where the colour they impart plays important roles in social and predator–prey interactions, thermoregulation and ultraviolet (UV) protection [29,30]. In addition, internal organs and tissues, such as the liver, spleen, brain and inner ear, also contain melanin,

which contributes to physiological processes and disease resistance [30, fig. 1].

The cellular site of melanin synthesis, storage and transportation is the melanosome—a membrane-bound organelle generated by melanocytes, melanophores and pigment-epithelial cells [29]. Melanosomes attain a broad range of sizes and shapes, ranging from sub-micrometre-sized spherical grains [21, fig. 2d] to elongate particles up to 4 μm long [31, fig. 2a]. Ellipsoidal forms are typically ascribed to eumelanosomes, whereas spherical structures are referred to pheomelanosomes (e.g. [21]). This subdivision of shape has been proposed to reflect the chemical composition of the type of melanin they contain ([21], but also see below).

Melanosome biogenesis follows four sequential stages (enumerated I–IV), where melanin deposition is initiated at stage III, and the organelle is fully melanized by stage IV [32, fig. 1a]. Polymerization of melanin within the developing melanosome results in the formation of granules (this term is inconsistently used in the literature, but we follow the definition of Simon & Peles [22] as a standard) on intraluminal fibrils, and continues until all other structures within the organelle are obliterated [28,33]. At this time (stage IV), the organelle is considered to be mature [22]. Fully grown melanin granules normally range from 10 to 30 nm in diameter [22,34,35]; however, larger grains up to 80 nm in diameter have been recorded within red human hair melanosomes [21]. The melanin granules cause the outer surface of the melanosomes to become rugose [36, figs 2 and 3], a characteristic trait that is most marked in spherical forms [23].

Whereas pure eumelanin is naturally occurring, pure pheomelanin has not yet been documented [22]. Instead, pheomelanosomes contain a mixture of eumelanin and pheomelanin [21,28,37]. Pheomelanin granules are thought to comprise a pheomelanin core surrounded by a eumelanin sheath (the casing model [22,38], but see Gorniak *et al.* [39] for a different interpretation), the thickness of which determines expressed colour, at least in iridal melanosomes [37].

3. Melanin synthesis in microorganisms

In addition to eumelanin and pheomelanin, bacteria and fungi also produce a third type of melanin, generically named allomelanin [18,40]. Allomelanins are synthesized from an array of sources and via different biochemical pathways. As a result, several major subtypes exist, the most ubiquitous being pyomelanin. Allomelanins usually form from nitrogen-free precursors and are hence devoid of this constituent (see Plonka & Grabacka [18] for a comprehensive review of melanin biosynthesis in microorganisms).

In contrast to vertebrates, whose melanogenesis is confined to specialized cellular organelles, melanin synthesis in fungi usually occurs within the cell wall [41,42]. Nonetheless, some fungal species deposit melanins intracellularly in the form of cytoplasmic bodies, whereas others secrete melanic pigments into the surrounding environment [43]. The melanized fungal cell wall is highly durable, and thus can be isolated by chemical treatments destructive to other cellular components [44]. The resulting melanin shells (often called melanin ghosts) are hollow, but retain both the shape and size of the original cells after degradation and removal of the non-melanized constituents [18,44]. Melanin ghosts are composed of tightly packed and occasionally laminated melanin granules between 30 and

150 nm in diameter [43,44]. These impart a nodular appearance to the external ghost wall [44, fig. 2], and are typically accompanied by diagnostic crater-like scars derived from the budding process ([44, fig. 5], [45, fig. 1]).

In prokaryotic organisms, melanogenesis normally occurs extracellularly, and hence most bacterial melanins form amorphous deposits when purified [18,46], although globular aggregates have been reported [47]. However, in some bacteria, melanins are localized to the cytoplasm and may appear as electron-dense spots [48, fig. 5e]. Melanin-like compounds have also been detected in bacterial endospore coats, where they probably protect the developing spore against harmful UV radiation (e.g. [49]).

4. Melanin and melanosomes in the fossil record

Reports describing fossil melanins and melanosomes have been published sporadically since the 1930s (e.g. [6,50,51]), yet the search for ancient melanic pigments only began in earnest in the late 2000s following the proposal that feather traces might infer evidence of original hues and shades [7,52]. Since then, a number of investigations have used chemical markers and presumed fossil melanosomes to explore aspects of the biology and ecology of extinct animals, including colour [8,9,53–57], behaviour [8,56] and physiology [10]. However, studies reporting remnant melanosomes have been met with controversy, and an alternative hypothesis has been put forth favouring a more conservative interpretation of the fossil microbodies as microbes colonizing the degrading tissues prior to burial [12,58]. Such criticism has sparked intense debate (see Edwards *et al.* [11] for review), that is further aggravated by the dearth of unequivocal molecular indicators for ancient melanic pigments, which thus far have only been recorded from cephalopod ink sacs [59,60], a fish ‘eye spot’ [61] and marine reptile integuments [56]. Indeed, most occurrences of fossil melanosomes reported so far (particularly in feathers) are based entirely on morphology, packing and distribution (e.g. [7–10, 52–54,62]), whereas chemical studies, with few exceptions (see above), have either been inconclusive (e.g. [14,63]) or lacking in specificity and/or relevant comparative material to rule out alternative hypotheses (e.g. [55,64,65]). Most critically, many alleged melanosomes occur only as imprints (‘mouldic melanosomes’ [53]), a preservation mode that implies preferential degradation of the bodies relative to the surrounding substrate [12]. To complicate matters further, impressions indistinguishable from those attributed to melanosomes are occasionally found also in clay minerals, on silica crystals, and other sedimentary grains associated with, but clearly distinct from, the fossilized tissue structures (e.g. [9,12,65]).

These conflicts highlight the need for clear and unambiguous criteria by which remnant melanosomes can be differentiated from microbial residues. Clearly, this is vital for any accurate inference of organismal colour and its subsequent influence on ancient behaviours or ecology. We therefore outline factors contributing to the preservation potential of both melanin and melanosomes, and evaluate published methodologies employed to identify fossil microbodies. We also propose an integrated structural and molecular approach to promote rigorous interpretation of fossil melanins and melanosomes in the future. Firstly, however, we address a series of untested assumptions regarding melanosome data derived from the vertebrate fossil record.

5. Assumptions underlying assignment of colour to fossil organisms

(a) Assumption 1: melanosomes are inherently resistant to degradation

Whereas melanosomes in living animals contain a variety of biomolecules in addition to melanins (including significant amounts of proteins and lipids [66, fig. 1]), only eumelanin has so far been confidently identified in fossil melanosomes [56,61]. This suggests that the fully melanized stage IV melanosomes have the greatest capacity for preservation given their internal architecture of densely aggregated melanin granules [56,61]. The cross-linked polymeric structure of the eumelanin macromolecule is most likely responsible for this survival in fossil form [56,61]. Support for this hypothesis has been gleaned from degradation experiments, which demonstrate the remarkable mechanical rigidity of the melanin framework and its ability to retain both the size and shape of hydrolysed melanosomes, even after the complete removal of proteins and lipids [31,66–68]. Yet despite this durability, melanin is still susceptible to breakdown via oxidative reactions [66] and by some enzymes [69]. Moreover, populations of specialized melanophages infest vertebrate tissues (e.g. [70,71]). These monocyte-derived cells engulf melanosomes and retain them within their cytoplasm where both organelles and pigments are degraded over relatively short spans of time (e.g. [70,71]). In accordance, melanin can disintegrate rapidly under natural conditions, and thus its architectural stability and chemical robustness do not unequivocally confer preservation potential over geological time.

(b) Assumption 2: melanin pigments confer resistance to degradation

Melanized epidermal tissues and their appendages are known to have increased resistance to physical abrasion relative to unmelanized ones (e.g. [69,72]). Melanin insolubility, imparted by abundant intramolecular cross-links, has been argued to contribute to the preservation of integumentary structures in fossils, and especially feathers (e.g. [54]). However, the assumption that melanin unambiguously confers degradation resistance to the enclosing organelles, or the surrounding keratinous tissues, has not yet been rigorously tested. This is critical for evaluating the many published accounts on presumed melanosomes in fossils, because the majority of those specimens where expressed colour, physiology, behaviour or evolutionary significance have been proposed do not illustrate three-dimensional bodies, but rather derive data from ovoid to elongate imprints within an uncharacterized matrix (e.g. [8–10,54]). This observation implies that the microbodies decay more rapidly than does the surrounding matrix, thus challenging the idea that melanin confers decay resistance to the bodies. Because the attribution of these imprints to melanosomes rests on assumptions of their inherent durability, this assignment is called into question when only voids are present. Taphonomic experiments designed to test the relative resistance of melanosomes in keratin, keratin alone and microbial cells in extracellular polymeric substance (EPS) under varying conditions may present a possible method for addressing this issue.

(c) Assumption 3: fossil microbody shape and size are reliable indicators of colour

Statistical correlations support coherency between the shape and size of melanosomes in living epidermal tissues and the expression of melanin-derived colours (e.g. [8,9]). However, in addition to melanins, many other factors contribute to organismal coloration, including diet, light conditions, tissue structure, gender and co-expressed pigments [73,74]. Melanosomes occurring in skin and skin derivatives have also been statistically compared to microbodies (or more frequently their imprints) in fossil-associated material, and used to assign hues and colour patterns (e.g. [8,9]). However, with one exception [10], these extrapolations have failed to consider potential diagenetic alterations of these parameters in the matrix; instead, most studies have assumed the measured impressions to accurately reflect the shape and size of the original bodies (e.g. [57]). Nonetheless, maturation experiments on extant feathers designed to simulate the fossilization process have shown that melanosome size can be altered by increasing temperature and/or pressure [75]. Notably though, no consistent morphological modification has yet been documented in presumed fossil melanosomes, and it remains feasible that varying decompositional conditions, as well as mineralization might also effect structural change [60].

Another problem is the possibility that the supposed melanosome imprints could represent microbial cells preserved in mineralized EPS. Microorganismal EPS has high preservation potential because of its inherent affinity for mineral ions, and is thus likely to persist in the rock record [17]. Moreover, bacteria are ubiquitous in degrading organic matter and were undoubtedly present with all fossilized specimens. Imprints produced in the EPS when microbes degrade or are lost in other ways are consistent in virtually every aspect with those attributed to fossil melanosomes (electronic supplementary material, figure S1).

To further complicate matters, melanosomes in other pigmented tissues, such as the retina and choroid of the vertebrate eye, also vary widely in shape and size [23,76]. In these tissues at least, melanosome morphologies might additionally differ during ontogeny, yet the main melanin component is eumelanin regardless of melanosome shape and surface topography [23,76]. Microstructures comparable to those in modern vertebrate eyes are occasionally found in the orbital region of animal fossils (e.g. [61,77]), demonstrating that diverse ocular melanosome morphologies are not limited to extant taxa. Whether similar conditions apply to melanosomes derived from integumentary tissues has yet to be verified (it was recently discovered that similarly shaped melanosomes obtained from modern iridescent feathers have a highly variable chemistry [78]); however, the fact that diverse melanosome shapes occur in the eyes of ectothermic vertebrates suggests that factor(s) other than colour, energetics and physiology [8–10] can influence melanogenesis and the resulting melanosome morphologies.

Given the degree of morphological variation observed in living tissues, diagenetic factors and the co-expression of other pigments that may not persist in the fossil record, as well as the fact that a microbial source for most of these fossil microbodies and impressions has not been eliminated, we question the validity of reconstructing organismal colour based on the external structure of fossil microbodies alone and conclude that rigorous extant correlations with the same anatomical

sources (i.e. comparing skin with skin and feathers with feathers) offer the only accurate paradigm for reliable interpretations.

6. A way forward: integrated morphological and geochemical approaches

The intrinsic resistance of melanin to degradation (except in the presence of cells/enzymes targeted specifically against it) and its preservation in fossils highlight significant potential for elucidating the biology of extinct organisms. Nevertheless, such interpretations are inherently equivocal, and further complicated by the fact that microbes: (1) overlap in size, shape and preservation potential with melanosomes; (2) can produce melanins; and (3) are innately associated with decaying organics [12]. Judicious elimination of alternative hypotheses for the origin of microbodies in fossils is therefore necessary prior to extrapolations of colour or function. While SEM imaging of external morphology and organisation provides a viable first step, it is not sufficient for a definitive diagnosis [12]. To augment morphology, higher resolution images should therefore be obtained from field emission gun scanning electron microscopy (FEG-SEM), which can reveal distinctive surface features, such as melanin granules (e.g. [56, fig. 2c]). TEM imaging can also yield complementary information about internal structures. Generally, microbial cells have an electron lucent core ([12, fig. 4], [79, figs 7, 9–13], [80, fig. 1]), as opposed to the electron opaque interior of mature melanosomes (see [61, electronic supplementary material, fig. S2], [81, fig. 3]). Exceptions do exist, however, such as hollow melanosomes [82] and solid, ‘carbonized’ bacteria [16, fig. 7c]. Therefore, for confident identification, chemical fingerprints of eumelanins, pheomelanins and/or their degradation products must be localized to the fossil microbodies (e.g. [56,59–61]). Ideally, these biomarkers should not occur only as trace metals because microbes and the EPS they secrete can concentrate metal ions from the environment [83]. Thus, elevated trace metal levels in fossilized animal tissues could be bacterially mediated [84,85] or artificially concentrated during diagenesis [11]. Furthermore, many enzymes employed by microbes to degrade keratinized tissues (including both white and pigmented feathers) are metalloenzymes that use a variety of metal ions which deposit on keratin surfaces during decomposition [86].

(a) Case study: structural and molecular identification of fossil melanosomes

To illustrate a proposed set of practical parameters for detecting endogenous pigment biomarkers and associated microstructures in an exemplary fossil, we undertook a series of stepwise microscopic and chemical analyses on microbodies obtained from the preserved ‘eye’ of a teleost fish (FUM-N-2268; MUSERUM) from the early Eocene of Denmark (figures 1 and 2; electronic supplementary material, figures S2–S6).

Initial macroscopic examination of the orbital residue showed a clearly delineated accumulation of a dense, brown substance that was superficially amorphous but distinct from the surrounding sediment in both texture and colour (figure 1*a,b*). FEG-SEM imaging revealed its composition to be a morphologically heterogeneous mass of spherical, oval and elongate bodies ranging from 0.2 to 3 μm in length (figure 1*c,d*). These structures were tightly

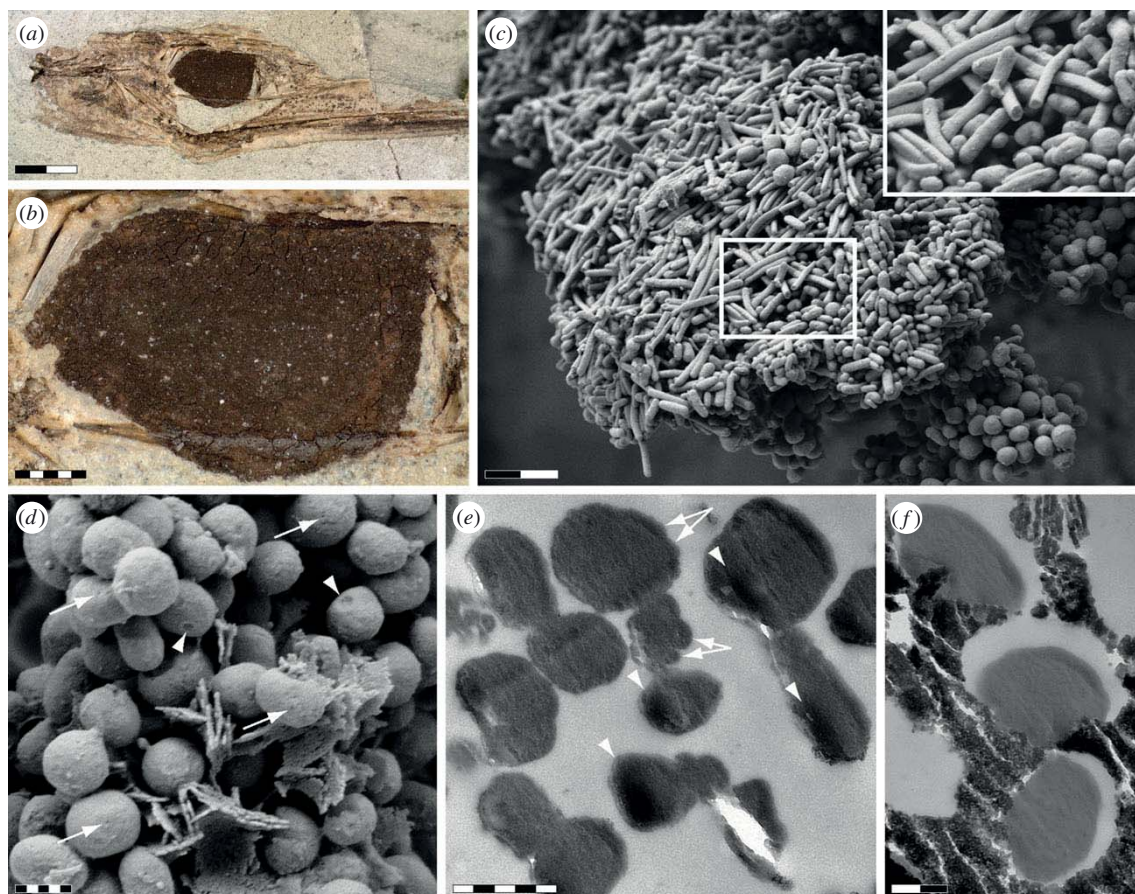


Figure 1. (a) Articulated skull of FUM-N-2268A. (b) Enlargement showing organic matter within the orbital cavity. (c) FEG-SEM micrograph of massed microbodies revealing morphological variation consistent with retinal melanosomes found in extant vertebrate eyes. Inset details elongate microbodies with homogeneous interior structure. (d) Surface pits (arrows) and depressions (arrowheads) on densely packed sub-spherical microbodies, the latter probably produced by diagenetic compression. Lamellar structures are infiltrating sedimentary matrix. Note distinct size difference between moulds formed by diagenetic minerals and microbodies (see also *f*). (e) TEM micrograph of sectioned, unstained microbodies exposing external nodules (arrows) and electron-dense interior. Corrugated internal texture might be diagenetic; darker coloration (arrowheads) may represent replacement by inorganic material, possibly (based on ToF-SIMS data) iron sulfate. (f) TEM micrograph indicating diagenetic shrinkage of microbodies within the enclosing matrix. Scale bars: (a) 2 mm; (b) 500 μm ; (c) 2 μm ; (d,e) 500 nm; (f) 200 nm.

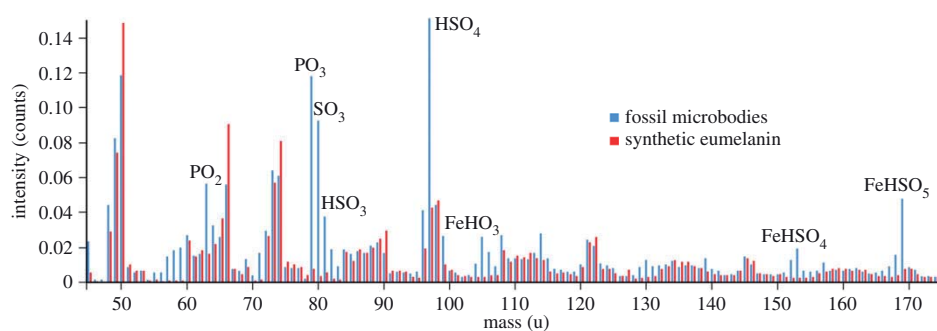


Figure 2. Negative ion ToF-SIMS spectra collected from fossil microbodies located within the 'eye spot' of FUM-N-2268 ('fossil microbodies') and synthetic eumelanin. Bars represent the integrated signal intensity at each nominal mass (the spectra are normalized to the sum intensity of the major eumelanin peaks). Peaks in the fossil spectrum that are not present in the eumelanin spectrum correspond to inorganic ions (as indicated), sulfur-containing organic ions (C_2HS^- at 57 u, CSN^- at 58 u and C_3SN^- at 82 u) and oxygen-containing organic ions ($\text{C}_2\text{H}_3\text{O}_2^-$ at 59 u and $\text{C}_3\text{H}_3\text{O}_2^-$ at 71 u), respectively.

packed but showed limited spatial overlap. Instead, some areas were characterized by stacks of rod-shaped microbodies (figure 1c), whereas other regions showed a predominance of globular forms (figure 1d). Superficially, the exterior surface of all microbodies appeared to be fairly smooth; however,

closer inspection revealed a fine granular fabric incorporating randomly scattered pits (figure 1d—arrows) and depressions (figure 1d—arrowheads).

TEM imaging of sectioned microbodies exposed a corrugated, electron-dense interior (figure 1e,f). A darker coloration in

some areas could indicate replacement of the presumed organic matter (see below) by inorganic material (figure 1e—arrowheads). A notable size difference between natural moulds formed by precipitated minerals and the microbodies indicates that the latter may have contracted during the fossilization process (figure 1d,f).

Energy dispersive X-ray microanalysis (EDX) identified carbon as the primary constituent in the orbital residue, with minor contributions from other elements, such as sulfur.

ToF-SIMS analysis targeting the fossil microbodies yielded mass spectra consistent with comparative data from synthetic and natural eumelanins, but which excluded pheomelanin and pyomelanin as significant surface components (figure 2; electronic supplementary material, figures S2–S5). Deviations were identified as ionic constituents of the sedimentary matrix (including phosphate and sulfate), as well as iron sulfate and sulfur-containing organics (figure 2; electronic supplementary material, figure S2). The latter suggest diagenetic incorporation of sulfur into the eumelanin macromolecule [56,61], or alternatively represent derivatives from a minor pheomelanin component.

These data were corroborated by IR microspectroscopic measurements, which produced broad-band absorbance in the 900–1800 and 2500–3700 cm^{-1} regions, consistent with natural eumelanin (electronic supplementary material, figure S6).

(b) Rationale for assignment of the fossil microbodies to remnant melanosomes

The co-localization of melanin and microbodies in the ‘eye spot’ of FUM-N-2268 advocates a common source, but whether this is endogenous or exogenous remains to be determined. Alternative hypotheses exist: (1) the minute bodies could be the fossilized remains of ocular melanosomes preserved as melanin ‘pseudomorphs’ with a morphology replicating that of the original melanosomes; (2) they might also represent preserved invasive microbes and/or their spores; or (3) be a mixture of both endogenous and exogenous melanin sources.

To discriminate between these possibilities, we first tested for hollowness and the presence/absence of budding scars indicative of fungal melanin ghosts. TEM imaging accordingly showed that the FUM-N-2268 microbodies were solid, unlike melanin ghosts. Even though intracellular melanogenesis has been documented in some microorganisms, the process is toxic and potentially inhibitory to cell growth [48]. Hence, internal microbial melanins are restricted to either small spots or rare globular aggregates [43,48], inconsistent with the pattern observed in this sample. To the best of our knowledge, no extant microorganism undergoes cytoplasmic melanin production to such an extent that it obscures all other cellular details. Additionally, although shallow, circular depressions exist on the surface of some microbodies, they do not exhibit the typical characteristics of budding scars (see [44, fig. 5]). Instead, these marks are most likely diagenetic, being formed during compaction when the microbodies were pressed against one another.

EDX analysis detected carbon and sulfur in the ‘eye’ residue. These elements are components of melanin but also occur in bacterial biofilms [87]. Hence, they are insufficient to determine the affinity of the fossil microbodies. On the other hand, the predominance of eumelanin biomarkers in intimate association with the bodies (as evidenced by ToF-SIMS analysis) allows more confident determination. Eumelanin is the

primary biochrome in vertebrate ocular melanosomes [76]. Moreover, modern vertebrate eyes contain a number of melanin-housing tissues, including the iris, retina and choroid [76]. Of these, the retinal pigment epithelium (RPE) is notable for its disparity in melanosome shapes and sizes (e.g. [24, fig. 1]). Furthermore, despite being located adjacent to one another, the various morphologies occur in functionally different parts of the RPE: rod-shaped forms proliferating in the apical processes wrapping the photoreceptor outer segments [88, fig. 6], and spherical forms dominating the basal cytoplasm immediately below the apical region [89]. Post-mortem degradation and subsequent collapse of the RPE and attendant tissues will inevitably result in a partial mixture of melanosome morphologies via stacking and/or close proximal packing (electronic supplementary material, figure S7), a distributional pattern consistent with that observed in FUM-N-2268. Conversely, if the fossil microbodies represent invading microorganisms, then multiple unrelated eumelanin-producing microbes, each with the ability to survive massive cytoplasmic melanin accumulation, must have independently colonized the orbital cavity during the decay of this fish. We deem this to be highly unlikely, and instead advocate a more parsimonious explanation of the microbodies as endogenous, being the fossilized remains of ocular melanosomes.

7. Summary

Organismal colour holds deep fascination because species recognition, gender differences and many other traits are intimately linked to pigmented epidermal tissues. There is no doubt that biochromes were, and are, an integral substrate for natural selection. Indeed, the various patterns, hues and shades that we observe today unquestionably also had equivalents in the distant past. Hence, characterizing pigments in extinct animals has enormous potential to shed light on evolutionary aspects of biology and ecology. Despite this, the study of colour through deep time is still very much in its infancy and can be impinged by numerous experimental pitfalls. Caution should therefore be exercised in this endeavour. Illuminating aspects of ancient organismal colour is achievable only by thorough evaluation of all plausible hypotheses. These remain valid until disproven and should not be swayed by popular opinion. Developing a comprehensive understanding of exceptional preservation processes through careful actualistic experiments must also be augmented by knowledge of diagenetic effects and how they potentially alter the morphology and chemistry of microbodies associated with decaying organics. Such approaches will ultimately facilitate more rigorous interpretations and reduce the risk of spectacular yet insufficiently supported claims propagating in the literature.

Data accessibility. FUM-N-2268 is deposited at MUSERUM. Additional supporting data can be accessed from the Department of Geology, Lund University.

Authors' contributions. J.L., A.M., M.H.S., D.E.N. and B.P.K. wrote the manuscript. J.L., A.M., P.S. and P.U. made the illustrations. J.L., A.M., P.S., P.U., J.H., A.E. and J.A.G. performed the analyses and interpreted the data. B.P.S. provided access to FUM-N-2268. All of the authors discussed the results and content of the manuscript.

Competing interests. We have no competing interests.

Funding. This research was supported by the Swedish Research Council, the Royal Physiographical Society in Lund and the Crafoord

Foundation to J.L., the David and Lucile Packard Foundation to M.H.S., and the US National Science Foundation to M.H.S. and A.M. **Acknowledgements.** Carina Rasmussen isolated melanosomes from a zebra obliquidens. Ola Gustafsson assisted during the SEM and TEM

analyses. Niels Christensen Bonde provided taxonomic information on FUM-N-2268. The micrographs in electronic supplementary material, figure S1, are credited to J. W. Costerton archives, courtesy MSU Center for Biofilm Engineering.

References

- Briggs DEG, Summons RE. 2014 Ancient biomolecules: their origins, fossilization, and role in revealing the history of life. *Bioessays* **36**, 482–490. (doi:10.1002/bies.201400010)
- Wuttke M. 1983 'Weichteil-Erhaltung' durch lithifizierte Mikroorganismen bei mittel-eozänen Vertebraten aus den Ölschiefern der 'Grube Messel' bei Darmstadt. *Senck. Leth.* **64**, 509–527.
- Franzen JL. 1985 Exceptional preservation of Eocene vertebrates in the lake deposit of Grube Messel (West Germany). *Phil. Trans. R. Soc. Lond. B* **311**, 181–186. (doi:10.1098/rstb.1985.0150)
- Davis PG, Briggs DEG. 1995 Fossilization of feathers. *Geology* **23**, 783–786. (doi:10.1130/0091-7613(1995)023<0783:FOF>2.3.CO;2)
- Toporski JKW, Steele A, Westall F, Avci R, Martill DM, McKay DS. 2002 Morphologic and spectral investigation of exceptionally well-preserved bacterial biofilms from the Oligocene Enspel formation, Germany. *Geochim. Cosmochim. Acta* **66**, 1773–1791. (doi:10.1016/S0016-7037(01)00870-5)
- Voigt E. 1988 Preservation of soft tissues in the Eocene lignite of the Geiseltal near Halle/S. *Cour. Forsch. Inst. Senck.* **107**, 325–343.
- Vinther J, Briggs DEG, Prum RO, Saranathan V. 2008 The colour of fossil feathers. *Biol. Lett.* **4**, 522–525. (doi:10.1098/rsbl.2008.0302)
- Li Q, Gao K-Q, Vinther J, Shawkey MD, Clarke JA, D'Alba L, Meng Q, Briggs DEG, Prum RO. 2010 Plumage color patterns of an extinct dinosaur. *Science* **327**, 1369–1372. (doi:10.1126/science.1186290)
- Li Q *et al.* 2012 Reconstruction of *Microraptor* and the evolution of iridescent plumage. *Science* **335**, 1215–1219. (doi:10.1126/science.1213780)
- Li Q, Clarke JA, Gao K-Q, Zhou C-F, Meng Q, Li D, D'Alba L, Shawkey MD. 2014 Melanosome evolution indicates a key physiological shift within feathered dinosaurs. *Nature* **507**, 350–353. (doi:10.1038/nature12973)
- Edwards NP, Manning PL, Wogelius RA. 2014 Pigments through time. *Pigment Cell Melanoma Res.* **27**, 684–685. (doi:10.1111/pcmr.12271)
- Moyer AE, Zheng W, Johnson EA, Lamanna MC, Li D-Q, Lacovara KJ, Schweitzer MH. 2014 Melanosomes or microbes: testing an alternative hypothesis for the origin of microbodies in fossil feathers. *Sci. Rep.* **4**, 4233. (doi:10.1038/srep04233)
- Knight TK, Bingham PS, Lewis RD, Savrda CE. 2011 Feathers of the Ingersoll Shale, Eutaw Formation (Upper Cretaceous), eastern Alabama: the largest collection of feathers from North American Mesozoic rocks. *Palaio* **26**, 364–376. (doi:10.2110/palo.2010.p10-091r)
- Barden HE, Wogelius RA, Li D, Manning PL, Edwards NP, van Dongen BE. 2011 Morphological and geochemical evidence of eumelanin preservation in the feathers of the Early Cretaceous bird, *Gansus yumenensis*. *PLoS ONE* **6**, e25494. (doi:10.1371/journal.pone.0025494)
- Pacton M, Fiet N, Gorin G. 2006 Revisiting amorphous organic matter in Kimmeridgian laminites: what is the role of the vulcanization process in the amorphization of organic matter? *Terra Nova* **18**, 380–387. (doi:10.1111/j.1365-3121.2006.00702.x)
- Preston LJ, Shuster J, Fernández-Remolar D, Banerjee NR, Osinski GR, Southam G. 2011 The preservation and degradation of filamentous bacteria and biomolecules within iron oxide deposits at Rio Tinto, Spain. *Geobiology* **9**, 233–249. (doi:10.1111/j.1472-4669.2011.00275.x)
- Westall F. 1999 The nature of fossil bacteria: a guide to the search for extraterrestrial life. *J. Geophys. Res.* **104**, 16 437–16 451. (doi:10.1029/1998JE900051)
- Plonka PM, Grabacka M. 2006 Melanin synthesis in microorganisms—biotechnological and medical aspects. *Acta Biochim. Polon.* **53**, 429–443.
- Gospodaryov D, Lushchak V. 2011 Some properties of melanin produced by *Azotobacter chroococcum* and its possible application in biotechnology. *Biotechnol. Acta* **4**, 61–69.
- Beimforde C, Schäfer N, Dörfelt H, Nascimbene PC, Singh H, Heinrichs J, Reitner J, Rana RS, Schmidt AR. 2011 Ectomycorrhizas from a lower Eocene angiosperm forest. *New Phytol.* **192**, 988–996. (doi:10.1111/j.1469-8137.2011.03868.x)
- Liu Y, Hong L, Wakamatsu K, Ito S, Adhyaru B, Cheng C-Y, Bowers CR, Simon JD. 2005 Comparisons of the structural and chemical properties of black and red human hair melanosomes. *Photochem. Photobiol.* **81**, 135–144. (doi:10.1562/2004-08-03-RA-259.1)
- Simon JD, Peles DN. 2010 The red and the black. *Acc. Chem. Res.* **43**, 1452–1460. (doi:10.1021/ar100079y)
- Zareba M, Szweczyk G, Sarna T, Hong L, Simon JD, Henry MM, Burke JM. 2006 Effects of photodegradation on the physical and antioxidant properties of melanosomes isolated from retinal pigment epithelium. *Photochem. Photobiol.* **82**, 1024–1029. (doi:10.1562/2006-03-08-RA-836)
- Lopes VS, Wasmeier C, Seabra MC, Futter CE. 2007 Melanosome maturation defect in Rab38-deficient retinal pigment epithelium results in instability of immature melanosomes during transient melanogenesis. *Mol. Biol. Cell* **18**, 3914–3927. (doi:10.1091/mbc.E07-03-0268)
- Riley PA. 1997 Melanin. *Int. J. Biochem. Cell Biol.* **29**, 1235–1239. (doi:10.1016/S1357-2725(97)00013-7)
- Kaxiras E, Tsolakidis A, Zonios G, Meng S. 2006 Structural model of eumelanin. *Phys. Rev. Lett.* **97**, 218102-1–218102-4. (doi:10.1103/PhysRevLett.97.218102)
- Banerjee A, Supakar S, Banerjee R. 2014 Melanin from the nitrogen-fixing bacterium *Azotobacter chroococcum*: a spectroscopic characterization. *PLoS ONE* **9**, e84574. (doi:10.1371/journal.pone.0084574)
- Simon JD, Hong L, Peles DN. 2008 Insights into melanosomes and melanin from some interesting spatial and temporal properties. *J. Phys. Chem. B* **112**, 13 201–13 217. (doi:10.1021/jp804248h)
- Wasmeier C, Hume AN, Bolasco G, Seabra MC. 2008 Melanosomes at a glance. *J. Cell Sci.* **121**, 3995–3999. (doi:10.1242/jcs.040667)
- Dubey S, Roulin A. 2014 Evolutionary and biomedical consequences of internal melanosins. *Pigment Cell Melanoma Res.* **27**, 327–338. (doi:10.1111/pcmr.12231)
- Broekhuysen RM, Kuhlmann ED, Winkens HJ. 1993 Experimental autoimmune anterior uveitis (EAAU). III. Induction by immunization with purified uveal and skin melanosins. *Exp. Eye Res.* **56**, 575–583. (doi:10.1006/exer.1993.1071)
- Chen KG, Leapman RD, Zhang G, Lai B, Valencia JC, Cardarelli CO, Vieira WD, Hearing VJ, Gottesman MM. 2009 Influence of melanosome dynamics on melanoma drug sensitivity. *J. Natl. Cancer Inst.* **101**, 1259–1271. (doi:10.1093/jnci/djp259)
- Ortolani-Machado CF, Freitas PF, Faraco CD. 2009 Melanogenesis in dermal melanocytes of Japanese silky chicken embryos. *Tissue Cell* **41**, 239–248. (doi:10.1016/j.tice.2008.11.005)
- Liu Y, Simon JD. 2003 Isolation and biophysical studies of natural eumelanins: applications of imaging technologies and ultrafast spectroscopy. *Pigment Cell Res.* **16**, 606–618. (doi:10.1046/j.1600-0749.2003.00098.x)
- Akazaki S *et al.* 2014 Three-dimensional analysis of melanosomes isolated from B16 melanoma cells by using ultra high voltage electron microscopy. *Microsc. Res.* **2**, 1–8. (doi:10.4236/mr.2014.21001)
- Liu Y, Kempf VR, Nofsinger JB, Weinert EE, Rudnicki M, Wakamatsu K, Ito S, Simon JD. 2003 Comparisons of the structural and chemical properties of human hair eumelanin following enzymatic and acid/base extraction. *Pigment Cell Res.* **16**, 355–365. (doi:10.1034/j.1600-0749.2003.00059.x)
- Peles DN, Hong L, Hu D-N, Ito S, Nemanich RJ, Simon JD. 2009 Human iridal stroma melanosomes

- of varying pheomelanin contents possess a common eumelanin outer surface. *J. Phys. Chem. B* **113**, 11 346–11 351. (doi:10.1021/jp904138n)
38. Agrup G, Hansson C, Rorsman H, Rosengren E. 1982 The effect of cysteine on oxidation of tyrosine, dopa, and cysteinyl dopas. *Arch. Dermatol. Res.* **272**, 103–115. (doi:10.1007/BF00510400)
39. Gorniak T *et al.* 2014 Support and challenges to the melanosomal casing model based on nanoscale distribution of metals within iris melanosomes detected by X-ray fluorescence analysis. *Pigment Cell Melanoma Res.* **27**, 831–834. (doi:10.1111/pcmr.12278)
40. Solano F. 2014 Melanins: skin pigments and much more—types, structural models, biological functions, and formation routes. *N. J. Sci.* **2014**, 498276. (doi:10.1155/2014/498276)
41. Romero-Martinez R, Wheeler M, Guerrero-Plata A, Rico G, Torres-Guerrero H. 2000 Biosynthesis and functions of melanin in *Sporothrix schenckii*. *Inf. Immunol.* **68**, 3696–3703. (doi:10.1128/IAI.68.6.3696-3703.2000)
42. Kizil'shtein LY, Shpitsgluz AL. 2014 The structure of fossil fungal spores based on the results of ion etching. *Solid Fuel Chem.* **48**, 81–84. (doi:10.3103/S0361521914020062)
43. Alviano CS, Farbiarz SR, de Souza W, Angluster J, Travassos LR. 1991 Characterization of *Fonsecaea pedrosoi* melanin. *J. Gen. Microbiol.* **137**, 837–844. (doi:10.1099/00221287-137-4-837)
44. Eisenman HC, Nosanchuk JD, Webber JBW, Emerson RJ, Camesano TA, Casadevall A. 2005 Microstructure of cell wall-associated melanin in the human pathogenic fungus *Cryptococcus neoformans*. *Biochemistry* **44**, 3683–3693. (doi:10.1021/bi047731m)
45. Nosanchuk JD, Casadevall A. 2003 The contribution of melanin to microbial pathogenesis. *Cell. Microbiol.* **5**, 203–223. (doi:10.1046/j.1462-5814.2003.00268.x)
46. Tarangini K, Mishra S. 2013 Production, characterization and analysis of melanin from isolated marine *Pseudomonas* sp. using vegetable waste. *Res. J. Eng. Sci.* **2**, 40–46.
47. Agodi A, Stefani S, Corsaro C, Campanile F, Gribaldo S, Sichel G. 1996 Study of melanic pigment of *Proteus mirabilis*. *Res. Microbiol.* **147**, 167–174. (doi:10.1016/0923-2508(96)80216-6)
48. Geng J, Yuan P, Shao C, Yu S-B, Zhou B, Zhou P, Chen X-D. 2010 Bacterial melanin interacts with double-stranded DNA with high affinity and may inhibit cell metabolism *in vivo*. *Arch. Microbiol.* **192**, 321–329. (doi:10.1007/s00203-010-0560-1)
49. McKenney PT, Driks A, Eichenberger P. 2013 The *Bacillus subtilis* endospore: assembly and functions of the multilayered coat. *Nat. Rev. Microbiol.* **11**, 33–44. (doi:10.1038/nrmicro2921)
50. Voigt E. 1936 Über das Haarkleid einiger Säugetiere aus der mitteleozänen Braunkohle des Geiseltales. *Nova Acta Leopoldina* **4**, 317–334.
51. Beyermann K, Hasenmaier D. 1973 Identifizierung 180 Millionen Jahre alten, wharscheinlich unverändert erhaltenen Melanins. *Zeitschrift Anal. Chem.* **266**, 202–205. (doi:10.1007/BF00428061)
52. Vinther J, Briggs DEG, Clarke J, Mayr G, Prum RO. 2010 Structural coloration in a fossil feather. *Biol. Lett.* **6**, 128–131. (doi:10.1098/rsbl.2009.0524)
53. Zhang F, Kearns SL, Orr PJ, Benton MJ, Zhou Z, Johnson D, Xu X, Wang X. 2010 Fossilized melanosomes and the colour of Cretaceous dinosaurs and birds. *Nature* **463**, 1075–1078. (doi:10.1038/nature08740)
54. Carney RM, Vinther J, Shawkey MD, D'Alba L, Ackermann J. 2012 New evidence on the colour and nature of the isolated *Archaeopteryx* feather. *Nat. Commun.* **3**, 637. (doi:10.1038/ncomms1642)
55. Manning PL *et al.* 2013 Synchrotron-based chemical imaging reveals plumage patterns in a 150 million year old early bird. *J. Anal. At. Spectrom.* **28**, 1024–1030. (doi:10.1039/c3ja50077b)
56. Lindgren J *et al.* 2014 Skin pigmentation provides evidence of convergent melanism in extinct marine reptiles. *Nature* **506**, 484–488. (doi:10.1038/nature12899)
57. Vinther J. 2015 A guide to the field of palaeo colour: melanin and other pigments can fossilise: reconstructing colour patterns from ancient organisms can give new insights to ecology and behaviour. *Bioessays* **37**, 643–656. (doi:10.1002/bies.201500018)
58. Schweitzer MH. 2011 Soft tissue preservation in terrestrial Mesozoic vertebrates. *Annu. Rev. Earth Planet. Sci.* **39**, 187–216. (doi:10.1146/annurev-earth-040610-133502)
59. Glass K *et al.* 2012 Direct chemical evidence for eumelanin pigment from the Jurassic period. *Proc. Natl Acad. Sci. USA* **109**, 2118–2123. (doi:10.1073/pnas.1118448109)
60. Glass K *et al.* 2013 Impact of diagenesis and maturation on the survival of eumelanin in the fossil record. *Org. Geochem.* **64**, 29–37. (doi:10.1016/j.orggeochem.2013.09.002)
61. Lindgren J, Uvdal P, Sjövall P, Nilsson DE, Engdahl A, Schultz BP, Thiel V. 2012 Molecular preservation of the pigment melanin in fossil melanosomes. *Nat. Commun.* **3**, 824. (doi:10.1038/ncomms1819)
62. Clarke JA, Ksepka DT, Salas-Gismondi R, Altamirano AJ, Shawkey MD, D'Alba L, Vinther J, DeVries TJ, Baby P. 2010 Fossil evidence for evolution of the shape and color of penguin feathers. *Science* **330**, 954–957. (doi:10.1126/science.1193604)
63. Barden HE, Bergmann U, Edwards NP, Egerton VM, Manning PL, Perry S, van Veelen A, Wogelius RA, van Dongen BE. 2015 Bacteria or melanosomes? A geochemical analysis of micro-bodies on a tadpole from the Oligocene Enspel Formation of Germany. *Palaebio. Palaeoenv.* **95**, 33–45. (doi:10.1007/s12549-014-0177-5)
64. Wogelius RA *et al.* 2011 Trace metals as biomarkers for eumelanin pigment in the fossil record. *Science* **333**, 1622–1626. (doi:10.1126/science.1205748)
65. Egerton VM *et al.* 2015 The mapping and differentiation of biological and environmental signatures in the fossil remains of a 50 million year old bird. *J. Anal. At. Spectrom.* **30**, 627–634. (doi:10.1039/C4JA00395K)
66. Borovanský J, Elleder M. 2003 Melanosome degradation: fact or fiction. *Pigment Cell Res.* **16**, 280–286. (doi:10.1034/j.1600-0749.2003.00040.x)
67. Ohtaki N, Seiji M. 1971 Degradation of melanosomes by lysosomes. *J. Invest. Dermatol.* **57**, 1–5. (doi:10.1111/1523-1747.ep12292038)
68. Borovanský J, Hach P, Duchoň J. 1977 Melanosome: an unusually resistant subcellular particle. *Cell Biol. Int. Rep.* **1**, 549–554. (doi:10.1016/0309-1651(77)90093-5)
69. Goldstein G, Flory KR, Browne BA, Majid S, Ichida JM, Burt Jr EH. 2004 Bacterial degradation of black and white feathers. *Auk* **121**, 656–659. (doi:10.1642/0004-8038(2004)121[0656:BDOBAW]2.0.CO;2)
70. Keefe JR. 1973 An analysis of urodelian retinal regeneration. III. Degradation of extruded melanin granules in *Notophthalmus viridescens*. *J. Exp. Zool.* **184**, 233–237. (doi:10.1002/jez.1401840208)
71. Kordylewski L. 1983 An ultrastructural study of the melanophages in the cerebrospinal fluid of the tadpoles of *Xenopus*. *J. Morph.* **176**, 315–324. (doi:10.1002/jmor.1051760305)
72. Gunderson AR, Frame AM, Swaddle JP, Forsyth MH. 2008 Resistance of melanized feathers to bacterial degradation: is it really so black and white? *J. Avian Biol.* **39**, 539–545. (doi:10.1111/j.0908-8857.2008.04413.x)
73. Jawor JM, Breitwisch R. 2003 Melanin ornaments, honesty, and sexual selection. *Auk* **120**, 249–265. (doi:10.1642/0004-8038(2003)120[0249:MOHASS]2.0.CO;2)
74. McGraw KJ. 2008 An update on the honesty of melanin-based color signals in birds. *Pigment Cell Melanoma Res.* **21**, 133–138. (doi:10.1111/j.1755-148X.2008.00454.x)
75. McNamara ME, Briggs DEG, Orr PJ, Field DJ, Wang Z. 2013 Experimental maturation of feathers: implications for reconstructions of fossil feather colour. *Biol. Lett.* **9**, 20130184. (doi:10.1098/rsbl.2013.0184)
76. Liu Y, Hong L, Wakamatsu K, Ito S, Adhyaru BB, Cheng C-Y, Bowers CR, Simon JD. 2005 Comparisons of the structural and chemical properties of melanosomes isolated from retinal pigment epithelium, iris and choroid of newborn and mature bovine eyes. *Photochem. Photobiol.* **81**, 510–516. (doi:10.1562/2004-10-19-RA-345.1)
77. Tanaka G *et al.* 2014 Mineralized rods and cones suggest colour vision in a 300 Myr-old fossil fish. *Nat. Commun.* **5**, 5920. (doi:10.1038/ncomms6920)
78. Liu SY, Shawkey MD, Parkinson D, Troy TP, Ahmed M. 2014 Elucidation of the chemical composition of avian melanin. *RSC Adv.* **4**, 40 396–40 399. (doi:10.1039/C4RA06606E)
79. Sergeev VN, Knoll AH, Grotzinger JP. 1995 Paleobiology of the Mesoproterozoic Billyakh Group, Anabar Uplift, northern Siberia. *Paleontol. Soc. Mem.* **1995**, 1–37.
80. Igsu M, Ueno Y, Shimojima M, Nakashima S, Awramik SM, Ohta H, Maruyama S. 2009 Micro-FTIR spectroscopic signatures of bacterial lipids in

- Proterozoic microfossils. *Precambrian Res.* **173**, 19–26. (doi:10.1016/j.precamres.2009.03.006)
81. Pfeiffer CJ, Jones FM. 1993 Epidermal lipid in several cetacean species: ultrastructural observations. *Anat. Embryol.* **188**, 209–218. (doi:10.1007/BF00188213)
82. Eliason CM, Bitton P-P, Shawkey MD. 2013 How hollow melanosomes affect iridescent colour production in birds. *Proc. R. Soc. B* **280**, 20131505. (doi:10.1098/rspb.2013.1505)
83. Hitchcock AP, Dynes JJ, Lawrence JR, Obst M, Swerhone GDW, Korber DR, Leppard GG. 2009 Soft X-ray spectromicroscopy of nickel sorption in a natural river biofilm. *Geobiology* **7**, 432–453. (doi:10.1111/j.1472-4669.2009.00211.x)
84. Choi DW *et al.* 2006 Spectral, kinetic, and thermodynamic properties of Cu(I) and Cu(II) binding by methanobactin from *Methylosinus trichosporium* OB3b. *Biochemistry* **45**, 1442–1453. (doi:10.1021/bi051815t)
85. Choi DW *et al.* 2006 Spectral and thermodynamic properties of Ag(I), Au(III), Cd(II), Co(II), Fe(III), Hg(II), Mn(II), Ni(II), Pb(II), U(IV), and Zn(II) binding by methanobactin from *Methylosinus trichosporium* OB3b. *J. Inorg. Biochem.* **100**, 2150–2161. (doi:10.1016/j.jinorgbio.2006.08.017)
86. Gupta R, Ramnani P. 2006 Microbial keratinases and their prospective applications: an overview. *Appl. Microbiol. Biotechnol.* **70**, 21–33. (doi:10.1007/s00253-005-0239-8)
87. Kühl M, Jørgensen BB. 1992 Microsensor measurements of sulfate reduction and sulfide oxidation in compact microbial communities of aerobic biofilms. *Appl. Environ. Microbiol.* **58**, 1164–1174.
88. Zang Q-X, Lu R-W, Messinger JD, Curcio CA, Guarcello V, Yao X-C. 2013 *In vivo* optical coherence tomography of light-driven melanosome translocation in retinal pigment epithelium. *Sci. Rep.* **3**, 2644.
89. Kim IT, Choi JB. 1998 Melanosomes of retinal pigment epithelium—distribution, shape, and acid phosphatase activity. *Korean J. Ophthalmol.* **12**, 85–91. (doi:10.3341/kjo.1998.12.2.85)

“Exakt! Men hur?”



PAPER IV

Overleaf: SEM image of a sectioned feather barb from a modern bird (*Corvus* sp.)

SCIENTIFIC REPORTS

OPEN

Molecular composition and ultrastructure of Jurassic paravian feathers

Received: 10 April 2015
Accepted: 29 July 2015
Published: 27 August 2015

Johan Lindgren¹, Peter Sjövall², Ryan M. Carney³, Aude Cincotta^{4,5}, Per Uvdal^{6,7}, Steven W. Hutcheson⁸, Ola Gustafsson⁹, Ulysse Lefèvre^{4,10}, François Escuillié¹¹, Jimmy Heimdal⁶, Anders Engdahl⁶, Johan A. Gren¹, Benjamin P. Kear^{12,13}, Kazumasa Wakamatsu¹⁴, Johan Yans⁵ & Pascal Godefroit⁴

Feathers are amongst the most complex epidermal structures known, and they have a well-documented evolutionary trajectory across non-avian dinosaurs and basal birds. Moreover, melanosome-like microbodies preserved in association with fossil plumage have been used to reconstruct original colour, behaviour and physiology. However, these putative ancient melanosomes might alternatively represent microorganismal residues, a conflicting interpretation compounded by a lack of unambiguous chemical data. We therefore used sensitive molecular imaging, supported by multiple independent analytical tests, to demonstrate that the filamentous epidermal appendages in a new specimen of the Jurassic paravian *Anchiornis* comprise remnant eumelanosomes and fibril-like microstructures, preserved as endogenous eumelanin and authigenic calcium phosphate. These results provide novel insights into the early evolution of feathers at the sub-cellular level, and unequivocally determine that melanosomes can be preserved in fossil feathers.

The Middle-Late Jurassic fossil assemblage found in the Tiaojishan Formation of Liaoning Province in northeastern China has yielded unparalleled evidence on the early evolution of birds^{1–4}. Most importantly, the identification of various feather-like integumental appendages in non-avian and stem avialan theropods has illuminated the diversity and distribution of plumage structures during their adaptive transition towards use in flight⁴. Epidermal traces in the Tiaojishan Formation are preserved as either faint impressions or phosphatised and carbonised residues^{4,5}. The latter were long thought to be a product of keratin-degrading bacteria⁶. However, more recent interpretations have favoured fossilised melanosomes; that is, melanin-bearing cellular organelles responsible in part for the colouration of skin and its structural derivatives⁷. This landmark hypothesis has spawned an entirely new field of exploratory inference into dinosaurian colour^{5,7–11}, behaviour⁵ and physiology¹².

¹Department of Geology, Lund University, 223 62 Lund, Sweden. ²SP Technical Research Institute of Sweden, Chemistry, Materials and Surfaces, 501 15 Borås, Sweden. ³Department of Ecology and Evolutionary Biology, Brown University, Providence, Rhode Island 02906, USA. ⁴Operational Direction 'Earth and History of Life', Royal Belgian Institute of Natural Sciences, 1000 Brussels, Belgium. ⁵Department of Geology, University of Namur, 5000 Namur, Belgium. ⁶MAX-IV laboratory, Lund University, 221 00 Lund, Sweden. ⁷Chemical Physics, Department of Chemistry, Lund University, 221 00 Lund, Sweden. ⁸Department of Cell Biology and Molecular Genetics, University of Maryland, College Park, Maryland 20742, USA. ⁹Department of Biology, Lund University, 223 62 Lund, Sweden. ¹⁰Department of Geology, Liège University, 4000 Liège, Belgium. ¹¹Eldonia, 9 Avenue des Portes Occitanes, 3800 Gannat, France. ¹²Museum of Evolution, Uppsala University, 752 36 Uppsala, Sweden. ¹³Palaeobiology Programme, Department of Earth Sciences, Uppsala University, 752 36 Uppsala, Sweden. ¹⁴Department of Chemistry, Fujita Health University School of Health Sciences, Toyoake, Aichi 470-1192, Japan. Correspondence and requests for materials should be addressed to J.L. (email: johan.lindgren@geol.lu.se)

Nevertheless, it has also met with vivid debate (see ref. 13 for review). This centres on the observation that microbes colonising the epidermal tissues during decay are virtually indistinguishable from the melanosome-like microbodies recognised in fossils^{14,15}. Such criticism is aggravated by the lack of unequivocal molecular traces from melanic pigments in ancient feathers and feather-like appendages^{15,16}. Indeed, claims of melanosomes found in the plumage of non-avian dinosaurs and stem avialans have fundamentally relied upon external morphology^{5,7–12}, but this is demonstrably inadequate for discriminating pigment organelles from pervasive bacteria¹⁵. Furthermore, chemical data^{17–20} have proven inconclusive or lacking in specificity²¹, and alleged melanosomes occurring as imprints (‘mouldic melanosomes’⁹) problematically imply that the surrounding substrate was more resistant to degradation than the microbodies themselves¹⁵. The matrix retaining ‘mouldic melanosomes’ is assumed to be either residual keratin⁹ or ‘remineralized melanin’⁵, yet no attempt has been made to test these hypotheses¹⁵. An alternative origin might therefore be plausible because melanosome-like impressions are occasionally found in clay minerals, together with silica crystals and other sedimentary grains adjacent to preserved integumentary structures^{15,20}.

Here we address the unresolved problem of accurately identifying microbodies, imprints and fibrous structures associated with fossilised feather remains via high-resolution imaging and molecular analysis of an exceptionally preserved new specimen (YFGP-T5199, housed in Yizhou Fossil and Geology Park) of the paravian *Anchiornis*²². Our results show that multiple local taphonomic pathways incorporating both organic and geochemical agents contributed to the retention of fibrils, eumelanin pigment and eumelanosomes in the integumentary filaments of YFGP-T5199.

Results

Fossil specimen and rationale for sample selection. An extensively feathered Jurassic paravian referable to *Anchiornis huxleyi* was recovered from the Yaolugou locality in Jianchang County, western Liaoning (see the Supplementary Methods section online). Although initially classified as a non-avian troodontid theropod¹, recent studies suggest that *Anchiornis* represents a stem avialan, more primitive than *Archaeopteryx*^{4,23}. The fossil is diagenetically flattened but otherwise essentially complete, comprising an articulated skeleton with plumage remnants forming a dark corona around the bones (Fig. 1a,b). Some integument residues were lost during preparation (see the Supplementary Methods section online); however, patches of feathers and feather-like structures extend along the back half of the skull, lateral to the shoulder girdle, above the pelvic girdle, and along the forelimbs, hind limbs and tail (Fig. 1a,b).

Fourteen samples (S1–S14) ranging in size from about 2 × 2 to 10 × 10 mm were removed from the plumage surfaces (Fig. 1b). One of these (S1) was selected for detailed morphological and molecular examination. S1 was collected some distance above the skull roof (Fig. 1b), in the region of the ‘fore-crown’ *sensu* ref. 5 (note that the inferred dorsal crest in *Anchiornis* may be an artefact of preservation^{11,24}). The sample was considered optimal for investigation because: (1) it showed greyish-brownish colouration indicative of organic remains; (2) was uncovered from a ‘fresh’ sub-surface layer within the sedimentary matrix; (3) produced part and counterpart sub-samples that revealed internal structuring of the filamentous epidermal appendages (Supplementary Fig. S1); and (4) similar ‘crest’ feathers from another *Anchiornis* fossil (see below) have been interpreted as housing pheomelanosomes⁵; that is, spheroid melanosomes dominated by pheomelanin pigment²⁵.

Description of the filamentous epidermal structures and microbodies. The integumentary appendages in S1 superficially resemble feathers of extant birds. They comprise a larger (and darker) central strand (Fig. 1c—arrowheads) with diffuse filamentous arrays branching off laterally at acute angles (Fig. 1c—arrows). In their current, somewhat compressed state, the finer filaments range in width from about 20 to 30 μm, whereas the larger strands measure approximately 40 to 50 μm across.

Under scanning electron microscopy (SEM) the individual filaments appear as thick, folded sheets of amorphous matter. This morphology is consistent with that of experimentally degraded feathers²⁶, and suggests distortion via diagenetic compression and/or elevated temperatures. However, some regions seemingly retain original structure, including continuous layers of densely packed fibrils organised into macrofibrils and/or fibril bundles with a predominantly longitudinal orientation (Fig. 2). Most fibrils are shown in relief, suggesting that they retain at least some of their original three-dimensional form (Fig. 2a); however, extensive folding, wrinkling and branching (Fig. 2d—arrows, e) are congruent with loss of tension during decomposition^{27,28}. Uneven fracturing has exposed the fibrous material in oblique tangential (Fig. 2a) and transverse views (Fig. 2c,d), revealing that it is part of larger structures (fibres or barbules) with a cylindrical shape (Fig. 2c). The fibrous elements range in size from about 80 nm (fibrils) to >10 μm (fibres/barbules) in diameter. These dimensions are broadly comparable to those recorded for keratinous components of extant bird feathers^{27–29}, despite the extent of diagenetic mineralisation (see below).

Ultrathin sections visualised using transmission electron microscopy (TEM) revealed micrometre-thick, layered structures (Fig. 3), superficially similar to sectioned keratin fibrils of extant feathers (see ref. 15, Fig. 1a).

Stacks of elongate microbodies are locally seen tightly adhering to, partially embedded in, or even merged with the fibrous substrate (Fig. 2a,b). These are crudely aligned in parallel to one another, and their overall orientation follows that of the fibrous tissues (Fig. 2a,b). Individual elements are rod-shaped

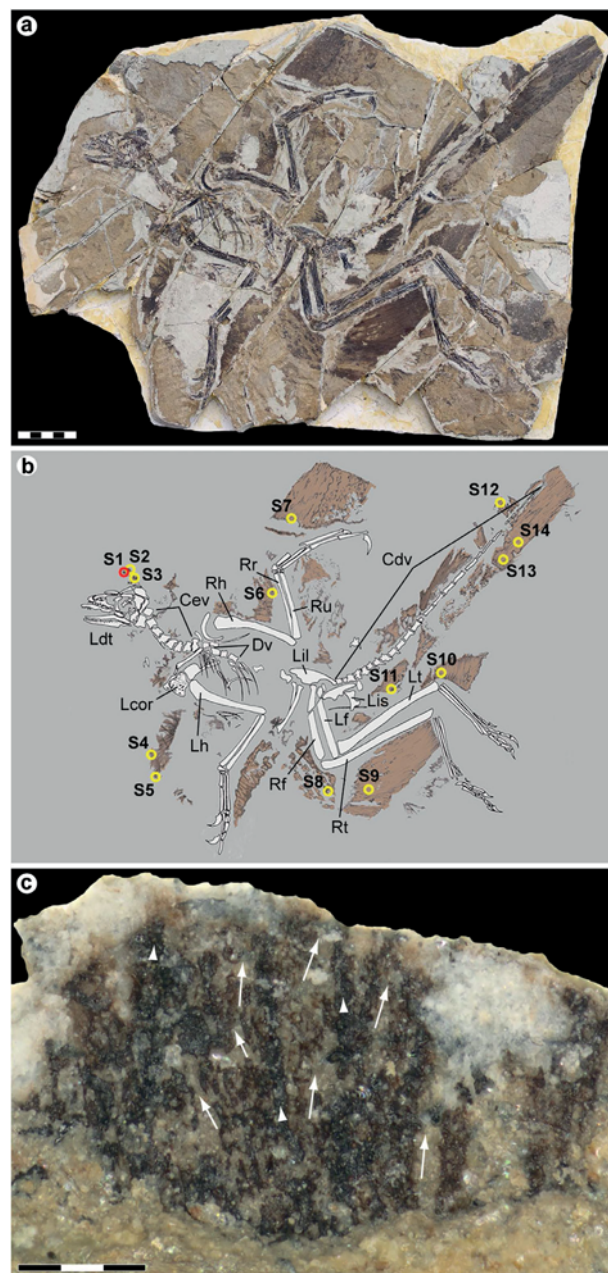


Figure 1. *Anchiornis huxleyi* specimen YFGP-T5199. (a) Photographic and (b) diagrammatic representation. Numbered circles denote location of plumage samples used for molecular and/or imaging analyses. Red circle (S1) demarcates the ‘forecrown’ sample used as the basis for our investigation; yellow circles (S2–S14) indicate samples used for supportive SEM imaging. Cdv, caudal vertebrae; Cev, cervical vertebrae; Dv, dorsal vertebrae; Lcor, left coracoid; Ldt, left dentary; Lf, left femur; Lh, left humerus; Lil, left ilium; Lis, left ischium; Lt, left tibia; Rf, right femur; Rh, right humerus; Rr, right radius; Rt, right tibia; Ru, right ulna. Scale bar: 5 cm. Photograph by Pascal Godefroit and Ulysse Lefèvre. Drawing by Ulysse Lefèvre. (c) Detail of S1 after initial preparation showing darker central strands (arrowheads) with diffuse arrays of filaments branching laterally at acute angles (arrows). Note that the analysed area is still covered by sedimentary matrix (see also Supplementary Fig. S1). Scale bar: 300 μ m. Photograph by Johan Lindgren.

with rounded termini, and substantially longer than wide. Most of these rods are straight or gently bent (Fig. 2b); however, others are strongly flexed (Supplementary Fig. S2d,e—arrow).

Within the matrix immediately adjacent to the fibrous tissues are densely spaced imprints infesting either a eumelanin/calcium phosphate residue (see discussion below and Supplementary Fig. S2c,d,f), clay

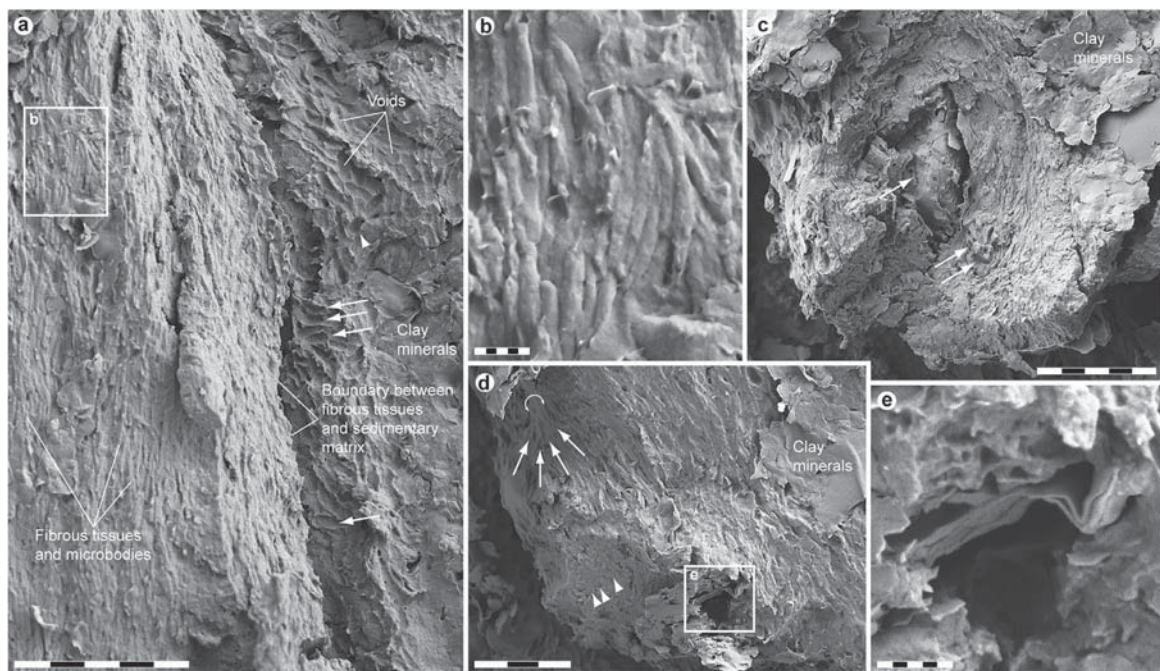


Figure 2. Ultrastructure of YFGP-T5199 ‘forecrown’ feathers. (a) FEG-SEM micrograph of fibril-like structures and solid microbodies (left side of image), and densely spaced voids made in the adjacent sedimentary matrix (‘Clay minerals’: right side of image). Note that the fibrous structures and microbodies are roughly aligned in parallel to one another, whereas the imprints are more randomly oriented (those with a longitudinal axis set almost perpendicular to the main direction of the fibrous tissues are marked with arrows). Also note highly variable shape of the voids (one with a sub-circular outline is marked with an arrowhead). Scale bar: 5 μm . (b) Enlargement of (a) showing aligned, rod-shaped microbodies with rounded termini. Scale bar: 500 nm. (c) Oblique transverse view of densely packed fibrils demonstrating their organisation into a larger cylindrical structure, presumably a fibre or barbule. Arrows point at sedimentary infill with randomly oriented elliptical impressions. Scale bar: 5 μm . (d) Cross-section of stacked and somewhat ragged fibril-like microstructures with a solid interior (arrowheads). The arrowhead hemi-circle partially encloses a presumed fibril bundle. Note branching patterns (arrows), possibly indicating loss of tension. Scale bar: 3 μm . (e) Detail of the area marked in (d) showing a wrinkled and partially folded microstructure roughly similar in dimensions to a macrofibril. Scale bar: 500 nm.

minerals (Fig. 2a) or microcrystalline aggregates (Fig. 2c and Supplementary Fig. S2h). Some impressions correspond in shape and size to the rod-shaped microbodies (Supplementary Fig. S2d,f,g). Additionally, they show similar alignment (Supplementary Fig. S2d,f,g), and rod-like elements are even retained in a few imprints (Supplementary Fig. S2d,e—arrow). Other impressions are morphologically more diverse, ranging from ovoid to elongate, and they are also more randomly oriented (sometimes with their long axis set almost perpendicular to that of the fibrous tissues; Fig. 2a—arrows and Supplementary Fig. S2h).

Ultimately, while the morphological and organisational similarities of the fibrous structures and microbodies to those of degraded feather keratin and remnant eumelanosomes are striking (Supplementary Fig. S3; see also refs 27,28,30,31), integration of chemical data is necessary to discriminate between endogenous residues and exogenous microorganisms that may occur associated with decaying keratinaceous substrates (see ref. 30, fig. 6).

Elemental and molecular analyses. Energy-dispersive X-ray microanalysis (EDX) identified carbon as the primary component in the integumentary remains, which suggests an organic source (Fig. 4). In addition, time-of-flight secondary ion mass spectrometric (ToF-SIMS) imaging analysis detected negative ions characteristic of melanic pigments localised specifically to areas with fibrous tissues and embedded microbodies (e.g., A1–A3; Figs 5b,c and 6a and Supplementary Figs S2a–e, S4a,e, S5). Detailed comparisons with modern reference samples further revealed that all ‘characteristic’ peaks of the eumelanin molecular structure were present in the fossil spectra, with considerable agreement in both mass position and relative signal intensity distribution (Fig. 6a and Supplementary Table S1). In contrast, the surrounding sediment yielded mainly silica-related negative ions indicative of silicate-rich minerals (e.g., A4; Fig. 5b,c and Supplementary Figs S2a, S4b,e, S5). Phosphate-containing ions were also encountered

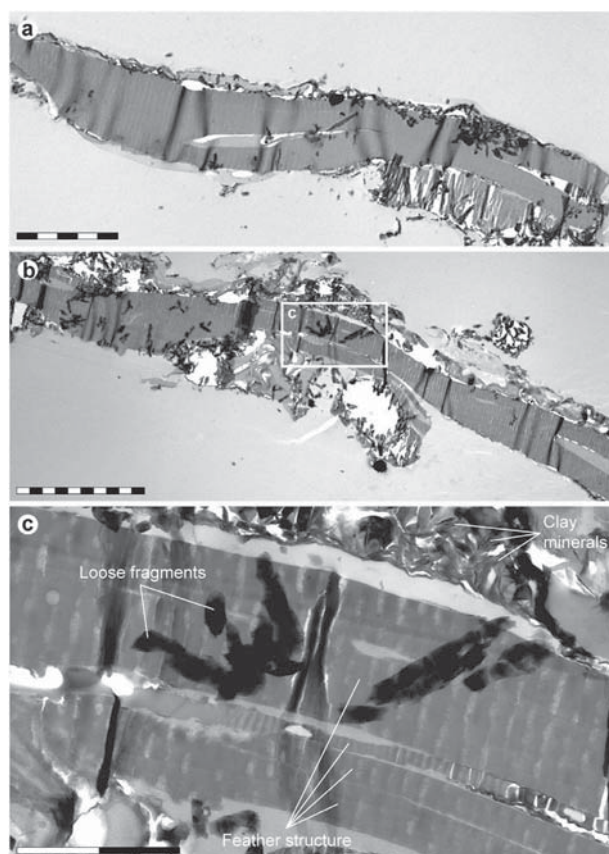


Figure 3. TEM micrographs of YFGP-T5199 ‘forecrown’ feathers. (a) Layered microstructures that are superficially similar in both size and organisation to keratin fibrils of extant bird feathers. The corrugated internal texturing and partial rupturing are artefacts of the TEM cutting process. This sample chip was also used for SEM-EDX (Fig. 4) and IR microspectroscopic (Fig. 8) analysis. Scale bar: 5 μm . (b) A separate section from the same chip a few micrometres deeper in the fossil feather substrate. Scale bar: 10 μm . (c) Enlargement of (b) showing details of the feather residues and adhering clay minerals. Scale bar: 2 μm .

over the entire surface, but at significantly higher intensities in the melanin-dominated areas (Fig. 5c and Supplementary Fig. S4d).

Positive ion mode spectra generated directly from the feather residues showed increased intensity of calcium phosphate-related ions, indicating preferential localisation of this mineral to the fibrous tissues and microbodies (e.g., A1–A3; Figs 5b,d and 6b and Supplementary Figs S6a,e, S7). Mineral-related ions, including aluminium, silicon, magnesium, and potassium, were found in the adjacent matrix (e.g., A4; Fig. 5b,d and Supplementary Figs S6b–e, S7); these probably denote illite group clay minerals³², as intimated by the TEM imaging (Fig. 3c).

ToF-SIMS spectra from areas with microbody imprints (e.g., A5–A7; Fig. 5 and Supplementary Figs S2c,d,f–h, S4–S7) detected varied molecular compositions, ranging from melanin/calcium phosphate-dominated residues (A5) to silicate minerals (A6 and A7), incorporating regionalised intensities of calcium phosphate-related ions (A6).

Comparative analyses were undertaken on synthetic and natural variants of eumelanin and pheomelanin, keratin, two peptidoglycans, five hopanoids, three porphyrins, and three microbial mats^{33–35}. We also examined a chemically derived pyomelanin, as well as pyomelanin from the bacterium *Vibrio cholerae* and eumelanin from the bacterium *Saccharophagus degradans* (Fig. 7). Based on these data, the fossil melanin from YFGP-T5199 displayed closest agreement with animal eumelanin (Fig. 7). Spectra acquired from the microbial melanins were also compatible in their ‘characteristic’ eumelanin peaks at 73, 74, 97, 98, 121, 122, 145, and 146 u; importantly though, these were significantly different in their relative abundances. The synthetic pyomelanin spectrum lacked all peaks corresponding to nitrogen-containing ions, including those indicative of eumelanin at 50, 66, 74, 98, 122, and 146 u.

Minor contributions from sulfur-containing organics were identified in the spectra from YFGP-T5199, including C_nNS^- ions at 58 (n = 1), 82 (n = 3) and 106 (n = 5) u, and C_nHS^- ions at 57 (n = 2), 81 (n = 4) and 105 (n = 6) u. These peaks were likewise prominent in the synthetic and natural pheomelanin samples

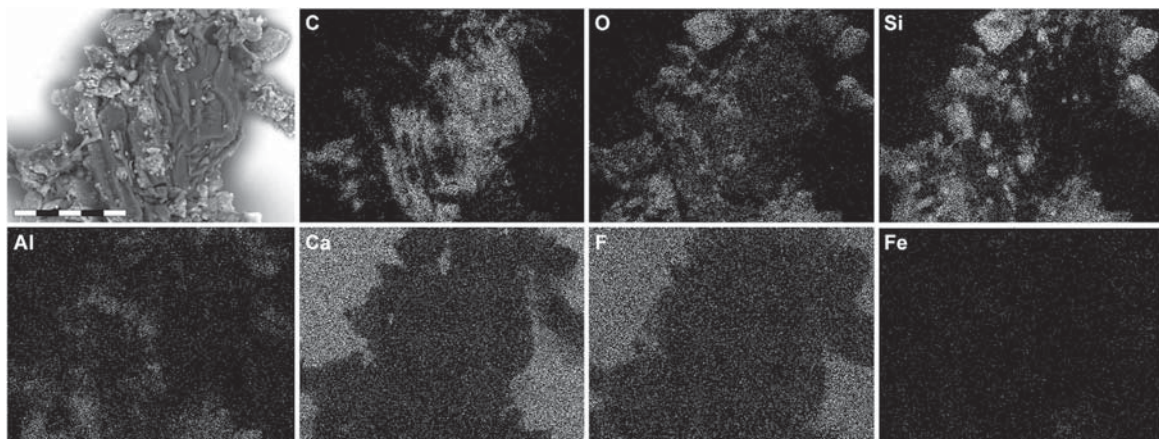


Figure 4. Single-element SEM-EDX maps of YFGP-T5199 ‘forecrown’ feathers. White indicates high intensity whereas black indicates low intensity. Note relatively high levels of carbon (C) in the fossil feather material, whereas the sediment is dominated by silica (Si) and oxygen (O), with minor quantities of aluminium (Al) and only trace amounts of iron (Fe). Intensities of calcium (Ca) and fluoride (F) derive from the underlying spectrophotometric window (for IR microspectroscopic analysis). Scale bar: 50 μm .

(Fig. 7), and showed significant co-localisation with ‘typical’ eumelanin-related peaks (Supplementary Fig. S4a,c). However, the sulfur-containing, possible pheomelanin-related peaks were conspicuously weak in the fossil spectra (Figs 6a and 7), thus preventing confident determination of pheomelanin or diagenetic incorporation of sulfur into the eumelanin molecular structure (as has been previously suggested for other fossil eumelanins^{33,35}).

No bacterial peptidoglycans or hopanoids were detected, and proteinaceous components consistent with keratins were also absent. Lastly, there were no signs of consolidants and/or preservatives that might potentially compromise the chemical integrity of the sample.

These results were corroborated by IR microspectroscopic measurements, which produced localised absorbance consistent with natural eumelanin, albeit with minor contributions from the surrounding sedimentary matrix (Fig. 8).

Discussion

The microscopic organisation of the epidermal remains in YFGP-T5199 closely resembles decayed keratin fibrils and eumelanosomes found in extant bird feathers, especially after selective biodegradation of the amorphous polymer matrix^{27,28,30,31}. The exceptional morphological fidelity of these filamentous appendages also reveals a fibrillar hierarchy reminiscent of the rachis and barb cortex²⁷, which may have imparted a flexural stiffness to the ‘forecrown’ feathers in YFGP-T5199. The mechanical architecture of paravian feathers can thus be shown to extend beyond gross macroanatomy^{36,37}, to a sub-cellular level of biological organisation.

Multiple independent lines of evidence advocate a eumelanosome origin for the rod-shaped microbodies in the epidermal tissues: (1) the presence of animal eumelanin; (2) the size, shape, distribution, and parallel alignment, which unlike bacterial cells do not form serial chains indicative of microbe fission (see ref. 15, figs 1e and 2a, S1c2 and ref. 30, fig. 6); and (3) the embedment within fibril-like structures similar to feather keratin. Yet despite this striking morphological resemblance, we failed to detect any proteinaceous components indicative of keratins. Instead, the fibrous tissues consisted of eumelanin and calcium phosphate, the latter possibly derived from mineral replacement. Indeed, post-burial melanin leakage might have provided a mechanism for either epidermal tissue stabilisation or replication in YFGP-T5199 that was further facilitated by the rapid growth of authigenic minerals^{38–40}. Early mineralisation is a common way of preserving labile soft tissues^{38–40}, and often involves calcium phosphate in fossilised melanic and/or keratinous structures, including ink sacs^{41,42}, feathers^{5,43} and claw sheath material⁴⁴.

The association of biomolecules with a mineral substrate is thought to increase the preservation potential of organic compounds, either via adsorptive inhibition of autolysis in decay-inducing enzymes, or by fixation of mineral ions into stable organometallic complexes that impede molecular breakdown^{44,45}. Polymer-calcium phosphate^{39,40,44} and/or polymer-clay^{38,45–47} interactions could thus be responsible for the retention of eumelanin molecules in YFGP-T5199. Regardless, eumelanin itself is resistant to decay⁴⁸ because of its extremely dense and insoluble polymer composition that is both antimicrobial and chemically robust^{49,50}, even in comparison with keratin⁹. Furthermore, mature melanosomes are essentially solid aggregations of melanin, which is polymerised onto an insoluble amyloid fibril scaffolding^{51,52}, thus

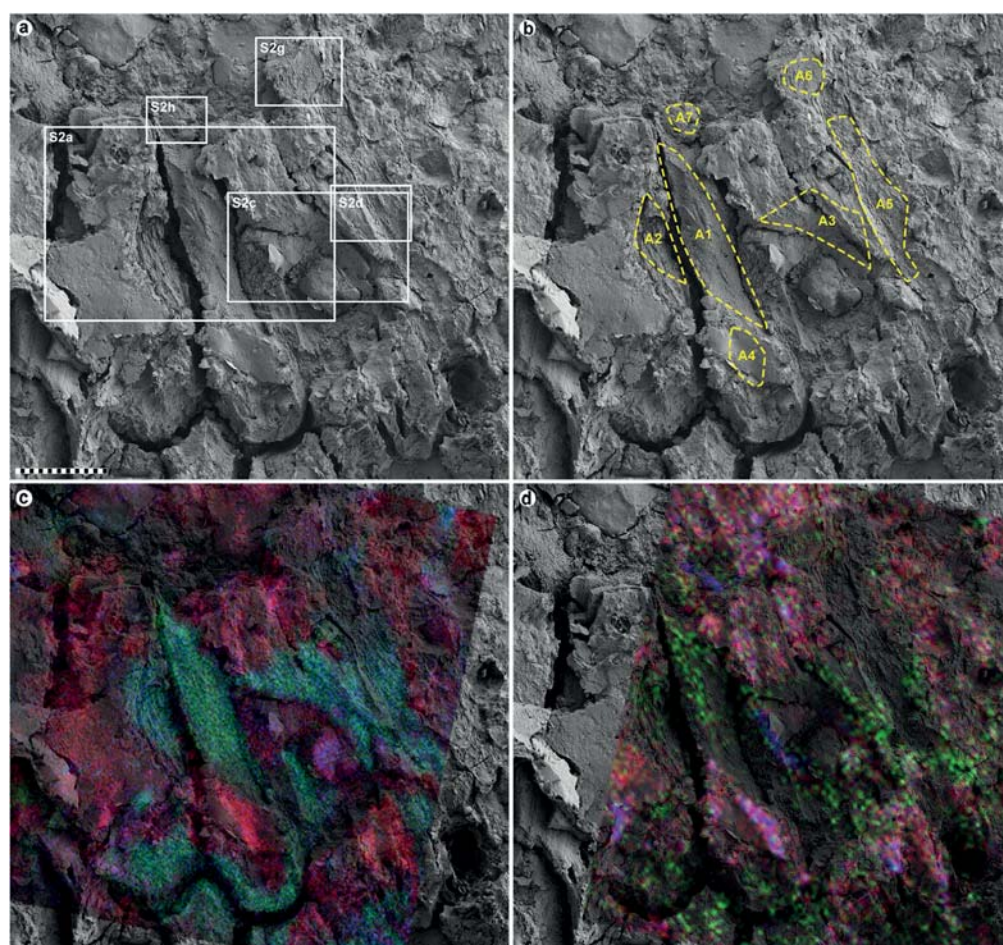


Figure 5. FEG-SEM and ToF-SIMS micrographs of YFGP-T5199 ‘forecrown’ feathers. (a) FEG-SEM micrograph of feather material and surrounding sediments. Close-up images of the delimited areas are shown in Supplementary Fig. S2. Scale bar: 20 μm . (b) Same image as in (a). Stippled yellow lines mark areas (A1–A7) from which the spectra in Figs 6 and 7 and Supplementary Figs S5 and S7 were collected. (c) A semi-transparent negative ion image showing the spatial distribution of peaks characteristic of eumelanin (green), phosphate (blue) and silica (red) superimposed onto the FEG-SEM image (see also Supplementary Fig. S4). (d) A semi-transparent positive ion image showing the spatial distribution of peaks corresponding to calcium phosphate (green), potassium (blue) and aluminium + silicon (red) superimposed onto the FEG-SEM image (see also Supplementary Fig. S6).

imparting an architectural stability that likely allows these specialised organelles to persist in the fossil record.

Some imprints observed in the matrix bordering the fibrous microstructures (e.g., A5) are reasonably interpreted as external moulds of pigment organelles based on their dimensional, distributional and chemical compatibility with the rod-like microbodies interpreted here as remnant eumelanosomes (Fig. 5 and Supplementary Fig. S2d–f), and might have been derived via sample preparation or disruption – e.g., impression from microbodies located on the counterpart (a scenario experimentally shown to produce melanosome imprints in the keratin matrix of modern feathers⁸).

A melanosome origin is also plausibly inferred for other mouldic structures in YFGP-T5199, including those exposed in A6 (note the continuous alignment of the impressions in A5 and A6; Fig. 5b). However, the molecular composition in this region broadly corresponds to that of the host rock (albeit with an increased amount of calcium phosphate), indicating mould formation primarily by aluminosilicate clays. It is therefore possible that local, rapid nucleation and precipitation of clay minerals proceeded in synchrony with the decomposition of the keratinous feather material, thereby encapsulating more stable organic structures (such as the eumelanosomes) within clay nanofabrics. At a later stage, the entombed organelles also decayed, leaving hollow void spaces that for unknown reasons remained

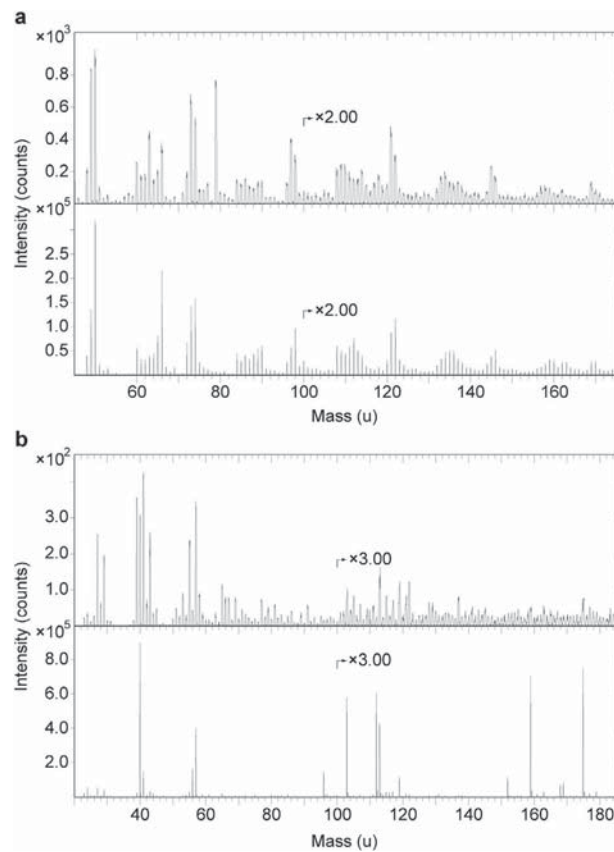


Figure 6. ToF-SIMS spectra from area A1 together with eumelanin and hydroxyapatite. (a) Negative ion ToF-SIMS spectra from A1 (top) and synthetic eumelanin (bottom). Note that all major peaks in the synthetic eumelanin spectrum are also present in the fossil spectrum, and that they occur with approximately the same relative signal intensity distribution (see also Supplementary Table S1), indicating the presence of significant amounts of eumelanin at the surface of the fibrous tissues. Additional peaks in the fossil spectrum originate from phosphate (PO_2^- and PO_3^- at 63 and 79 u, respectively) and silicate-related ions (SiO_2^- , SiO_3^- and SiO_3H^- at 60, 76 and 77 u, respectively). (b) Positive ion ToF-SIMS spectra from A1 (top) and hydroxyapatite (bottom). Note characteristic calcium phosphate peaks at 103, 159 and 175 u in the fossil spectrum, corresponding to CaPO_2^+ , Ca_2PO_3^+ and Ca_2PO_4^+ , respectively (see Supplementary Table S2 for peak assignments).

empty (assuming that these melanosome ‘pseudomorphs’ are not negatives from positive reliefs on the counterpart slab).

The affinity of other imprints is more enigmatic, including those in A7 (Supplementary Fig. S2h). Not only are these voids morphologically more diverse, but they are also highly disorganised in comparison to the solid eumelanosomes (Fig. 2a and Supplementary Fig. S2h). Spatially, these impressions are also seemingly restricted to aluminosilicate clays and microcrystalline clay aggregates along the bedding plane (Fig. 2a and Supplementary Fig. S2h). We were unable to locate any three-dimensional microstructures matching the imprints, implying that maker(s) of these moulds were less resistant to decay than the eumelanosomes.

In modern feathers, melanosomes can be organised into discrete layers where individual organelles are either consistently aligned or more erratically oriented with only local uniformity in directions^{8,53}. Thus, the fossil imprints may comprise moulds of melanosomes that exhibit more variability in shape, and originated from the outer cortex (which can exhibit less melanosome alignment⁸). These organelles may also be more prone to degradation because of greater exposure. Alternatively, preservational biases and diagenesis could potentially modify the appearance of fossil structures^{46,54}, although this would require the pigment organelles to be transformed not only in size (as has been previously demonstrated²⁶), but also in shape and orientation during the fossilisation process (assuming that they were originally aligned in approximate parallel with the bedding plane).

On the other hand, colonies of keratin-degrading microorganisms often comprise a consortium of taxa, resulting in a mixture of shapes and sizes³⁰. They are also inherently associated with decaying

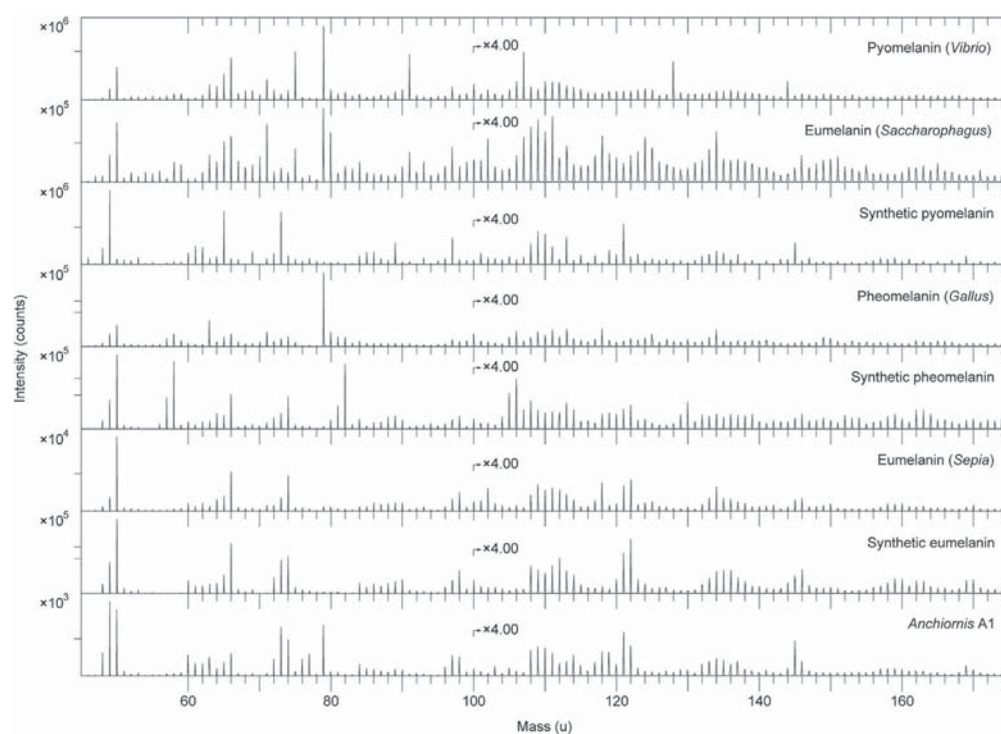


Figure 7. ToF-SIMS spectra acquired from melanin reference samples and A1. Negative ion ToF-SIMS spectra from various melanin standards and reference samples together with the spectrum from area A1. All spectra were acquired with the ToF-SIMS instrument optimised for high mass resolution. The prominent peak at 79 u (PO_3^-) in the spectra from pyromelanin (*Vibrio*), eumelanin (*Saccharophagus*) and pheomelanin (*Gallus*) derives from phosphate-containing contaminants, most likely originating from the melanin extraction and/or purification process.

feathers, and can form clustering patterns where neighbouring cells are oriented in common directions (see ref. 30, Fig. 6). Furthermore, because some decay is necessary to initiate mineralisation³⁹, and because calcium phosphate precipitation can be microbially induced^{40,55}, a microorganismal mediator could be rationally invoked in the partial replacement of the feather material. This, coupled with morphological evidence of fossilised microbes⁵⁶, has implications for the interpretation of the more enigmatic imprints observed in the matrix bordering the fibrous microstructures in YFGP-T5199 (Fig. 2a and Supplementary Fig. S2h). Given the extensive fossil record of microorganisms^{56,57}, and that some of these voids were not associated with an animal eumelanin molecular signature (e.g., A7), a microbial origin for these particular imprints cannot be excluded. Accordingly, we argue caution against interpreting all fossilised microbodies and impressions as melanosomes, and reconstructing plumage colours based on morphology alone.

An interesting aspect of the fossilised melanosomes in YFGP-T5199 is their exclusively elongate shape (Fig. 2b and Supplementary Fig. S2e). This deviates markedly from the relatively stocky microbodies reported from the ‘forecrown’ feathers of another referred specimen of *A. huxleyi* (BMNHC PH828, housed in Beijing Museum of Natural History)⁵. With a few possible exceptions (Fig. 2a—arrowhead), we also detected no pheomelanosome-like structures (see ref. 5). Several explanations might account for these discrepancies, including ontogeny, intraspecific variability and sexual dimorphism, as well as taphonomy, and/or sampling (that is, different regions within a multi-coloured crest). We also have to entertain the possibility that: (1) YFGP-T5199 and BMNHC PH828 represent different taxa; (2) integumentary melanosomes intermingle with melanosomes from other parts of the body in one of the two specimens; and (3) the microbodies and impressions reported by Li *et al.*⁵ and us are different structures altogether.

Indeed, BMNHC PH828 is considerably smaller (~60% by ulna and tibiotarsus length) than YFGP-T5199, and hence it may represent an earlier ontogenetic stage of *A. huxleyi*. Furthermore, YFGP-T5199 possesses a uniquely short dorsodistal process of the ischium (see the Supplementary Methods section online), which suggests the possibility of intraspecific and/or sexual differences that may also be reflected in the expressed colour pattern. However, the referral of BMNHC PH828 to *A. huxleyi* is problematic, and we cannot exclude that this specimen represents a closely related but different paravian taxon (see the Supplementary Methods section online).

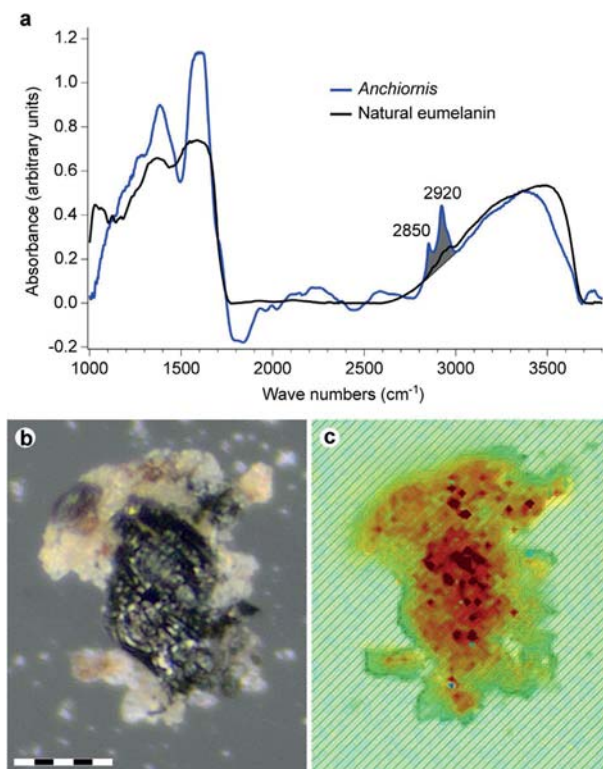


Figure 8. IR absorbance data from YFGP-T5199 ‘forecrown’ feathers. (a) Single point IR spectrum recorded from the lower part of the sample chip illustrated in (b,c). Broad-band absorbance occurs in the 900–1800 and 2500–3700 cm^{-1} regions, consistent with natural eumelanin. The YFGP-T5199 spectrum was recorded using transmission mode and a $15 \times 15 \mu\text{m}$ aperture to reduce sediment contributions. The C-H stretch region used for the absorbance imaging in (c) is shaded in grey. (b) Optical and (c) IR absorbance image (superimposed onto an optical image), the latter recorded by a focal plane array detector (see the Supplementary Methods section online). The IR image is based on the absorbance of the C-H stretches in the 2820–3000 cm^{-1} region from 2,760 individual spectra (the absorbance increases from yellow to red). The C-H stretches are associated with eumelanin-like spectra, which in conjunction with the lack of other organics on the sample chip (as evidenced by ToF-SIMS), suggest derivation primarily from eumelanin residues. Note that the spatial distribution of the C-H stretch absorbance intimately follows the blackish feather material (see consistency with the carbon distribution recorded by SEM-EDX; Fig. 4). Scale bar: 50 μm .

Additionally, while it has been shown that increased temperature and pressure can reduce the size of melanosomes²⁶, such alterations may not also include shape (but also see ref. 10). Taphonomy, therefore, presumably cannot account for the different microstructures seen in YFGP-T5199 and BMNHC PH828. Even though melanosomes can potentially disperse during decay⁵⁸, the microbodies in S1 are located deeply within a fibrous matrix interpreted as fossilised keratin. We thus conclude that the melanosomes most feasibly derive from the ‘forecrown’ feathers of YFGP-T5199 as opposed to other dermal tissues and/or internal organs (but whether this is also true for BMNHC PH828 has yet to be determined).

Although a re-investigation of the affinity and preservation of BMNHC PH828 is beyond the scope of this study, we note that the ‘pheomelanosome’ imprints reported by Li *et al.* (ref. 5, Fig. S5) are preserved in sedimentary grains rather than recognisable feather traces, similar to our more enigmatic impressions. Thus, these imprints may also represent either remobilised melanosomes or non-melanosome microstructures.

Our integrated structural and direct chemical approach provides compelling evidence that eumelanosomes and endogenous eumelanin pigment are preserved in the feather remains of YFGP-T5199. This result adds to a growing chronicle of molecular eumelanin detection in fossils^{33,35,42,59,60}, and demonstrates the aptitude of rigorous experimental techniques for identifying ancient biomolecules and their use in characterising ‘palaeo-colours’.

Methods

Fourteen feather samples (denoted S1–S14) were removed from YFGP-T5199 using either a sterile scalpel or a hand-operated saw. One sample (S1) selected for molecular analysis was triple-washed successively in acetone, 96% ethanol and Milli-Q water to remove potential contaminants from human handling. The sample was then dried under a hood, wrapped loosely in fresh aluminium foil and stored in isolation inside a sealed sterile glass container. ‘Fresh’ feather material was exposed prior to analysis by removing encasing sediment with a sterile scalpel; the resulting sample chip was subsequently split into part and counterpart pieces. Fresh aluminium foil was used to cover all work areas, and sterile surgical gloves were used during all handling and preparation. Our treatment procedure was identical for all modern reference samples. All experiments were repeated in order to validate the results.

SEM and FEG-SEM. Initial screening of S1 was performed using a Hitachi S-3400N SEM on the uncoated sample under low vacuum, and the elemental composition was determined via elemental mapping using EDX analysis (1900 sec scanning time at 15 keV, 62.0 μ A and a working distance of 10 mm). Following ToF-SIMS analysis, S1 was sputter-coated with a gold/palladium mixture and re-examined using a Zeiss Supra 40VP FEG-SEM (2 keV, working distance 3–5 mm, Everhart-Thornley secondary electron detector). Samples S2–S14 were sputter-coated with gold or gold/palladium and analysed using an environmental QUANTA 200 (FEI) SEM and a Zeiss Supra 40VP FEG-SEM.

TEM. Fossil feather material was removed from S1 using a sterile scalpel and placed in pure alcohol. The alcohol was then replaced with acetone, and stepwise substituted with epoxy resin (AGAR 100 Resin kit, R1031) to fully infiltrate the remnant tissues. The epoxy was left to polymerise at 60°C for 48 h. Infiltrated sub-samples were trimmed with a razor blade and then 1.5 μ m thick sections were cut using a glass knife mounted on an ultratome (Leica Ultracut UCT). A diamond knife was employed for the ultra-thin sectioning at 50 nm, after which slices were fixed to pioloform-coated copper grids. These were inserted into a JEOL JEM-1230 transmission electron microscope run at 80 kV. Areas of interest were photographed using a Gatan MultiScan 794 CCD camera.

ToF-SIMS. The ‘freshly’ prepared part and counterpart sub-samples of S1 were fixed on a metal block using double-sided tape (Supplementary Fig. S1) and then immediately inserted into a ToF-SIMS IV instrument (IONTOF GmbH). ToF-SIMS analyses in the static SIMS mode were performed using 25 keV Bi_3^+ primary ions and low energy electron flooding for charge compensation. High mass resolution data were acquired in the bunched mode ($m/\Delta m \sim 5000$) at a spatial resolution of $\sim 3\text{--}4 \mu\text{m}$, whereas high image resolution data were obtained without bunching ($m/\Delta m \sim 300$, spatial resolution $\sim 0.2\text{--}0.5 \mu\text{m}$); in both cases at 256×256 pixels. The coordinates for all positions investigated were monitored in order to allow for subsequent FEG-SEM analysis of the same areas.

IR microspectroscopy. Fossil tissues and sediments were removed from S1 using a sterile scalpel, suspended in Milli-Q water, and then placed on sterile CaF_2 infrared windows and left to air dry under a hood at room temperature. Likewise, standard samples were dissolved in Milli-Q water and then casted onto CaF_2 infrared windows. Infrared microspectroscopic measurements were recorded at two beam-lines: SMIS at the SOLEIL synchrotron radiation facility, France, and D7, MAX-IV laboratory, Sweden. At SOLEIL, the infrared photon source was coupled to a Thermo Fisher Nicolet Nexus 5700 FTIR spectrometer equipped with a Continuum XL microscope. A single point MCT-A detector and a $15 \times 15 \mu\text{m}$ aperture were used for the measurements. At MAX-IV laboratory, the set up combined a Hyperion 3000 microscope with a Bruker IFS66/v FTIR spectrometer. The image spectra were recorded in off-line mode using a MCT focal plane array detector consisting of 128×128 individual detector elements. Both microscopes operated in transmission mode at 4 cm^{-1} resolution.

References

- Hu, D., Hou, L., Zhang, L. & Xu, X. A pre-*Archaeopteryx* troodontid theropod from China with long feathers on the metatarsus. *Nature*. **461**, 640–643 (2009).
- Xu, X., You, H., Du, K. & Han, F. An *Archaeopteryx*-like theropod from China and the origin of Avialae. *Nature*. **475**, 465–470 (2011).
- Godefroit, P. *et al.* Reduced plumage and flight ability of a new Jurassic paravian theropod from China. *Nat Commun*. **4**, 1394 (2013).
- Godefroit, P. *et al.* A Jurassic avialan dinosaur from China resolves the early phylogenetic history of birds. *Nature*. **498**, 359–362 (2013).
- Li, Q. *et al.* Plumage color patterns of an extinct dinosaur. *Science*. **327**, 1369–1372 (2010).
- Davis, P. G. & Briggs, D. E. G. Fossilization of feathers. *Geology*. **23**, 783–786 (1995).
- Vinther, J., Briggs, D. E. G., Prum, R. O. & Saranathan, V. The colour of fossil feathers. *Biol Lett*. **4**, 522–525 (2008).
- Vinther, J., Briggs, D. E. G., Clarke, J., Mayr, G. & Prum, R. O. Structural coloration in a fossil feather. *Biol Lett*. **6**, 128–131 (2010).
- Zhang, F. *et al.* Fossilized melanosomes and the colour of Cretaceous dinosaurs and birds. *Nature*. **463**, 1075–1078 (2010).
- Carney, R. M., Vinther, J., Shawkey, M. D., D’Alba, L. & Ackermann, J. New evidence on the colour and nature of the isolated *Archaeopteryx* feather. *Nat Commun*. **3**, 637 (2012).
- Li, Q. *et al.* Reconstruction of *Microraptor* and the evolution of iridescent plumage. *Science*. **335**, 1215–1219 (2012).
- Li, Q. *et al.* Melanosome evolution indicates a key physiological shift within feathered dinosaurs. *Nature*. **507**, 350–353 (2014).
- Edwards, N. P., Manning, P. L. & Wogelius, R. A. Pigments through time. *Pigment Cell & Melanoma Res*. **27**, 684–685 (2014).

14. Schweitzer, M. H. Soft tissue preservation in terrestrial Mesozoic vertebrates. *Annu Rev Earth Planet Sci.* **39**, 187–216 (2011).
15. Moyer, A. E. *et al.* Melanosomes or microbes: testing an alternative hypothesis for the origin of microbodies in fossil feathers. *Sci Rep.* **4**, 4233 (2014).
16. McNamara, M. E. The taphonomy of colour in fossil insects and feathers. *Palaeontology.* **56**, 557–575 (2013).
17. Barden, H. E. *et al.* Morphological and geochemical evidence of eumelanin preservation in the feathers of the Early Cretaceous bird, *Gansus yumenensis*. *PLoS ONE.* **6**, e25494 (2011).
18. Wogelius, R. A. *et al.* Trace metals as biomarkers for eumelanin pigment in the fossil record. *Science.* **333**, 1622–1626 (2011).
19. Manning, P. L. *et al.* Synchrotron-based chemical imaging reveals plumage patterns in a 150 million year old early bird. *J Anal At Spectrom.* **28**, 1024–1030 (2013).
20. Egerton, V. M. *et al.* The mapping and differentiation of biological and environmental elemental signatures in the fossil remains of a 50 million year old bird. *J Anal At Spectrom.* **30**, 627–634 (2015).
21. Vinther, J. A guide to the field of palaeo colour: melanin and other pigments can fossilise: reconstructing colour patterns from ancient organisms can give new insights to ecology and behaviour. *Bioessays.* **37**, 643–656 (2015).
22. Xu, X. *et al.* A new feathered maniraptoran dinosaur fossil that fills a morphological gap in avian origin. *Chin Sci Bull.* **54**, 430–435 (2009).
23. Foth, C., Tischlinger, H. & Rauhut, O. W. M. New specimen of *Archaeopteryx* provides insights into the evolution of pennaceous feathers. *Nature.* **511**, 79–82 (2014).
24. Foth, C. On the identification of feather structures in stem-line representatives of birds: evidence from fossils and actuopalaeontology. *Paläontol Z.* **86**, 91–102 (2012).
25. Liu, Y. *et al.* Comparisons of the structural and chemical properties of black and red human hair melanosomes. *Photochem Photobiol.* **81**, 135–144 (2005).
26. McNamara, M. E., Briggs, D. E. G., Orr, P. J., Field, D. J. & Wang, Z. Experimental maturation of feathers: implications for reconstructions of fossil feather colour. *Biol Lett.* **9**, 20130184 (2013).
27. Lingham-Soliar, T., Bonser, R. H. C. & Wesley-Smith, J. Selective biodegradation of keratin matrix in feather rachis reveals classic bioengineering. *Proc R Soc B.* **277**, 1161–1168 (2010).
28. Lingham-Soliar, T. & Murugan, N. A new helical crossed-fibre structure of β -keratin in flight feathers and its biomechanical implications. *PLoS ONE.* **8**, e65849 (2013).
29. Martínez-Hernández, A. L., Velasco-Santos, C., de Icaza, M. & Castaño, V. M. Microstructural characterisation of keratin fibres from chicken feathers. *Int J Environ Poll.* **23**, 162–178 (2005).
30. Ichida, J. M. *et al.* Bacterial inoculum enhances keratin degradation and biofilm formation in poultry compost. *J Microbiol Meth.* **47**, 199–208 (2001).
31. Rodziewicz, A. & Łaba, W. Biodegradation of feather keratin by *Bacillus cereus* in pure culture and compost. *EJPAU.* **11**, 03 (2008).
32. Meunier, A. *Clays* (Springer-Verlag, 1986).
33. Lindgren, J. *et al.* Molecular preservation of the pigment melanin in fossil melanosomes. *Nat Commun.* **3**, 824 (2012).
34. Leefmann, T. *et al.* Spectral characterization of ten cyclic lipids using time-of-flight secondary ion mass spectrometry. *Rapid Commun Mass Spectrom.* **27**, 565–581 (2013).
35. Lindgren, J. *et al.* Skin pigmentation provides evidence of convergent melanism in extinct marine reptiles. *Nature.* **506**, 484–488 (2014).
36. Xu, X., Zhou, Z.-H. & Prum, R. O. Branched integumental structures in *Sinornithosaurus* and the origin of feathers. *Nature.* **410**, 200–204 (2001).
37. Xu, X., Zheng, X. & You, H. A new feather type in a nonavian theropod and the early evolution of feathers. *Proc Natl Acad Sci.* **106**, 832–834 (2009).
38. Gabbott, S. E., Norry, M. J., Aldridge, R. J. & Theron, J. N. Preservation of fossils in clay minerals; a unique example from the Upper Ordovician Soom Shale, South Africa. *Proc Yorkshire Geol Soc.* **53**, 237–244 (2001).
39. Briggs, D. E. G. The role of decay and mineralization in the preservation of soft-bodied fossils. *Annu Rev Earth Planet Sci.* **31**, 275–301 (2003).
40. Briggs, D. E. G. & Wilby, P. R. The role of the calcium carbonate-calcium phosphate switch in the mineralization of soft-bodied fossils. *J Geol Soc London.* **153**, 665–668 (1996).
41. Kear, A. J., Briggs, D. E. G. & Donovan, D. T. Decay and fossilization of non-mineralized tissue in coleoid cephalopods. *Palaeontology.* **38**, 105–131 (1995).
42. Glass, K. *et al.* Impact of diagenesis and maturation on the survival of eumelanin in the fossil record. *Org Geochem.* **64**, 29–37 (2013).
43. Bergmann, U. *et al.* *Archaeopteryx* feathers and bone chemistry fully revealed via synchrotron imaging. *Proc Natl Acad Sci.* **107**, 9060–9065 (2010).
44. Schweitzer, M. H. *et al.* Keratin immunoreactivity in the Late Cretaceous bird *Rahonavis ostromi*. *J Vert Paleontol.* **19**, 712–722 (1999).
45. Yu, B. *et al.* The role of clay minerals in the preservation of organic matter in sediments of Qinghai Lake, NW China. *Clays Clay Min.* **57**, 213–226 (2009).
46. Pan, Y., Sha, J. & Fürsich, F. T. A model for organic fossilization of the Early Cretaceous Jehol Lagerstätte based on the taphonomy of “*Ephemeropsis trisetalis*”. *Palaios.* **29**, 363–377 (2014).
47. Edwards, N. P. *et al.* Infrared mapping resolves soft tissue preservation in 50 million year-old reptile skin. *Proc R Soc B.* **278**, 3209–3218 (2011).
48. Hollingworth, N. T. J. & Barker, M. J. in *The Processes of Fossilization* (ed. Donovan, S. K.) 105–119 (Belhaven Press, 1991).
49. Sulaimon, S. S. & Kitchell, B. E. The biology of melanocytes. *Vet Derm.* **14**, 57–65 (2003).
50. McGraw, K. J. in *Bird Coloration* Vol. 1 (eds Hill, G. E. & McGraw, K. J.) 243–294 (Harvard Univ. Press, 2006).
51. Watt, B., Raposo, G. & Marks, M. S. in *Functional Amyloid Aggregation* (eds Rigacci, S. & Bucciantini, M.) 89–113 (Research Signpost, 2010).
52. Delevoeye, C., Giordano, F., Marks, M. S. & Raposo, G. in *Melanins and Melanosomes: Biosynthesis, Biogenesis, Physiological, and Pathological Functions* (eds Borovanský, J. & Riley, P. A.) 247–294 (Wiley-VCH Verlag GmbH & Co. KGaA, 2011).
53. Shawkey, M. D., D’Alba, L., Xiao, M., Schutte, M. & Buchholz, R. Ontogeny of an iridescent nanostructure composed of hollow melanosomes. *J Morph.* **276**, 378–384 (2015).
54. Orange, F., Lalonde, S. V. & Konhauser, K. O. The formation and preservation of *Synechococcus elongatus* cell molds in simulated silica sinter: implications for the identification of microfossils. *Geomicrobiol J.* **30**, 327–336 (2013).
55. Hirschler, A., Lucas, J. & Hubert, J.-C. Bacterial involvement in apatite genesis. *FEMS Microbiol Ecol.* **73**, 211–220 (1990).
56. Westall, F. The nature of fossil bacteria: a guide to the search for extraterrestrial life. *J Geophys Res.* **104**, 16,437–16,451 (1999).
57. Paction, M., Fiet, N. & Gorin, G. Revisiting amorphous organic matter in Kimmeridgian laminites: what is the role of the vulcanization process in the amorphization of organic matter? *Terra Nova.* **18**, 380–387 (2006).

58. McNamara, M. E., Kaye, J. S., Benton, M. J. & Orr, P. J. Non-integumentary melanosomes can bias reconstructions of the colours of fossil vertebrate skin. Paper presented at 4th *International Palaeontological Congress. The history of life: a view from the Southern Hemisphere*, Mendoza, Argentina. Abstract volume: Ianigla, CCT-Conicet (2014, September 28–October 3).
59. Glass, K. *et al.* Direct chemical evidence for eumelanin pigment from the Jurassic period. *Proc Natl Acad Sci.* **109**, 10218–10223 (2012).
60. Tanaka, G. *et al.* Mineralized rods and cones suggest colour vision in a 300 Myr-old fossil fish. *Nat Commun.* **5**, 5920 (2014).

Acknowledgements

C. Rasmussen assisted during the laboratory work. S. N. Wai provided a colony of *Vibrio cholerae* mutant isolate SNW28, and L. Hederstedt grew the bacterium. L. Carlred assisted in the purification of the natural melanin standards. Beamtime was allocated at SMIS, SOLEIL synchrotron radiation facility, France (proposal 20131382), and D7, MAX-IV laboratory, Sweden. P. Dumas assisted during the IR measurements at SOLEIL. This research was supported by grants from the Swedish Research Council (J.L.), Crafoord foundation (J.L. and P.U.) and National Geographic Society (R.M.C.).

Author Contributions

J.L., P.S. and R.M.C. designed the project and planned the experiments. J.L., P.S., R.M.C. and B.P.K. wrote the main manuscript, whereas P.G. and U.L. described the fossil. J.L., P.S., P.U. and U.L. made the illustrations. P.S. and J.L. performed the ToF-SIMS analyses, P.U., J.H. and A.E. conducted the IR experiments, P.S., A.C., J.A.G., J.Y. and J.L. executed the FEG-SEM and SEM studies, and O.G. and J.L. did the TEM analyses. F.E. and P.G. made YFGP-T5199 available for study. S.W.H. provided eumelanin from *Saccharophagus degradans*, whereas K.W. provided synthetic pheomelanin. All authors discussed the results and provided input on the manuscript.

Additional Information

Supplementary information accompanies this paper at <http://www.nature.com/srep>

Competing financial interests: The authors declare no competing financial interests.

How to cite this article: Lindgren, J. *et al.* Molecular composition and ultrastructure of Jurassic paravian feathers. *Sci. Rep.* **5**, 13520; doi: 10.1038/srep13520 (2015).



This work is licensed under a Creative Commons Attribution 4.0 International License. The images or other third party material in this article are included in the article's Creative Commons license, unless indicated otherwise in the credit line; if the material is not included under the Creative Commons license, users will need to obtain permission from the license holder to reproduce the material. To view a copy of this license, visit <http://creativecommons.org/licenses/by/4.0/>

“Each time I came to my Master with the flower that never wilted nor faded - how I grew to hate that flower! - and told him what I'd learned, he would say, ‘Is that all, my son?’ And, crushed, I'd go back to my study of that silly little flower. In time my distaste for it grew less. The more I studied it, the better I came to know it, and I eventually grew fond of it.”

- Belgarath the Sorcerer, David & Leigh Eddings

The image features a textured, brownish-gold background with a central, dark, fibrous, feather-like structure. The structure is composed of numerous fine, dark fibers that fan out from a central point, creating a feather-like appearance. The overall texture is grainy and organic, suggesting a natural or handmade material. A black horizontal bar is positioned across the middle of the image, containing the text "PAPER V" in white, serif, uppercase letters.

PAPER V

Overleaf: The isolated feather specimen FUM-1980b

[Palaeontology, 2016, pp. 1–18]

MOLECULAR AND MICROSTRUCTURAL INVENTORY OF AN ISOLATED FOSSIL BIRD FEATHER FROM THE EOCENE FUR FORMATION OF DENMARK

by JOHAN A. GREN¹, PETER SJÖVALL², MATS E. ERIKSSON¹, RENE L. SYLVESTERSEN³, FEDERICA MARONE⁴, KAJSA G. V. SIGFRIDSSON CLAUSS⁵, GAVIN J. TAYLOR⁶, STEFAN CARLSON⁵, PER UVDAL⁷ and JOHAN LINDGREN¹

¹Department of Geology, Lund University, Sölvegatan 12, 223 62 Lund, Sweden; johan.gren@geol.lu.se, mats.eriksson@geol.lu.se, johan.lindgren@geol.lu.se

²SP Technical Research Institute of Sweden, Box 857, 501 15 Borås, Sweden; peter.sjovall@sp.se

³MUSERUM, Brårupgade 18, 7800 Skive, Denmark; rlsy@muserum.org

⁴Swiss Light Source, Paul Scherrer Institute, 5232 Villigen, Switzerland; federica.marone@psi.ch

⁵MAX IV Laboratory, Box 118, 221 00 Lund, Sweden; kajsa.sigfridsson_clauss@maxiv.lu.se, stefan.carlson@maxiv.lu.se

⁶Department of Biology, Lund University, Sölvegatan 35/37, 223 62 Lund, Sweden; gavin.taylor@biol.lu.se

⁷Department of Chemical Physics, Lund University, Box 124, 221 00 Lund, Sweden; per.uvdal@chemphys.lu.se

Typescript received 7 June 2016; accepted in revised form 7 October 2016

Abstract: An isolated, yet virtually intact contour feather (FUM-1980) from the lower Eocene Fur Formation of Denmark was analysed using multiple imaging and molecular techniques, including field emission gun scanning electron microscopy (FEG-SEM), X-ray absorption spectroscopy and time-of-flight secondary ion mass spectrometry (ToF-SIMS). Additionally, synchrotron radiation X-ray tomographic microscopy (SRXTM) was employed in order to produce a digital reconstruction of the fossil. Under FEG-SEM, the proximal, plumulaceous part of the feather revealed masses of ovoid microstructures, about 1.7 µm long and 0.5 µm wide. Microbodies in the distal, pennaceous portion were substantially smaller (averaging 0.9 × 0.2 µm), highly elongate, and more densely packed. Generally, the microbodies in both the plumulaceous and pennaceous segments were aligned along the barbs and located within shallow depressions on the exposed surfaces. Biomarkers consistent with

animal eumelanins were co-localized with the microstructures, to suggest that they represent remnant eumelanosomes (i.e. eumelanin-housing cellular organelles). Additionally, ToF-SIMS analysis revealed the presence of sulfur-containing organics – potentially indicative of pheomelanins – associated with eumelanin-like compounds. However, since there was no correlation between melanosome morphology and sulfur content, we conclude these molecular structures derive from diagenetically incorporated sulfur rather than pheomelanin. Melanosomes corresponding roughly in both size and morphology with those in the proximal part of FUM-1980 are known from contour feathers of extant parrots (Psittaciformes), an avian clade that has previously been reported from the Fur Formation.

Key words: Eocene, eumelanin, Fur Formation, melanosome, parrot, Psittaciformes.

DUE to rapid methodological advances and re-evaluations of existing hypotheses pertaining to the retention of original biomolecules and soft tissue structures across deep time (e.g. Schweitzer *et al.* 2005, 2007; Vinther *et al.* 2008), the field of palaeontology is currently undergoing a paradigm shift (Gibbons 2010). A broad array of sensitive and selective techniques has greatly improved our understanding of processes and factors contributing to exceptional preservation (e.g. Schweitzer *et al.* 2007, 2009; Wogelius *et al.* 2011; Glass *et al.* 2012, 2013; Lindgren *et al.* 2012, 2015a, b). To further augment this knowledge, it is necessary to pursue this methodological development

and apply these new techniques to fossils representing different ages, affinities, depositional settings and preservational modes (Colleary *et al.* 2015). Consequently, over the last few decades a number of studies have documented potentially endogenous molecular remains associated with body fossils ranging from the Palaeozoic to the Recent (Briggs & Summons 2014). Noteworthy recent discoveries include presumed original biomolecular components of Silurian sea scorpion cuticle (Cody *et al.* 2011) and proteinaceous compounds of Cretaceous bird claw sheaths and non-avian dinosaur bone (Gurley *et al.* 1991; Schweitzer *et al.* 1997, 1999, 2007).

2 PALAEOLOGY

Moreover, fossilized feathers and plumage of early birds and non-avian dinosaurs have recently become the focus of molecular and/or imaging investigations. The renewed interest in these ancient integumental traces centres on the presence of micrometre-sized, sub-spherical to elongate bodies, or, more often, imprints thereof, originally thought to represent lithified keratinophilic bacteria (e.g. Wuttke 1983; Davis & Briggs 1995). However, in 2008, Vinther *et al.* re-interpreted the fossil microbodies as remnant melanosomes; i.e. eukaryotic, melanin-containing cellular organelles. Vinther *et al.*'s (2008) hypothesis has since gained increasing popularity, not least because it potentially allows for partial reconstructions of original colours and pigment patterns (Vinther *et al.* 2008; Clarke *et al.* 2010; Li *et al.* 2010, 2012; Colleary *et al.* 2015; Vinther 2015). Additionally, presumed fossil melanosomes have also been used to infer ancient animal behaviour (Li *et al.* 2010) and physiology (Li *et al.* 2014; Lindgren *et al.* 2014).

It has been argued that the superficial similarity between fossil microbodies and melanosomes is insufficient for confident determination, and that supporting molecular data are required before an exogenous origin can be excluded (Moyer *et al.* 2014; Lindgren *et al.* 2015a). This assertion has spurred a vivid debate (for review, see Edwards *et al.* 2014) and different criteria for melanosome recognition have been proposed (Lindgren *et al.* 2015a; Schweitzer *et al.* 2015; Vinther 2015, 2016); however, so far without consensus. Hence, as it stands, the most careful way to proceed is to analyse each fossil individually and as rigorously as possible (*contra* Vinther 2016), thereby minimizing the risk of insufficiently supported claims propagating in the literature (Lindgren *et al.* 2015a).

Accordingly, we used an integrated suite of sophisticated molecular and imaging techniques, including field emission gun scanning electron microscopy (FEG-SEM), X-ray absorption spectroscopy (XAS), time-of-flight secondary ion mass spectrometry (ToF-SIMS) and synchrotron radiation X-ray tomographic microscopy (SRXTM) to examine the microstructural and molecular inventory of an isolated, yet virtually intact fossil bird feather (FUM-1980; MUSERUM) from the Eocene Fur Formation of Denmark. In this contribution, we report the results of our integrated geochemical and ultrastructural approach.

GEOLOGICAL SETTING

Specimen FUM-1980 is preserved in a calcareous concretion belonging to the Fur Formation (or 'Moler' – an informal name used in Danish literature; e.g. Bøggild 1918; Pedersen *et al.* 2011) of Denmark. It was collected at Knudeklint – the type locality of the formation – which

is represented by a costal cliff section located on the Island of Fur, northern Jutland (Fig. 1).

The Fur Formation comprises an up to 60 m thick, fossil-rich and tephra-bearing marine diatomite of earliest Eocene (Ypresian) age (Pedersen *et al.* 2011). The diatomite formed below the storm wave-base under alternating dysoxic and anoxic conditions (Pedersen 1981). Thus, parts of the sedimentary sequence consist of finely laminated (0.1–0.3 mm) deposits that are generally uninterrupted by the actions of benthic organisms, whereas other parts lack clearly defined laminations, to suggest periodically higher oxygen and/or energy levels (Pedersen *et al.* 2011). Nonetheless, the absence of a diverse benthic fauna testifies to a generally low oxygen supply in the lower part of the water column (Pedersen & Surlyk 1983). Much of the oxygen consumption may be linked to the decomposition of diatoms that periodically accumulated in large amounts on the sea floor (Pedersen *et al.* 2011).

The diatomite is interbedded with more than 200 distinct volcanic ash layers originating from emissions during the early stages of the North Atlantic Igneous Province (Pedersen & Surlyk 1983; Pedersen *et al.* 2011). Two volcanic ash layers have been radiometrically dated at 55.39 ± 0.12 (Layer –17) and 54.04 ± 0.14 Ma (Layer +19), respectively (see Chambers *et al.* 2003; Storey *et al.* 2007). Based on these absolute dates, the Fur Formation has been correlated with contemporary deposits across Europe (e.g. Knox & Holloway 1992; Heilmann-Clausen 1995; Egger & Brückl 2006).

The Fur Formation is a so-called Konservat-Lagerstätte and consequently yields a wealth of exceptionally preserved fossils. Although the preserved flora and fauna are dominated by marine taxa (e.g. fish, invertebrates and planktonic algae), they also include abundant remains of terrestrial plants and animals (Bonde *et al.* 2008; Pedersen *et al.* 2011), ranging from insects to tree-trunks. In certain calcareous horizons, fossils (such as FUM-1980) are particularly well preserved (Pedersen & Buchardt 1996) and many of these have been designated as 'Danekræ'; i.e. specimens with extraordinary scientific and/or display value (Christensen & Hald 1990; Bonde *et al.* 2008).

Several fossil groups, including insects (Larsson 1975; Rust 1999) bony fishes (Bonde 1979) and palynomorphs (Willumsen 2004), have been used for palaeoenvironmental interpretations. Henriksen (1922) analysed the insect fauna of the Fur Formation and concluded that it was indicative of a subtropical environment, with yearly mean temperatures being up to 10°C higher than those experienced in the region today. The presence of psittaciform birds (parrots) also attests to a greenhouse climate (Waterhouse *et al.* 2008), as do isotope data from the Paleocene–Eocene thermal maximum, a prominent

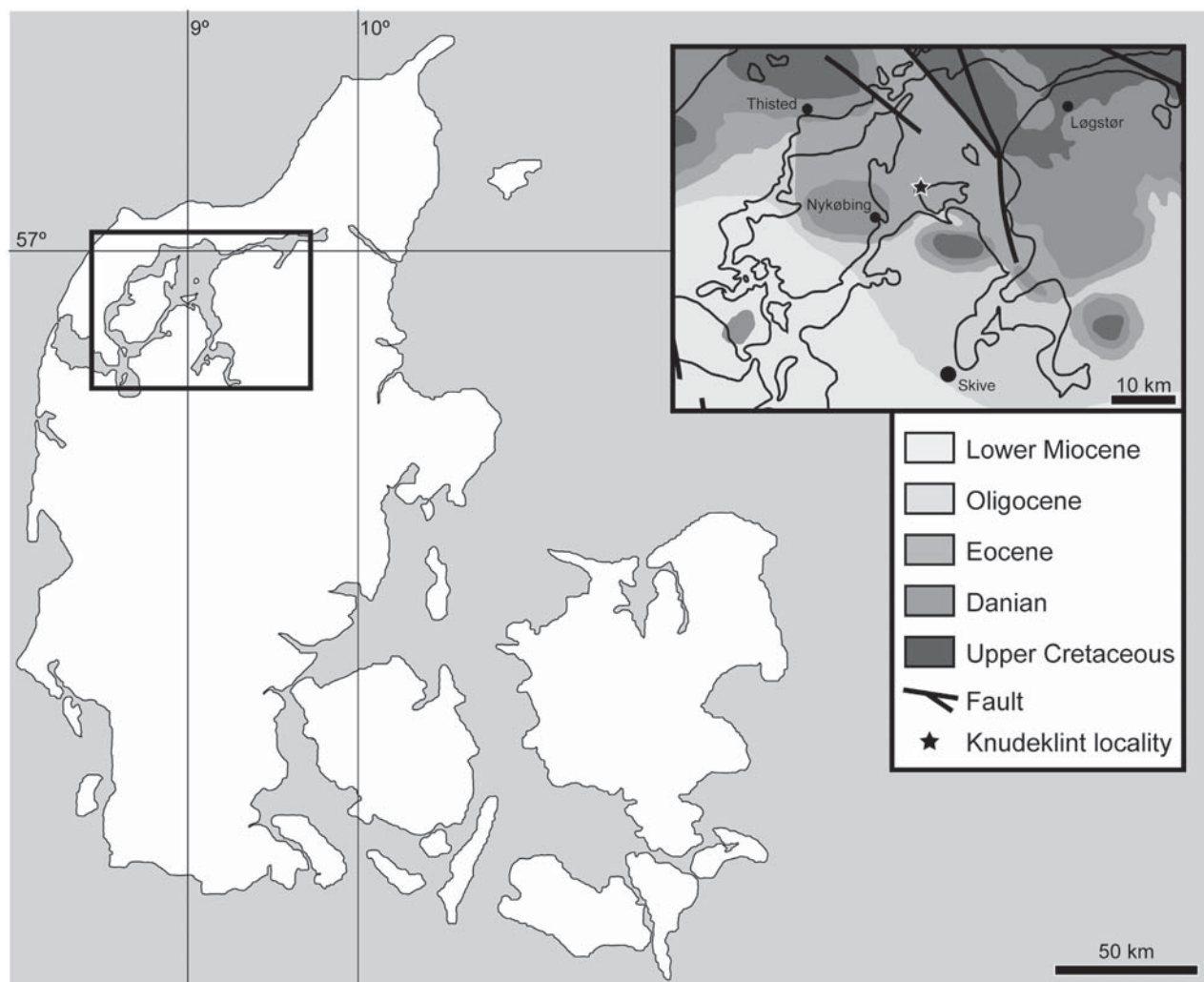


FIG. 1. Sketch map showing the extension of the Fur formation in Jutland, Denmark (modified from Karl & Madsen 2012, fig. 1a). Inset is a geological map of the area with the location of Knudeklint marked with a star (modified from Pedersen *et al.* 2011, fig. 2).

climatic event which is traceable in rock successions across the globe (e.g. Schmitz *et al.* 2004; Schoon *et al.* 2015).

METHOD

Preparation and optical microscopy

The fossil has been split along its longitudinal axis, and is thus represented by both part (FUM-1980a) and counterpart (FUM-1980b; collectively FUM-1980). No preservatives or consolidants were applied during the preparation of the fossil, and samples for ToF-SIMS analysis were carefully removed using sterile scalpels and surgical gloves. For general assessment, the feather traces were examined under an Olympus SZX16 optical microscope and photographed using an Olympus SC30 camera. For

swift recognition of morphological details, the terminology follows that of extant bird feathers (see Lucas & Stettenheim 1972).

Scanning electron microscopy (SEM)

Initially, both part and counterpart were examined uncoated under low vacuum using a Hitachi S-3400N scanning electron microscope (SEM), and the elemental composition of FUM-1980a was recorded using energy-dispersive X-ray (EDX) microanalysis (1900 s scanning time, 15 keV, 62.0 mA, 5–10 mm working distance). Following ToF-SIMS examination (see details below), feather samples were sputter coated with a conducting gold film and then imaged using a Zeiss Supra 40VP field emission gun scanning electron microscope (2 keV, working distance 3–5 mm, Everhart–Thornley secondary electron

4 PALAEOLOGY

detector). Measurements of microstructures were taken on FEG-SEM micrographs using Fiji ImageJ v1.49 m (<http://imagej.nih.gov/ij>) software.

Time-of-flight secondary ion mass spectrometry (ToF-SIMS)

Minute samples were removed from FUM-1980a using a sterile scalpel and placed on metal blocks using double-sided tape. ToF-SIMS analyses were carried out in a TOF-SIMSIV instrument (IONTOF GmbH, Germany) using 25 keV Bi₃⁺ primary ions and low energy electron flooding for charge compensation. Positive and negative ion data were collected with the instrument optimized either for high lateral resolution (lateral resolution 0.5–0.6 μm, mass resolution $m/\Delta m = 300$) or for high mass resolution (lateral resolution 3–5 μm, mass resolution $m/\Delta m = 3000$ –5000). The accumulated primary ion dose density for all measurements taken on individual sample areas was kept below 2×10^{12} ions/cm² to ensure static SIMS conditions. Principal components analysis (PCA) of ion images was conducted using the SurfaceLab 6.5 software supplied with the ToF-SIMS instrument.

X-ray absorption spectroscopy (XAS)

XAS was performed *in situ* on FUM-1980a by focusing the X-ray beam on different parts of the slab. Data were recorded from two spots on the plumulaceous part, one spot on the pennaceous segment, and two spots on the sediment. In the experimental set-up, a Ni-filter in front of the energy dispersive detector was used to decrease the elastic scattering peak, and thus the measured Ni K α fluorescence peak could be used for normalization between different sample spots. Eumelanin from *Sepia officinalis* ink and powders of CuO and Cu₂S (Sigma-Aldrich) were placed in acrylic glass holders and used as reference samples. At the Cu K-edge (8979 eV), XAS spectra were collected at the wiggler beam-line I811, synchrotron MAX II (1.5 GeV ring with current range of 150–250 mA), at MAX IV Laboratory (Lund University, Sweden). A double crystal Si(111) monochromator was used and the second monochromator crystal was detuned to 20% of maximum intensity to minimize higher order harmonics. X-ray fluorescence was detected with an energy dispersive detector, Vortex SDD (or Amptek XR-100SDD) with the region of interest set to the Cu K α peak. The fluorescence signal was normalized using an upstream ion chamber, and a Cu foil standard was measured in between all sample spots. The fossil was measured at 45° to the incident beam and fluorescence detector, using a beam spot size of 1.5 × 1.5 mm. The final XAS spectra were an average of 10–45 scans at 40 min. Data reduction, energy

calibration, normalization, extraction of EXAFS oscillations ($k = 2$ –11 Å⁻¹), and conversion of energy to wave vector were performed as described by Dau *et al.* (2003), prior to the analysis of the X-ray absorption near edge structure (XANES) and the extended X-ray absorption fine structure (EXAFS) parts of the XAS spectrum.

Synchrotron radiation X-ray tomographic microscopy (SRXTM)

SRXTM measurements were acquired at the TOMCAT beamline, Swiss Light Source, Paul Scherrer Institute in Villigen, Switzerland. Due to the large size of the sample, the slabs (FUM-1980a, b) were mounted using a clamp system developed specifically for this cumbersome object. For optimal penetration (even in the direction parallel to the bedding plane), the X-ray energy was set at 50 keV using a W/Si multilayer monochromator with 2% bandwidth. The X-rays transmitted by the fossil were converted into visible light using a 20 μm thick Ce-doped lutetium aluminium garnet scintillator screen (Crytur, Czech Republic) and magnified using a microscope (Optique Peter, France). The projection data were then digitized using a CCD camera (PCO.2000; PCO GmbH, Germany). For each scan, 3000 raw projections were collected equiangularly over 180°. After flat- and dark-field corrections, the data were assembled using a tomographic reconstruction algorithm based on the Fourier method with re-gridding (Marone & Stampanoni 2012); the resulting volumetric data had a voxel size of 0.74 μm.

TIFF images acquired from the SRXTM examination of FUM-1980a were analysed using the software AMIRA 5.3.3 (<https://www.fei.com/software/amira-3d-for-life-sciences/>). The difference in contrast between the sample and background noise was not enough to perform an automatic segmentation; instead, a conservative threshold was applied such that all pixels belonging to the sample and some of the background regions were labelled, after which erroneously labelled background regions were manually unlabelled in each TIFF image. To visualize the surface topography, the Isosurface, SurfaceGen, SurfaceThickness and SurfaceView modules of AMIRA were utilized.

RESULTS

Macroscopic examination

FUM-1980 comprises a gently curved and somewhat flattened fossilized feather measuring 20.8 mm in length from the base of the calamus to the tips of the distal most barbs. As preserved, the calamus is 0.3 mm wide and at

least 1.1 mm long (the proximal part is faint and thus hard to distinguish from the sedimentary matrix). At its base, the rachis measures approximately 350 μm in diameter; distally, it tapers gradually to a width of *c.* 80 μm before becoming untraceable. Although generally evenly bent, there is a distinct 'kink', interpreted as a taphonomic artefact, in the feather shaft near its apex (Fig. 2A, arrow); however, no corresponding deviation is apparent in the adjacent barbs or barbules.

Surrounding the rachis are two vanes of sub-equal dimensions; these can be divided into a proximal, plumulaceous part (with a blackish colouration) and a distal, pennaceous part (displaying a more greyish hue; Fig. 2A, B). This colour pattern is readily apparent on both the part and counterpart (Fig. 2A, B), and is thus not an artefact of uneven splitting.

In the plumulaceous portion, masses of barbs extend laterally at acute angles from the rachis. The majority of these protrusions are not preserved as individual structures, although some are more or less separate at, or near, the base, and occasionally also close to the tip (Fig. 2A–C). However, in those areas where individual barbs can be distinguished they seem to comprise a darker cortex straddling a more brightly coloured central cavity

(Fig. 2C). Most barbs are virtually straight, although the tips are often slightly curved inwards; nonetheless, folding and wrinkling patterns are also apparent in some places (Fig. 2A, B). Proximal barbs generally measure between 0.5–2.5 mm in length, whereas distal barbs are considerably longer, averring *c.* 7 mm in length. The maximum width of the plumulaceous segment amounts to approximately 7.1 mm.

Close to the base of the rachis, a few barb-like protrusions extend laterally almost perpendicular to the longitudinal axis of the rachis (Fig. 2A, B). It is not known whether these structures represent dislocated barbs from the primary vane or remnants of an afterfeather, although no 'typical' afterfeather features (such as a hyporachis; see Lucas & Stettenheim 1972), were observed.

Preserved barbules are scarce in this part of the fossil; those that can be observed rise at approximately 35–40° to the longitudinal axis of the barbs without any sign of interlocking (Fig. 2C). They measure, on average, 85 μm in length and 4 μm in width and, notably, show more or less even thicknesses throughout their length (Fig. 2C).

In the pennaceous segment, the length of the barbs gradually decreases distally. Consequently, the longest barbs are the proximal ones, and they measure up to

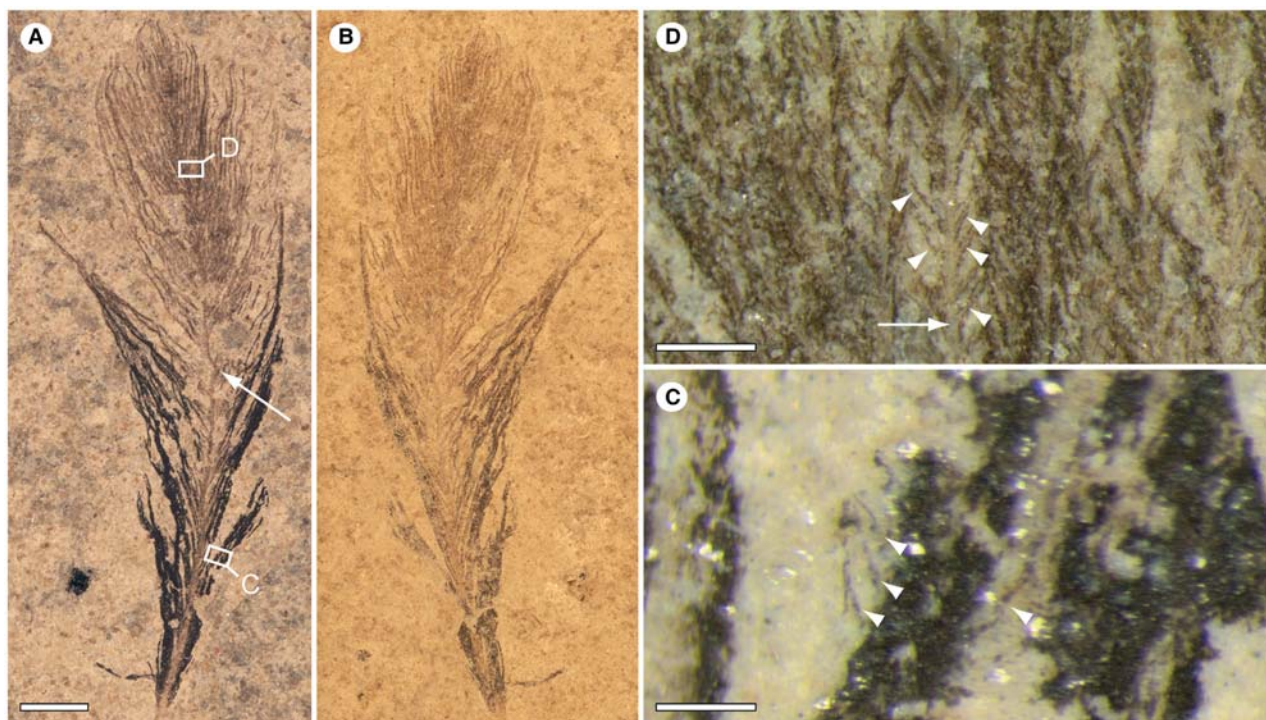


FIG. 2. Fine structures of FUM-1980. A, photograph of FUM-1980a; arrow indicates a 'kink', separating the proximal, plumulaceous part from the distal, pennaceous segment. B, photograph of FUM-1980b; note that the proximal part of the fossil is visually darker on both slabs, indicating that the patterning is not an artefact of uneven splitting. C, close-up image of proximal area demarcated in A; arrowheads indicate plumulaceous barbules. D, close-up image of distal area demarcated in A; arrow indicates pennaceous barb ramus, while arrowheads indicate pennaceous barbules. Scale bars represent: 2 mm (A, B); 100 μm (C, D). Colour online.

6 PALAEOONTOLOGY

c. 10 mm in length. Distal barbs are considerably shorter (down to c. 2 mm) and seem to be offset at more acute angles relative to those in the proximal portion of the pennaceous vane. Close to the feather apex, the barbs are preserved with their longitudinal axes set almost parallel to one another, thereby forming a gently rounded, plume-like structure (Fig. 2A, B). Individual barbs are preserved as dark cortices surrounding a brighter core (Fig. 2D).

Barbules are numerous and best preserved near the central parts of the pennaceous unit. They extend at angles of 30–40° to the barb rami and can be traced for 100–150 µm before being obscured by neighbouring barbs or barbules (Fig. 2D).

Microscopic features

Under SEM and FEG-SEM, it was readily apparent that the feather shaft preserves few original structures; instead,

those areas representing the calamus and rachis (particularly the central parts) were dominated by sedimentary matrix. The barbs, on the other hand, comprised dense mats of oval to elongate depressions, each measuring 3–10 µm in length and 1–4 µm in width (Fig. 3A, B). Such shallow excavations were visible on both the part and counterpart, to suggest that they all, prior to splitting, formed part of an extensive pattern of three-dimensional, sub-spherical to elongate cavities arranged longitudinally along the barbs (Fig. 3A, B).

Associated with the pits were dense clusters of microbodies. Most of these were located within the depressions, although some occurred embedded in the surrounding walls (Fig. 3B). Microbodies in the plumulaceous segment exhibited an oval shape with evenly rounded ends (Fig. 3C, E). Their surface texture was finely granulated with sparse, nm-sized perforations (Fig. 3C, inset), whereas the interior appeared solid (Fig. 3C, short arrow). Microbodies from the pennaceous unit were

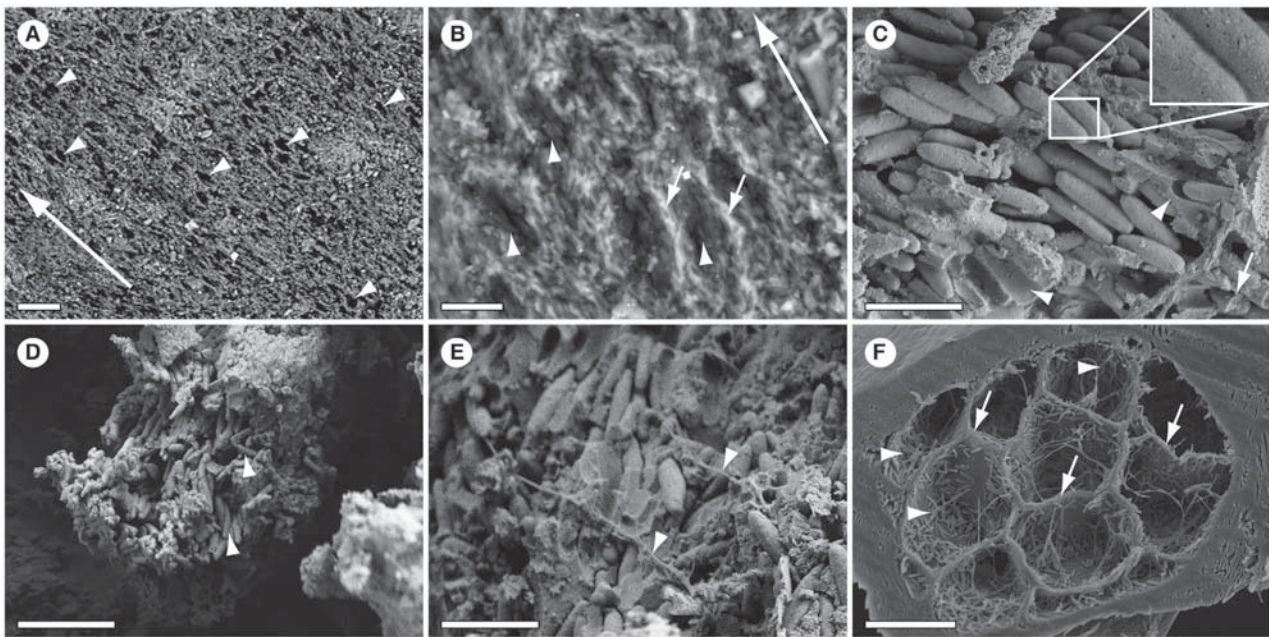


FIG. 3. SEM (A, B) and FEG-SEM (C–E) micrographs of various microstructures preserved in FUM-1980a, together with a SEM micrograph of a transversally sectioned extant feather barb (*Corvus* sp.; F). A, overview of the exposed surface in the plumulaceous portion of FUM-1980; the long arrow indicates the longitudinal axis of the barb; arrowheads indicate elongate depressions, aligned along the barbs. B, close-up view of the depressions; the long arrow indicates the longitudinal axis of the barb; short arrows indicate anastomosing ridges, separating the elongate excavations from one another; arrowheads indicate depressions containing clusters of tightly packed microbodies, aligned lengthwise in the depressions. C, FEG-SEM micrograph of proximal microbodies; inset shows the surface texture of the microbodies, revealing a granulated texture with scattered nm-sized perforations; the short arrow indicates a fragmented microbody with a seemingly homogenous interior; arrowheads indicate amorphous matrix, partly enclosing the microbodies and occasionally retaining imprints of them. D, FEG-SEM micrograph of distal microbodies; note that these structures are substantially smaller and more elongate than the proximal ones; arrowheads indicate heavily curved microbodies. E, FEG-SEM micrograph of proximal microbodies; arrowheads indicate a thread-like network, possibly representing fossilized keratin fibrils. F, a transversally sectioned barb originating from an extant bird feather (*Corvus* sp.), showing microstructures morphologically comparable to those seen in FUM-1980 (B); short arrows indicate keratinous ridges, separating the individual cells of the central pith; arrowheads indicate clusters of melanosomes situated along the pith cell walls. Scale bars represent: 20 µm (A); 5 µm (B); 2 µm (C–E); 10 µm (F).

considerably smaller and more elongate than those in the plumulaceous part (Fig. 3D). They were also frequently curved and occasionally showed an almost sinusoidal shape (Fig. 3D, arrowheads). Those microbodies with a longitudinal axis set more or less perpendicular to the field of view were measured and their shape was assessed by calculating their aspect ratio (AR; i.e. length/width). In the plumulaceous portion, the microbodies were notably larger (mean $1.7 \times 0.5 \mu\text{m}$; $n = 20$) and more rounded (AR = 3.7) than in the pennaceous part (mean $0.9 \times 0.2 \mu\text{m}$, AR = 4.6; $n = 15$).

When not closely stacked on top of each other, the microbodies were entrenched in an amorphous matrix with a seemingly homogeneous texture (Fig. 3C). Some microbodies were almost completely embedded by this medium. Notably, imprints were left behind in the matrix where microbodies had degraded or been artificially removed during splitting (Fig. 3C). In a few places, thread-like structures were observed, each measuring *c.* 70–100 nm in width and several μm in length, branching into threads of even narrower widths (Fig. 3E).

The SRXTM analysis corroborated the presence of numerous elongate depressions, each measuring up to *c.* 10 μm in depth and *c.* $15 \times 5 \mu\text{m}$ in size, scattered over the exposed feather surface (Fig. 4). The excavations corresponded in both size and shape to the structures observed in the SEM images (Fig. 3A, B, arrowheads).

Elemental composition

The elemental composition was determined using EDX microanalysis (Fig. 5), and revealed enrichment of carbon and, to a lesser extent, sulfur in the feather traces relative to the surrounding sediment. The sedimentary matrix, on the other hand, was dominated by silicon, but with significant amounts of calcium and oxygen (these latter elements were present also in the fossil). Trace metals, such as aluminium and iron, occurred at low concentrations, primarily within the sediment.

Molecular analyses

ToF-SIMS images of selected negative ions, used previously to identify eumelanin, silica and the underlying tape (see Lindgren *et al.* 2012, 2014, 2015a, b), revealed heterogeneous spatial distributions (Fig. 6B–E). For instance, ions presumed to represent eumelanin were localized primarily to distinct spots, although areas with high ‘eumelanin’ signal intensity also occurred unevenly scattered across the investigated surfaces (Fig. 6B, E). The spatial distribution of silica, on the other hand, indicated that sedimentary matrix dominated the samples.

Nonetheless, semi-transparent overlay images showed that the silica signal was markedly reduced in areas with enhanced ‘eumelanin’ intensity (Fig. 6B–C, E). Ions representing the underlying tape were localized to positions spatially separated from the fossil material and sedimentary particles (Fig. 6D).

In order to verify the presence of melanic components in the feather traces, spectra from selected areas, or regions of interest (ROI), were generated and compared to reference spectra obtained from various melanin standards (see Lindgren *et al.* 2012, 2014, 2015a, b). From these comparisons, it was readily apparent that all relevant peaks in the eumelanin reference spectra occurred also in spectra obtained from the feather (Fig. 6F). Moreover, the signal intensity distribution of the peaks was virtually identical in the extant and fossil spectra (Fig. 6F, ROI 1; *Sepia*). Conversely, spectra acquired from the sedimentary matrix were dominated by peaks corresponding to silica-related ions (including 60, 76, 77, 119, and 137 u; Fig. 6F, ROI 2), whereas those from the underlying tape displayed yet another set of distinct peaks (Fig. 6F, ROI 3).

To further examine the spatial distribution and spectral properties of the different molecular components on the sample surfaces, principal component analysis (PCA) was employed, using 104 individual ion images in the mass range between 47 and 150 u. In this type of analysis, ions with similar spatial distributions are identified and displayed together in new images; i.e. principal components. This statistical approach (Fig. 7) showed that the third principal component closely matched the original ‘eumelanin’ image (Fig. 6B), indicating that the spatial distribution reflected comparable spectral properties in the entire mass range between 47 and 150 u (and not only properties of those ions used to generate the ‘eumelanin’ image in Fig. 6B). Furthermore, the loadings plot for PC3 (which identifies contributions from the original ion images to the PC3 image) exhibited spectral features that were strikingly similar to those of the eumelanin reference spectra, to suggest that the PC3 image (and hence also the ‘eumelanin’ image) represents the actual spatial distribution of a molecular species that generates negative ion spectra very similar to those obtained from modern eumelanin standards (Fig. 7).

Negative ion data were also recorded with the ToF-SIMS instrument optimized for high mass resolution in order to investigate whether or not the peaks assigned to ‘eumelanin’ originated from the same ions as those in the eumelanin reference spectra. Our analysis revealed that the observed mass positions for all ‘eumelanin’ peaks in the entire mass range between 45 and 150 u were identical (within measurement uncertainties) in the fossil and modern spectra (Table 1).

Collectively, the negative ion data collected from the feather traces exhibited close spectral agreement with

8 PALAEOONTOLOGY

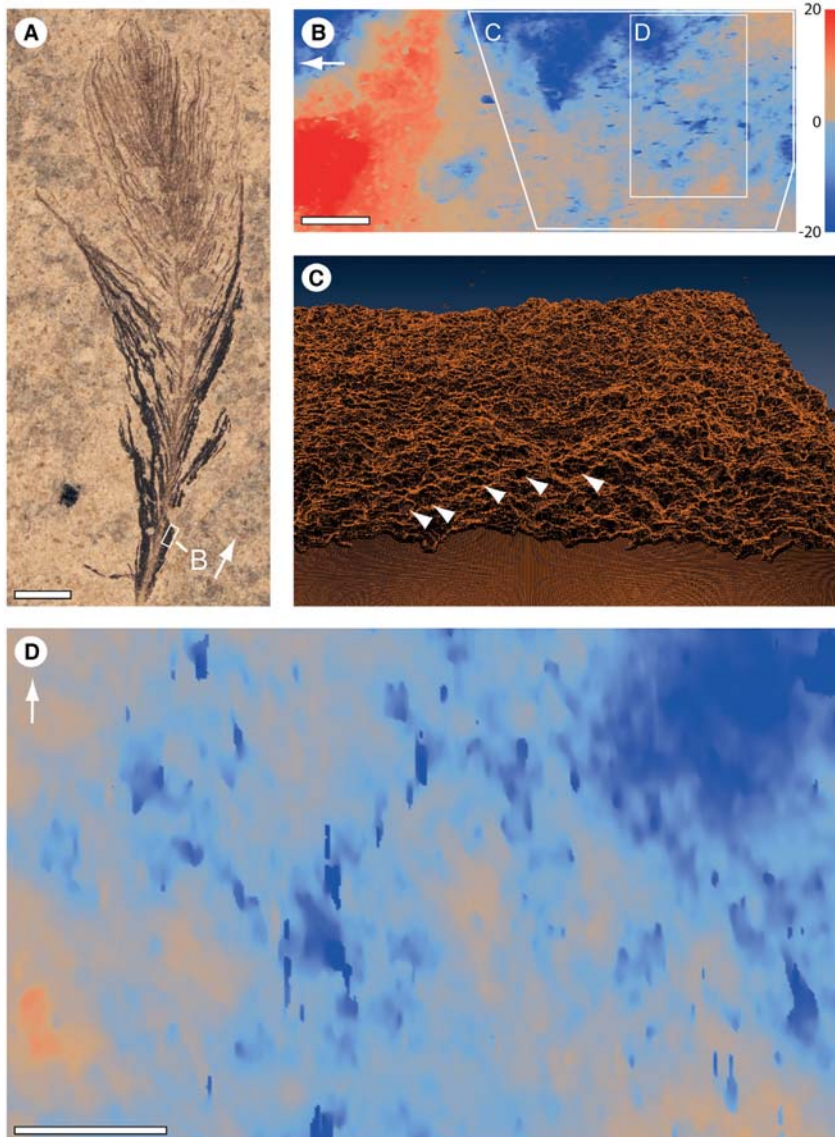


FIG. 4. Surface topography of FUM-1980a, illustrated using SRXTM analysis. A, the fossil with the examined area demarcated by a white rectangle; white arrow indicates the same direction as similar arrows in B and D. B, smoothed surface image of the analysed SRXTM area, highlighting local deviations in topography; red represents peaks of $\geq 20 \mu\text{m}$, whereas blue represents depressions of $\leq -20 \mu\text{m}$ from the normalized mean surface of the analysed area. C, 3D-model (isosurface) of the area demarcated in B; arrowheads indicate shallow excavations covering the surface. D, detail of area demarcated in B; note numerous elongate depressions (blue) on the examined surface. Scale bars represent: 2 mm (A); 100 μm (B); 50 μm (D).

modern eumelanin reference samples. This indicates the presence of this biochrome, or a molecular species very similar to it, in FUM-1980.

The inorganic components of FUM-1980 were further investigated in positive ion mode. These spectra showed strong signal intensity from various Ca_xO_y^+ -related ions, indicating the presence of calcium carbonate and/or calcium oxide at the fossil surfaces. Furthermore, increased signal intensity was observed also for Na^+ , Al^+ , Si^+ , and K^+ , whereas much lower amplitudes were recorded for Mg^+ , Fe^+ and Mn^+ . Images of selected positive ions acquired from the same area as those presented in Figure 6 showed heterogeneous distributions with significant differences between the ions (Fig. 8A–F). For instance, Ca_xO_y^+ -related ions were largely separated from Si^+ ions, as was apparent in overlay images (Fig. 8F). Positive ion spectra from those ROI previously analysed in negative

ion mode (Fig. 6F) indicated slightly increased signal intensity from Ca_xO_y^+ ions in the ‘eumelanin’-rich areas, whereas Al^+ , Si^+ and K^+ intensities were higher in the surrounding sediment. However, direct comparison between the Ca_xO_y^+ (positive ion mode; Fig. 8A) and ‘eumelanin’ (negative ion mode; Fig. 6B) images did not indicate any apparent correlation between these two chemical species.

Finally, the molecular compositions of the plumulaceous and pennaceous parts of FUM-1980 were compared in order to investigate potential differences in eumelanin and pheomelanin content (Colleary *et al.* 2015). Pheomelanin can be distinguished from eumelanin primarily by the presence of strong peaks at 57, 58, 81, 82, 105, 106, 129, and 130 u (Fig. 9), corresponding to sulfur-containing negative ions (i.e. $\text{C}_{n+1}\text{HS}^-$ and C_nNS^- , where $n = 1, 3, 5, 7$). Signal from these ions was evident in both the

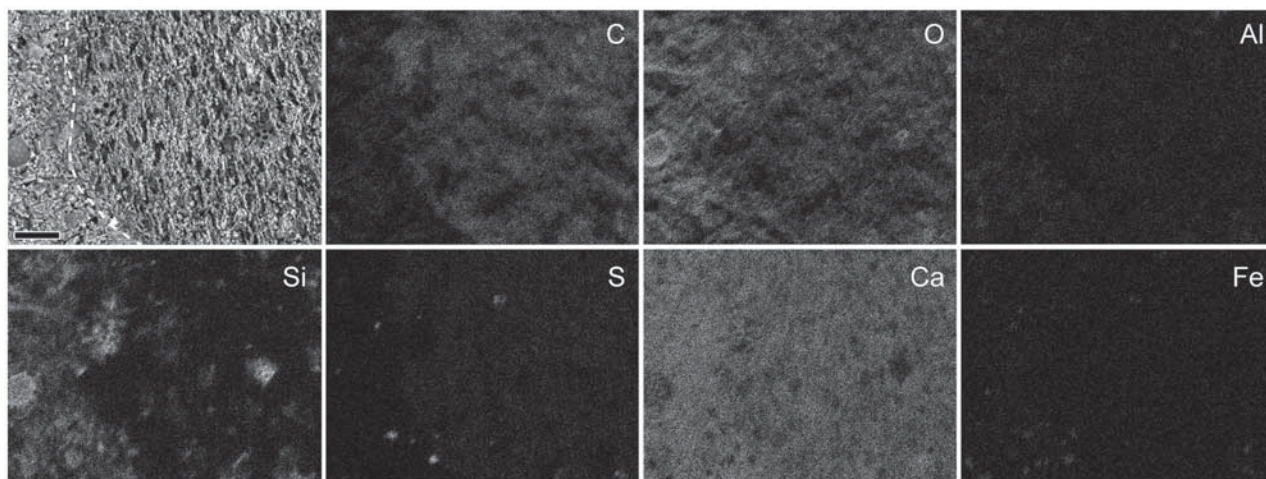


FIG. 5. Single element SEM-EDX maps of FUM-1980a. The top left micrograph represents the analysed area; dashed line separates sediment (left) from feather traces (right). In the element maps, white indicates high intensity whereas black reflects low intensity. The feather trace is dominated by carbon (C), whereas the sediment shows high silicon (Si) intensity. Patches of higher Si intensities surrounded by carbonaceous material can be linked to diatom fragments occurring on the surface. Calcium (Ca) and oxygen (O) are present both in the sediment and, to a slightly lesser degree, in the feather material. Sulfur (S) is also detected, primarily in the feather, and the investigated sample also contains trace amounts of aluminium (Al) and iron (Fe). Scale bar represents 20 μm .

proximal and distal parts of FUM-1980. Importantly though, there were no obvious differences between the plumulaceous and pennaceous parts of FUM-1980 in the relative signal intensity of these peaks compared to 'typical' eumelanin peaks (Fig. 9).

In order to assess the metal content of the fossil and surrounding sedimentary matrix, XAS was employed and a total fluorescence spectrum for the fossil was recorded. XAS provides average spectra of all materials excited by the X-ray beam. Additionally, at the excitation energy level used in this analysis (9600 eV), photons penetrate the carbonaceous feather trace and enter the underlying sediment (which is dominated by Si, O and Ca; see Fig. 5). Carbon absorbs much less of the incoming photons compared to a silicon-based mineral; the absorption length (absorption of c. 63% of the beam) at 9600 eV is 1.7 mm for carbon, whereas in the silicon-based mineral it would be in the order of about 0.1 mm (based on element composition, density, and X-ray energy). Therefore, the spectra taken from the sample spots on the feather were influenced by the underlying sediments. However, at these spots the signal from the sediment was attenuated by the feather residue (first as exciting photons entered the sample, and again as emitted photons left the excited sediment) before photons reached the fluorescence detector. Additionally, the large beam size (1.5 mm) may have resulted in that the adjacent sediment contributed to the signal. Collectively, this caused the metal content of the sediment to dominate all sample spots investigated, but with decreased fluorescence intensity of the Mn and Fe peaks at spots taken on the feather. In Figure 10A, this is visible as a decreased

intensity of the fluorescence peaks in the spectra from the distal (dashed black) and proximal (solid black) spots, correlating with the dark colouration of the fossil; the lowest peak intensities were observed for the darkest sample spot (proximal, solid black spectrum) due to the largest attenuation effect. Typically, *Sepia* eumelanin contains both Fe and Cu, whereas its Mn content is substantially lower (Liu *et al.* 2004). There was, however, no straight-forward way to quantitatively estimate the attenuation effect, since the photon energy also affected the penetration depth of the photons.

Though an attenuation effect was clearly noticeable in the fluorescence data for the Mn and Fe peaks (signal from the sediment was orders of magnitude stronger than signal from the proximal part of the feather; Fig. 10A, grey vs solid black spectra), the Cu signal from these two regions was of similar intensity. Hence, it is feasible that a fair amount of the Cu signal originated from the feather; an assumption that was subsequently corroborated by our Cu EXAFS data.

From analysis of the Cu XANES spectra, indicative of oxidation state and coordination, it was clear that Cu^{II} was the dominating species both in the Cu-containing mineral(s) of the sedimentary matrix (Fig. 10B, grey spectrum) and in *Sepia* eumelanin (Fig. 10B, solid black spectrum); however, importantly, the coordination geometry and ligand identity differed, as was indicated by the dissimilar shape and position of the edges.

The Cu EXAFS spectrum from the proximal part of the feather was compared to spectra from *Sepia* eumelanin and the sedimentary matrix (Fig. 10C). The sediment (grey spectrum) was significantly different from eumelanin

10 PALAEOONTOLOGY

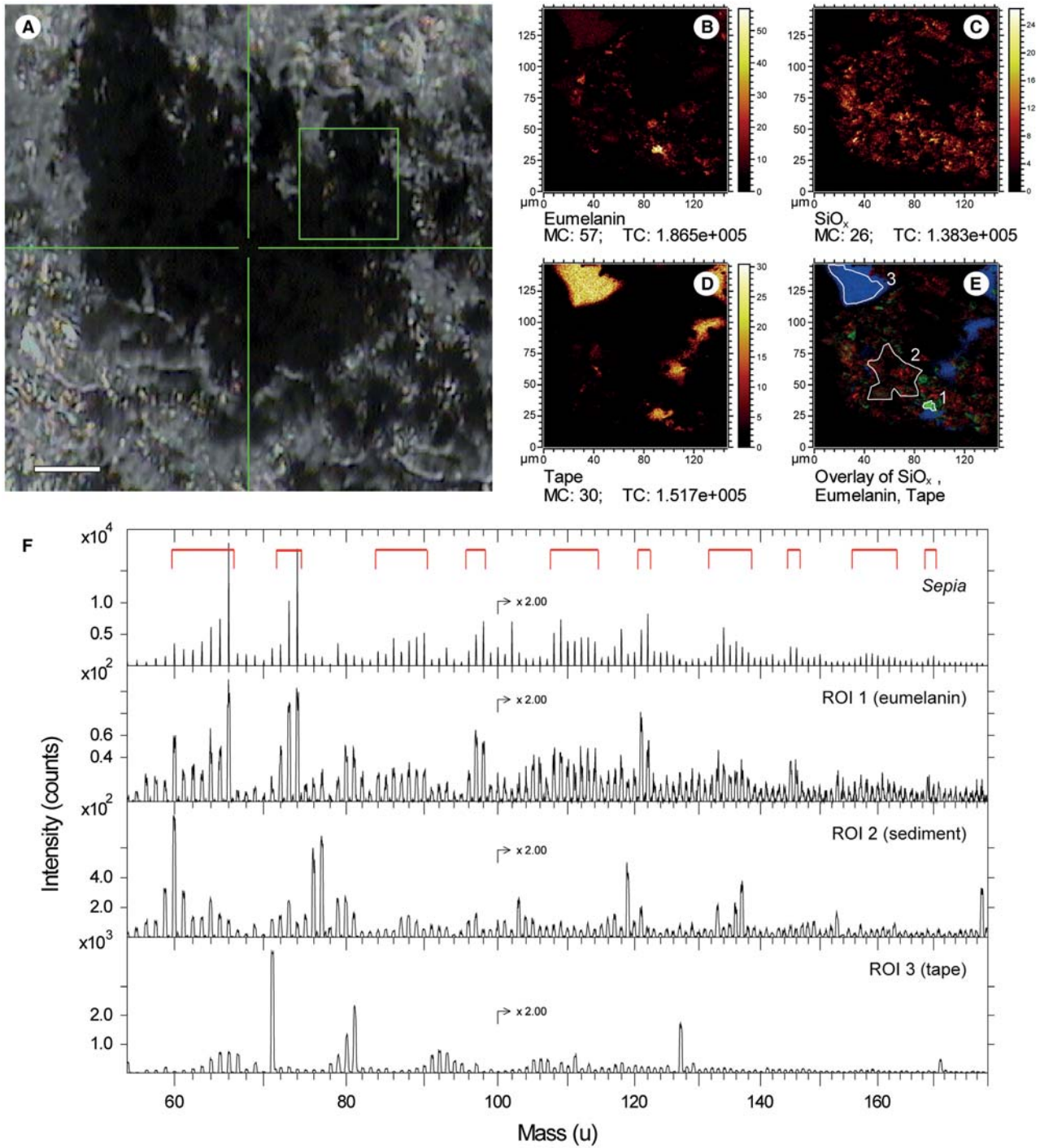


FIG. 6. Negative ion ToF-SIMS analysis of sample removed from the plumulaceous portion of FUM-1980a. A, a camera image of fossil sample particles (deposited on double-sided tape) taken during the ToF-SIMS analysis; the green square indicates the analysis area. B–D, ToF-SIMS images showing the signal intensity distributions of ions possibly representing: B, eumelanin (49 + 50 + 66 + 73 + 74 u); C, silica (60 + 76 + 77 u); D, the tape substrate (71 + 81 u). E, overlay image of silica (red), eumelanin (green) and tape (blue); MC, maximum signal (counts) per pixel; TC, total counts in the image. F, negative ion spectra from a natural eumelanin reference sample (*Sepia*) and selected regions of interest (ROI 1–3) indicated in E; ROI 1 represents an area with strong eumelanin signal, ROI 2 sediment and ROI 3 the underlying tape substrate; peaks that originate from the eumelanin molecular structure are indicated by the red brackets. Scale bar represents 100 μm .

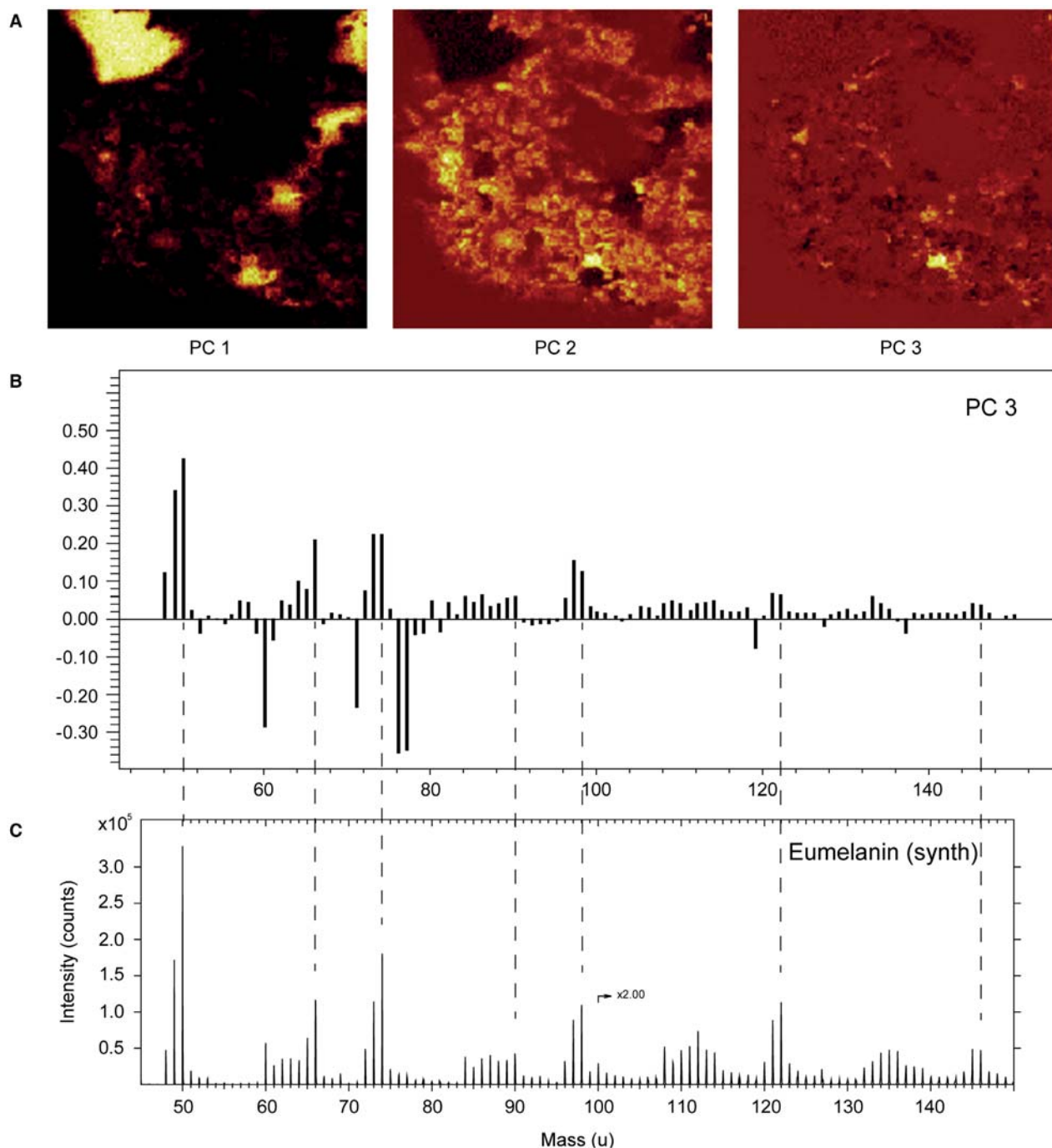


FIG. 7. Results from principal components analysis (PCA) of the negative ion data partially presented in Figure 6. The analysis included all peaks between 47 and 150 u. A, ion images of principal components (PC) 1–3; the PC 1 image highlights features related to the tape, whereas the PC 2 image outlines the signal intensity distribution from the fossil particles; the PC 3 image shows intensities with a similar distribution as the ‘eumelanin’ image presented in Figure 6B. B–C, comparison of the loadings plot for PC 3 (B) with the reference spectrum of synthetic eumelanin (C) confirms the link between the PC 3 image and the eumelanin distribution, in that the general features of the eumelanin spectrum is reproduced as positive loadings in PC 3. The peaks with negative loadings are characteristic for tape (52, 71, 81 and 127 u) and SiO_x (60, 76, 77, 119 and 137 u). Peaks corresponding to sulfur-containing ions in the pheomelanin spectrum (at 57, 58, 81, 82, 105, 106, 129 and 130 u) occur with positive loadings in PC 3, indicating that these ions have a spatial distribution similar to that of eumelanin. Colour online.

12 PALAEOLOGY

TABLE 1. Observed peak positions (u) of major eumelanin peaks in negative ion spectra obtained from FUM-1980a together with natural (*Sepia*) and synthetic eumelanin standards.

Ion	Theoretical mass	Observed mass		
		FUM-1980	<i>Sepia</i> eumelanin	Synthetic eumelanin
C ₄	48.000	47.997	48.000	47.998
C ₄ H	49.008	49.001	49.009	49.009
C ₃ N	50.003	50.007	50.006	50.006
C ₄ HO	65.003	65.011	65.011	65.007
C ₃ NO	65.998	65.998	66.001	66.001
C ₆	72.000	71.995	72.001	71.997
C ₆ H	73.008	73.008	73.009	73.007
C ₅ N	74.003	74.002	74.005	74.004
C ₇	84.000	83.993	83.999	83.997
C ₇ H	85.008	85.000	85.008	85.004
C ₆ N	86.003	86.007	86.006	86.005
C ₆ HN	87.011	87.015	87.011	87.011
C ₅ HN ₂	89.009	89.004	89.011	89.008
C ₅ NO	89.998	90.002	90.000	90.000
C ₈	96.000	95.988	95.998	95.995
C ₈ H	97.008	97.004	97.008	97.005
C ₇ N	98.003	97.999	98.003	98.002
C ₉	108.000	107.992	107.992	107.995
C ₉ H	109.008	109.002	109.002	109.003
C ₈ N	110.003	109.998	110.005	110.004
C ₈ HN	111.011	111.008	111.010	111.009
C ₇ HN ₂	113.008	112.982	113.012	113.011
C ₇ NO	113.998	113.924	113.998	113.996
C ₁₀ H	121.008	121.000	121.005	121.003
C ₉ N	122.003	121.999	122.000	121.999
C ₁₂ H	145.008	144.985	145.003	145.000
C ₁₁ N	146.003	145.971	146.000	146.000

The spectra were acquired with the ToF-SIMS instrument optimized for high mass resolution. Putative ion assignments and corresponding theoretical ion mass values are included for comparison.

(dashed black spectrum), again suggesting a dissimilar coordination of Cu^{II} in the mineral(s) (as observed via XANES). At the proximal sample spot (located in the darkest part of the feather), a spectrum clearly deviating from the sedimentary EXAFS spectrum was observed (Fig. 10C, solid black and grey spectra; in particular, compare at 6 Å⁻¹ and above). In the Fourier transforms (FT) of EXAFS (Fig. 10D), the first dominating FT peak represents the distance to the nearest atom neighbours, given as the reduced distance (to get the actual distance the EXAFS has to be simulated taking the scattering phases into account, +0.2–0.5 Å). Clearly, the dominating FT peak from the proximal, dark feather spot (solid black) was located between the most pronounced FT peaks from *Sepia* eumelanin (Fig. 10D, dashed black) and sediment (Fig. 10D, grey). Translated into reduced distances, *Sepia*

eumelanin was centred at 1.5 Å, the feather at 1.8 Å and the sediment at 2.0 Å. Accordingly, Cu^{II} ions in the proximal part of the feather (solid black), corresponding to the darkest part of the specimen, had an average Cu-to-nearest neighbour distance of 1.8 Å (reduced distance). The peak position for the proximal part of the feather (Fig. 10D) could therefore be the result of a mixed spectrum from the ‘eumelanin’ coordinated Cu ions within the feather trace, and the Cu mineral(s) from the underlying sedimentary matrix. However, simulation of EXAFS was complicated by the fact that the sediment seemed to contain a mix of unknown Cu-species, and consequently was not attempted. The Cu EXAFS of the distal spot and one additional proximal spot (not shown) were completely dominated by Cu signal from the underlying sediment. We attribute the difference of the proximal spectra and sediment to a low amount of eumelanin in that part of the feather.

DISCUSSION

Structure and ultrastructure of FUM-1980

With its symmetrical vanes, sub-divided into distinct plumulaceous and pennaceous segments, FUM-1980 can be confidently identified as a contour feather (see Lucas & Stettenheim 1972). The extent of the plumulaceous portion (comprising roughly half of the length of the rachis) further distinguishes it from both remiges and rectrices (Lucas & Stettenheim 1972). Consequently, the fossil most likely represents a body feather, although its precise location remains unknown. The size of FUM-1980 further indicates that it must have originated from a bird at least the size of a modern thrush (A. Hedenström, pers. comm. 2016).

In extant avialans, the rigid pennaceous portion helps to protect the feather against physical stress and mechanical damage (Lucas & Stettenheim 1972; Bonser 1995). This part is often also prominently coloured, thereby aiding in camouflage or advertisement (Savalli 1995). The downy section, on the other hand, is usually more or less covered by neighbouring feathers and primarily functions as an insulator (Lucas & Stettenheim 1972). In FUM-1980, individual barbs of the plumulaceous vanes are hard to discriminate; instead, they appear to be intertwined into bundles of variable thicknesses (Fig. 2A–C). With few exceptions (see below), this part also lacks clearly distinguishable barbules (Fig. 2C). In modern feathers, plumulaceous barbules generally lack a stabilizing function (Lucas & Stettenheim 1972), and the absence of this characteristic may have facilitated adherence of the barbs when the feather was deposited. Conversely, the preservation of individual barbs in the pennaceous vanes may, at least partially, be attributed to stiffening actions by barbules (Lucas & Stettenheim 1972).

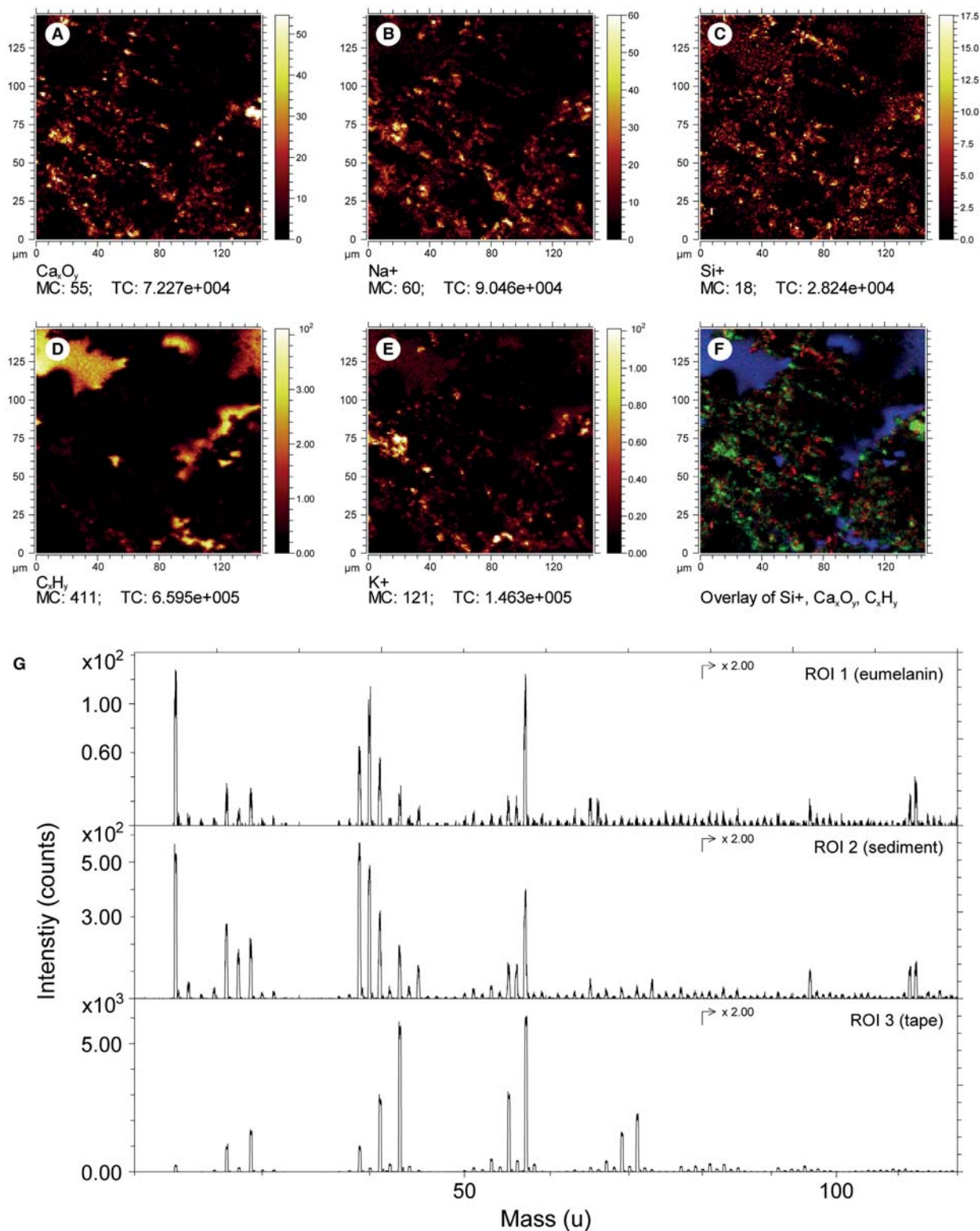


FIG. 8. Positive ion ToF-SIMS analysis of fossil feather particles from the same area as in Figure 6. A, Ca_xO_y (representing calcium oxide/carbonate) obtained by addition of peak signals at 96 (Ca_2O^+), 112 (Ca_2O_2^+), 113 ($\text{Ca}_2\text{O}_2\text{H}^+$), 152 (Ca_3O_2^+), 168 (Ca_3O_3^+) and 169 u ($\text{Ca}_3\text{O}_3\text{H}^+$). B, Na^+ (signal at 23 u). C, Si^+ (signal at 28 u). D, C_xH_y (representing the tape substrate) obtained by adding the peak signals at 29 (C_2H_5^+), 43 (C_3H_7^+), 57 (C_4H_9^+) and 71 u ($\text{C}_5\text{H}_{11}^+$). E, K^+ (signal at 39 u). F, overlay image of Si^+ (red), Ca_xO_y (green) and C_xH_y (blue). G, positive ion spectra obtained from ROI 1–3 (as indicated in Fig. 6E), representing areas with eumelanin, sediment and tape, respectively. *Abbreviations:* MC, maximum signal (counts) per pixel; TC, total counts in the image.

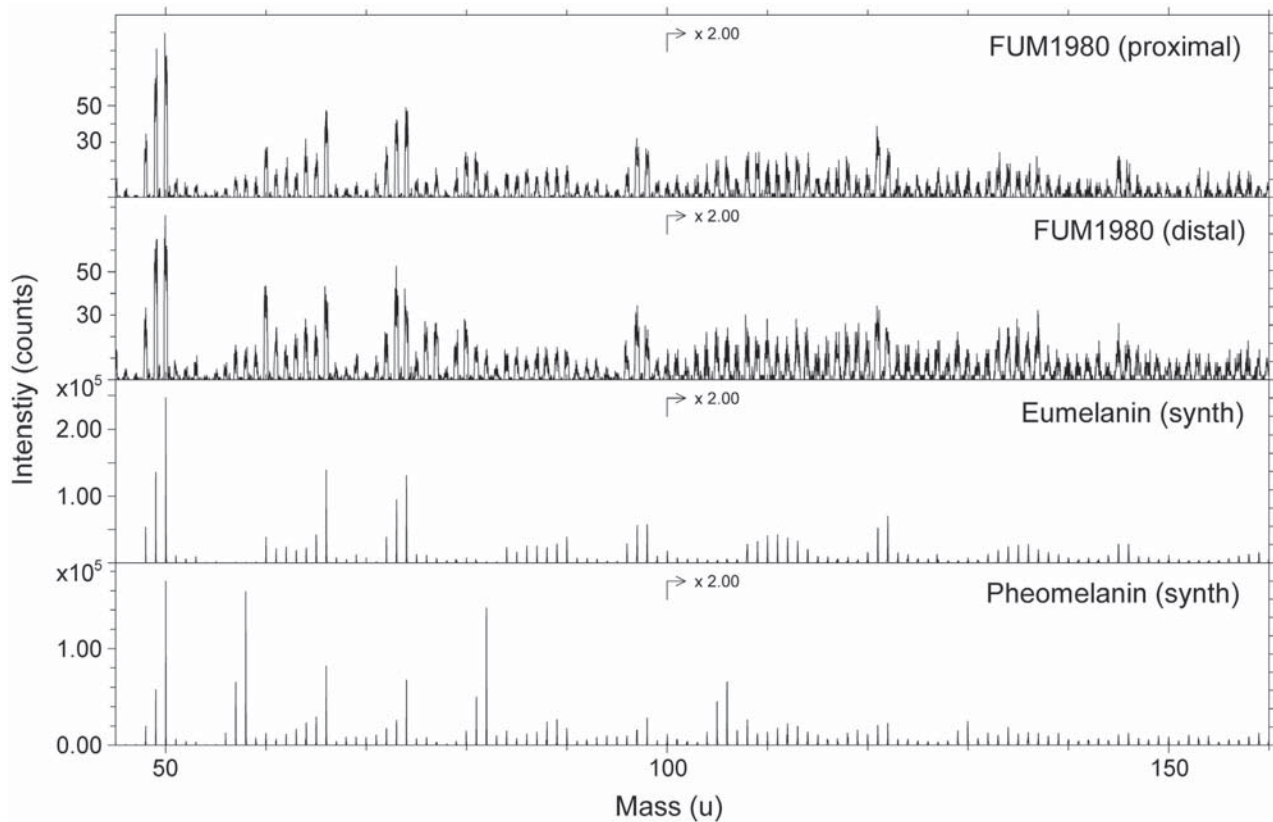


FIG. 9. Negative ion ToF-SIMS spectra obtained from the distal and proximal parts of FUM-1980a, together with spectra acquired from synthetic eumelanin and pheomelanin, respectively.

Despite its somewhat flattened state, FUM-1980 reveals important ultrastructural details. For instance, under SEM and FEG-SEM, 5–10 μm long, oval to elongate depressions can be seen along the centre of the barbs on both the part and counterpart (Fig. 3A, B). Our SRXTM analysis corroborated the presence of such features, and also confirmed their three-dimensional nature and organisation (Fig. 4). The cavities are separated from one another by anastomosing ridges, and appear similar to microscopic features previously described in a fossil feather from the Lower Cretaceous of China (Zhang *et al.* 2010, fig. 1). Collectively, these voids resemble the medullary pith (or ‘cytoplasmic voids’; Prum *et al.* 2009) of modern feather barbs (Fig. 3F), which primarily consists of air-filled cells separated from one another by keratinous walls (Lucas & Stettenheim 1972). Notably though, we did not detect any biomarkers indicative of keratinous proteins, although a fine network of thread-like structures, possibly representing remnant keratin fibrils, was observed in some places (Fig. 3E). A perforated, almost spongy texture is present also in some acid-treated bacterial biofilms (Pacton *et al.* 2006); however, in these secretions the pitting does not appear to be as organized and regularly spaced as in FUM-1980. Additionally, there is also a considerable size

difference between these structures; the voids in bacterial biofilms measure about 1–2 μm (Pacton *et al.* 2006) compared to the 5–10 μm pits observed in the feather (Fig. 3A, B).

Identification and implications of preserved melanosomes

In modern feathers, colour is produced in part by melanic pigments (McGraw 2006), of which two main types have been recognized: eumelanin, imparting dark brown to black colours, and pheomelanin, which is partially responsible for yellow to reddish hues (Prota 1980; McGraw 2006). Animal melanins are synthesized, packaged and stored in melanosomes; i.e. intracellular, lysosome-related organelles (Seiji *et al.* 1961; Marks & Seabra 2001). It has been suggested that the shape of these microscopic structures is indicative of the main type of melanin they possess: melanosomes in which pheomelanin predominates are generally considered to be small and spherical, whereas eumelanin-dominated melanosomes are larger and more elongate (Liu *et al.* 2005a; McGraw 2006; Colleary *et al.* 2015). Notable exceptions do exist, however, such as retinal melanosomes. In these organelles the size and shape may vary despite the fact

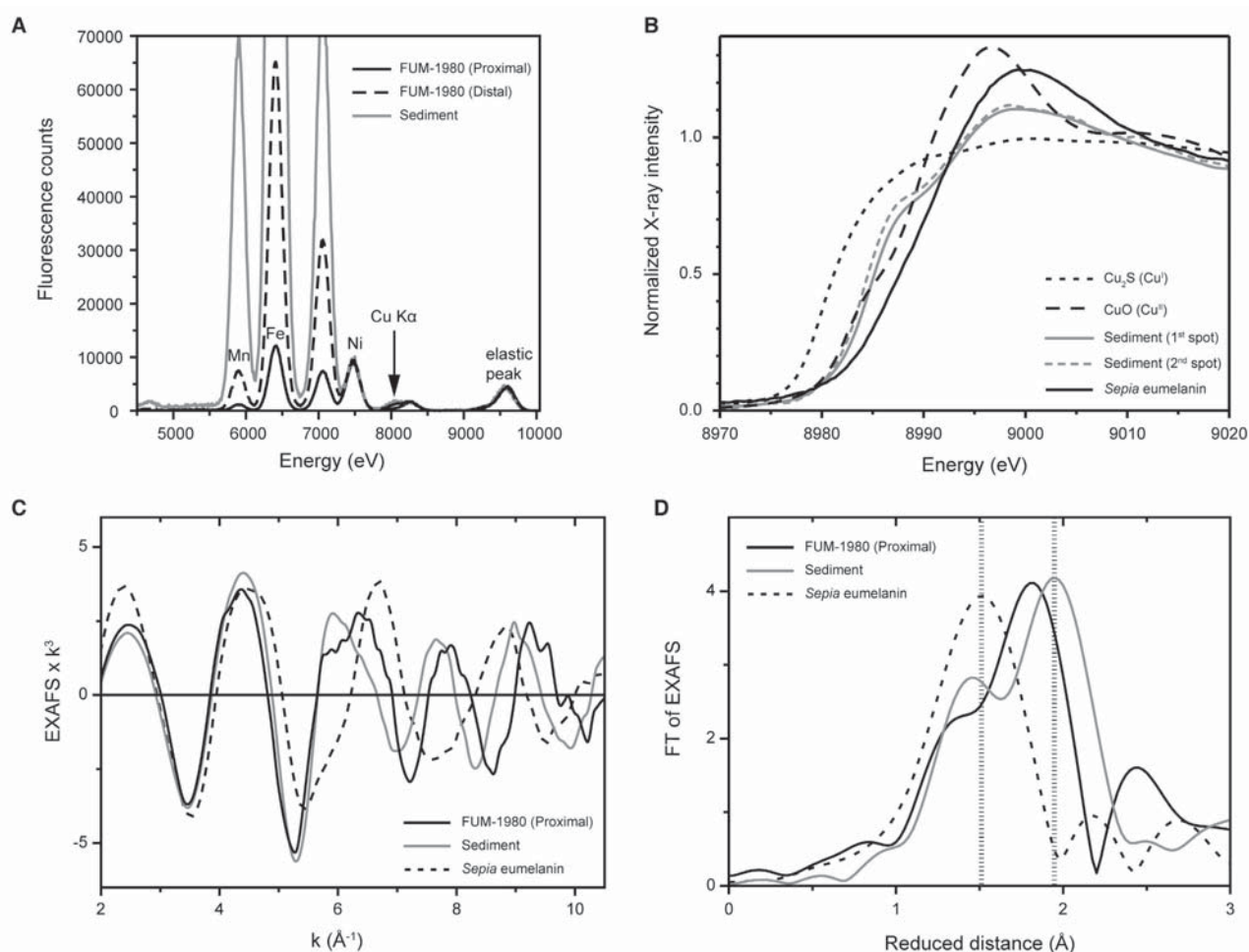


FIG. 10. Results from XAS analysis of FUM-1980a. A, total fluorescence spectrum after excitation at 9600 eV, normalized on the Ni K α emission line from proximal (solid black), distal (dashed black) and sediment (grey) sample spots on FUM-1980a. The Mn, Fe, Ni and Cu K α emission lines are marked, as well as the elastic scattering peak. B, the Cu K-edge of FUM-1980a sedimentary matrix (solid and dashed grey) compared to Cu^I (Cu₂S, short dashed black) and Cu^{II} (CuO, long dashed black) minerals and *Sepia eumelanin* (solid black). C, k^3 weighted EXAFS at the Cu K-edge of FUM-1980a; ‘darkest’ spot of proximal part (solid black) and sediment (grey), compared to *Sepia eumelanin* (dashed black). D, Fourier transforms of the EXAFS (in same colour code as C). The dotted vertical lines mark the major peaks in *Sepia eumelanin* and sediment, respectively.

that the melanin content is eumelaninic (Liu *et al.* 2005b; Zareba *et al.* 2006; Lindgren *et al.* 2015a).

Our ToF-SIMS analyses did identify animal eumelanin, or a molecular compound very similar to this biochrome, in some areas of FUM-1980 (Figs 6B, F, 9). Moreover, under SEM and FEG-SEM, it was readily apparent that the exposed surfaces were littered by micrometre-sized, elliptical to highly elongate bodies (Fig. 6B–E). Although many microorganisms overlap in both shape and size with vertebrate pigment organelles (Moyer *et al.* 2014), the co-localisation of an animal eumelanin-like molecule (or molecules) provides compelling evidence to suggest that the microbodies in FUM-1980 represent remnant eumelanosomes rather than microbial traces.

Although the presumed fossil melanosomes within each feather segment were morphologically more or less

homogenous, they were noticeably different between the plumulaceous and pennaceous parts of the feather (Fig. 3C–E). This divergence was reflected also at the macroscopic level: in the fossil, the downy portion is distinctly black, whereas the pennaceous segment has a more greyish hue (Fig. 2A, B). Despite these differences, however, ToF-SIMS spectra generated from the proximal and distal parts of the feather were conspicuously similar to one another; i.e. they were dominated by eumelanin-related ions, but with clear signals from presumed pheomelanin-related peaks (including sulfur-containing ions at 57, 58, 81, 82, 105, 106, 129 and 130 u). Additionally, we did not detect any significant differences in relative intensity of the pheomelanin-like peaks compared to ‘typical’ eumelanin peaks in spectra collected from the plumulaceous and pennaceous parts of the feather

16 PALAEOONTOLOGY

(Fig. 9). Thus, pheomelanin could be present in both the proximal and distal parts of FUM-1980 or, alternatively, the sulfur-containing ions could originate from diagenetically incorporated sulfur in the eumelanin molecular structure. Sulfur could potentially stem from surrounding sediments (McNamara *et al.* 2016) or from degraded β -keratin (a major feather constituent containing the sulfur-rich amino acid cysteine; Alibardi & Toni 2006). A diagenetic incorporation of sulfur would imply that pheomelanin is present either at very low concentrations, or at locations where it is not accessible for ToF-SIMS analysis (such as the interior of the melanin granules; Simon & Peles 2010). Alternatively, pheomelanin may have been lost through degradation or was absent altogether from the beginning. Because the presumed melanosomes are of two distinct morphologies yet possess virtually identical molecular compositions (based on our ToF-SIMS data), we consider the sulfur-containing, seemingly pheomelanin-related ions in FUM-1980 primarily to have a diagenetic origin, in accordance with McNamara *et al.* (2016) and *contra* Colleary *et al.* (2015).

Another interesting aspect of the fossil microbodies relate to their appearance. Notwithstanding possible taphonomic, geochemical and/or diagenetic alterations (see Glass *et al.* 2013; McNamara *et al.* 2013; Lindgren *et al.* 2015a), the pigment organelles in the pennaceous portion of FUM-1980 compare favourably in morphology with melanosomes in modern iridescent feathers (Li *et al.* 2012). The microstructures in the downy part, on the other hand, correspond in both size and aspect ratio to melanosomes in grey contour feathers of extant parrots (Clarke *et al.* 2010; Li *et al.* 2010, 2012) an avian clade that has previously been reported from the Fur Formation (Waterhouse *et al.* 2008). Thus, FUM-1980 could belong to a psittaciform bird, a tentative assignment that is corroborated by the form of the (few) preserved barbules in the plumulaceous segment. As is the case in extant parrots, these exhibit nearly constant widths rather than tapering distally, as is common in most other avialans (Lucas & Stettenheim 1972).

Acknowledgements. Ola Gustafsson, Department of Biology, Lund University, assisted during the SEM analyses. Basil el Jundi, Department of Biology, Lund University, provided access to the AMIRA software. Anders Hedenström, Department of Biology, Lund University, provided helpful comments that greatly benefited the description of FUM-1980. This project was funded through grant from the Royal Physiographic Society in Lund to JAG and grants from the Swedish Research Council to MEE (grant 2015-05084) and JL (grant 642-2014-3773). Alison Moyer and an anonymous reviewer provided feedback on an earlier version of the manuscript.

Editor. Sarah Gabbott

REFERENCES

- ALIBARDI, L. and TONI, M. 2006. Cytochemical, biochemical and molecular aspects of the process of keratinization in the epidermis of reptilian scales. *Progress in Histochemistry & Cytochemistry*, **40**, 73–134.
- BØGGLID, O. B. 1918. Den vulkanske aske i Moleret samt en oversigt over Danmarks ældre Tertiærbjergarter. *Danmarks Geologiske Undersøgelse*, **2**, 1–159.
- BONDE, N. 1979. Palaeoenvironment in the 'North Sea' as indicated by the fish bearing Mo-Clay deposit (Paleocene/Eocene), Denmark. *Mededelingen van de Werkgroep voor Tertiaire en Kwartaire Geologie*, **16**, 3–16.
- ANDERSEN, S., HALD, N. and JAKOBSEN, S. L. 2008. *Danekræ – Danmarks bedste fossiler*. Gyldendal, Copenhagen.
- BONSER, R. H. C. 1995. Melanin and the abrasion resistance of feathers. *The Condor*, **97**, 590–591.
- BRIGGS, D. E. and SUMMONS, R. E. 2014. Ancient biomolecules: their origins, fossilization, and role in revealing the history of life. *Bioessays*, **36**, 482–490.
- CHAMBERS, L., PRINGLE, M., FITTON, J. G., LARSEN, L. M., PEDERSEN, A. K. and PARRISH, R. 2003. Recalibration of the Paleocene-Eocene boundary (P-E) using high precision U-Pb and Ar-Ar isotopic dating. EGS-AGU-EUG Assembly, Nice 6–11 April. *Geophysical Research Abstracts*, **5**, 09681.
- CHRISTENSEN, E. F. and HALD, N. 1990. Danekræ – et nyt begreb i dansk museumslovgivning. *Arkæologiske udgravninger i Danmark*, **1990**, 7–16.
- CLARKE, J. A., KSEPKA, D. T., SALAS-GISMONDI, R., ALTAMIRANO, A. J., SHAWKEY, M. D., D'ALBA, L., VINTHER, J., DEVRIES, T. J. and BABY, P. 2010. Fossil evidence for evolution of the shape and color of penguin feathers. *Science*, **330**, 954–957.
- CODY, G. D., GUPTA, N. S., BRIGGS, D. E. G., KILCOYNE, A. L. D., SUMMONS, R. E., KENIG, F., PLOTNICK, R. E. and SCOTT, A. C. 2011. Molecular signature of chitin-protein complex in Paleozoic arthropods. *Geology*, **39**, 255–258.
- COLLEARY, C., DOLOCAN, A., GARDNER, J., SINGH, S., WUTTKE, M., RABENSTEIN, R., HABERSETZER, J., SCHAAL, S., FESEHA, M., CLEMENS, M., JACOBS, B. F., CURRANO, E. D., JACOBS, L. L., SYLVESTERSEN, R. L., GABBOTT, S. E. and VINTHER, J. 2015. Chemical, experimental, and morphological evidence for diagenetically altered melanin in exceptionally preserved fossils. *Proceedings of the National Academy of Sciences*, **112**, 12592–12597.
- DAU, H., LIEBISCH, P. and HAUMANN, M. 2003. X-ray absorption spectroscopy to analyze nuclear geometry and electronic structure of biological metal centers – potential and questions examined with special focus on the tetra-nuclear manganese complex of oxygenic photosynthesis. *Analytical & Bioanalytical Chemistry*, **376**, 562–583.
- DAVIS, P. G. and BRIGGS, D. E. G. 1995. Fossilization of feathers. *Geology*, **23**, 783–786.
- EDWARDS, N. P., MANNING, P. L. and WOGELIUS, R. A. 2014. Pigments through time. *Pigment Cell & Melanoma Research*, **27**, 684–685.

- EGGER, H. and BRÜCKL, E. 2006. Gigantic volcanic eruptions and climatic change in the early Eocene. *International Journal of Earth Sciences*, **95**, 1065–1070.
- GIBBONS, A. 2010. Tiny time machines revisit ancient life. *Science*, **330**, 1616.
- GLASS, K., ITO, S., WILBY, P. R., SOTA, T., NAKAMURA, A., BOWERS, C. R., VINTHER, J., DUTTA, S., SUMMONS, R., BRIGGS, D. E., WAKAMATSU, K. and SIMON, J. D. 2012. Direct chemical evidence for eumelanin pigment from the Jurassic period. *Proceedings of the National Academy of Sciences*, **109**, 10218–10223.
- — — — — MILLER, K. E., DUTTA, S., SUMMONS, R. E., BRIGGS, D. E. G., WAKAMATSU, K. and SIMON, J. D. 2013. Impact of diagenesis and maturation on the survival of eumelanin in the fossil record. *Organic Geochemistry*, **64**, 29–37.
- GURLEY, L. R., VALDEZ, J. G., SPALL, W. D., SMITH, B. F. and GILLETTE, D. D. 1991. Proteins in the fossil bone of the dinosaur, *Seismosaurus*. *Journal of Protein Chemistry*, **10**, 75–90.
- HEILMANN-CLAUSEN, C. 1995. Palæogene aflejringer over danskekalken. 70–114. In NIELSEN, O. B. (ed.) *Danmarks Geologi Fra Kridt Til I Dag*. Aarhus Geokompender, **1**, Geologisk Institut, Aarhus Universitet, 290 pp.
- HENRIKSEN, K. L. 1922. Eocene insects from Denmark. *Danmarks Geologiske Undersøgelse*, **2**, 1–36.
- KARL, H.-V. and MADSEN, H. 2012. *Tasbacka danica* n. sp., a new Eocene marine turtle of Denmark (Testudines: Chelonioidae). *Studia Geologica Salmanticensia*, **9**, 193–204.
- KNOX, R. W. O. and HOLLOWAY, S. 1992. Paleogene of the central and northern North Sea. In KNOX, R. W. O. and CORDEY, W. G. (eds.) *Lithostratigraphic nomenclature of the UK North Sea*. British Geological Survey, 206 pp.
- LARSSON, S. G. 1975. Paleobiology and mode of burial of the insects of the Lower Eocene Mo-Clay of Denmark. *Bulletin of the Geological Society of Denmark*, **24**, 193–209.
- LI, Q., GAO, K. Q., VINTHER, J., SHAWKEY, M. D., CLARKE, J. A., D'ALBA, L., MENG, Q., BRIGGS, D. E. and PRUM, R. O. 2010. Plumage color patterns of an extinct dinosaur. *Science*, **327**, 1369–1372.
- — — MENG, Q., CLARKE, J. A., SHAWKEY, M. D., D'ALBA, L., PEI, R., ELLISON, M., NORELL, M. A. and VINTHER, J. 2012. Reconstruction of Microraptor and the evolution of iridescent plumage. *Science*, **335**, 1215–1219.
- — — CLARKE, J. A., GAO, K.-Q., ZHOU, C.-F., MENG, Q., LI, D., D'ALBA, L. and SHAWKEY, M. D. 2014. Melanosome evolution indicates a key physiological shift within feathered dinosaurs. *Nature*, **507**, 350–353.
- LINDGREN, J., UVDAL, P., SJÖVALL, P., NILSSON, D. E., ENGD AHL, A., SCHULTZ, B. P. and THIEL, V. 2012. Molecular preservation of the pigment melanin in fossil melanosomes. *Nature Communications*, **3**, 824.
- — — SJÖVALL, P., CARNEY, R. M., UVDAL, P., GREN, J. A., DYKE, G., SCHULTZ, B. P., SHAWKEY, M. D., BARNES, K. R. and POLCYN, M. J. 2014. Skin pigmentation provides evidence of convergent melanism in extinct marine reptiles. *Nature*, **506**, 484–488.
- — — MOYER, A., SCHWEITZER, M. H., SJÖVALL, P., UVDAL, P., NILSSON, D. E., HEIMDAL, J., ENGD AHL, A., GREN, J. A., SCHULTZ, B. P. and KEAR, B. P. 2015a. Interpreting melanin-based coloration through deep time: a critical review. *Proceedings of the Royal Society B*, **282**, 20150614.
- — — SJÖVALL, P., CARNEY, R. M., CINCOTTA, A., UVDAL, P., HUTCHESON, S. W., GUSTAFSSON, O., LEFEVRE, U., ESCUILLIE, F., HEIMDAL, J., ENGD AHL, A., GREN, J. A., KEAR, B. P., WAKAMATSU, K., YANS, J. and GODEFROIT, P. 2015b. Molecular composition and ultrastructure of Jurassic paravian feathers. *Scientific Reports*, **5**, 13520.
- LIU, Y., HONG, L., KEMPF, V. R., WAKAMATSU, K., ITO, S. and SIMON, J. D. 2004. Ion-exchange and adsorption of Fe(III) by *Sepia* melanin. *Pigment Cell Research*, **17**, 262–269.
- — — WAKAMATSU, K., ITO, S., ADHYARU, B. B., CHENG, C.-Y., BOWERS, C. R. and SIMON, J. D. 2005a. Comparisons of the structural and chemical properties of melanosomes isolated from retinal pigment epithelium, iris, and choroid of newborn and mature bovine eyes. *Photochemistry & Photobiology*, **81**, 510–516.
- — — — — ADHYARU, B., CHENG, C. Y., BOWERS, C. R. and SIMON, J. D. 2005b. Comparison of structural and chemical properties of black and red human hair melanosomes. *Photochemistry & Photobiology*, **81**, 135–144.
- LUCAS, A. M. and STETTENHEIM, P. R. 1972. *Avian anatomy integument*. US Government Printing Office, Washington, DC.
- MARKS, M. S. and SEABRA, M. C. 2001. The melanosome: membrane dynamics in black and white. *Nature Reviews Molecular Cell Biology*, **2**, 738–748.
- MARONE, F. and STAMPANONI, M. 2012. Regriding reconstruction algorithm for real-time tomographic imaging. *Journal of Synchrotron Radiation*, **19**, 1029–1037.
- McGRAW, K. J. 2006. Mechanics of melanin-based coloration. In HILL, G. E. and McGRAW, K. J. (eds.) *Bird coloration. Vol. 1. Mechanisms and measurements*. Harvard University Press, 640 pp.
- McNAMARA, M. E., BRIGGS, D. E. G., ORR, P. J., FIELD, D. J. and WANG, Z. 2013. Experimental maturation of feathers: implications for reconstructions of fossil feather colour. *Biology Letters*, **9**, 20130184.
- — — DONGEN, B. E. VAN, LOCKYER, N. P., BULL, I. D. and ORR, P. J. 2016. Fossilization of melanosomes via sulfurization. *Palaeontology*, **59**, 337–350.
- MOYER, A. E., ZHENG, W., JOHNSON, E. A., LAMANNA, M. C., LI, D., LACOVARA, K. J. and SCHWEITZER, M. H. 2014. Melanosomes or microbes: testing an alternative hypothesis for the origin of microbodies in fossil feathers. *Scientific Reports*, **4**, 4233.
- PACTON, M., FIET, N. and GORIN, G. 2006. Revisiting amorphous organic matter in Kimmeridgian laminites: what is the role of the vulcanization process in the amorphization of organic matter? *Terra Nova*, **18**, 380–387.
- PEDERSEN, G. K. 1981. Anoxic events during sedimentation of a Palaeogene diatomite in Denmark. *Sedimentology*, **28**, 487–504.

18 PALAEOONTOLOGY

- and BUCHARDT, B. 1996. The calcareous concretions (cementsten) in the Fur Formation (Paleogene, Denmark): isotopic evidence of early diagenetic growth. *Bulletin of the Geological Society of Denmark*, **43**, 78–86.
- and SURLYK, F. 1983. The Fur Formation, a late Paleocene ash-bearing diatomite from northern Denmark. *Bulletin of the Geological Society of Denmark*, **32**, 43–65.
- PEDERSEN, S. A. S., BONDE, N., HEILMANN-CLAUSEN, C., LARSEN, L. M., LINDOW, B., MADSEN, H., PEDERSEN, A. K., RUST, J., SCHULTZ, B. P., STOREY, M. and WILLUMSEN, P. 2011. Molerområdets geologi – sedimenter, fossiler, askelag og glaicalteknik. *Geologisk Tidsskrift*, 41–135.
- PROTA, G. 1980. Recent advances in the chemistry of melanogenesis in mammals. *Journal of Investigative Dermatology*, **75**, 122–127.
- PRUM, R. O., DUFRESNE, E. R., QUINN, T. and WATERS, K. 2009. Development of colour-producing β -keratin nanostructures in avian feather barbs. *Journal of The Royal Society Interface*, **6**, S253–S265.
- RUST, J. 1999. *Biologie der Insekten aus dem ältesten Tertiär Nordeuropas*. Habilitation thesis, University of Göttingen.
- SAVALLI, U. M. 1995. The evolution of bird coloration and plumage elaboration – a review of hypotheses. 141–190. In POWER, D. M. (ed.) *Current ornithology*. Vol. 12. Plenum Press, 278 pp.
- SCHMITZ, B., PEUCKER-EHRENBRINK, B., HEILMANN-CLAUSEN, C., ÅBERG, G., ASARO, F. and LEE, C. T. A. 2004. Basaltic explosive volcanism, but no comet impact, at the Paleocene–Eocene boundary: high-resolution chemical and isotopic records from Egypt, Spain and Denmark. *Earth & Planetary Science Letters*, **225**, 1–17.
- SCHOON, P. L., HEILMANN-CLAUSEN, C., SCHULTZ, B. P., SINNINGHE DAMSTÉ, J. S. and SCHOUTEN, S. 2015. Warming and environmental changes in the eastern North Sea Basin during the Palaeocene–Eocene thermal maximum as revealed by biomarker lipids. *Organic Geochemistry*, **78**, 79–88.
- SCHWEITZER, M. H., JOHNSON, C., ZOCCO, T. G., HORNER, J. R. and STARKEY, J. R. 1997. Preservation of biomolecules in cancellous bone of *Tyrannosaurus rex*. *Journal of Vertebrate Paleontology*, **17**, 349–359.
- WATT, J. A., AVCI, R., FORSTER, C. A., KRAUSE, D. W., KNAPP, L., ROGERS, R. R., BEECH, I. and MARSHALL, M. 1999. Keratin immunoreactivity in the Late Cretaceous bird *Rahonavis ostromi*. *Journal of Vertebrate Paleontology*, **19**, 712–722.
- WITTMAYER, J. L., HORNER, J. R. and TOPORSKI, J. K. 2005. Soft-tissue vessels and cellular preservation in *Tyrannosaurus rex*. *Science*, **307**, 1952–1955.
- SUO, Z., AVCI, R., ASARA, J. M., ALLEN, M. A., ARCE, F. T. and HORNER, J. R. 2007. Analyses of soft tissue from *Tyrannosaurus rex* suggest the presence of protein. *Science*, **316**, 277–280.
- ZHENG, W., ORGAN, C. L., AVCI, R., SUO, Z., FREIMARK, L. M., LEBLEU, V. S., DUNCAN, M. B., VANDER HEIDEN, M. G., NEVEU, J. M., LANE, W. S., COTTRELL, J. S., HORNER, J. R., CANTLEY, L. C., KALLURI, R. and ASARA, J. M. 2009. Biomolecular characterization and protein sequences of the Campanian hadrosaur *B. canadensis*. *Science*, **324**, 626–631.
- LINDGREN, J. and MOYER, A. E. 2015. Melanosomes and ancient coloration re-examined: a response to Vinther 2015 (DOI 10.1002/bies.201500018). *BioEssays*, **37**, 1174–1183.
- SEIJI, M., FITZPATRICK, T. B. and BIRBECK, M. S. C. 1961. The melanosome: a distinctive subcellular particle of mammalian melanocytes and the site of melanogenesis. *Journal of Investigative Dermatology*, **36**, 243–252.
- SIMON, J. D. and PELES, D. N. 2010. The red and the black. *Accounts of Chemical Research*, **43**, 1452–1460.
- STOREY, M., DUNCAN, R. A. and SWISHER, C. C. 2007. Paleocene-Eocene thermal maximum and the opening of the Northeast Atlantic. *Science*, **316**, 587–589.
- VINTHER, J. 2015. A guide to the field of palaeo colour. *BioEssays*, **37**, 643–656.
- 2016. Fossil melanosomes or bacteria? A wealth of findings favours melanosomes. *BioEssays*, **38**, 220–225.
- BRIGGS, D. E., PRUM, R. O. and SARANATHAN, V. 2008. The colour of fossil feathers. *Biology Letters*, **4**, 522–525.
- WATERHOUSE, D. M., LINDOW, B. E. K., ZELENKOV, N. V. and DYKE, G. J. 2008. Two new parrots (Psittaciformes) from the lower Eocene Fur Formation of Denmark. *Palaeontology*, **51**, 575–582.
- WILLUMSEN, P. S. 2004. Palynology of the Lower Eocene deposits of northwest Jutland, Denmark. *Bulletin of the Geological Society of Denmark*, **51**, 141–157.
- WOGELIUS, R. A., MANNING, P. L., BARDEN, H. E., EDWARDS, N. P., WEBB, S. M., SELLERS, W. I., TAYLOR, K. G., LARSON, P. L., DODSON, P., YOU, H., DA-QING, L. and BERGMANN, U. 2011. Trace metals as biomarkers for eumelanin pigment in the fossil record. *Science*, **333**, 1622–1626.
- WUTTKE, M. 1983. Weichteil-Erhaltung durch lithifizierte Mikroorganismen bei mittel-eosänen Vertebraten aus den Ölschiefern der Grube Messel bei Darmstadt. *Senckenbergiana Lethaea*, **64**, 509–527.
- ZAREBA, M., SZEWCZYK, G., SARNA, T., HONG, L., SIMON, J. D., HENRY, M. M. and BURKE, J. M. 2006. Effects of photodegradation on the physical and antioxidant properties of melanosomes isolated from retinal pigment epithelium. *Photochemistry & Photobiology*, **82**, 1024–1029.
- ZHANG, F., KEARNS, S. L., ORR, P. J., BENTON, M. J., ZHOU, Z., JOHNSON, D., XU, X. and WANG, X. 2010. Fossilized melanosomes and the colour of Cretaceous dinosaurs and birds. *Nature*, **463**, 1075–1078.



PAPER VI

Overleaf: The skull of the Permian amphibian specimen LO-JG1

Skeletal and soft tissue anatomy of an Early Permian temnospondyl amphibian from the Saar-Nahe Basin of south-western Germany

JOHAN A. GREN¹, STEPHEN A. HALL², SVEN SACHS^{3,4} AND ULLA KOKFELT⁵

¹Department of Geology, Lund University, Sölvegatan 12, 223 62 Lund, Sweden; e-mail: johan.gren@geol.lu.se

²Division of Solid Mechanics, Lund University, Ole Römers väg 1, 223 63 Lund, Sweden; e-mail: stephen.hall@solid.lth.se

³Naturkundemuseum Bielefeld, Abteilung Geowissenschaften, Adenauerplatz 2, 33602 Bielefeld, Germany; e-mail: sachs.pal@gmail.com

⁴Im Hof 9, 51766 Engelskirchen, Germany

⁵Stokholmsvej 31, 3060 Esbjerg, Denmark; e-mail: ukokfelt@gmail.com

Abstract: The Saar Nahe Basin of south-western Germany has yielded a diverse assemblage of Late Carboniferous–Early Permian temnospondyl amphibian fossils, many of which retain traces of soft tissues. Here, we describe and illustrate an exceptionally preserved temnospondyl amphibian larva from the ancient lake Jeckenbach (Lower Lebach Group, Meisenheim Formation) of the Saar-Nahe Basin. The specimen comprises the skull and anterior half of the body, and is here tentatively referred to the genus *Micromelerpeton*. In addition to a semi-articulated skeleton, the fossil displays several types of soft tissues, including a glossy black residue in one of the orbits, a dark halo demarcating the body outline, and traces of external gills, associated with remains of the branchial arches. Scanning and transmission electron microscopic analysis revealed dense accumulations of sub-spherical and electron dense microbodies (about 0.5 µm in diameter) in the orbital pigmentation. We employed X-ray computed tomography to produce a digital volume rendering of the fossil. In addition to visualising the three-dimensional structure of the exposed skeleton, this model also revealed bones and teeth obscured by the sedimentary matrix.

Introduction

Lacustrine deposits of Late Carboniferous to Early Permian age in the Saar-Nahe Basin, south-western Germany, have produced a diverse fauna of temnospondyl amphibians (Boy 1972, 2007). The remarkable preservation and completeness of the fossils in the assemblage has, among other things, elucidated predator-prey relationships otherwise rarely observed among Palaeozoic amphibians (Boy 1998; Lohmann & Sachs 2001; Schoch 2009). Moreover, the abundance of virtually intact and largely articulated skeletal material has provided important insights into the ontogeny and evolution of the Temnospondyli (Boy 1972, 1995; Schoch 2002, 2003; Witzmann & Pfretzschner 2003).

The exceptional preservation of amphibian fossils from the Saar-Nahe Basin and other *Konservat-Lagerstätten*, such as the Eocene Messel Pit of south-western Germany (Franzen & Schaal 2000) and Pleistocene Shiobara Group of north-eastern Japan (Allison *et al.* 2008), has prompted investigations into various normally highly decay-prone anatomical features, such as skin, eyes and respiratory organs (e.g. Schoch 2014 and references therein). In

the Saar-Nahe Basin, dark-coloured soft tissue traces are intimately associated with micrometre-sized bodies that were initially interpreted as lithified bacteria (Willems & Wuttke 1987). However, similar microstructures also occur in vertebrate fossils from other depositional settings, and these are nowadays more-or-less routinely referred to as remnant melanosomes; i.e. melanin-bearing eukaryotic cellular organelles (Vinther *et al.* 2008; but see also Lindgren *et al.* 2015a). This reinterpretation has influenced a number of studies dealing with different biological and ecological aspects, including original colouration (e.g. Vinther *et al.* 2008; Li *et al.* 2010, 2012; Colleary *et al.* 2015; Vinther 2015), physiology (Clarke *et al.* 2010; Li *et al.* 2014; Lindgren *et al.* 2014) and even behaviour (Li *et al.* 2010) of extinct organisms. These inferences have been based largely on the anatomical localization, arrangement, spatial distribution, and/or morphology of the conserved microbodies (e.g. Vinther *et al.* 2008; Clarke *et al.* 2010; Li *et al.* 2010, 2012). Nonetheless, because the methodologies used to characterize the minute structures differ considerably between studies (e.g. Vinther *et al.* 2008; Li *et al.* 2010; Wogelius *et al.* 2011; Glass *et al.* 2012; Lindgren *et al.* 2012, 2015b; Barden *et al.* 2014; McNamara *et al.* 2016; Gren *et al.* 2017), there is an ongoing debate

regarding what criteria to use for confident identification (see Schweitzer *et al.* 2015; Vinther 2015, 2016). Some authors (e.g. Lindgren *et al.* 2015a; Schweitzer *et al.* 2015) favour a multi-proxy approach that includes integrated ultrastructural and molecular methods if not to avoid, so at least to minimize the risk of reaching erroneous conclusions; others (Vinther 2015, 2016) argue that existing evidence is enough to treat ‘all’ fossil microbodies as relict melanosomes more or less by default.

In the present contribution, we use both scanning (SEM) and transmission electron microscopy (TEM) to examine the fine- and ultrastructure of a black residue located within one of the orbits of a larval temnospondyl amphibian (LO-JG1) from the Saar-Nahe Basin. Our results indicate that the dark-coloured pigmentation coincides with closely stacked, electron-dense microbodies with a morphology corresponding to that of ocular melanosomes (but also to bacterial cells).

Moreover, we employ X-ray computed tomography (XRCT) – a technique that greatly facilitates anatomical studies (particularly of remains hidden within the sedimentary matrix) while minimising the risk of damaging prized fossils – to produce a virtual 3D model of the skeleton. This reconstruction exposed some bones and teeth that were otherwise obscured by sediments, and also revealed the orientation of some skeletal parts that were displaced and/or overturned during the initial stages of fossilization.

Geological setting

The Saar-Nahe Basin of south-western Germany is about 90 km long and 40 km wide (Fig. 1), and retains sediments spanning the Carboniferous-Permian boundary (Falke 1954). Approximately 300 million years ago, the region was located within the tropical zone, about 10–

20° north of the equator (Boy 2003). The formation of the basin took place at a fairly high altitude (at least 2000 m; Boy 2003) within a mountain range depression associated with the Variscan orogeny (Henk 1993; Korsch & Schäfer 1995; Dietze 2000; Schoch 2009). In the Saar-Nahe area, Lower Permian sediments are subdivided into the Upper and Lower Rotliegend, respectively (Falke 1954). Whereas the Upper Rotliegend primarily comprises red beds of terrestrial origin (Falke 1954; Schäfer & Stapf 1978) the Lower Rotliegend is rich in lacustrine deposits (Falke 1954; Schäfer & Stapf 1978; Boy 1987; Schoch 2009). As previously documented (Falke 1954), the Rotliegend consists of a series of fluvio-lacustrine depositional cycles that collectively form the foundation for the stratigraphy in the area. Each cycle begins with sandy conglomerates; these are overlain by finely laminated mudrocks and/or relatively homogenous greywackes (Boy 1978; Schäfer & Stapf 1978; Dietze 2000; Schoch 2009). The succession of freshwater deposits comprises ten distinct lacustrine units labelled M1 to M10 (formerly L-O1 to L-O10; cf. Boy and Fichter 1982; Schindler 2007) representing ‘fossil lakes’ with considerable differences in size, depth and sedimentary accumulation rates (e.g. Boy 1987; Schindler 2007; Schoch 2009).

Some stratigraphic units are particularly fossiliferous, containing abundant remains of invertebrates (Boy 1976), cartilaginous and bony fish (Gardiner 1963; Heidtke 1986, 1990; Schindler 1993), and amphibians (Boy 1972, 1978, 2007; Schoch 2009). The quality of the vertebrate remains is highly variable between sites; some produce fossils showing pristine skeletal articulation, whereas others yield specimens with soft tissue traces (although the bones may be in a rather poor condition).

Specimen LO-JG1, described in this paper, was collected from the ancient lake Jeckenbach (unit M6), belonging to the Meisenheim Formation of the Lower Lebach Group of the Lower Rotliegend, which equals the Autunian (Schäfer & Stapf 1978; Boy & Fichter 1982; Schindler 2007; Schoch 2009; Schoch & Witzmann 2009). The lake is located in the north-eastern part of the Saar-Nahe Basin (Fig. 1 – star). At the time of deposition, lake Jeckenbach measured about 30 km in diameter, and it has been interpreted as a moderately deep lake (i.e. about 20–50 m; Boy 2003; Schoch 2009) with a stratified water column and an oxygen-depleted, possibly toxic bottom zone (Boy 1987; Schindler 2007; Schoch 2009).

Methods

LO-JG1 was photographed using a Sony DSLR-A200 digital camera (Fig. 2A). To enhance contrast and highlight surface features, the fossil was also photographed while covered with ammonium chloride (Fig. 2B). For



Fig. 1: Simplified map of Germany showing the location of the ancient lake Jeckenbach and its relation to the Saar-Nahe Basin (modified with permission from Schoch 2009, fig. 1). Star demarcates the locality where LO-JG1 was collected.

general assessment, LO-JG1 was examined under an Olympus SZX16 optical microscope, photographed using an Olympus SC30 camera and compared with various specimens in the temnospondyl collection housed at Urweltmuseum GEOSKOP, Thallichtenberg, Germany. Measurements of the fossil were taken in the digital photographs, between the anterior and posterior ends of exposed elements, using the straight line tool in the Fiji ImageJ v1.49m (<http://imagej.nih.gov/ij>) software.

Electron microscopy examination

Minute samples of the glossy black 'eye' residue were removed from the left orbit of LO-JG1 using a scalpel and mounted on a silicon wafer using carbon tape. Samples for SEM imaging were sputter coated with gold and examined using a Hitachi S-3400N electron microscope (15 keV, 62.0 μ A, 5–10 mm working distance). Additional SEM imaging and EDX element analysis were performed under low vacuum on the uncoated specimen using a Tescan Mira3 FEG-SEM, equipped with an Oxford Instruments X-MaxN 80 EDX detector.

For TEM analysis, a small fossil sample was first placed in pure alcohol which was then replaced by acetone. To achieve full infiltration, the acetone was thereafter stepwise replaced with epoxy resin (AGAR 100 Resinkit, R1031) and left to polymerise at 60 °C for 48 h. The embedded sample was trimmed with a razor blade before being sectioned on an ultratome (Leica Ultracut UCT). Ultra-thin (50 nm) sections were mounted onto pioloform-coated copper grids and examined using a JEOL JEM-1230 transmission electron microscope at 80 kV and imaged employing a Gatan MultiScan 794 CCD camera.

Measurements of microstructures were taken on SEM and TEM micrographs using Fiji ImageJ v1.49m (<http://imagej.nih.gov/ij>) software.

X-ray computed tomography

X-ray computed tomography was performed at the 4D-Imaging Lab at the Division of Solid Mechanics, Lund University, using a Zeiss XRadia XRM520 X-ray tomograph. An X-ray tube voltage of 50 kV was used with a source power of 4 W and the manufacturer-supplied Le5 source filter to minimise beam-hardening effects. The applied tube voltage results in a broad spectrum of X-ray energies, with a maximum of 50 keV and, with the Le5 filter, an effective energy of 28.3 kV. The cone-beam produced by the source provides a geometrical magnification of the image depending on the source-detector distance and the position of the sample between the two; in this case, the sample was placed at 43.99 mm from the source and at 76.98 mm from the detector. The optics after the scintillator give a magnification of $\times 0.4$. The manufacturer-supplied Le5 filter was used on the source to minimise

beam hardening effects. 1601 radiographs were acquired over 360° with an exposure time of 8 sec for each image. The subsequent tomographic reconstruction, using the Zeiss reconstructor software with a correction for the centre of rotation, provided cubic voxels with side lengths of 24.724 microns.

Acquired TIFF images of LO-JG1 were mounted and analysed in the AMIRA 5.3.3 and Fiji ImageJ v1.49m softwares. A threshold was applied to separate pixels belonging to the fossil from the sediment and the background noise, after which a 3D volume was rendered employing a tricubic smooth interpolation in the Fiji ImageJ Volume Viewer v2.01.

Description

Skeletal features

LO-JG1 comprises the anterior half of a dorsoventrally flattened, yet largely articulated skeleton of a larval temnospondyl amphibian (Fig. 2). The fossil is embedded in a mudrock showing fine (<1 mm) horizontal laminations of alternating dark and light bands.

When measured from the tip of the premaxillae to the posterior end of the parasphenoid, the total skull length amounts to 14.1 mm. Most of the articular facets and sutures are indistinguishable and, accordingly, accurate measurements of the skeletal elements were difficult. As preserved, the fossil is resting obliquely on its right side, which has resulted in displacement of some bones, whereas others are obscured by the sedimentary matrix. Nonetheless, several bones (particularly on the left side of the skull) are readily identifiable (Fig. 2).

Both premaxillae are exposed and although the right one is poorly defined, the left element is well preserved and in contact with the left maxilla and vomer (Fig. 2B). No premaxillary teeth could be distinguished by means of optical microscopy; however, XRCT revealed at least four large teeth in each premaxilla (Fig. 3 – arrows). The left maxilla is well preserved; it is exposed in lingual view, holds 12 visible teeth, and measures 12.5 mm in overall length. The suture abutting the distal part of the maxilla and traces of the left quadratojugal can be seen in ventral view. Conversely, the right maxilla is not well exposed, being partly covered by sediments and with its posterior end obscured by the overlying pterygoid. As revealed by our digital volume rendering of the XRCT data, the right maxilla has been rotated and is exposed in dorsal view. Furthermore, a few teeth in the right maxilla, undetected using conventional microscopy, were also identified in the digital reconstruction (Fig. 3). The right dentary is partially preserved in labial view adjacent to the maxilla.

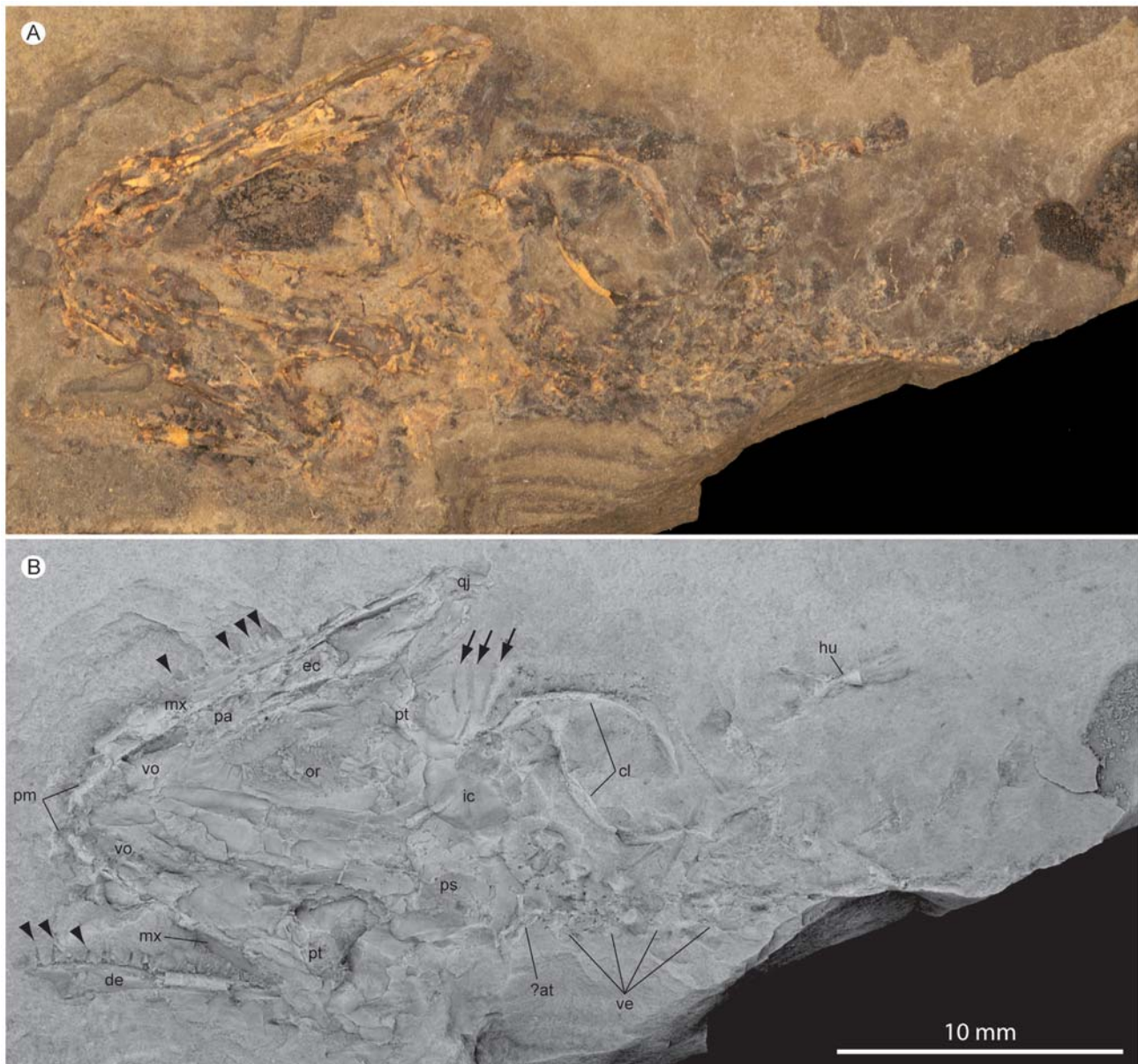


Fig. 2: Photographs of LO-JG1. A, photograph under conventional light. In addition to a semi-articulated skeleton, soft tissue residues are visible as a dark halo around the bones and as a distinct blackish film within one orbit. B, Ammonium chloride-covered sample to enhance surface features, such as individual skeletal elements. Poor preservation and compactional deformation preclude confident assignment of several bones and sutures. Arrowheads demarcate maxillary and dentary teeth. Arrows indicate branchial arches. Abbreviations: at, atlas; cl, clavicular; de, dentary; ec, ectopterygoid; hu, humerus; ic, interclavicular; mx, maxilla; or, orbit; pa, palatine; pm, premaxillae; ps, parasphenoid; pt, pterygoid; qj, quadratojugal; ve, vertebrae; vo, vomer. Scale bar: 10 mm.

Most of the dentary is preserved as an imprint, although its medial portion occurs as a three-dimensional structure. The total length of the element is at least 8.8 mm, although its posterior part is obscured by the maxilla and pterygoid. Anteriorly, the (imprint of the) dentary is substantially wider, tapering towards its posterior end, although this may be an artefact of deformation. Seven teeth are preserved in the dentary; these are readily visible together with an additional four teeth that are only preserved as imprints. Posterior to the premaxillae, part of the left vomer protrudes from the sediment and is visible as an elliptic structure located anterior to the palatine. Its anterior portion and articular facets with the maxilla, premaxilla and right vomer are relatively poorly preserved and partially covered by sediment. A few tooth sockets

can be seen close to the left maxilla, though neither of the vomers have a particularly well defined surface preservation. Moreover, compressional deformation, together with the slight displacement of the parasphenoid towards the right of the fossil, further obscures the visibility of the right vomer and adjacent bones. The sub-triangular shaped palatine ends in an irregular, blunt suture with the vomer. Apart from its long lateral contact with the maxilla, the posterior portion of the palatine is in contact with the ectopterygoid and pterygoid. On the exposed surface of the palatine, a few round structures of different sizes can be seen aligned in a single line close to the maxilla, probably representing shallow tooth sockets. The left ectopterygoid is evenly wide and its posterior end is relatively wide and blunt. Despite that the ectopterygoid

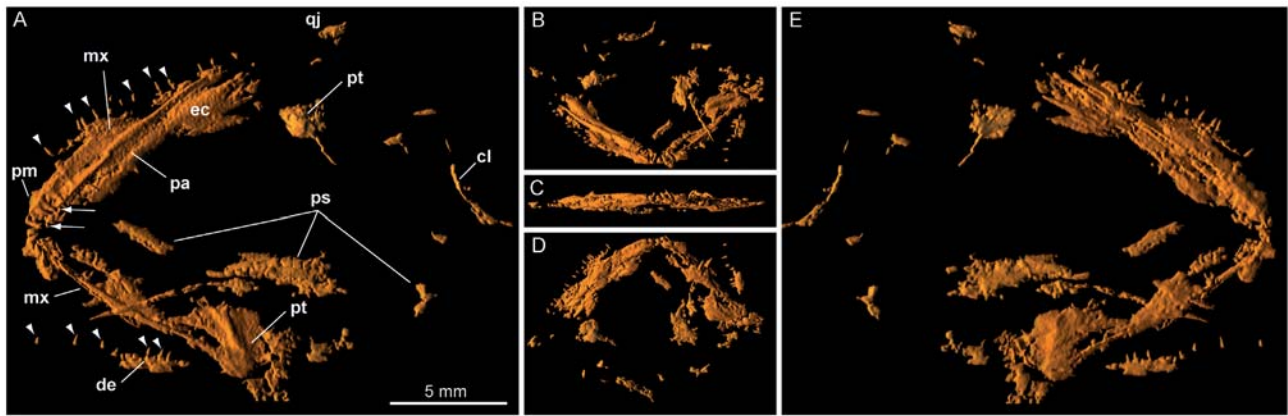


Fig. 3: Volume rendering of LO-JG1 skeletal remains based on μ CT, in A: ventral, B: anterior (rotated 30° toward ventral view), C: anterior, D: anterior (rotated 30° toward dorsal view), and E: dorsal view, respectively. Arrowheads indicate maxillary and dentary teeth, whereas arrows mark premaxillary teeth. For abbreviations, see Figure 2.

is poorly preserved, its articular contacts with the maxilla, palatine and pterygoid are discernible, something that is particularly evident in the tomographic reconstruction (Fig. 3). No teeth or tooth-sockets are observable in the ectopterygoid or in the pterygoid. The left pterygoid is well preserved in three dimensions and protrudes from the sediment. As exposed, its maximum length is c. 7.5 mm and its width is 2.7 mm. The anterior part of the pterygoid lies in contact with the ectopterygoid and reaches about half the length of the palatine before the element tapers. On the right side of the skull, the pterygoid is not as readily visible. It has been slightly displaced and overturned, protruding up through the right orbit. Posterior to the left maxilla, part of the quadratojugal is visible in ventral view, in clear contact with the pterygoid. Also on the right side of the skull, a trace of the quadratojugal can be seen, although it is fainter and partly covered by matrix.

The cultriform process of the parasphenoid can be traced for 8.8 mm, gradually tapering anteriorly from a 2.7 mm wide posterior base. Immediately posterior to the process, the basal plate of the parasphenoid is visible as a sub-triangular shaped area, c. 3.2 mm long and 2.2 mm wide. It contains about 20 round structures, interpreted as remnant denticles, each measuring about 0.2 mm in diameter. Due to the poor state of preservation, it is difficult to deduce the boundary between the denticle field and the adjacent basicranial articulation. Nevertheless, the basal plate can be seen delineating the posterior part of the left interpterygoid vacuity together with the left pterygoid. In addition to abundant presumed soft tissue remains (see below), some bony remnants of uncertain origin are observable within the left orbit. These may be part of the prefrontal or an adjacent bone of the skull roof, or bony platelets associated with the upper eyelid, previously described as ‘sclerotic plating’ (Boy 1972, 1995). On the right side of the fossil, the orbit is difficult to discriminate due to displacement of the right pterygoid.

Preserved postcranial elements include the left front limb, where the humerus is the only clearly visible bone. Whereas the distal end is preserved in three dimensions, the proximal termination appears damaged by compaction. The bone measures 2.9 mm in length and it is substantially wider proximally than distally. Distal to the humerus, traces of the radius and ulna can be seen as faint impressions. Both clavicae are preserved as narrow and strongly curved structures, each measuring about 6 mm in overall length. Anterior to the left clavicle, the interclavicle is present as a poorly preserved, sub-rounded structure. The right clavicle has been displaced towards the left side of the fossil and the element is partially embedded in sediment. The preserved part of the vertebral column consists of seven vertebrae, the most anterior one being the atlas. The atlas is hourglass-shaped and considerably larger than the other vertebrae. To the left of the vertebral column, several dislocated ribs can be seen, all of which are in a fairly poor condition. It is uncertain whether this is due to diagenetic compaction or (originally) poor ossification. In addition to the skeletal remains, traces of the cartilaginous hyobranchial skeleton are visible posterior to the left pterygoid (Fig. 2B – arrows). These consist of three slightly curved branchial arches (ceratobranchials), each measuring c. 1.5 mm in length.

Soft tissues

Several types of soft tissue structures occur in LO-JG1, including a faint ‘skin’ imprint outlining the body wall (Fig. 2A), and a glossy black residue within the left orbit (Fig. 4A–B). Additionally, traces of external gills can be seen on the left side of the specimen, posterior to the pterygoid. These occur as a dense, black accumulation alongside and distal to the three ceratobranchials. External gill branches have previously been reported from several genera of temnospondyl larvae (see Schoch 2014 and references therein), including specimens from the Saar-Nahe area (Witzmann & Pfretzschner 2003). The external gill branches in LO-JG1 are poorly preserved

and retain no distinct branchial dentition or filaments. 'Skin' impressions are visible as a dark 'halo' around the preserved part of the trunk. It is noticeably darker in areas where remnants of poorly preserved bones are present, such as along the ribs and around the left radius and ulna.

In addition to the matt black 'skin' imprint, patches of a glossy black residue can be seen within the left orbit and adjacent to the right mandible. Both of these patches are interpreted as remains of eyes, where the right eye has been somewhat displaced during the initial stages of fossilization. Similar black pigmentations have also been observed in other temnospondyl fossils from the Saar-Nahe Basin (e.g. the branchiosaurids *Apateon caducus* and *A. pedestris*) and these have tentatively been interpreted as remnant eye pigments (Schoch 1992).

Under scanning electron microscope, the soft tissue remains are visible as flattened areas of carbonaceous mat-

ter, separated by cracks that strongly resemble desiccation cracks on the c. 100 μm scale. Our SEM-EDX element analysis shows that the dark residue is dominated by carbon in contrast to the silica-based sediment. Furthermore, SEM revealed masses of ovoid microbodies (Fig. 4C) with a mean size of $0.65 \pm 0.12 \mu\text{m} \times 0.43 \pm 0.09 \mu\text{m}$ ($n = 30$) and a mean aspect ratio (length/width) of 1.57. The microbodies are packed tightly together and occur almost in a sheet-like manner, and some of the contacts between microbodies appear faint as if they have 'melted' together (possibly an effect of diagenetic processes). Such deformations may also have caused the occasional depressions visible on the surfaces of some microbodies (Fig. 4C—arrows; cf. Lindgren *et al.* 2015b). Most microbodies are sub-spherical, although some have a somewhat more angular appearance. The tight arrangement is visible also under TEM, which furthermore reveals a solid interior of the microbodies (Fig. 4D).

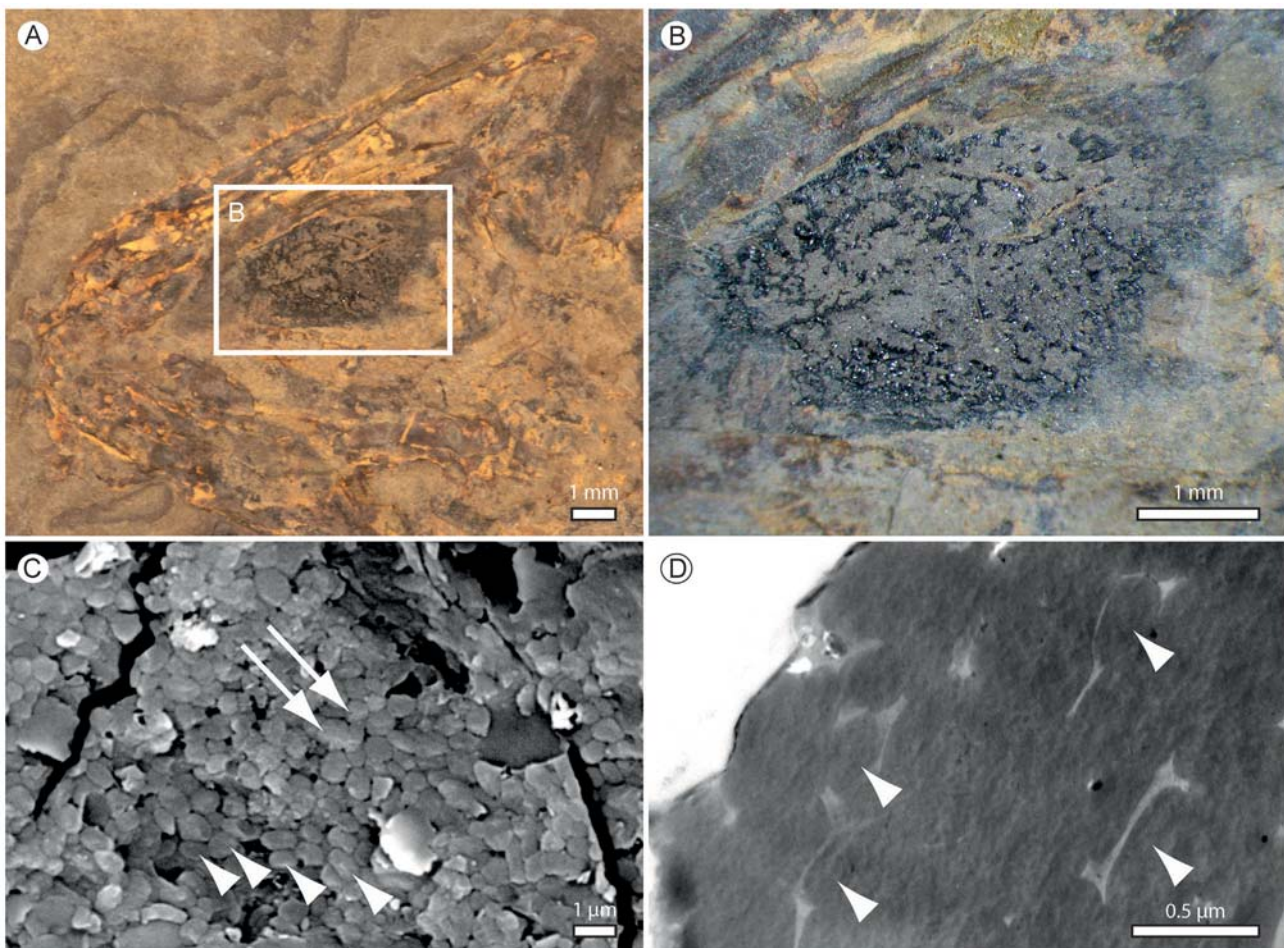


Fig. 4: Close-up photographs of the orbit of LO-JG1 (A–B), and electron microscopy micrographs of organic residues collected from the orbital pigmentation (C–D). A, photograph of the head of LO-JG1. The orbit is highlighted by a white rectangle. B, close-up photograph of the orbit. Note distinct traces of glossy blackish matter. C, SEM micrograph of organic residues obtained from within the orbit. Arrowheads indicate round to elongate and densely packed microbodies. Arrows indicate shallow depressions on microbody surfaces. D, TEM micrograph of the organic residues. Arrowheads indicate microbodies with a solid and homogenous interior. Scale bars: 1 mm (A–B); 1 μm (C); 0.5 μm (D).

Discussion

Classification of LO-JG1

For general assessment and diagnosis, LO-JG1 was compared with temnospondyl fossils housed in the collection at Urweltmuseum GEOSKOP, Thallichtenberg, Germany. In particular, specimens of the genera *Apateon*, *Micromelerpeton* and *Sclerocephalus* were examined, including individuals representing various ontogenetic stages and preservational modes. Despite the abundance of well-preserved fossil amphibians from the Saar-Nahe area, precise systematic placement of LO-JG1 was not possible due to the relatively poor condition of its skeletal elements, but also because of the extensive ontogenetic variation among larval temnospondyls (see Boy 1972). Nevertheless, some characteristics were particularly helpful for a tentative classification of LO-JG1, including: (i) the overall shape of the skull which is sub-triangular, consistent with micromelerpetontid temnospondyls, as opposed to the quadrangular skulls of branchiosaurids and amphibamids, and the rectangular skull shape seen in eryopoid amphibians, such as *Sclerocephalus* (Schoch 2003, 2009; Schoch & Milner 2014); (ii) the short palatine ramus of the pterygoid and the sub-triangular basal plate of the parasphenoid. These elements most closely resemble corresponding structures in branchiosaurids and *Micromelerpetontids* (cf. Schoch 1992, 2003; Boy 1995; Schoch & Milner 2014). Furthermore, LO-JG1 displays a short humerus (2.9 mm) relative to skull length (14.1 mm), and putative sclerotic plating in the left orbit. These features are more consistent with *Micromelerpeton* than with *Apateon* (the most common branchiosaurid genus in the Saar-Nahe area) of corresponding ontogenetic stage (cf. Schoch 1992; Witzmann and Pfretzschner 2003). Accordingly, LO-JG1 is here tentatively assigned to *Micromelerpeton*, a genus that has previously been documented in the same stratigraphic unit (M6) as LO-JG1 (Witzmann & Pfretzschner 2003).

Soft tissue preservation

Among the soft tissue remains preserved in LO-JG1, the glossy black material within the left orbit is visually the most pronounced structure. Upon close examination (Fig. 4A–B), these remnants occur in aggregates in between areas where sediment either covers the residue or where the underlying sedimentary matrix is exposed. Furthermore, the microscopic structure of the black matter strongly resembles desiccation cracks on the 0.1 mm-scale, probably developed sometime during diagenesis (see below). In addition to the preserved left ‘eye’, glossy black remains are also found adjacent to the mandible on the right side of the fossil, presumably representing traces of the right eye. Our SEM-EDX elemental analysis showed that the dark residue contains carbon intimately associated with dense

accumulations of sub-spherical microbodies (Fig. 4C). In overall morphology, these minute structures correspond to microstructures previously assigned to fossil melanosomes (e.g. Vinther *et al.* 2008; Li *et al.* 2010), but also bacterial cells (see Moyer *et al.* 2014). The solid interior of the microbodies (Fig. 4D) favour a melanosome affinity; however, in light of the unsettled debate on fossil melanosome recognition criteria (see the introduction section above), an unambiguous affinity of the observed microbodies is not attainable without more in-depth chemical analyses, an undertaking that is beyond the scope of the present study.

Some previously examined *Micromelerpeton* larvae, similar in size to LO-JG1, have shown the presence of gill arches and external gills (Milner 1982; Witzmann & Pfretzschner 2003; Witzmann 2013). Similarly, LO-JG1 displays three faint imprints of putative branchial arches measuring c. 1.5 mm in length (Fig. 2B — arrows), consistent with other temnospondyl and modern urodele larvae (Stebbins & Cohen 1995). Furthermore, along and distal to the arches is a concentration of matt black carbonaceous residue. These remains presumably represent external gills, although their state of preservation does not reveal any filaments or other structural characteristics. Nevertheless, an incomplete preservation of soft external gills is to be expected, given the highly labile nature of such structures (see below).

Surrounding the postcrania is a dark, matte halo showing parts of the body outline. SEM-EDX revealed that the dark areas are enriched in carbon and distinct from the surrounding siliceous sediment. Moreover, the darkest patches display prominent desiccation cracks similar to the structures observed in the orbit. These features cannot be seen in areas with only sediments and thus they are interpreted as being connected to the taphonomy of soft tissue structures (see below).

Taphonomy of LO-JG1

While the Saar-Nahe Basin has yielded a rich fauna of fossil amphibians, preservational quality differs considerably between the various fossil lakes (M1–M10; Boy and Fichter 1982). Because LO-JG1 displays a rather uncommon preservational mode (several types of soft tissues, yet many bones are in poor condition and, in places, disarticulated), this raises questions pertaining to the taphonomy of the specimen. Plausibly, this is a case of so called “stick ‘n’ peel”, where decay products from the carcass have infiltrated the surrounding sediments, thereby adhering skin and other features to the substrate, whereas skeletal elements have been remobilised and damaged at a later stage (Orr *et al.* 2016). Several studies have been conducted regarding the palaeoenvironment of the Saar-Nahe Basin, most of which indicating that Jeckenbach was a relatively deep lake setting (e.g. Boy 2003; Schoch 2009). The fine

laminations observed in lake sediments of the Saar-Nahe area have been proposed to be the result of seasonal variations in bioaccumulation, with higher net production occurring in rainy summers than during the drier winter months (Clausing *et al.* 1992; Clausing 1996). Additionally, the undisturbed horizontal laminations are also an indication that the sediments were deposited at depths below the storm wave base and were not reworked by a benthic fauna (Boy 2003).

Differences in preservation between the various fossil lakes may be related to water depth; a deeper environment would more likely keep the bones in articulation, partly because the carcass is kept concealed from near-shore scavengers but also because the high water pressure at the bottom may aid in keeping the bones in place and prevent the carcass from floating (a common scenario often affecting animals buried in warm and shallow waters; see Elder and Smith 1984, 1988). A deeper environment would also likely result in lower oxygen levels, diminishing the amount of smaller scavengers scattering the bones, which, in turn, would promote a more complete skeletal preservation (Elder & Smith 1984; Boy 2003). Nevertheless, although a hypoxic or anoxic environment may favour the preservation of skeletal elements, it does not necessarily promote the conservation of soft tissues, since anaerobic decay may act nearly as fast as aerobic decomposition (Allison 1988a, b).

Despite the deep, stratified and oxygen-depleted setting proposed for lake Jeckenbach (Boy 1987, 2003; Schindler 2007; Schoch 2009), the preservation of the skeleton of LO-JG1 is rather poor. The flattened and, in places, dislocated bones indicate that the fossil has been subjected to substantial pressure after burial and it is plausible that the displacement and poor preservation of the bones occurred later in diagenesis rather than during burial and decay. Recent decay experiments have shown that soft external gill branches are extremely decay prone and would be completely lost within days when exposed in seawater (Sansom *et al.* 2013). Sansom *et al.* (2013) also showed that, although the cartilaginous branchial arches are slightly more resistant, they start losing shape within weeks. This supports a rapid burial of LO-JG1, again indicating that the partial loss of articulation occurred later during diagenesis.

Acknowledgements

We thank Sebastian Voigt for access to the temnospondyl collections of Urweltmuseum GEOSKOP, Thallichtenberg. Furthermore, we thank the “Imaging 3D Structures Research School”, Lund University, for supporting the X-ray computed tomography, Carl Alwmark, Department of Geology, Lund University, for assistance during

the FEG-SEM analysis, and Basil el Jundi, Department of Biology, Lund University, for providing access to the AMIRA visualization software. Thanks also to Johan Lindgren and Mats Eriksson, Department of Geology, Lund University, and Florian Witzmann, Museum für Naturkunde, Berlin, for valuable comments on the manuscript. The authors have no conflict of interest to declare.

References

- Allison, P.A. 1988a: Konservat-Lagerstätten: cause and classification. *Paleobiology* 14, 331–344.
- Allison, P.A. 1988b: The role of anoxia in the decay and mineralization of proteinaceous macro-fossils. *Paleobiology* 14, 139–154.
- Allison, P.A., Maeda, H., Tuzino, T. and Maeda, Y. 2008: Exceptional preservation within Pleistocene lacustrine sediments of Shiobara, Japan. *Palaios* 23, 260–266.
- Barden, H.E., Bergmann, U., Edwards, N.P., Egerton, V.M., Manning, P.L., Perry, S., van Veelen, A., Wogelius, R.A. and van Dongen, B.E. 2014: Bacteria or melanosomes? A geochemical analysis of micro-bodies on a tadpole from the Oligocene Enspel Formation of Germany. *Palaeobiodiversity and Palaeoenvironments* 95, 33–45.
- Boy, J.A. 1972: Die Branchiosaurier (Amphibia) des saarpfälzischen Rotliegenden (Perm, SW-Deutschland). *Hessisches Landesamt für Bodenforschung* 65.
- Boy, J.A. 1976: Überblick über die Fauna des saarpfälzischen Rotliegenden (Unter-Perm). *Mainzer geowissenschaftliche Mitteilungen* 5, 13–85.
- Boy, J.A. 1978: Die Tetrapodenfauna (Amphibia, Reptilia) des saarpfälzischen Rotliegenden (Unter-Perm, SW-Deutschland). 1. *Branchiosaurus*. *Mainzer geowissenschaftliche Mitteilungen* 7, 27–76.
- Boy, J.A. 1987: Die Tetrapoden-Lokalitäten des saarpfälzischen Rotliegenden (?Ober-Karbon – Unter-Perm; SW-Deutschland) und die Biostratigraphie der Rotliegend-Tetrapoden. *Mainzer geowissenschaftliche Mitteilungen* 16, 31–65.
- Boy, J.A. 1995: Über die Micromelerpetontidae (Amphibia: Temnospondyli). 1. Morphologie und Paläoökologie des *Micromelerpeton credneri* (Unter-Perm; SW-Deutschland). *Paläontologische Zeitschrift* 69, 429–457.
- Boy, J.A. 1998: Möglichkeiten und Grenzen einer Ökosystem-Rekonstruktion am Beispiel des spätpaläozoischen lakustrinen Paläo-Ökosystems. 1. Theoretische und methodische Grundlagen. *Paläontologische Zeitschrift* 72, 207–240.

- Boy, J.A. 2003: Paläoökologische Rekonstruktion von Wirbeltieren: Möglichkeiten und Grenzen. *Paläontologische Zeitschrift* 77, 123–152.
- Boy, J.A. 2007: Als die Saurier noch klein waren: Tetrapoden im Permokarbon. In Schindler, T., Heidtke, U. H. J. (eds.), *Kohlesümpfe, Seen und Halbwüsten*, 258–286. Pollichia, Bad Dürkheim.
- Boy, J.A. and Fichter, J. 1982: Zur Stratigraphie des saarpfälzischen Rotliegenden (?Ober-Karbon – Unter-Perm; SW-Deutschland). *Zeitschrift der Deutschen Geologischen Gesellschaft* 133, 607–642.
- Clarke, J.A., Ksepka, D.T., Salas-Gismondi, R., Altamirano, A.J., Shawkey, M.D., D’Alba, L., Vinther, J., DeVries, T.J. and Baby, P. 2010: Fossil evidence for evolution of the shape and color of penguin feathers. *Science* 330, 954–957.
- Clausing, A. 1996: Überlegungen zur organischen Produktion und Degradation in Seen des europäischen Rotliegend. *Hallesches Jahrbuch für Geowissenschaften (B)* 18, 89–108.
- Clausing, A., Schmidt, D. and Schindler, T. 1992: Sedimentologie und Paläoökologie unterpermischer Seen in Mitteleuropa. 1. Meisenheim-See (Rotliegend; Saar-Nahe-Becken). *Mainzer geowissenschaftliche Mitteilungen* 21, 159–198.
- Colleary, C., Dolocan, A., Gardner, J., Singh, S., Wuttke, M., Rabenstein, R., Habersetzer, J., Schaal, S., Fesha, M., Clemens, M., Jacobs, B.F., Currano, E.D., Jacobs, L.L., Sylvestersen, R.L., Gabbott, S.E. and Vinther, J. 2015: Chemical, experimental, and morphological evidence for diagenetically altered melanin in exceptionally preserved fossils. *Proceedings of the National Academy of Sciences* 112, 12592–12597.
- Dietze, K. 2000: A revision of paramblypterid and amblypterid actinopterygians from Upper Carboniferous–Lower Permian lacustrine deposits of Central Europe. *Palaeontology* 43, 927–966.
- Elder, R.L. and Smith, G.R. 1984: Fish taphonomy and paleoecology. *Geobios* 17, 287–291.
- Elder, R.L. and Smith, G.R. 1988: Fish taphonomy and environmental inference in paleolimnology. *Palaeogeography, Palaeoclimatology, Palaeoecology* 62, 577–592.
- Falke, H. 1954: Leithorizonte, Leitfolgen und Leitgruppen im pfälzischen Unterrotliegenden. *Neues Jahrbuch für Geologie und Paläontologie, Abhandlungen* 99, 298–360.
- Franzen, J.L. and Schaal, S. 2000: Der eozäne See von Messel. In Meischner, D. (ed.), *Europäische Fossilagerstätten*, 177–183. Springer Berlin Heidelberg.
- Gardiner, B.G. 1963: Certain palaeoniscoid fishes and the evolution of the snout in actinopterygians. *Bulletin of the British Museum (Natural History), Geology Series* 8, 255–355.
- Glass, K., Ito, S., Wilby, P.R., Sota, T., Nakamura, A., Bowers, C.R., Vinther, J., Dutta, S., Summons, R., Briggs, D.E., Wakamatsu, K. and Simon, J.D. 2012: Direct chemical evidence for eumelanin pigment from the Jurassic period. *Proceedings of the National Academy of Sciences* 109, 10218–10223.
- Gren, J.A., Sjövall, P., Eriksson, M.E., Sylvestersen, R.L., Marone, F., Sigfridsson Clauss, K.G.V., Taylor, G.J., Carlson, S., Uvdal, P. and Lindgren, J. 2017: Molecular and microstructural inventory of an isolated fossil bird feather from the Eocene Fur Formation of Denmark. *Palaeontology* 60, 73–90.
- Heidtke, U. 1986: Über Neufunde von *Conchopoma gadiforme* Kner (Dipnoi: Pisces). *Paläontologische Zeitschrift* 60, 299–312.
- Heidtke, U. 1990: Studien über *Acanthodes* (Pisces: Acanthodii) aus dem saarpfälzischen Rotliegend (?Ober-Karbon – Unter-Perm, SW-Deutschland). In Heidtke, U. (ed.), *New Research on Permo-Carboniferous Faunas*, 1–86. Pollichia Buch 19, Bad Dürkheim.
- Henk, A. 1993: Late orogenic basin evolution in the Variscan Internides: the Saar-Nahe Basin, southwest Germany. *Tectonophysics* 223, 273–290.
- Korsch, R.J. and Schäfer, A. 1995: The Permo-Carboniferous Saar-Nahe Basin, south-west Germany and north-east France: basin formation and deformation in a strike-slip regime. *Geologische Rundschau* 84, 293–318.
- Li, Q., Gao, K.Q., Meng, Q., Clarke, J.A., Shawkey, M.D., D’Alba, L., Pei, R., Ellison, M., Norell, M.A. and Vinther, J. 2012: Reconstruction of *Microraptor* and the evolution of iridescent plumage. *Science* 335, 1215–1219.
- Li, Q., Clarke, J.A., Gao, K.-Q., Zhou, C.-F., Meng, Q., Li, D., D’Alba, L. and Shawkey, M.D. 2014: Melanosome evolution indicates a key physiological shift within feathered dinosaurs. *Nature* 507, 350–353.
- Li, Q., Gao, K.Q., Vinther, J., Shawkey, M.D., Clarke, J.A., D’Alba, L., Meng, Q., Briggs, D.E. and Prum, R.O. 2010: Plumage color patterns of an extinct dinosaur. *Science* 327, 1369–1372.
- Lindgren, J., Sjövall, P., Carney, R.M., Uvdal, P., Gren, J.A., Dyke, G., Schultz, B.P., Shawkey, M.D., Barnes, K.R. and Polcyn, M.J. 2014: Skin pigmentation provides evidence of convergent melanism in extinct marine reptiles. *Nature* 506, 484–488.
- Lindgren, J., Moyer, A., Schweitzer, M.H., Sjövall, P., Uvdal, P., Nilsson, D.E., Heimdal, J., Engdahl, A., Gren, J.A., Schultz, B.P. and Kear, B.P. 2015a: In-

- terpreting melanin-based coloration through deep time: a critical review. *Proceedings of the Royal Society B* 282, 20150614.
- Lindgren, J., Sjövall, P., Carney, R.M., Cincotta, A., Uvdal, P., Hutcheson, S.W., Gustafsson, O., Lefevre, U., Escuillie, F., Heimdal, J., Engdahl, A., Gren, J.A., Kear, B.P., Wakamatsu, K., Yans, J. and Godefroit, P. 2015b: Molecular composition and ultrastructure of Jurassic paravian feathers. *Scientific Reports* 5, 13520.
- Lindgren, J., Uvdal, P., Sjövall, P., Nilsson, D.E., Engdahl, A., Schultz, B.P. and Thiel, V. 2012: Molecular preservation of the pigment melanin in fossil melanosomes. *Nature Communications* 3, 824.
- Lohmann, U. and Sachs, S. 2001: Observations on the postcranial morphology, ontogeny and palaeobiology of *Sclerocephalus haeuseri* (Amphibia: Actinodontidae) from the Lower Permian of Southwest Germany. *Memoirs of the Queensland Museum* 46, 771–782.
- McNamara, M.E., van Dongen, B.E., Lockyer, N.P., Bull, I.D. and Orr, P.J. 2016: Fossilization of melanosomes via sulfurization. *Palaeontology* 59, 337–350.
- Milner, A.R. 1982: Small temnospondyl amphibians from the Middle Pennsylvanian of Illinois. *Palaeontology* 25, 635–664.
- Moyer, A.E., Zheng, W., Johnson, E.A., Lamanna, M.C., Li, D., Lacovara, K.J. and Schweitzer, M.H. 2014: Melanosomes or microbes: testing an alternative hypothesis for the origin of microbodies in fossil feathers. *Scientific Reports* 4, 4233.
- Orr, P.J., Adler, L.B., Beardmore, S.R., Furrer, H., McNamara, M.E., Peñalver-Mollá, E. and Redelstorff, R. 2016: “Stick ‘n’ peel”: Explaining unusual patterns of disarticulation and loss of completeness in fossil vertebrates. *Palaeogeography, Palaeoclimatology, Palaeoecology* 457, 380–388.
- Sansom, R.S., Gabbott, S.E. and Purnell, M.A. 2013: Atlas of vertebrate decay: a visual and taphonomic guide to fossil interpretation. *Palaeontology* 56, 457–474.
- Schindler, T. 1993: ‘*Elonichthys palatinus* n. sp., a new species of actinopterygian from the Lower Permian of the Saar-Nahe-Basin (SW-Germany). In Heidtke, U. (ed.), *New Research on Permo-Carboniferous Faunas*, 67–81. Pollichia Buch 29, Bad Dürkheim.
- Schindler, T. 2007: Geologie, Stratigraphie und Genese des permokarbonischen Saar-Nahe-Beckens. In Schindler, T., Heidtke, U. H. J. (eds.), *Koblesümpfe, Seen und Halbwüsten*, 4–37. Pollichia, Bad Dürkheim.
- Schoch, R.R. 1992: Comparative ontogeny of Early Permian branchiosaurid amphibians from southwestern Germany. *Paleontographica Abteilung A* 222, 43–83.
- Schoch, R.R. 2002: The early formation of the skull in extant and Paleozoic amphibians. *Paleobiology* 28, 278–296.
- Schoch, R.R. 2003: Early larval ontogeny of the Permo-Carboniferous temnospondyl *Sclerocephalus*. *Palaeontology* 46, 1055–1072.
- Schoch, R.R. 2009: Life-cycle evolution as response to diverse lake habitats in Paleozoic amphibians. *Evolution* 63, 2738–2749.
- Schoch, R.R. 2014: *Amphibian evolution: The life of early land vertebrates*. Wiley, New York.
- Schoch, R.R. and Witzmann, F. 2009: The temnospondyl *Glanochthon* from the Permian Meisenheim Formation of Germany. *Special papers in Palaeontology* 81, 121–136.
- Schoch, R.R. and Milner, A.R. 2014: *Handbook of paleoherpetology, Part 3A2, Temnospondyli I*. In Sues, H.-D. (ed.) Verlag Dr. Friedrich Pfeil, München.
- Schweitzer, M.H., Lindgren, J. and Moyer, A.E. 2015: Melanosomes and ancient coloration re-examined: A response to Vinther 2015 (DOI 10.1002/bies.201500018). *BioEssays* 37, 1174–1183.
- Schäfer, A. and Stapf, K.R.G. 1978: Permian Saar-Nahe Basin and Recent Lake Constance (Germany): Two environments of lacustrine algal carbonates. In *Modern and Ancient Lake Sediments, Vol. 2*, 83–107. Blackwell Publishing Ltd., Oxford, UK.
- Stebbins, R.C. and Cohen, N.W. 1995: *A natural history of amphibians*. Princeton University Press, New Jersey.
- Vinther, J. 2015: A guide to the field of palaeo colour. *BioEssays* 37, 643–656.
- Vinther, J. 2016: Fossil melanosomes or bacteria? A wealth of findings favours melanosomes. *BioEssays* 38, 220–225.
- Vinther, J., Briggs, D.E., Prum, R.O. and Saranathan, V. 2008: The colour of fossil feathers. *Biology Letters* 4, 522–525.
- Willems, H. and Wuttke, M. 1987: Lithogenese lakustriner Dolomite und mikrobiell induzierte Weichteilerhaltung bei Tetrapoden des Unter-Rotliegenden (Perm, Saar-Nahe Becken, SW-Deutschland). *Neues Jahrbuch für Geologie und Paläontologie, Abhandlungen* 174, 213–238.
- Witzmann, F. 2013: Phylogenetic patterns of character evolution in the hyobranchial apparatus of early tetrapods. *Earth and Environmental Science Transactions of the Royal Society of Edinburgh* 104, 145–167.
- Witzmann, F. and Pfretzschner, H.-U. 2003: Larval ontogeny of *Micromelerpeton credneri* (Temnospondy-

li, Dissorophoidea). *Journal of Vertebrate Paleontology* 23, 750–768.

Wogelius, R.A., Manning, P.L., Barden, H.E., Edwards, N.P., Webb, S.M., Sellers, W.I., Taylor, K.G., Larson, P.L., Dodson, P., You, H., Da-qing, L. and Bergmann, U. 2011: Trace metals as biomarkers for eumelanin pigment in the fossil record. *Science* 333, 1622–1626.

Dissertations

1. *Emma F. Rehnström, 2003*: Geography and geometry of pre-Caledonian western Baltica : U-Pb geochronology and palaeomagnetism.
2. *Oskar Paulsson, 2003*: U-Pb geochronology of tectonothermal events related to the Rodinia and Gondwana supercontinents : observations from Antarctica and Baltica.
3. *Ingela Olsson-Borell, 2003*: Thermal history of the Phanerozoic sedimentary succession of Skåne, southern Sweden, and implications for applied geology.
4. *Johan Lindgren, 2004*: Early Campanian mosasaurs (Reptilia; Mosasauridae) from the Kristianstad Basin, southern Sweden.
5. *Audrius Cecys, 2004*: Tectonic implications of the ca. 1.45 Ga granitoid magmatism at the southwestern margin of the East European Craton.
6. *Peter Dahlgvist, 2005*: Late Ordovician-Early Silurian facies development and stratigraphy of Jämtland, central Sweden.
7. *Mårten Eriksson, 2005*: Silurian carbonate platform and unconformity development, Gotland, Sweden.
8. *Jane Wigforss-Lange, 2005*: The effects of Late Silurian (mid-Ludfordian) sea-level change : a case study of the Öved-Ramsåsa Group in Skåne, Sweden.
9. *Erik Eneroth, 2006*: Nanomagnetic and micromagnetic properties of rocks, minerals and sulphide-oxidation products.
10. *Niklas Axheimer, 2006*: The lower and middle Cambrian of Sweden : trilobites, biostratigraphy and intercontinental correlation.
11. *Fredrik Terfelt, 2006*: Upper middle Cambrian through Furongian of Scandinavia with focus on trilobites, paleoenvironments and correlations.
12. *Andrius Rimsa, 2007*: Understanding zircon geochronology : constraints from imaging and trace elements.
13. *Mårten Eriksson 2007*: Silurian carbonate platforms of Gotland, Sweden : archives of local, regional and global environmental changes.
14. *Jane Wigforss-Lange, 2007*: Geochemical and sedimentary signatures of Phanerozoic events.

15. *Tobias Hermansson, 2007*: The tectonic evolution of the western part of the Svecofennian orogen, central Sweden : Insight from U/Pb and $^{40}\text{Ar}/^{39}\text{Ar}$ geochronology at Forsmark.
16. *Pia Söderlund, 2008*: $^{40}\text{Ar}-^{39}\text{Ar}$, AFT and (U-Th)/He thermochronologic implications for the low-temperature geological evolution in SE Sweden.
17. *Anders Cronholm, 2009*: The flux of extraterrestrial matter to Earth as recorded in Paleogene and Middle Ordovician marine sediments.
18. *Carl Alwmark, 2009*: Traces in Earth's geological record of the break-up of the L-chondrite parent body 470 Ma.
19. *Linda Larsson-Lindgren, 2009*: Climate and vegetation during the Miocene : evidence from Danish palynological assemblages.
20. *Ingemar Bergelin, 2010*: $^{40}\text{Ar}/^{39}\text{Ar}$ whole-rock geochronology of Mesozoic basalts in Scania : evidence for episodic volcanism over an extended period of ca. 80 Myr.
21. *Johanna Mellgren, 2011*: Conodont biostratigraphy, taxonomy and palaeoecology in the Darriwilian (Middle Ordovician) of Baltoscandia : with focus on meteorite and extraterrestrial chromite-rich strata.
22. *Johan Olsson, 2012*: U-Pb baddeleyite geochronology of Precambrian mafic dyke swarms and complexes in southern Africa : regional-scale extensional events and the origin of the Bushveld complex.
23. *Kristina Mehlqvist, 2013*: Early land plant spores from the Paleozoic of Sweden : taxonomy, stratigraphy and paleoenvironments.
24. *Andreas Petersson, 2015*: Evolution of continental crust in the Proterozoic : growth and reworking in orogenic systems.
25. *Karolina Bjärnberg, 2015*: Origin of the Kleva Ni-Cu sulphide mineralisation in Småland, southeast Sweden.
26. *Lorraine Tual, 2016*: P–T evolution and high-temperature deformation of Precambrian eclogite, Sveconorwegian orogen.
27. *Mimmi Nilsson, 2016*: New constraints on paleoreconstructions through geochronology of mafic dyke swarms in North Atlantic Craton.
28. *Sanna Alwmark, 2016*: Terrestrial consequences of hypervelocity impact : shock metamorphism, shock barometry, and newly discovered impact structures.
29. *Anders Lindskog, 2017*: Early–Middle Ordovician biotic and sedimentary dynamics in the Baltoscandian paleobasin.

30. *Ashley Gumsley, 2017: Validating the existence of the supercraton Vaalbara in the Mesoarchaeon to Palaeoproterozoic.*
31. *Johan Gren, 2018: Molecular, micro- and ultrastructural investigations of labile tissues in deep time.*